Hybrid Modelling of Roll Compaction

Inaugural-Dissertation

zur Erlangung des Doktorgrades
der Mathematisch-Naturwissenschaftlichen Fakultät
der Heinrich-Heine-Universität Düsseldorf

vorgelegt von

Hannah Lou Keizer (geb. Reimer)
aus Kiel

Hamburg, März 2021

aus dem Institut für Pharmazeutische Technologie und Biopharmazie
der Heinrich-Heine-Universität Düsseldorf

Gedruckt mit der Genehmigung der
Mathematisch-Naturwissenschaftlichen Fakultät der
Heinrich-Heine-Universität Düsseldorf

Berichterstatter:

1. Prof. Dr. Dr. h.c. Peter Kleinebudde

2. Prof. Dr. Jörg Breitkreutz

Tag der mündlichen Prüfung: 21. Mai 2021

„Der Beginn aller Wissenschaften ist das Erstaunen, dass die Dinge sind, wie sie sind.“

- Aristoteles -

Table of Contents

List of Abbreviations

Abbreviation	Explanation
API	Active pharmaceutical ingredient
CP	Compression pressure
DCPA	Dibasic calcium phosphate
GW	Gap width
HCT	Hydrochlorothiazide
HPMC	Hydroxypropylmethylcellulose
HR	Hausner ratio
Kp	Kp correction factor
MCC	Microcrystalline cellulose
NCE	New chemical entity
RC/DG	Roll compaction / dry granulation
RH	Relative humidity
RMSE	Root mean square error
rpm	Rounds per minute
RS	Roll speed
RW	Roll width
SCF	Specific compaction force
SD	Standard deviation
SF	Solid fraction

List of Publications

Peer reviewed articles

- Reimer H.L., Kleinebudde P.; *Hybrid modeling of roll compaction processes with the Styl'One Evolution;* Powder Technology, 2019
- Keizer H.L., Kleinebudde P.; *Elastic recovery in roll compaction simulation;* International Journal of Pharmaceutics, 2019
- Keizer H.L., Kleinebudde P.; working title: *Process simulation of different types of roll compactors;* in progress

Oral presentations

- User Group Meeting Medelpharm, Lyon (2017): *Hybrid modeling of roll compaction*
- Granulation Workshop, Sheffield (2017): *Hybrid modeling of roll compaction*
- JRS Symposium, Holzmühle (2017): *Hybrid modeling of roll compaction – granulation and tableting*
- PBP World Meeting, Granada (2018): *Hybrid modeling of roll compaction – improved predictability of ribblet solid fraction*
- JRS Symposium, Holzmühle (2018): *Roll compaction simulation – Is hybrid modeling material independent?*
- Alumni-Meeting, Düsseldorf (2018): *Hybrid modeling des Walzenkompaktierens – Ein neuer Ansatz zur Optimierung der Prozessentwicklung*

Poster presentations

- ParTec Nürnberg (2019): *Roll compaction – Influence of the screw speed ratio on the ribbon solid fraction*
- Granulation Workshop Lausanne (2019): *Estimation of nip angle by roll compaction simulation*

Combined oral and poster presentations

- Compaction Simulation Forum Ghent (2017): *Hybrid modeling of roll compaction – granule size distribution*
- Compaction Simulation Forum Cambridge (2018): *Roll compaction simulation – connection between specific compaction force, compression pressure and gap width*

Eigenanteil der veröffentlichten Manuskripte

H.L. Reimer, P. Kleinebudde, 2019. Hybrid Modeling of Roll Compaction Processes with the Styl'One Evolution. Powder Technology 341, 66-74.

Eigenanteil: 70 %

Erläuterung zum Eigenanteil: Hannah Lou Keizer hat die praktischen Versuche konzipiert, durchgeführt und ausgewertet. Bei der praktischen Durchführung wurde sie teilweise durch Bruno Leclercq unterstützt. Das Manuskript hat sie selbständig verfasst. Peter Kleinebudde war an der Konzeption der Studie beteiligt, hat die Interpretation begleitet und das Manuskript korrigiert.

H.L. Keizer, P. Kleinebudde, 2020. Elastic recovery in roll compaction simulation. International Journal of Pharmaceutics 573, 118810

Eigenanteil: 90 %

Erläuterung zum Eigenanteil: Hannah Lou Keizer hat die praktische Arbeit geplant und mit teilweiser Unterstützung von Hanna Plappert und Nina Baumann durchgeführt. Die Auswertung der Daten sowie das Entwerfen des Manuskriptes hat Hannah Lou Keizer selbständig durchgeführt. Peter Kleinebudde war an der Konzeption der Studie beteiligt, hat die Interpretation begleitet und das Manuskript korrigiert.

1 Introduction

1.1 Granulation

Granules are solid and dry aggregates, which have a sufficiently high robustness and are coarser compared to the particles from which they are produced. Granules can be divided into three main types according to their production technique. The first one is wet granulation: Granules are formed by wetting and aggregating the powder. In this case, the particles can be either directly enlarged or smaller granules are formed by sieving a wet mass (Ennis, 2005). The second one is dry granulation: The powder is compacted into larger intermediate compacts, which are subsequently milled into granules. In this case, the particle size enlargement is achieved by the size reduction of previously dry compacted powder (Miller, 2005). The third one is melt granulation: The granulation agent, which is solid at room temperature, is melted during granulation to agglomerate the particles (Kristensen and Schaefer, 1987).

The European and the United States Pharmacopoeia differentiate between effervescent granules, coated granules, gastro-resistant and modified-release granules or delayed- and extended-release granules (Council of Europe, 2020c, United States Pharmacopeial Convention, 2021). The formed granules can either be the final dosage form or they can be further processed into tablets or filled into capsules.

The reasons for granulation are numerous and summarised in the following.

- Improvement of flow properties: It is known that the particle size has a distinct influence on the flow properties of powders and that poor flowability is connected to tablet weight variations (Fassihi and Kanfer, 1986). Mehrotra et al. (2009) simulated the die filling and compression behaviour of granular systems by 3D discrete element method. It was found that the die filling for cohesive materials takes longer than for less cohesive powders and this can adversely affect the tablet weight uniformity. The enlargement of particles by granulation should improve their flowability by decreasing the specific surface area and the particle-particle interaction (Schiano et al., 2018), since larger particles have a favourable ratio of weight forces to attractive forces.
- Reduction of bulk volume: A high bulk volume can be problematic for direct compression, since it requires a large die filling height, which can cause problems when filling the die (Zettler et al., 2016). Furthermore, the deaeration during the compaction becomes difficult, which may result in capping/lamination of the tablets (Long and Alderton, 1960, Mazel et al., 2015). By granulation, the bulk volume is reduced and thus also the space required for storage (Parrott, 1981).

- Avoiding segregation and improving content uniformity of tablets: Segregation is one of the most relevant mechanisms in non-uniform die filling on a tablet press. It has been shown that differences in particle size as well as differences in the particle density in a blend can induce a segregation (Guo et al., 2011a, Guo et al., 2011b), which can lead to a false dosing in the tablet (Hildebrandt et al., 2019). The tendency of powder blend particle size segregation during die filling can be lowered by granulation, since the particle size distribution can be narrowed (Wennerstrum, 2000). Especially for tablets containing low doses of the active pharmaceutical ingredient (API), the content uniformity can be problematic (Hausman et al., 2005). By granulation, the mixture of the different primary particles and their percentage is fixed in the larger granules (Cantor, 2008), so that an inhomogeneous distribution of the API should be prevented. Hausman (2004), Railkar and Schwartz (2000) and Ende et al. (2007), e.g., have shown that granulation can improve the content uniformity of tablets.

- Reduction of safety hazards for operators: The dust generation is diminished by reducing the fraction of fines and thus the risk for operators handling with high potent drugs can be reduced (Rumpf, 1958a, b).

Wet granulation is the most used granulation method in the pharmaceutical industry (Seem et al., 2015, Thapa et al., 2019), since the granules obtained by wet granulation show good flow properties due to their smooth surface and narrow granule size distribution (Fu et al., 2004). Three wet granulation techniques are used in the pharmaceutical industry: twin-screw granulation, high shear wet granulation, fluid bed granulation (Thapa et al., 2019). The bonding mechanisms within the granules are mainly based on solid bridges. They are built by hardening of the liquid binder polymers or by the formation of crusts after the removal of the liquid granulating agent (Parikh, 2005). Depending on the chosen technique and the process parameters, the granules show different properties. For example, high shear granulation results in granules with higher density due to the greater forces acting on the particles compared to fluid bed granulation (Faure et al., 2001). Important process parameters, which can be varied to influence the granule properties, are for example the liquid to solid ratio in general, the wet massing time in high shear granulation, the screw configuration and throughput in twin-screw granulation and the airflow and inlet air temperature in fluid bed granulation (Arndt et al., 2018). The presence of liquids (water or organic solvents) causes several disadvantages: The liquids must be removed in a drying step that leads to high energy consumption. The high energy consumption and the recycling of solvents make the multi-stage process cost and time intensive. Furthermore, the granules

are exposed to heat stress, which can cause degradation processes and accelerate reactions such as decarboxylation, oxidation etc.

Dry granulation is a suitable alternative, especially for heat- and moisture-sensitive materials since a liquid addition is not required. The drying step is omitted and thus the materials are not exposed to a relevant heat stress. In literature, temperatures between 30° C and 70° C for freshly produced lactose ribbons (Omar et al., 2015) and between 20° C and 45° C for MCC (microcrystalline cellulose) ribbons (Al-Asady et al., 2016, Wiedey and Kleinebudde, 2018) were observed by using infrared thermography. Since the temperature decreases rapidly after the compaction, the exposure of the material to heat stress is only temporary and less critical regarding possible degradation processes.

There are two ways of dry granulation: One is slugging, in which the powder is compressed to compacts, and subsequently the tablets are comminuted to granules. The other is roll compaction, in which powder is densified between two counter-rotating rolls before the compacts are milled to granules. Slugging merely has historical relevance and is no longer used, since it has many disadvantages, like the comparatively low throughput, the poor process control and the single batch processing (Miller, 2005). Roll compaction can be used in continuous manufacturing, overcomes the low throughput of slugging and is capable to process poorly flowing powder blends, which may have problems to fill the die properly in the slugging process, since screw conveyors can be used (Miller, 2005, Parrott, 1981). Drawbacks of the process may be the amount of formed fine particles (Kleinebudde, 2004) and a partial loss in tabletability after roll compaction/dry granulation (Sun and Kleinebudde, 2016), which is described in more detail in section 1.4. Inghelbrecht and Remon (1998a) were able to minimise the formation of dust and fine particles by adding a controlled wetting process before roll compaction, in order to improve the dry binder distribution. Arndt and Kleinebudde (2018c) stated that the fraction of fines could be reduced by using dry binders with optimised dry binding properties and that the use of efficient dry binders could partially compensate for the loss in tabletability. Despite the above mentioned disadvantages, the manufacturing classification system introduced by Leane et al. (2015) ranks the roll compaction/dry granulation process between direct compression and wet granulation at the second place with regard to the simplicity of the process. The process characteristics make roll compaction/dry granulation a time-, energy- and cost-saving process and finally an attractive choice for heat- and moisture-sensitive materials and continuous manufacturing lines (Kleinebudde, 2004). It is described in the following section 1.2 in more detail.

1.2 Roll Compaction/Dry Granulation

1.2.1 General

In roll compaction/dry granulation, a powder blend is densified between two counter-rotating rolls into intermediate compacts, called ribbons, which are consequently milled to granules. Roll compaction/dry granulation is a continuous granulation method and has gained interest as it can be integrated into continuous manufacturing lines (Leuenberger, 2001, Mangal, 2018, Vervaet and Remon, 2005).

The pharmaceutical application of roll compaction/dry granulation was first mentioned by Jaminet and Hess (1966). The roll compaction process can be divided into three parts (Guigon and Simon, 2003, Shlieout et al., 2002). In the first part, the powder is conveyed towards the rolls, either by gravity or by one or several screws. The second part of the process is the compaction, in which the powder is densified between the two counter-rotating rolls. The resulting intermediates - ribbons - are milled to granules in the third part, the granulation unit. This main principle is valid for all roll compactors, but they differ in their designs, depending on the supplier.

1.2.2 Roll Compaction

In most modern roll compactors, the following process variables can be adjusted to influence the properties of the ribbons, which in turn have a decisive influence on the properties of the granules.

- *Specific compaction force.* The specific compaction force (SCF) is expressed in kN per cm roll width. The specific compaction force is the process parameter in roll compaction which influences the ribbon and granule properties the most (Peck, 2008).
- *Roll speed.* The counter-rotating rolls are moving simultaneously with the same speed. The roll speed (RS) can be expressed, e.g., in rounds per minute (rpm) or for the circumferential speed e.g., in meter per second (m/s) to be able to compare the roll speed of roll compactors with different roll diameters.
- *Screw speed.* In case of roll compactors, which are not gravity fed but use feeding (and tamping) screws to convey the powder towards the gap, the feeding screw speed (FSS) is determining the amount of conveyed material.
- *Gap width.* The gap width describes the distance between the rolls. In the following, the minimum distance between the rolls is called gap width (GW) for reasons of simplification. In some roll compactors, the gap width is not controlled but a result of the other process parameters.

According to Johanson (1965), the space between the rolls is divided into three zones as shown in Figure 1.2-1. The feeding, compaction and extrusion zones are characterised by varying stresses and powder velocities (Michrafy et al., 2011b). First is the feeding zone (I): It is characterised by low stresses and mainly particle rearrangement takes place in this zone. The circumferential roll speed is higher compared to the one of the particles in contact with the rolls, which slip on the roll surface. Second is the compaction zone (II): The beginning of the compaction zone is described by the nip angle α (further explanations are given in section 3.3). This is the angle at the point of the transition between slip and non-slip of the powder on the roll surface, where the powder is dragged in between the rolls. In the compaction zone, the powder is densified depending on the used materials by either plastic flow and/or particle fragmentation and creation of new bonding areas. The pressure exerted on the powder increases until it reaches its maximum at the neutral angle, which does not have to be identical with the minimum gap width (Guigon and Simon, 2003, Schönert and Sander, 2002). In contrast to other granulation methods, which use liquid binders for example, the bonds between the particles in roll compaction do not consist of solid bridges but of inter-molecular van-der-Waals forces and hydrogen bonds or interlocking bonds for fibrous materials. Since the distance between the individual powder particles is strongly reduced by the applied pressure, the van-der-Waals forces and number of hydrogen bonds increase (Rumpf, 1958a). They can hold the particles together and ribbons are formed. Third is the extrusion zone (III): After passing through the minimum gap width, the formed ribbons exit the rolls. The ribbons undergo an elastic recovery when the pressure exerted by the rolls is removed so that the final ribbon thickness can be higher than the minimum gap width (Gamble et al., 2010, Guigon and Simon, 2003, Nkansah et al., 2008). The phenomenon of elastic recovery is discussed in section 3.2. The ribbons are removed by scrapers to avoid multiple compactions and sticking of the ribbons on the roll surface.

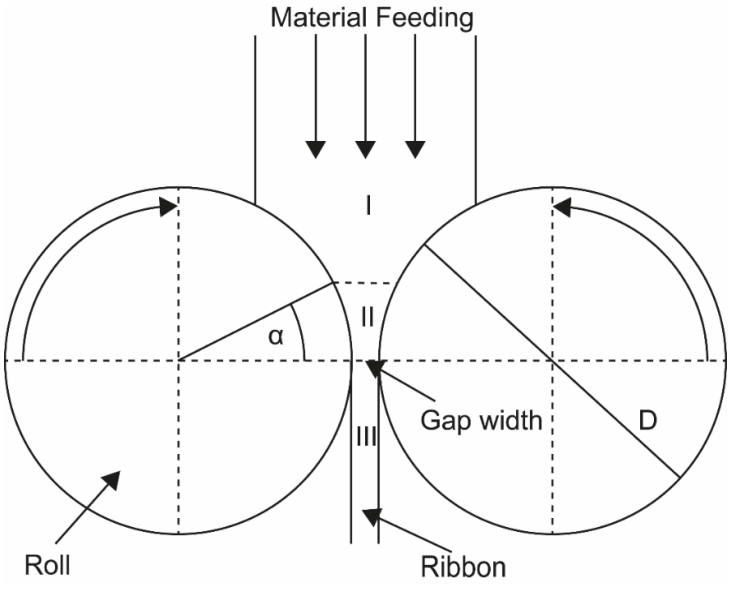

Figure 1.2-1: Zones between the rolls - I, feeding or slip zone; II, compaction zone; III, extrusion or release zone; α, nip angle; D, diameter; adapted from Kleinebudde (2004)

Ribbon Properties

Ribbons are mainly characterised by the following two key attributes:

Solid fraction / relative density. The ribbon solid fraction (SF) or relative density (in the following both expressions are used equivalently) is a valuable parameter, which can be used during production, to track the ribbon quality and the process performance (Hancock et al., 2003). The solid fraction is defined as the ratio between the envelope density of the compact $\rho_{envelope}$ and the powder density of the starting material ρ_{powder} and can be determined by helium and powder pycnometry (sections 5.2.9.5 and 5.2.10.1).

$$SF[\%] = \frac{\rho_{envelope}}{\rho_{powder}} \times 100 \qquad (1)$$

Tensile strength. The tensile strength (TS) of ribbons expresses the minimum tensile stress, which can induce a fracture within the compact, and is useful if the roll compaction process is evaluated for different materials (Zinchuk et al., 2004). It can be measured by using a three-point beam bending test (Hancock et al., 2000, Jaminet and Hess, 1966).

The specific compaction force is the process parameter with the highest impact on the ribbon solid fraction (Csordas et al., 2018, Inghelbrecht and Remon, 1998c) and tensile strength and finally influences the quality of the granules and tablets decisively. In modern roll compactors, this parameter is therefore prioritised and is maintained constant by master control loops, even if the feeding fluctuates (Csordas and Kleinebudde, 2018). Several authors have investigated the effect of the specific

compaction force on the ribbon solid fraction. Generally, an increase in specific compaction force or actual roll pressure results in ribbons with higher solid fractions. Roll compaction/dry granulation of different types of lactose and microcrystalline cellulose were evaluated. It was found for both materials that the roll pressure has the highest impact on the granule friability and that a high roll pressure results in granules of good quality (Inghelbrecht and Remon, 1998b, c).

Control loops allow to achieve a constant gap width throughout the process by automatically adjusting the feed screw speed and thus the amount of powder which is conveyed between the rolls (Csordas and Kleinebudde, 2018). If the automatic gap control is not used or not available, the ratio between the feeding screw speed and the roll speed is decisive for the resulting gap width and the occurrence of under- or over-feeding (Hervieu et al., 1994). Pishnamazi et al. (2019) investigated roll compaction of different pharmaceutical powders and developed a process mapping. It was found that varying the screw speed at constant pressure, which results in a larger gap width, has an influence on the ribbon solid fraction, but to a smaller extent than the pressure itself.

The roll speed can as well have an influence on the ribbon solid fraction, depending on the deformation behaviour of the processed material. Khorasani et al. (2016), for example, observed that for a binary mixture of MCC and acetylsalicylic acid decreasing the roll speed - while keeping the roll pressure and the gap width constant - resulted in ribbons with higher solid fraction. The effect of the roll speed can be explained by the prolonged time, in which the powder is exposed to the pressure. This allows a higher viscoelastic deformation (Armstrong, 1989) and leads to an increased ribbon solid fraction. On the other hand, Souihi et al. (2013b) found that varying the roll speed - while keeping the roll force and the gap width constant - has no impact on the solid fraction of ribbons from a model formulation containing large amount of mannitol. This confirms the assumption, that plastically deforming materials are more sensitive to variations of compaction speed than brittle materials (Rees and Rue, 1978).

The solid fraction is not equally distributed over the ribbon length and width. This is related to the friction between the powder and the used sealing system, which leads to density variations across the ribbon width (Funakoshi et al., 1977). Additionally, the periodical pattern of the screw feeder is visible along the ribbon length in a sinusoidal curve of more densified material (Simon and Guigon, 2000).

The addition of lubricants to the powder mixture prior to roll compaction can be useful to avoid sticking issues on the rolls but it can lead to altered compaction behaviour. Miguelez-Moran et al. (2008) studied the effect of using magnesium stearate on roll compaction of microcrystalline cellulose (MCC). It was

found that the nip angle and the pressure applied to the powder decreased significantly when magnesium stearate was used on the roll surface and even more when the powder itself was lubricated. Furthermore, a change in density distribution was observed due to the reduced friction between the powder and the side cheek plates. Yu et al. (2013) confirmed these effects for MCC and di-calcium phosphate dihydrate. Bulk lubrication altered the bonding properties which negatively influenced the tensile strength of MCC tablets (Almaya and Aburub, 2008, Paul and Sun, 2018, Zuurman et al., 1999).

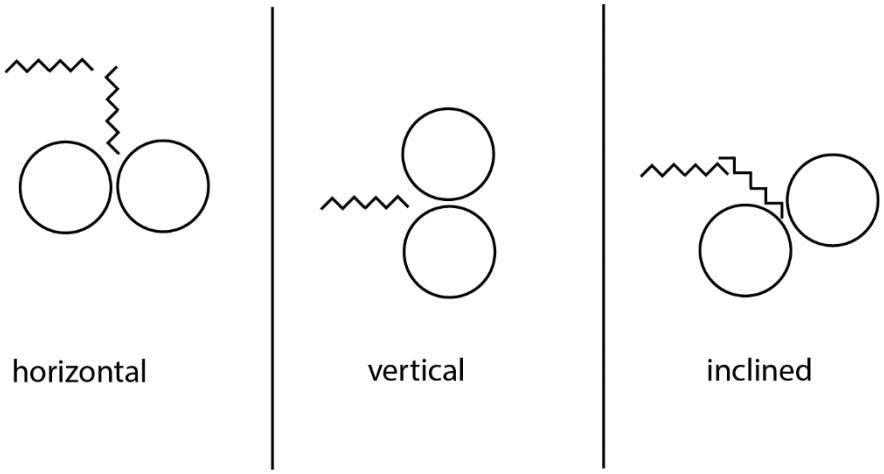

Figure 1.2-2: Schematic roll and screw positions

The compactors used in the present work have one fixed and one floating roll, which allows a dynamic adjustment of the gap width during the process and results in a more stable specific compaction force compared to roll compactors using a constant gap width (Haeffler et al., 2019). The specific compaction force on the rolls is generated either by a hydraulic system (WP120, WP200 – Alexanderwerk; Mini-Pactor - Gerteis) or by an electrical spindle motor (BRC25 - LB Bohle). The arrangement of the rolls and the feeding principle vary from manufacturer to manufacturer and are depicted in Figure 1.2-2. While Alexanderwerk uses vertically arranged rolls and one horizontal screw, LB Bohle works with horizontally arranged rolls and two screws, one horizontal feeding screw and one vertical tamping screw. Gerteis compactors are equipped with inclined (angle of 30°) rolls, one horizontal feeding screw and one inclined tamping screw. The horizontal feeding system of Alexanderwerk compactors may lead to a smaller fraction of uncompacted powder, since the powder bypass can be lowered. However, a drawback can be the partially insufficient powder draw between the rolls, especially when smooth rolls are used (Csordas and Kleinebudde, 2018). The vertical tamping screw used in the Bohle compactor benefits from gravity to transport enough powder to the rolls. Nevertheless, there is a risk of an increased fraction of fines, as powder tends to flow past the rolls without being compacted. The inclined rolls and

tamping screw used in the Mini-Pactor may combine the advantages of the afore-mentioned configurations.

The rolls of the different compactors can vary in their diameter and width. These roll parameters are important for adjusting the desired throughput and can be used for the scale-up of the process (Alleso et al., 2016). The roll dimensions of the roll compactors investigated in the present work are summarised in Table 1.2-1.

Table 1.2-1: Roll dimensions of the investigated roll compactors

Roll compactor	**Supplier**	**Roll diameter [mm]**	**Roll width [mm]**
Mini-Pactor	Gerteis	250	25
BRC25	LB Bohle	250	25
WP120	Alexanderwerk	120	25; 40
WP200	Alexanderwerk	200	75

The roll surface can either be smooth, slightly roughened, or shaped (knurled, grooved, squared). A shaping can improve the intake of the powder compared to smooth rolls since it increases the friction between powder and roll surface (Csordas and Kleinebudde, 2018, Johanson, 1965). The powder intake and compaction can be further improved by using a deaeration unit in the feeding zone (Miller, 2005).

One disadvantage of the roll compaction process is the relatively high fraction of fines. It is mainly caused by two mechanisms – on the one hand by powder that passes the rolls without being compacted and on the other hand by particles generated during the dry granulation step (section 1.2.3). Two main principles are used to seal the rolls – cheek plates and rim rolls. Rim rolls were found to be useful to achieve a more uniform pressure distribution along the ribbon width and to reduce the amount of uncompacted material. Regarding the density distribution along the ribbon width, it was found that cheek plates lead to ribbons with higher density in the centre of the ribbons, whereas rim rolls result in a distribution with a trend of higher density at the edges (Akseli et al., 2011, Funakoshi et al., 1977, Miguelez-Moran et al., 2008, Wiedey and Kleinebudde, 2017). As mentioned above, the rotation of the screw influences the ribbon density distribution. The result is a sinusoidal periodic pattern over the

length of the ribbon (Simon and Guigon, 2003). Nevertheless, the density distribution was found to be of small relevance for the properties of the final tablets (Wiedey et al., 2018).

1.2.3 Dry Granulation

In pharmaceutical applications, ribbons are not the final product but intermediates. The ribbons are milled into granules in a dry granulation step in less than one minute after they were formed between the rolls (Mangal and Kleinebudde, 2018). The granules can be the final product or again an intermediate, which is further processed to tablets or filled into capsules. It is thus of high importance to understand the parameters influencing the granule properties.

Depending on the roll compactor supplier, different types of mills are used to granulate the ribbons. Gerteis compactors, e.g., can be equipped with a pocket mould granulator or an oscillating star granulator. The latter was used in the present work and forces the ribbons through a sieve insert of defined mesh width and with an adjustable distance between the sieve and the star granulator. Bohle roll compactors are designed with a conical rasp sieve as granulation unit, in which the ribbons are pressed through holes of a defined diameter by an impeller. In some compactors several units can be connected in series, first for a coarse crushing and then for the milling into granules. The particle size distributions are varying between the type of mills, so that the transfer to another equipment while maintaining the particle size distribution is a challenging task (Vendola and Hancock, 2008).

Dry granulation results in a bimodal granule size distribution due to the fraction of fines, which is higher compared to other granulation methods (Arndt et al., 2018, Kleinebudde, 2004, Perez Gago and Kleinebudde, 2017). The fine particles are either uncompacted powder bypass, as described above (section 1.2.2), or are created during the milling in the granulation unit. Abrasive processes produce fine particles, their number is amongst others depending on the strength of the ribbons (Schiano et al., 2016).

The solid fraction of the ribbons is decisive for the strength of the granules, the particle size distribution, the compressibility, the tabletability and in connection with these, also for other properties such as granule flowability. It was shown by Jaminet and Hess (1966) that the particle size distribution is affected by the strength of the ribbons, which in turn depends on the process settings during roll compaction. Stronger ribbons led to coarser granules. Wagner et al. (2013) investigated the influence of roll compaction process parameters on the properties of mannitol granules. It was found that an increase of the specific compaction force had a significant positive effect on the granule flowability. These results

confirm the findings of Inghelbrecht and Remon (1998c), who stated that the specific compaction force has the greatest influence on the flowability of lactose granules.

The granule flowability relates to the granule size and the granule shape. Generally, the larger the granules the better is their flowability and the higher the ribbon solid fraction the larger are the resulting granules. However, an irregular granule shape can have a negative influence on the granule flowability compared to round shaped starting particles (Schiano et al., 2018).

Mangal and Kleinebudde (2018) evaluated the effect of the roll compaction/dry granulation (RC/DG) process parameters on the granule size of different materials. The results confirmed that the effect of the specific compaction is decisive for the granule size distribution and that an increase of the specific compaction force resulted in a decreased fraction of fines. In comparison, the granulation parameters themselves are secondary. However, by changing the impeller speed, the granule size could be adapted without changing the granule porosity, which was claimed advantageous for continuous manufacturing.

It can be concluded that the type of the used granulation unit and the ribbon properties are decisive factors for the granule properties. It is thus of importance to choose the correct roll compaction process parameters to obtain ribbons of the desired quality.

1.3 Roll Compaction Simulation

1.3.1 Need for Simulation

The interest in simulating roll compaction processes is high. Especially in the early phase of formulation development, the available amount of new chemical entities is limited and they are often expensive. The roll compaction process is time and material consuming. With an accurate simulation, it would be possible to find the appropriate process parameters quickly and thus, simulation could shorten the development process and reduce the costs considerably. Simulation is also interesting for the process transfer from one compactor to another. This could be the case, e.g., when a production process is relocated to another site. The transfer time could be shortened and the process optimisation could be simplified. Another application for roll compaction simulation is the scale-up. The scale-up from small laboratory to big production machines is challenging (Alleso et al., 2016, Liu et al., 2011). Simulation would make the step from lab to pilot scale largely superfluous and one could quicker move on to the production scale.

1.3.2 Existing Approaches

Numerous models have been developed to simulate roll compaction and to gain a better understanding of the roll compaction process. Some of them are purely theoretical considerations, others have a more experimental focus or are a mixture of both.

Johansons Theory and Extensions of it. The rolling theory of Johanson (1965) might be the approach in pharmaceutical area, to which many of the recently developed models refer. Johanson incorporated the steady state flow model into the theory of roll compaction (Sommer and Hauser, 2003). He used several material properties - the compressibility factor of the material, its angle of wall friction and the angle of internal friction in combination with the roll dimensions - to predict the pressure profile and nip angle for the roll compaction of powders. Several authors have evaluated and extended the rolling theory. Sommer and Hauser (2003) criticised that a simplified material model is used to describe the pressure distribution and that the influence of feed screws is not considered by the approach. This can lead to inaccurate prediction of the nip angle and maximum pressure. Bindhumadhavan et al. (2005) performed an experimental validation of Johanson's theory with a gravity fed roll compactor, which was equipped with pressure transducers. MCC was used as a model substance. It was found that the model can predict the peak pressures. However, the experimentally determined roll pressures deviated from the calculated ones the more the larger the gap width was. Some limitations of Johanson's model were pointed out: The parameter roll speed is not considered, and it cannot account for the complexity of screw fed roll compactor design. Reynolds et al. (2010) extended the rolling theory by the parameter pre-consolidation relative density and provided an approach that allows to predict the ribbon solid fraction as a function of process parameters, roll geometry and material properties for screw controlled and roll separation controlled roll compactors. It was found that predictions of ribbon properties by uniaxial compaction overestimate the ribbon solid fraction, so that data from roll compaction was used to build the model. The model can predict the influence of scale changes on the ribbon density. Sajjia et al. (2017) developed a mechanistic model of the roll compaction process based on Reynold's method with sufficient accuracy and pointed out the importance of the methodology used for determining the model input parameters. Park et al. (2018) performed flowsheet modelling for roll compaction/dry granulation of MCC based on the approach introduced by Reynolds et al. (2010). The effect of the process parameters roll speed and roll force on the ribbon relative density and the granule size distribution were evaluated and compared with experimental results. Generally, the prediction of the critical quality attributes was good, but the determination of the model input parameter was difficult, and the model could not reproduce the

influence of the dwell time on powder deformation. Rowe et al. (2013) provided a method based on Reynolds extension of Johanson's theory that assists in scale-up processes and in finding the design space for a new formulation. An iterative process for the determination of the feed pressure was established. Furthermore, a dimensionless number, which links the ribbon solid fraction with the roll compaction process conditions, was included into the model.

Intelligent Software. Mansa et al. (2008) used intelligent software to evaluate the effects of several process input parameters on the ribbon density, the maximum roll compaction pressure and the nip angle. The software was trained with experimental data and could be used to predict the process conditions to reach a certain ribbon porosity. However, deviations were found when the settings were outside of the trained area.

Unified Compaction Curve. Farber et al. (2008) evaluated the differences in tensile strength of tablets which were either made by direct compression or by roll compaction and subsequent compression of the granules. The authors assume that compaction is a cumulative process and introduced a unified compaction curve for the compaction behaviour of a powder, which combines roll compaction and tableting with direct compression. The unified compaction curve is only valid for materials or blends that show a considerable plastic deformation behaviour and for compaction pressures larger than 200 MPa, since a constant tablet density is required for the calculation. The approach of Hilden et al. (2011) aims to provide a simple mathematical equation to calculate the peak stress equivalent to tableting as a function of roll force, radius and width. The model only requires the solid fraction – compaction stress relation of the material as an input and assumes a material independent angular "working zone", in which most of the mechanical work takes place. The comparison of ribbon and tablet solid fraction data correlated with the compaction stress suggested a single compaction profile for the material like reported by Farber et al. (2008).

Experimental Approaches. Yu et al. (2012) presented a practical method to determine the nip angles of MCC and dibasic calcium dihydrate directly from instrumented roll data by using pressure gradients as a function of the angular position. The intersection between the ascending and descending part of the curve represents the nip angle. An advantage is that the method is applicable to different roll speeds. It was shown that the flow and compaction properties of the powders have a great influence on the nip angle. Since data from instrumented rolls is needed, this approach has no predictive capability. A model-based approach was introduced, in which low-throughput roll compaction experiments were used for

process design and scale-up (Toson et al., 2019). An iterative calibration process was established to determine the compressibility factor and the pre-consolidation solid fraction. The ribbon solid fraction and the throughput of two ibuprofen containing mixtures were successfully predicted. Disadvantages might be the one-dimensional perspective of the powder flow and the relatively high material consumption. It was stated that the approach of Johanson (1965) is better suited for gap-controlled systems whereas the model of Reynolds et al. (2010) is more useful for screw speed-controlled systems. Tan et al. (2016) investigated different methods to determine the nip angle of a roll compactor equipped with serrated rolls. The results of physical measurements and model calculations based on Johanson were in acceptable agreement. However, the removal of powder until the first sign of densification seems difficult to standardise.

Multivariate Data Analysis. Systematic multivariate data analysis of roll compaction can provide insights into the relationships between material properties, process parameters and the critical quality attributes of the product. A preliminary study evaluated the effects of process parameters and material properties of different MCC and lactose grades on the ribbon, granule and tablet properties (Soh et al., 2008). The process parameters, which had the biggest influence on the gap width, were the roll speed and roll pressure. The model quality could be improved also using the material properties. Based on these results, Boersen et al. (2015) investigated, whether it is possible to transfer a model for an API containing formulation to another formulation containing a different API. Considering the percolation threshold for the formulation improves the prediction quality. The tablet properties were influenced more by the ribbon and granule properties and less by the raw material properties. A method for roll compaction scale-up and transfer of a formulation was presented (Boersen et al., 2016), in which a dimensionless variable is used to connect the process parameters and the raw material properties with the ribbon relative density. This dimensionless number consists of the roll pressure, the roll speed, the horizontal feed screw speed, the true density and the roll diameter. The variable was successfully used for the transfer between two roll compactors, but its applicability may not be valid for compactors with larger differences in equipment design. Souihi et al. (2013a) investigated the effect of different mannitol and dicalcium phosphate qualities and found that the particle morphology is important for the roll compaction performance. Roll compaction of spray dried, agglomerated particles resulted in decreased flowability due to particle breakage into smaller primary particles. OPLS (orthogonal projections to latent structures) models were built and validated with excipient qualities not used during model development, showing good predictive ability for quality attributes of intermediates and final drug

product. In a further study, Souihi et al. (2013b) have used statistical design of experiment and multivariate data analysis to estimate the design space for a roll compaction process. Some authors provided systematic studies on the effect of changes in roll compaction equipment on ribbon, granule and tablet properties. The influence of horizontal and vertical screw feeding was evaluated and a method was presented to predict ribbon relative density for different roll compactors (Souihi et al., 2015) based on the approach of Reynolds (2010). The normal stress was found to be the main influencing factor for ribbon relative density for both investigated feeding mechanisms and a quadratic relationship was identified. However, a possible drawback of the method is that for roll compactors without gap control the screw constant must be determined in preliminary experiments. Haeffler et al. (2019) compared roll compactors from different suppliers and found that it might not be enough to keep ribbon porosity equal in order to get the same granule size distribution and final product properties when differences in compactor design are present. In this case, the force control – by hydraulic pressure or by regulation of the feeders – and sealing systems were the major differences resulting in differences in granule size distribution. The general disadvantages of models based on multivariate data analysis are the relatively high experimental effort for model building and the limited applicability to materials with distinct flow and compaction properties.

Finite Elements and Discrete Elements Methods. Several authors have used finite elements methods (FEM) and discrete elements methods (DEM) to model the roll compaction process. The compaction parts of the models are mainly based on the Drucker Prager Cap model. Dec et al. (2003) reviewed different approaches of roll compaction simulation – the rolling theory by Johanson, slab methods and finite elements methods. It was stated that the FEM approaches are advantageous compared to the other methods because they take into account accurate information about the process. Cunningham et al. (2010) have investigated the roll compaction process regarding the inhomogeneous density distribution in ribbons with instrumented rolls. High velocity and shear gradients were observed and further analysed by using 2D FEM. Differences in velocity of up to 20 % between the powder at the centre and the powder close to the rolls were found. With 3D modelling, it was possible to predict the pressure and density distribution near the edges connected to side seal fraction. Michrafy et al. (2011b) modelled roll compaction of MCC with an 2D FEM approach, whereby the compaction behaviour was modelled by a modified Drucker Prager Cap model. In a further study, the approach was extended to 3D FEM and the density distribution over the ribbon width could be modelled (Michrafy et al., 2011a). In a study by Muliadi et al. (2012), the rolling theory for granular solids (Johanson, 1965) was compared to a 2D FEM

model. The nip angle determination followed the same trends for both approaches, but large quantitative differences were observed. The approach of Johanson is limited to a one-dimensional perspective, whereas the FEM revealed material velocity gradients within the gap width. It was shown that the mass flow and consequently the material relative density were over-predicted by Johanson's approach. In a further study (Muliadi et al., 2013), a 3D FEM was validated with experimental roll compaction experiments. It was found that 3D FEM was able to picture the experimentally determined ribbon density distribution and the overall ribbon density. A limitation of the model was that the elastic recovery of the ribbons after passing the minimum gap width could not be simulated. Mazor et al. (2018) combined DEM and FEM approaches for roll compaction modelling, whereby the DEM approach described the flow behaviour in the feeding zone and the FEM approach the densification behaviour in the compaction zone. The sinusoidal density pattern in the ribbons could be linked with the duration of one screw turn. FEM and DEM models require high computational effort and might not be useful for process development and process control, but they provide a detailed insight into the process.

Uniaxial Compaction. Several authors developed modelling approaches using uniaxial compaction as a tool to mimic the densification in the compaction zone of a roll compactor. Zinchuk et al. (2004) introduced a method to simulate the roll compaction process by using a uniaxial compaction simulator. The resulting compacts were analysed regarding their solid fraction and tensile strength to compare them with real ribbons from roll compaction. The roll movement was transferred to the punch movement by a simple sine function. Since die compression is not a continuous but a batch process, it cannot simulate the shear forces occurring on the roll surface and the inhomogeneous powder transport. Nevertheless, it was considered to be sufficiently representative for the roll compaction process, because it takes into account the parameters roll pressure, roll speed and roll diameter, which have a great influence on the ribbon key attributes solid fraction and tensile strength. In the study of Hein et al. (2008) roll compaction of MCC and different types of lactose was simulated using an eccentric tablet press. These compacts were milled and tableted. In order to identify the most suitable material for roll compaction, the final tablets were characterised for their tensile strength and compared with the tablets made of uncompacted powder. Anhydrous β-lactose was claimed to be the most advantageous material due to the small loss in tabletability, but the simulation was not verified with actual roll compaction. Patel et al. (2010) investigated the prediction of the pressure distribution in roll compaction by uniaxial compaction. The results from uniaxial compaction were compared to roll compaction data, which were obtained using an instrumented roll press. It was found that the pressures predicted by uniaxial compaction and a modified

Johanson equation were smaller than the ones measured by the pressure transducers. This was mainly attributed to the non-uniform pressure distribution across the ribbon width and the non-uniform powder flow between the rolls. Nesarikar et al. (2012b) combined the use of roll instrumentation, uniaxial compaction analysis and statistical linear models for the design space development of a roll compaction process. Ribbon density was the critical quality attribute and a correlation between the ribbon properties and the process parameters gap width and normal stress was found. It was stated that maintaining the normal stress results in ribbons with the same porosity. In a further study Nesarikar et al. (2012a) presented a modified Johanson approach, which was developed by experimental calibration with data from instrumented rolls. The placebo model was used to predict ribbon densities of API containing blends. Additionally, a scale-up approach was developed, which is based on experimental calibration with the small-scale compactor. Bi et al. (2014) assumed that similar compression pressures should result in compacts with similar solid fractions and compared roll compaction of three model formulations with uniaxial compaction. The maximal roll surface pressure was overpredicted by using Johanson's model. They corrected the model by introducing a mass correction factor, which considers the inhomogeneous powder transport between the rolls. However, the correction factor was found to be material dependent. Liu and Wassgren (2016) modified Johanson's theory in a similar way, a mass correction factor was incorporated, which accounts for the multi-dimensional powder flow. The predictions for the ribbon relative density obtained with the modified Johanson theory were compared to FEM models and showed good agreement.

Equipment Transfer and Scale-Up. One way to facilitate the transfer from a small- to a large-scale roll compactor is a practical approach, in which the roll diameter is kept constant and the roll width is changed instead (Alleso et al., 2016). However, a limitation of this approach is that the density distribution across the roll width differs between the scales. The systematic study of Haeffler et al. (2019) indicated that it is not enough to maintain the ribbon porosity when a transfer between roll compactors should be performed, since the granule properties were different depending on the type of mill. The equipment design, e.g. floating or fixed rolls, has a large influence on the ribbon quality. In a recent study by Moroney et al. (2020), roll compaction simulation for a formulation with high API load was performed using the Johanson model, which was extended by a screw function for the powder transportation in the feeding system. A scale-up on the same equipment by increasing the roll width was conducted successfully but the approach showed limitations when the roll compactor was changed.

Thin Layer Model. The thin layer model presented by Peter et al. (2010) serves as the basis for the approach used in this thesis. It was developed to predict the density of the powder between the rolls and the forces that occur during the compaction. It is assumed that the powder consists of infinitesimal thin layers, similar to an approach for metal powders by Katashinskii (1966), and that for each layer a certain density is given at a certain position between the rolls. One layer is defined by its thickness, by the width of the roll and the distance between the rolls. The latter is variable and decreases as it approaches the minimum gap width. The correlation between the density of each layer and the corresponding compression pressure of a layer is determined by tableting experiments. The total force, applied to the rolls, can be estimated by adding up the forces of each layer during the compression and the decompression phase. Peter et al. (2010) used several excipients and one placebo blend for their experiments. The density was determined by the throughput method, which does not consider the elastic recovery after compaction but represents the "at gap" density. The modelling divides the process into the polynomial rearrangement phase, the exponential densification phase, and the recovery phase, which is characterised by a double compression of the same powder. It is defined that the model calculations start with a layer whose density corresponds to a pressure of 0.2 MPa. The authors mention the importance of the compression profile that is used to determine the pressure-density correlation and recommend using a profile as close as possible to a roll compaction profile. However, the thin layer model assumes a one-dimensional and continuous powder densification, which may lead to deviations, since powder flow is more complex. Experimental results showed systematic deviations of the predicted forces, which could be corrected.

1.4 Tableting and Loss in Tabletability after Roll Compaction

Tablets are solid preparations intended for oral use, which usually consist of one or more active pharmaceutical ingredients and are obtained by the compression of a constant volume of particles. Excipients (e.g. binders, disintegrating agents, lubricants) can be added to tailor the properties of the powder blend and the final tablet (Council of Europe, 2020d). A powder blend can be directly compressed to tablets. The advantage of direct compression is its simplicity and economy. Furthermore, it is a suitable process for continuous manufacturing, which is of growing importance in the pharmaceutical industry. However, not all powder blends can be used for direct compression, since they must fulfill some essential requirements in terms of compressibility, segregation tendency and flowability. Recently, particle engineering of excipients and APIs has been used to create particles optimised for direct compression (Li et al., 2017). Alternatively, the tableting can be preceded by a

granulation step to optimise the properties of the powder blend (described in section 1.1). In a second step, the granules, which can be obtained by varying granulation techniques, are compressed to the final tablets.

The use of granulation prior to tableting and its influence on the tablet properties compared to direct compression has already been thoroughly investigated. It is known that the tensile strength of tablets is strongly influenced by the ribbon and granule properties, and to a smaller extent by the process parameters and the properties of the starting materials (Boersen et al., 2015). Malkowska and Khan (1983) studied the effect of re-compression on the properties of tablets prepared by slugging. They found that the tablet tensile strength was reduced after re-compression and that this effect was more pronounced the higher the initial compression pressure was. This effect is the so-called work hardening, is described as “the resistance to permanent deformation of a material increasing with the amount of deformation” and was found to be present for plastic and, less pronounced, as well for brittle deforming materials (Malkowska and Khan, 1983). Since then, the phenomenon of work hardening was investigated by several authors and different mechanisms were proposed (Farber et al., 2008, Mosig and Kleinebudde, 2015, Riepma et al., 1993). Sun and Kleinebudde (2016) reviewed the different proposed mechanisms. They stated that not a single mechanism is sufficient to explain the phenomenon of loss in tabletability, but that granule hardening and size enlargement together, which are mainly acting via bonding area and bonding strength, have an influence, depending on which materials and process settings are used. It was shown that the use of dry binders can reduce the effect of loss in tabletability after roll compaction as they increase the interparticle bonding strength and allow to work at lower compaction forces while maintaining sufficient granule and tablet quality (Arndt and Kleinebudde, 2018b).

2 Aims and Outline

The roll compaction/dry granulation process has grown in importance in the production of solid dosage forms containing heat- or moisture-sensitive excipients or APIs. Nevertheless, the available amount of the often expensive NCEs is limited in the early phase of the formulation development. To overcome these issues, the aim of this work is the development of a time and material saving method for the mimicking and simulation of the roll compaction process on a uniaxial compaction simulator.

The elastic recovery of ribblets after compaction is investigated selecting materials with different deformation and compaction behaviours. The dependence of the elastic recovery on the compression pressure and speed as well as on the mimicked gap width is evaluated. One challenge is to implement the elastic recovery of the compacts, which takes place inside and outside the die, into the model and thus to optimise the prediction accuracy for the ribbon solid fraction.

Furthermore, a deeper understanding of the roll compaction process should be gained. A method to estimate the nip angle in dependence of the material properties, the specific compaction force, the roll speed and the gap width is developed and implemented to the simulation software.

To investigate the influence of the machine design, four roll compactors with rolls of different dimensions (diameter and width) as well as of different feeding systems are selected for comparison. The influence of the arrangement of the rolls and their surface are also considered. In addition, the usefulness of the parameter specific compaction force for the roll compaction process is critically assessed.

Finally, the whole downstream process - from the preparation of the powder blend, through roll compaction and granulation to tableting - is to be mimicked and compared with roll compaction/dry granulation by evaluating the properties of ribbons, ribblets, granules and tablets.

3 Results and Discussion

3.1 Insights to Roll Compaction and Kp Factor Determination for Hybrid Modelling[1]

3.1.1 Introduction and Objectives

The simulation of the roll compaction process is a beneficial step in formulation and process development. The hybrid modelling approach, which is evaluated and further developed in the present thesis, can be classified as an experimental approach, combining uniaxial tableting experiments with model calculations and is based on the thin layer model (Peter et al., 2010).

The key element of the hybrid modelling approach is the R&D tablet press Styl'One Evolution (Medelpharm) and its software Analis. Equipped with high-precision displacement and force transducers, the Styl'One is able to simulate and analyse tableting processes and can produce tablets equivalent to those from industrial scale tablet presses (Medelpharm, 2020). In the present case, however, the Styl'One is used to mimic the roll compaction process. Since the hybrid modelling approach is not particularly elaborate in terms of experimental effort, it could be a simple method to predefine the required process parameters for roll compaction with only a small amount of material. It is not known whether the hybrid modelling approach is universally applicable for different materials, process parameters and types of compactors. For the present thesis four compactors were chosen for the evaluation of the model: Mini-Pactor (Gerteis Maschinen + Processengineering AG), BRC25 (LB Bohle Maschinen und Verfahren GmbH), WP120 and WP200 (Alexanderwerk AG).

The hybrid modelling approach can be divided into two parts – one is the mechanical mimicking of the roll compaction process on a uniaxial compaction simulator (Styl'One Evolution, Medelpharm). Figure 3.1-1 illustrates the simulation/mimicking schematically and shows the respective correspondences of roll compactor (exemplarily for the Gerteis Mini-Pactor) and tablet press. The surface of the rectangular (10 mm x 20 mm) flat faced punches represents the mimicked roll surface. The punch movement, which has a rounded profile imitating the rolls, corresponds to the roll diameter and roll speed (Zinchuk et al., 2004). The minimum distance between the upper and the lower punch during compression corresponds to the gap width.

[1] Parts of this chapter were published in the article **Reimer, H. L. and P. Kleinebudde,** 2019. Hybrid Modeling of Roll Compaction Processes with the Styl'One Evolution. Powder Technology 341, 66-74.

The second part of the hybrid modelling approach is the mathematical calculation, which converts the compression pressure used on the Styl'One Evolution into the corresponding specific compaction force on the simulated roll compactor. Ribbon solid fraction is a result of the material properties and the chosen process parameters. The solid fraction was defined as the critical quality attribute to compare the ribbons with the compacts produced on the Styl'One – called ribblets (a combination of the words ribbon and tablet). Provided that the mimicking was correct, the ribblets produced on the Styl'One should have the same mean solid fraction as the ribbons of the roll compactor.

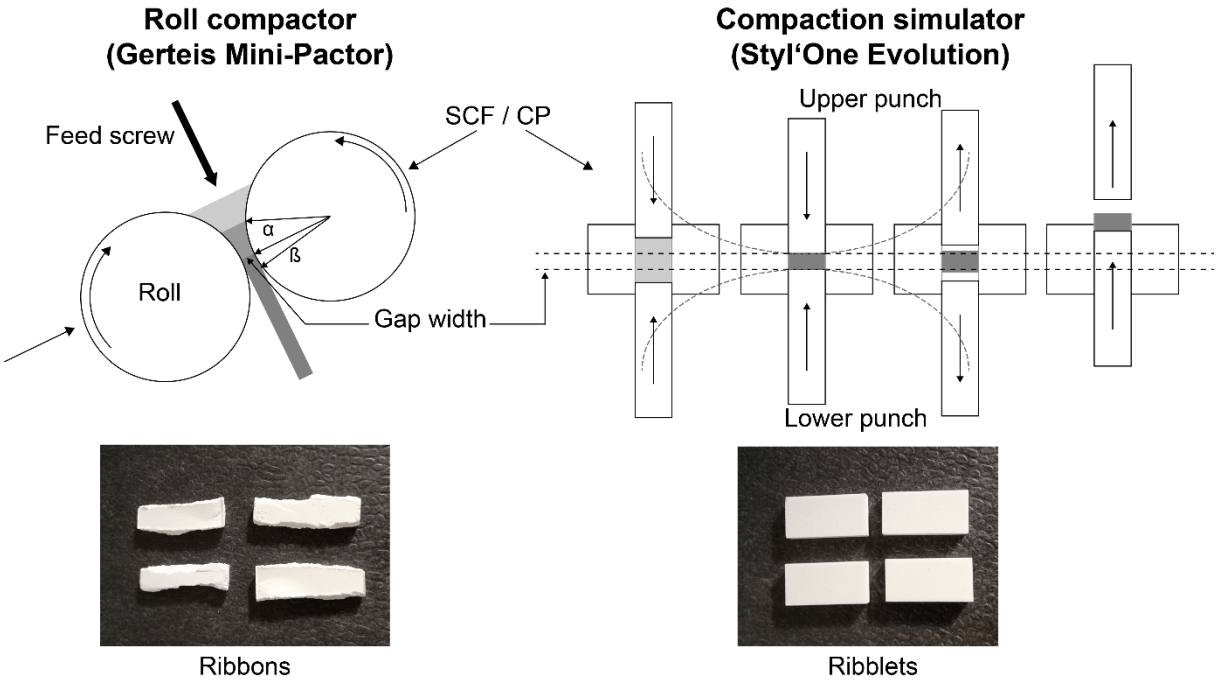

Figure 3.1-1: Hybrid modelling approach, SCF: specific compaction force, CP: compression pressure, α: nip angle, β: relaxation angle

In the following, the calculations behind the hybrid modelling approach are explained, which are performed automatically by the software of the Styl'One Evolution.

At first, a relationship between the density of each layer and the corresponding pressure must be found by the uniaxial tableting experiments. In theory, the powder between the rolls is divided to infinitely small layers (Figure 3.1-2). The layers are of constant weight, have a defined width, which corresponds to the roll width *w*, and a constant height. Only the layer length differs depending on the layer position between the rolls. Since all layers have the same weight, width and height, the density of the powder layer depends only on its length. In practice, on the Styl'One one layer is defined as the difference between two acquisition points. The density of each layer increases during the compaction process approaching the minimum distance between the rolls. The quotient of the distance between the rolls at

the nip angle (T_{nip}) and the gap width (T_{gap}) is called the compression coefficient (CC) and characterises the degree of powder densification (Keizer and Kleinebudde, 2020). This ratio is equivalent to the ratio between the layer density at the gap width (ρ_{gap}) and the layer density at the nip angle (ρ_{nip}) as displayed in equation (2).

$$CC = \frac{T_{nip}}{T_{gap}} = \frac{\rho_{gap}}{\rho_{nip}} = \frac{T_{gap} + D \times \left(1 - \cos \alpha_{nip}\right)}{T_{gap}} \quad (2)$$

After the powder has passed the minimum gap width, each layer exerts a force on the rolls due to the elastic recovery of the material.

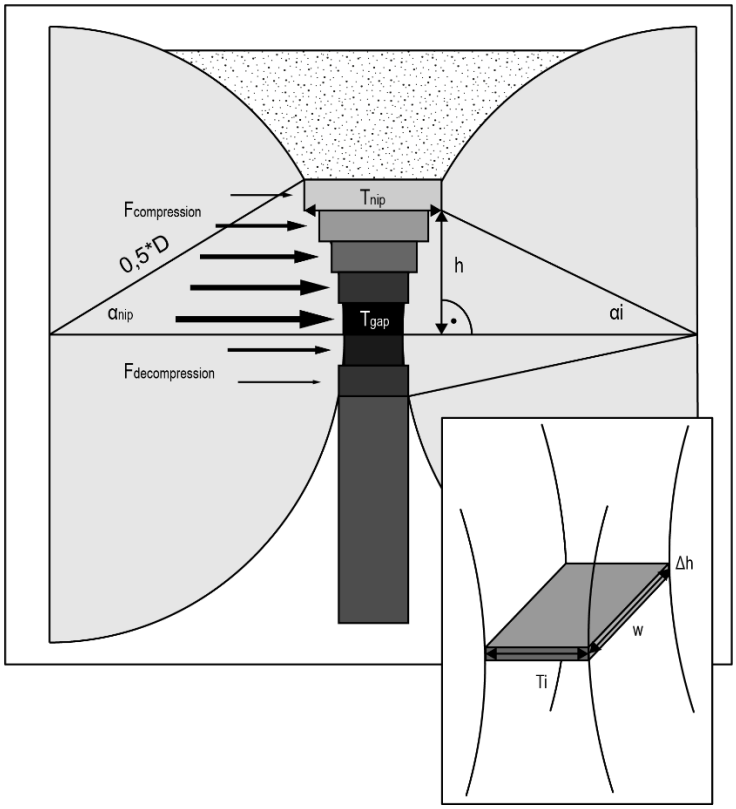

Figure 3.1-2: Thin layer model (modified after Peter et al. (2010). D: roll diameter, w: roll width, Δh: layer hight, T_{nip}: layer length at nip angle, T_{gap}: layer length at gap width, T_i: layer length at position i, α_{nip}: nip angle, α_i: angle at position i

For the conversion of the compression pressure into the specific compaction force, all forces exerted during the compression as well as during the decompression phase must be integrated.

The total compaction force is calculated by integrating the product of roll pressure and roll surface within the limits of the nip angle α_{nip} and the relaxation angle β, as shown in equation (3).

$$CF = \iint_{\alpha_{nip}}^{\beta} P \times \partial S \tag{3}$$

where P is the pressure in MPa. S is the surface of the roll, which can be decomposed into the roll circumference and the roll width. This integral is converted to cylindrical coordinates (equation (4)):

$$CF = \iint_{\alpha_{nip}}^{\beta} P(\alpha) \times R \times \cos\alpha \times d\alpha \times dw \tag{4}$$

where R is the radius of the roll, α represents a certain angle on the roll and $P(\alpha)$ is the pressure at an angle α. The repartition of the pressure over the roll width w is assumed constant. Other assumptions are, that there is no fluctuation on the densification, no impact from the feeding system and no powder recirculation. The roll width w is combined with the total compaction force (equation (5))

$$\frac{CF}{w} = \int_{\alpha_{nip}}^{\beta} P(\alpha) \times R \times \cos\alpha \times d\alpha \tag{5}$$

and therefore, the specific compaction force SCF [kN/cm] is calculated as shown in equation (6).

$$SCF = \int_{\alpha_{nip}}^{\beta} P(\alpha) \times R \times \cos\alpha \times d\alpha \tag{6}$$

Since the radius is equal to the diameter D divided by two, this results finally in equation (7).

$$SCF = \frac{D}{2} \times \int_{\alpha_{nip}}^{\beta} P(\alpha) \times \cos\alpha \times d\alpha \tag{7}$$

The theoretical calculation of the specific compaction force shown in equation (7) is now adapted to the acquisition data from the uniaxial tableting experiments on the Styl'One. While infinitesimal small layers are assumed in the theoretical calculation, the difference between two consecutive punch displacement points is now considered as one layer. The integral is replaced by the sum of the product of the average pressure at an angle α, the $cos\ \alpha$ and the delta of α obtained by the displacement between two points within the limits of the deaeration thickness T_{nip} and the elastic recovery thickness T_{ER} as can be seen in equation (8).

$$SCF = \frac{D}{2} \times \sum_{T_{nip}}^{T_{ER}} P(\alpha) \times \cos\alpha \times d\alpha \quad (8)$$

The deaeration thickness T_{nip} is the powder bed thickness at which a first significant increase in force is detected by the force sensors of the Styl'One. The elastic recovery thickness T_{ER} is the powder bed thickness at the upper punch position when the force decreases to zero in the upward movement after compression. This approximate integration is performed with the trapezoidal rule. To put it visually, the $P(\alpha)$ is put on the ordinate and the $\cos\alpha \times d\alpha$ on the abscissa of a coordinate system. Depending on the used material and the acquisition frequency, approximately at least 1000 data points are acquired for the compression phase and approximately another 500 for the decompression phase. This number of acquisition points is sufficiently high to neglect the non-linear response of the pressure.

The cos α is calculated as described below in equation (9).

$$\cos\alpha = 1 + \frac{(T_{gap} - T_{\alpha})}{D} \quad (9)$$

where T_{gap} is the minimum thickness corrected by the punch deformation, T_{α} the thickness at an angle α and D the radius of the roll.

The $d\alpha$ is obtained by forming the difference between the arccos at an angle α and the arccos at α+1, as described in equation (10).

$$d\alpha = \cos^{-1}\left(1 + \frac{(T_{gap} - T_{\alpha+1})}{D}\right) - \cos^{-1}\left(1 + \frac{(T_{gap} - T_{\alpha})}{D}\right) \quad (10)$$

After calculating the specific compaction force according to the formulae shown above, a correction factor (Kp factor) must be applied, which is determined experimentally. This is described in the following sections (3.1.2 - 3.1.5) for the roll compactor of interest. In summarised form, the practical calculation of the specific compaction force results in equation (11).

$$SCF\left[\frac{kN}{cm}\right] = \frac{\sum_{T_{nip}}^{T_{ER}}(P_{\alpha} \times \cos\alpha \times d\alpha)}{2 \times Kp} \times 0.01 \times D \quad (11)$$

It must be noted that the sign is reversed between the ascending and the descending phases, if one is looking at the data from acquisition point to acquisition point. For the compression phase, the thickness of the powder bed decreases more and more from the starting point until the minimum distance is reached. Since in the decompression phase the thickness increases again when starting from minimum thickness until the elastic recovery thickness is reached, one must revert sign at the end of the calculation

for the decompression phase. It was shown above, that tableting experiments allow to build a relationship between the compression pressure on the uniaxial compaction simulator and the specific compaction force on the mimicked roll compactor.

The thin-layer-model works with the “at gap” ribbon density and a throughput method (Peter et al., 2010). In contrast, the hybrid modelling approach shall consider not only the forces during the elastic recovery process but also the volume expansion and connected to that the changing ribbon and ribblet relative density. The consideration of the elastic recovery was part of the model development in the present thesis and is further discussed in the results section 3.2. It is evident that simulation and mimicking on a uniaxial compaction simulator, like it is done in the hybrid modelling approach, cannot cover all important parameters of the roll compaction process. This includes the feeding system, the inhomogeneous density distribution within the ribbons due to powder velocity gradients and powder feeding patterns due to the rotational movement of the screw and the fraction of fines. The influence of the sealing system on the ribbon properties is also not considered by the model. Nevertheless, Zinchuk et al. (2004) have hypothesised that real and simulated ribbons with the same tensile strengths have the same mechanical properties decisive for the subsequent milling step. It was found that the tensile strengths for real and simulated ribbons with the same solid fraction are equivalent. Furthermore, they concluded that the shear forces occurring during roll compaction but not in die compression do not lead to relevant differences in the mechanical properties.

Figure 3.1-3 illustrates schematically the dependence of the ribbon or ribblet solid fraction on the specific compaction force. The solid curve represents the ribbon solid fraction in dependence of the specific compaction force, whereas the dashed curve shows the ribblet solid fraction in dependence of the simulated specific compaction force. On the left side of the figure, the curves of simulated and actual specific compaction force deviate systematically from each other. In this case, setting the same specific compaction force on the roll compactor and on the compaction simulator would result in compacts with different solid fractions. By adjusting the simulated specific compaction force for the Styl’One using the so called Kp correction factor, the two curves overlap each other, as shown on the right side of the figure. In this case, ribbons and ribblets would show the same solid fraction if the same specific compaction force is set on the roll compactor and on the Styl’One.

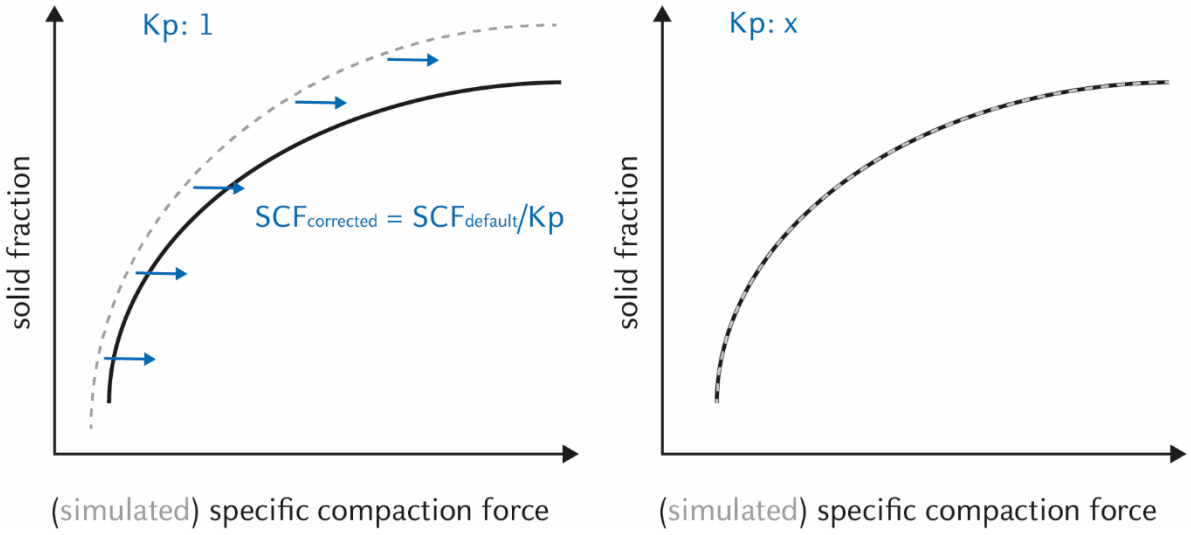

Figure 3.1-3: Visual Kp-factor determination (left: default Kp factor of 1, right: adapted Kp factor); schematical dependence of the ribbon/ribblet solid fraction on the (simulated) specific compaction force; dashed lines: simulated

This leads to several questions: Is there a universal Kp factor for all types of roll compactors and is the Kp factor valid for all types of material? Or in the other extreme, might it be necessary to determine a Kp factor for each material and roll compactor individually? To answer these questions, the Kp correction factor shall be experimentally determined for four roll compactors differing in their machine design, using a wide range of process parameters and several materials differing in their compression behaviour. The advantages and limitations of the hybrid modelling approach shall be demonstrated. Additionally, the influence of roll compactor design and the process parameters on the ribbon solid fraction shall be investigated to extend the understanding of the roll compaction process and to show possible limitations of the process.

3.1.2 Gerteis Mini-Pactor

3.1.2.1 Roll Compaction with the Gerteis Mini-Pactor

Roll compaction of three pure excipients – MCC, lactose and DCPA - was performed on the Gerteis Mini-Pactor. The roll compaction experiments were created using the design of experiment concept (section 5.2.1). The full-factorial multilevel experimental designs are displayed in Table 3.1-1. The influence of two factors, gap width and specific compaction force, on the ribbon solid fraction was evaluated. The factor gap width was investigated at two levels, 2 and 4 mm. The specific compaction force was tested at several levels from 3 up to 18 k/cm to gain a more detailed understanding of its effect on the ribbon solid fraction. The centre point, which is repeated three times, was used to check the reproducibility of the process settings.

Table 3.1-1: Full-factorial multilevel experimental plan for roll compaction of MCC, lactose and DCPA on the Gerteis Mini-Pactor

Material	Gap width [mm]	Specific compaction force [kN/cm]
MCC	2	3, 3.5, 4, 4.5, 5, 6, 7, 8, 9, 10, 11, 12, 14, 16, 18
	3 (centre point)	9
	4	3, 3.5, 4, 4.5, 5, 6, 7, 8, 9, 10, 11, 12, 14, 16, 18
Lactose	2	5, 6, 7, 8, 9, 10, 11, 12, 13, 14, 15
	3 (centre point)	10
	4	5, 6, 7, 8, 9, 10, 11, 12, 13, 14, 15
DCPA	2	5, 7, 9, 11, 13, 15, 17
	3 (centre point)	11
	4	5, 7, 9, 11, 13, 15, 17

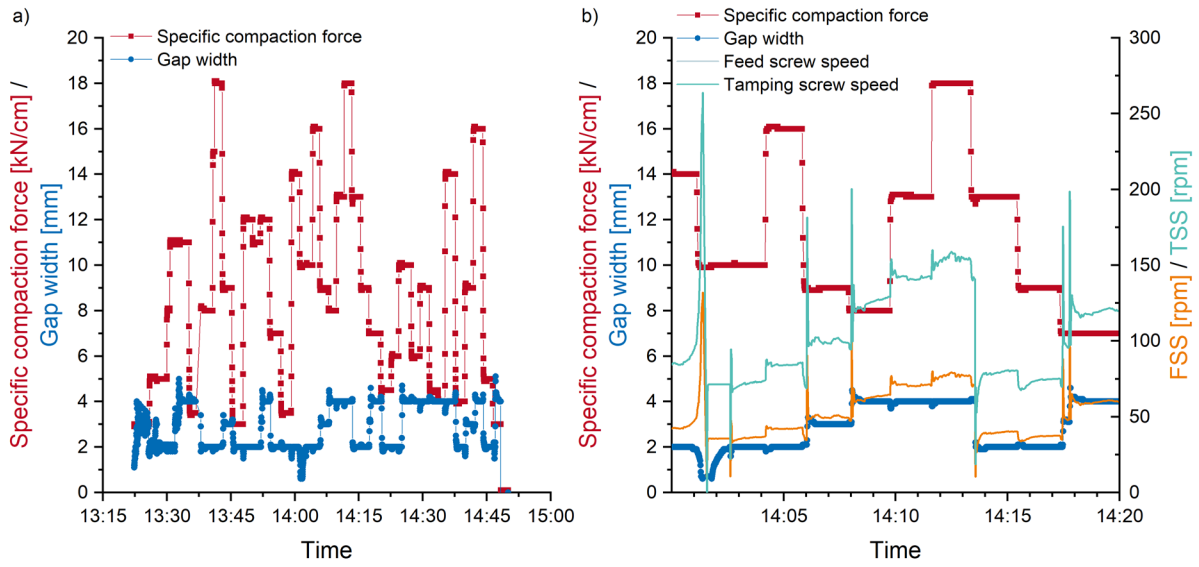

Figure 3.1-4: Process data of MCC roll compaction on the Mini-Pactor; a) overview of the process, b) detailed view of the process including the feeding (FSS) and tamping screw speeds (TSS); acquisition frequency: 1 Hz

The roll compactor was equipped with smooth rolls and a rim roll sealing system (section 5.2.4). Figure 3.1-4 a) shows an overview of the process parameters specific compaction force and gap width over the time. The roll compactor adapted quickly to every change in gap width and specific compaction force.

All settings of the experimental plan could be executed. The gap width and the specific compaction force were kept constant over the sampling periods of one minute (Figure 3.1-4 b). The powder is conveyed to the rolls via two screws, a feeding screw and a tamping screw. The ratio of tamping to feeding screw speed was 2:1. The detailed view shows the reaction of feeding and tamping screw to the changes in process settings. The screw speeds increase with an increasing gap width, e.g., from 3 to 4 mm (14:08 min). The screw speeds increase as well with an increasing specific compaction force, which can be observed when the force increases from 8 kN/cm to 13 kN/cm and from 13 kN/cm to 18 kN/cm (14:10-14:12 min). When the gap width or the specific compaction force are enlarged or reduced, the screws initially over- or under-steer until they settle to a constant speed. This phenomenon is more pronounced for changes in the gap width than for changes in the specific compaction force. The roll compaction results in ribbons with a length between approximately 0.5 and 1 cm (Figure 3.1-5). The ribbon width mostly corresponds to the width of the rolls (2.5 cm).

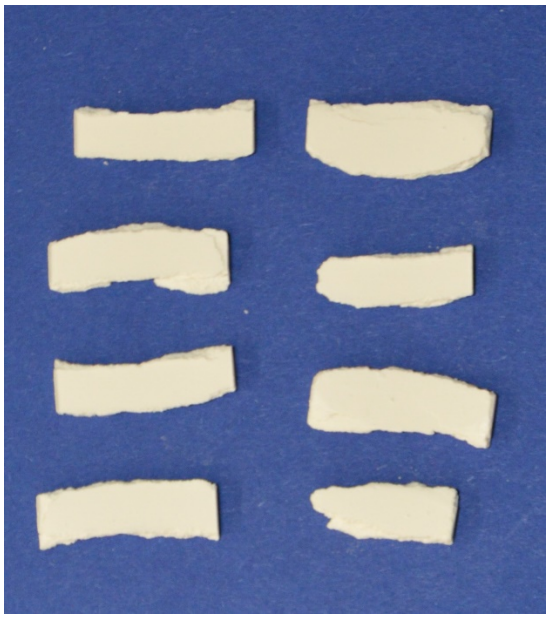

Figure 3.1-5: MCC ribbons produced at 5 kN/cm and 2 mm GW with the Mini-Pactor

In Figure 3.1-6 the roll compaction process of lactose is presented. Figure 3.1-6 a gives and overview of the whole process. All settings, which were planned in the experimental design, could be realised. However, compared to the roll compaction process with MCC, lactose caused some issues. The lactose ribbons were generally smaller than the MCC ribbons and the fragments did not have the full roll width. The compactor had difficulties to keep the gap width constant as can be seen in Figure 3.1-6 b. The feed and tamping screw speeds at higher forces and smaller gap widths fluctuated more than at small forces and bigger gap widths. The higher fluctuations are a result of powder sticking on the rolls since the

powder layers on the roll surface reduced the gap width. The powder layer was not covering the entire roll surface. Therefore, the feed screw compensated for the seemingly fluctuating gap width by constantly adjusting the speed. The thin powder layer affected the 2 mm gap width more than the 4 mm gap width. Due to the sticking on the rolls, parts of the powder were probably compacted several times, which could affect the ribbon solid fraction. It is reported in literature that internal and external lubrication can be used to prevent powder sticking on the rolls. However, adding magnesium stearate to the powder can alter the compaction behaviour and that external lubrication of the rolls can change the compaction process regarding nip angle and maximum roll pressure (Miguelez-Moran et al., 2008, Yu et al., 2013). Since the behaviour of the pure material was to be tested and the material properties should not be altered, no lubricants were used. Despite the powder sticking, it was possible to produce lactose ribbons of acceptable quality for further analysis.

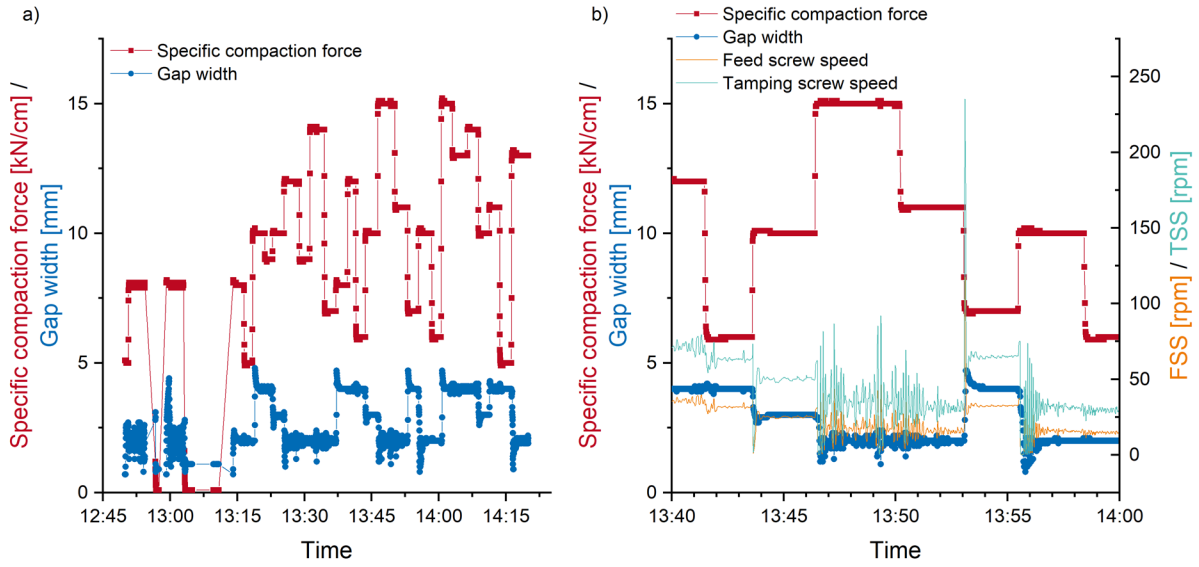

Figure 3.1-6: Process data of lactose roll compaction on the Mini-Pactor; a) overview of the process, b) detailed view of the process, including feeding (FSS) and tamping screw speeds (TSS); acquisition frequency: 1 Hz

Figure 3.1-7 a gives an overview of the roll compaction process for DCPA and shows the evaluation of specific compaction force and gap width over time. The Mini-Pactor adjusted quickly within seconds to every new setting. The gap width and the specific compaction force were kept constant over the sampling periods. Even big changes in gap width and force at the same time (11:22) from 2 mm to 4 mm and from 7 kN/cm to 17 kN/cm were smoothly performed. As observed for MCC and lactose, the screw speeds initially overreacted when the gap width and the specific compaction force were increased (Figure 3.1-7 b), before a constant level was reached. The produced DCPA ribbons were fragile and

irregular shaped small fragments were obtained. This behaviour was also observed for other brittle materials like mannitol (Perez-Gandarillas et al., 2016).

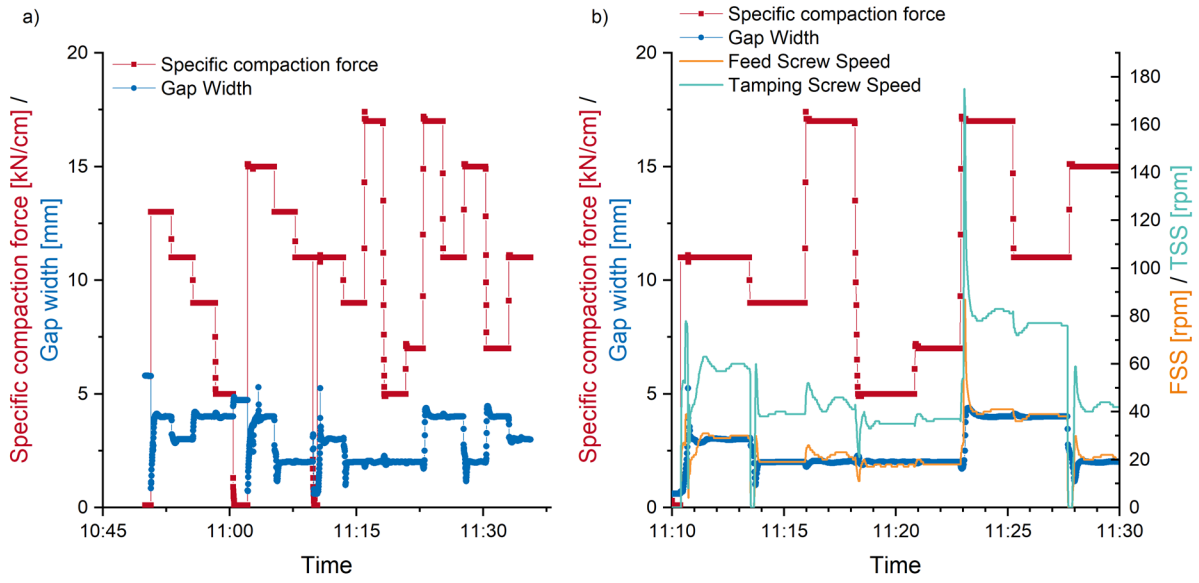

Figure 3.1-7: Process data of DCPA roll compaction on the Mini-Pactor; a) overview of the process, b) detailed view of the process, including feeding (FSS) and tamping screw speeds (TSS); acquisition frequency: 1 Hz

The produced MCC, lactose and DCPA ribbons were analysed regarding their solid fraction, which was measured by powder pycnometry (section 5.2.10.1). The powder density of the raw materials, which is needed to calculate the ribbon solid fraction, was measured by helium pycnometry (section 5.2.9.5). The powder densities of MCC, lactose and DCPA are listed in Table 3.1-2.

Table 3.1-2: Powder density of MCC, lactose and DCPA for roll compaction experiments with Gerteis Mini-Pactor; n = 3, mean ± SD

Material	**Powder density [g/cm³]**
MCC	1.5517 ± 0.0029
Lactose	1.5014 ± 0.0023
DCPA	2.8555 ± 0.0090

Figure 3.1-8 shows the relation between the specific compaction force and the ribbon solid fraction at gap widths of 2 mm and 4 mm and the centre points at 3 mm. The solid fraction raises with an increasing specific compaction force for the three tested materials. The changes in solid fraction are higher at small specific compaction forces. The curves flatten at higher specific compaction forces, which was observed

as well by Hancock et al. (2001). The relationship between specific compaction force and solid fraction can be described by a logarithmic function (Equation (12)).

$$y = a - b \times \ln(x + c) \tag{12}$$

$$y' = -\frac{b}{x + c} \tag{13}$$

where y is the ribbon solid fraction and x the specific compaction force. a is the y-axis intercept. b and c determine the slope of the curve, which varies depending on the x-value as displayed in the first derivative (Equation (13)). The coefficient of determination was > 0.96 for all fits shown in Figure 3.1-8.

The solid fraction of ribbons produced at a small gap width is higher than the solid fraction of ribbons which were produced at bigger gap widths. At a gap width of 4 mm, more powder is densified between the rolls compared to the 2 mm gap width. Since the specific compaction force was the same for both gap widths, but the amount of powder was smaller at a small gap width, the powder was densified to a higher extent.

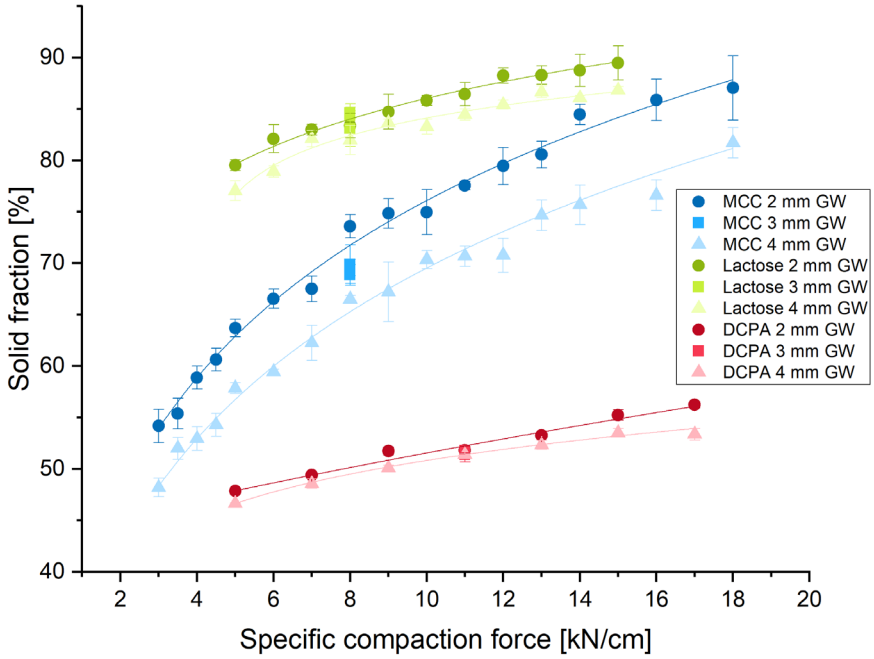

Figure 3.1-8: Solid fraction of MCC, lactose and DCPA ribbons in dependence on the specific compaction force (SCF) and the gap width (GW); Mini-Pactor; n=3, mean ± SD

Lactose ribbons had the highest solid fractions, followed by MCC ribbons. The DCPA ribbons showed the lowest solid fractions of the tested materials. The difference in solid fraction may be related to the material characteristics and their compaction behaviour. The used lactose is a spray-agglomerated alpha-lactose monohydrate. The primary particles of the agglomerated powder tend to break more easily into

smaller fragments. These small fragments create bigger bonding areas and can fill the gaps between the particles (Omar et al., 2015). The increased bonding area and the interlocking lead to lactose ribbons with higher solid fractions compared to MCC and DCPA. The used DCPA grade is an agglomerate with increased porosity. The resulting ribbons show a comparably small solid fraction, confirming findings from literature (Grote and Kleinebudde, 2018). The solid fraction of MCC ribbons is stronger affected by changes in the specific compaction force than lactose and DCPA ribbons. In a similar range of specific compaction forces, the solid fraction of MCC ribbons increases by appr. 40 percentage points, whereas the increase in solid fraction for lactose and DCPA ribbons is only about 10 percentage points. MCC has a higher compressibility or in other words it has a higher ability to deform under pressure than lactose and DCPA.

The influence of specific compaction force and the gap width on the ribbon solid fraction was statistically evaluated. An excellent model was obtained for MCC with a R^2=0.985 and Q^2=0.981. In Figure 3.1-9 the coefficient plot for the solid fraction of MCC ribbons is depicted. The factors specific compaction force and gap width were significant. The specific compaction force has the biggest influence on the ribbon solid fraction. The positive effect confirms the findings depicted in Figure 3.1-8. Additionally, a significant negative quadratic effect of the specific compaction force was detected, which was also reported in literature (Souihi et al., 2013b). The effect of the gap width on the ribbon solid fraction is negative and smaller compared to the specific compaction force.

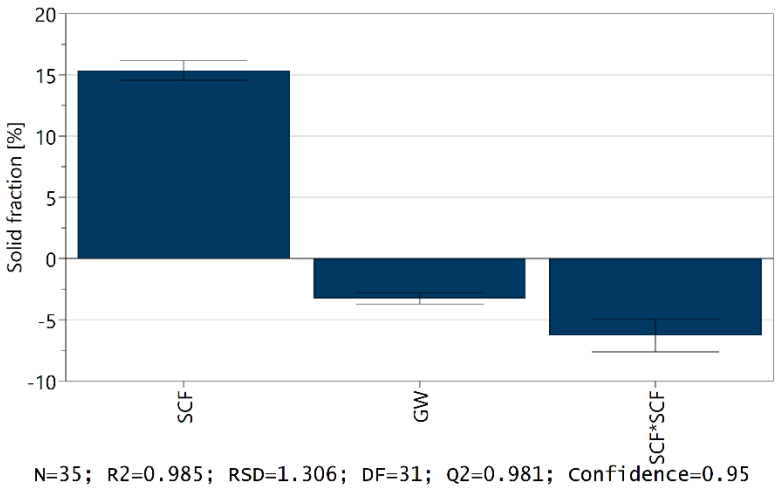

Figure 3.1-9: Coefficient plot for the effects of the specific compaction force (SCF) and the gap width (GW) on the solid fraction of MCC ribbons produced with the Mini-Pactor

The contour plot (Figure 3.1-10) visualises the negative quadratic effect of the specific compaction force on the solid fraction: The higher the specific compaction force, the smaller are the changes in the solid fraction.

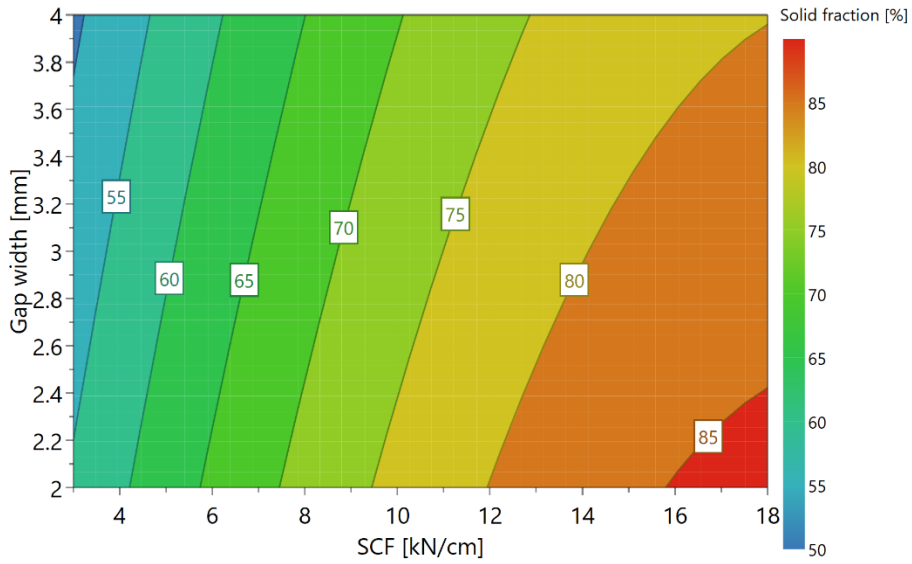

Figure 3.1-10: Contour plot for the solid fraction of MCC ribbons produced with the Mini-Pactor in dependence on the gap width (GW) and the specific compaction force (SCF)

For lactose, a good model was built with a R^2 of 0.955 and a Q^2 of 0.938. The coefficient plot for the solid fraction of lactose ribbons is shown in Figure 3.1-11. As observed with MCC, the specific compaction force has a significant positive and the gap width a significant negative effect on the ribbon solid fraction. The negative quadratic effect of the specific compaction force was observed as well. The extent of the effects on the solid fraction was smaller than it was for MCC.

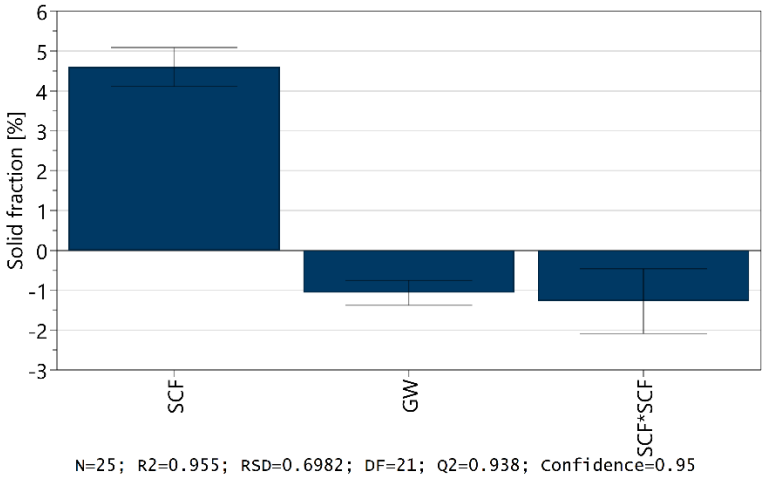

Figure 3.1-11: Coefficient plot for the effects of the specific compaction force (SCF) and the gap width (GW) on the solid fraction of lactose ribbons produced with the Mini-Pactor

Figure 3.1-12 shows the contour plot for the solid fraction of lactose ribbons and illustrates again the smaller influence of the factor specific compaction force on the solid fraction compared to MCC. The negative quadratic effect can be seen from the curved shape of the lines representing the same solid fraction.

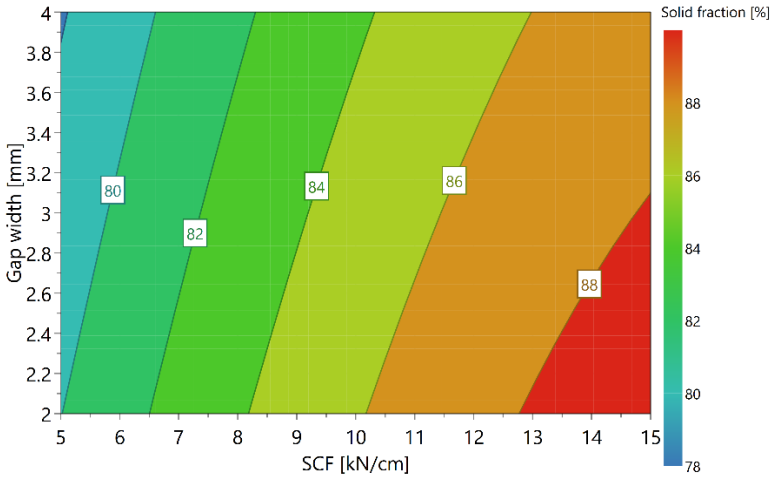

Figure 3.1-12: Contour plot for the solid fraction of lactose ribbons produced with the Mini-Pactor in dependence on the gap width (GW) and the specific compaction force (SCF)

For DCPA, the resulting model has good R^2 and Q^2 values of 0.969 and 0.934, respectively. The effect of the specific compaction force and the gap width on the solid fraction of DCPA ribbons is even smaller than for lactose ribbons, which is shown in the coefficient plot (Figure 3.1-13). Again, the specific compaction force has a significant positive effect and the gap width a significant negative one on the ribbon solid fraction. In the case of DCPA, the negative quadratic effect of the specific compaction force is not significant, but it is included in the model since it has a positive influence on the Q^2 value.

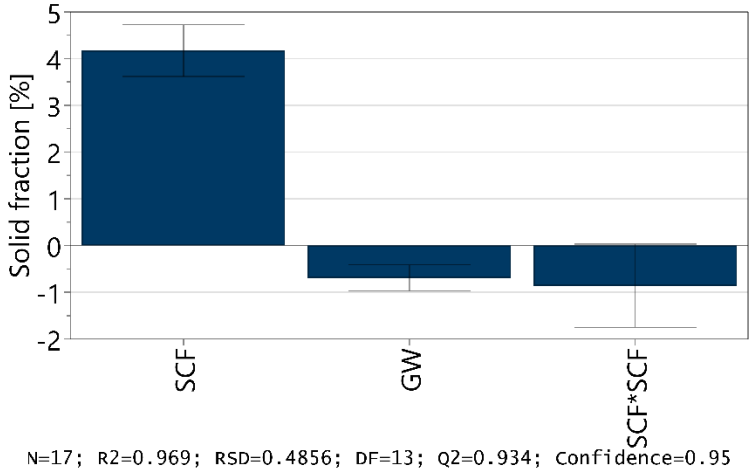

Figure 3.1-13: Coefficient plot for the effects of the specific compaction force (SCF) and the gap width (GW) on the solid fraction of DCPA ribbons produced with the Mini-Pactor

The contour plot (Figure 3.1-14) for DCPA underlines the observations made above. The isopycnes are less curved than for the other two investigated materials and the range of the ribbon solid fractions is smaller.

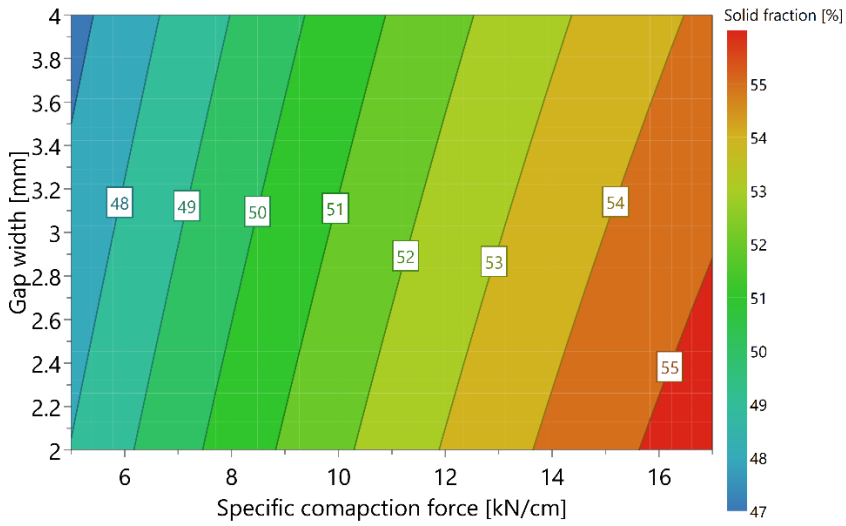

Figure 3.1-14: Contour plot for the solid fraction of DCPA ribbons produced with the Mini-Pactor in dependence on the gap width (GW) and the specific compaction force (SCF)

Overall, it was shown that roll compaction of MCC, lactose and DCPA was feasible on the Mini-Pactor in a wide range of process parameters. The influences of the process parameter specific compaction force and gap width on the critical quality attribute ribbon solid fraction were analysed and found to be significant. Models were built to describe these relationships for the three tested materials MCC, lactose and DCPA. The models have a R^2 of at least 0.955 and a Q^2 of at least 0.934, which underlines their high prediction quality.

3.1.2.2 Kp Factor Determination for the Gerteis Mini-Pactor

Solid Fraction Dependence on Specific Compaction Force

After the investigation of the roll compaction process itself with the Mini-Pactor, the roll compaction process was mimicked on the Styl'One. The procedure is described in detail in section 5.2.5.2. Figure 3.1-15 illustrates exemplarily the compression profile for DCPA, which is used to mimic the roll compaction on the Mini-Pactor. The mimicked specific compaction force was 9 kN/cm at a roll speed of 2 rpm and a gap width of 2 mm. The figure displays the punch displacement of upper and lower punch (solid lines), which mimic the roll speed as well as the roll diameter of the Mini-Pactor. The minimum distance between the punches represents the gap width, in this case 2 mm. The compression profile

(dashed lines) is similar to the profiles obtained by using a roll compactor with instrumented rolls (Bindhumadhavan et al., 2005, Nesarikar et al., 2012a).

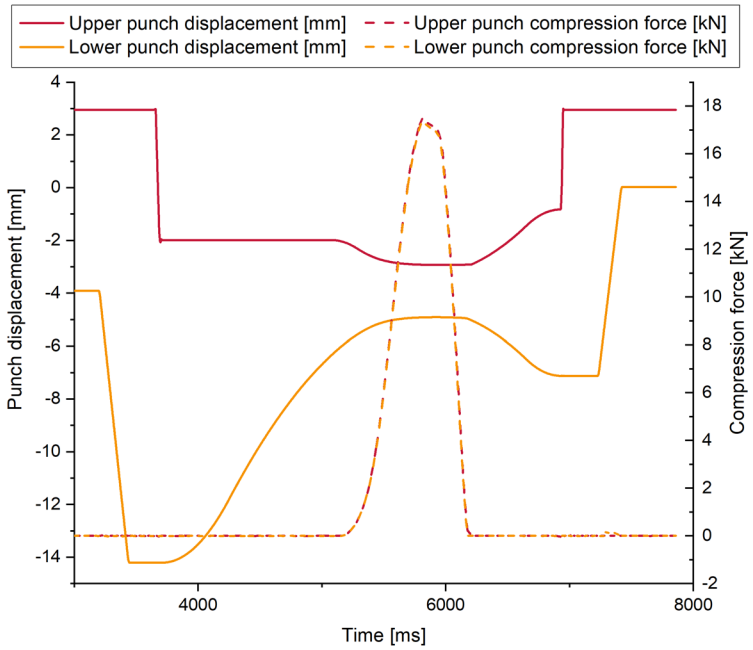

Figure 3.1-15 Punch displacement and compression force of one compression cycle mimicking the roll compaction process of the Mini-Pactor on the Styl'One; material: DCPA, simulated specific compaction force: 9 kN/cm, roll speed: 2 mm

As the punches approach each other in a rounded movement reminiscent of two rolls, the compression force starts to rise quickly. It reaches a maximum and decreases again rapidly as the punches separate and the ribblet is ejected, which is visible in a small peak in the lower punch compression force curve. The conversion from compression force on the Styl'One to the corresponding specific compaction force on the roll compactor is described in section 3.1.1.

The experimental plan for the production of ribblets was the same as that of the ribbons (Table 3.1-1). It must be considered that the Kp correction factor was not altered, but the default value of 1 was used to produce the ribblets. The goal was to produce ribblets of equal solid fraction as ribbons from roll compaction. The ribblets were analysed regarding their solid fraction by powder pycnometry (section 5.2.10.1). Figure 3.1-16 depicts the relation between (simulated) specific compaction force and the resulting ribbon/ribblet solid fraction for MCC and lactose. For the ribblet production, the same excipient batches were used as for roll compaction. The powder densities of the materials are listed in Table 3.1-2.

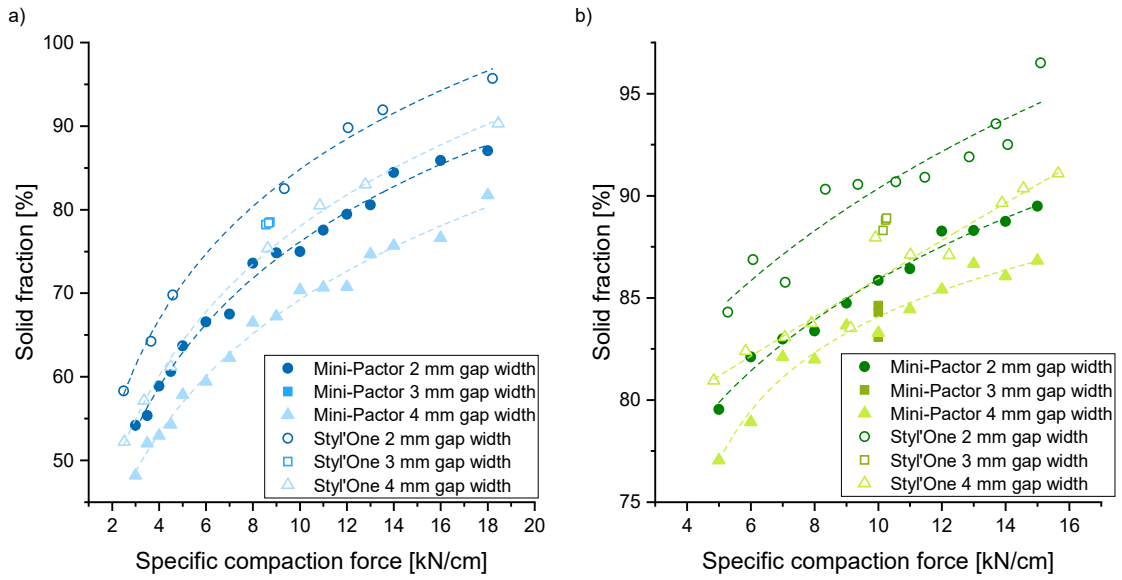

Figure 3.1-16: Solid fraction of ribbons and ribblets in dependence on the specific compaction force (SCF) and the gap width (GW) for a) MCC and b) lactose (Kp factor: 1); Mini-Pactor; n=3, mean

Similar curve shapes compared to the ribbons were obtained for the ribblets. In the Styl'One experiments, the same general relations as in roll compaction were observed between the solid fraction, the gap width and the specific compaction force. It is noticeable that the Styl'One produced ribblets with a systematically higher solid fraction than the Mini-Pactor at the same specific compaction force. The solid fraction of lactose ribblets ranged between 80 % and 96 % and the ribbon solid fraction between 77 % to 89 %. Equivalent results were observed for MCC – ribblet solid fraction from 52 % to 95 % but ribbon solid fraction from 48 % to 87 %. It can be assumed that similar compression pressures usually result in similar ribbon solid fractions (Bi et al., 2014). This indicates that the computed specific compaction force might not be correct, since the specific compaction force necessary to obtain a certain ribblet solid fraction is lower on the Styl'One than on the Mini-Pactor. Or to put it in another way: The Styl'One seems to overestimate the solid fraction resulting from a given specific compaction force. Hybrid modelling assumes constant powder transport between the rolls at a constant speed of the powder. However, it has been shown that velocity gradients and non-uniform powder transport exist during roll compaction (Muliadi et al., 2012). Shear and frictional forces during roll compaction may reduce the pressure, which is exerted on the powder, compared to powder compaction in a tablet press. Another difference is the feeding system – screw conveying in roll compaction and a force feed shoe in uniaxial compaction, which could cause another starting bulk density. These factors may lead to the observed overestimation of the ribblet solid fraction by the Styl'One at a certain specific compaction

force and it must be corrected for to obtain a correct correlation between the solid fraction and the simulated specific compaction force.

The curve form and the slopes of the specific compaction force-solid fraction relations for the Mini-Pactor and the Styl'One (Figure 3.1-16) are similar, but the curves of the ribblets seem to be equally shifted to the left compared to the ribbons. As described in section 5.2.5.2, the Kp factor was determined by adapting the default factor of 1 until the best visual match of the ribbon and ribblet curves was achieved for both materials. Finally, a common Kp correction factor for MCC and lactose of 0.667 was found.

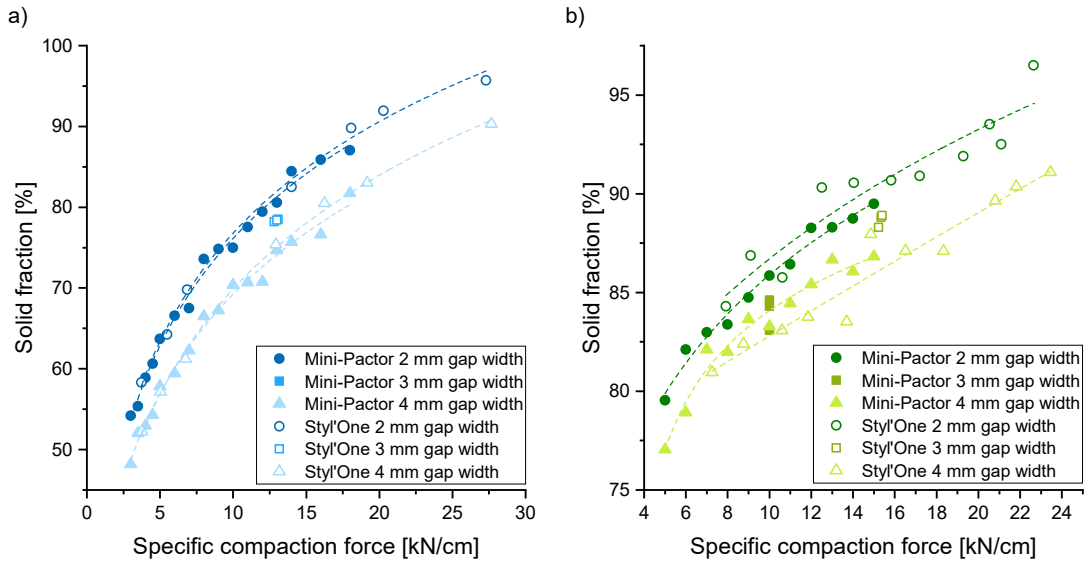

Figure 3.1-17: Solid fraction of ribbons and ribblets in dependence on the specific compaction force (SCF) and the gap width (GW) for a) MCC and b) lactose (Kp factor: 0.667); Mini-Pactor; n=3, mean

Figure 3.1-17 depicts the results which are obtained when the Kp factor of 0.667 is applied on the default computed specific compaction force. The shift caused by the Kp factor resulted in specific compaction forces higher than 20 kN/cm, which cannot be realised in practice. A good alignment between the ribbon and the ribblet results was achieved for MCC (Figure 3.1-17 a). The curves for ribbon and ribblet solid fraction overlap for both tested gap widths, so that it is possible to produce MCC ribblets with the same solid fraction as real ribbons. The alignment between ribbon and ribblet data was better for MCC than for lactose. This can be explained by issues during the production of lactose ribbons and ribblets. As described above, sticking occurred during roll compaction. During the compaction of the ribblets with the Styl'One, sticking on the punch surfaces was observed. This led to capping issues and probably had an influence on the internal ribblet structure. Regarding the higher discrepancies between ribbon and

ribblet curves, one must consider by contrast the smaller solid fraction range for lactose in the investigated specific compaction force region in comparison to MCC. Furthermore, the errors between lactose ribbon and ribblet solid fraction were generally small so that the match can be considered acceptable.

Since the same Kp factor was applicable to two materials with different compaction behaviour and physical properties, the hypothesis is made that the Kp correction factor is material independent. To test this hypothesis, a third excipient was investigated. The roll compaction of DCPA was mimicked on the Styl'One Evolution. Hereby, the Kp factor of 0.667, which was found for lactose and MCC, was set in the Styl'One software to produce the DCPA ribblets. An external magnesium stearate lubrication unit was used since DCPA tends to stick on the punches and has an abrasive effect. Figure 3.1-18 depicts the relation between specific compaction force and solid fraction for DCPA ribbons and ribblets. The ribbon solid fractions ranged between 46.6 % and 56.2 %, and the ribblet solid fractions between 46.7 % and 56.5 %. The ribbon and ribblet solid fractions for the 4 mm gap width overlap very well, whereas the results for the 2 mm gap width show larger differences. Due to the very flat curve, even small deviations in the y-values (solid fraction) lead to large deviations in the x-values (specific compaction force). However, the highest total error between ribbon and ribblet solid fraction was 2.5 %. This overall good agreement between the ribbon and the ribblet solid fractions supports the hypothesis that the Kp factor is a material and process parameter independent value within the studied design space.

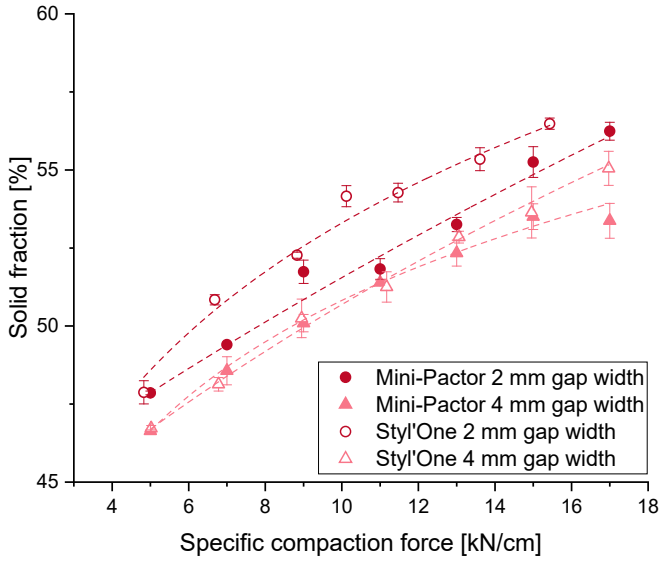

Figure 3.1-18: Solid fraction of DCPA ribbons and ribblets in dependence on the specific compaction force (SCF) and the gap width (GW) (Kp factor: 0.667); Mini-Pactor; n=3, mean ± SD

3.1.2.3 General interrelationships in roll compaction (simulation)

Dosage Height - Feed Screw Speed – Specific Compaction Force – Gap Width

The dosage height (section 5.2.5.1) is the equivalent on the Styl'One for the feed screw speed on the Mini-Pactor, since it determines the amount of powder which is compressed to a certain thickness or simulated gap width. Figure 3.1-19 illustrates the relationship between the specific compaction force, the feed screw speed and the dosage height for MCC, lactose and DCPA and illustrates the influence of the gap width as well.

The feed screw speed increases with an increasing specific compaction force at a constant gap width. If the same amount of material is compacted at a higher specific compaction force, this would result in a smaller gap width. Thus, to keep the gap width constant at an increasing specific compaction force, more material must be transported between the rolls. This is realised by an increase in the feed screw speed. This relationship can be transferred to mimicking of the roll compaction process on the Styl'One. The dosage height increases in the same extent as the feed screw speed does on the roll compactor.

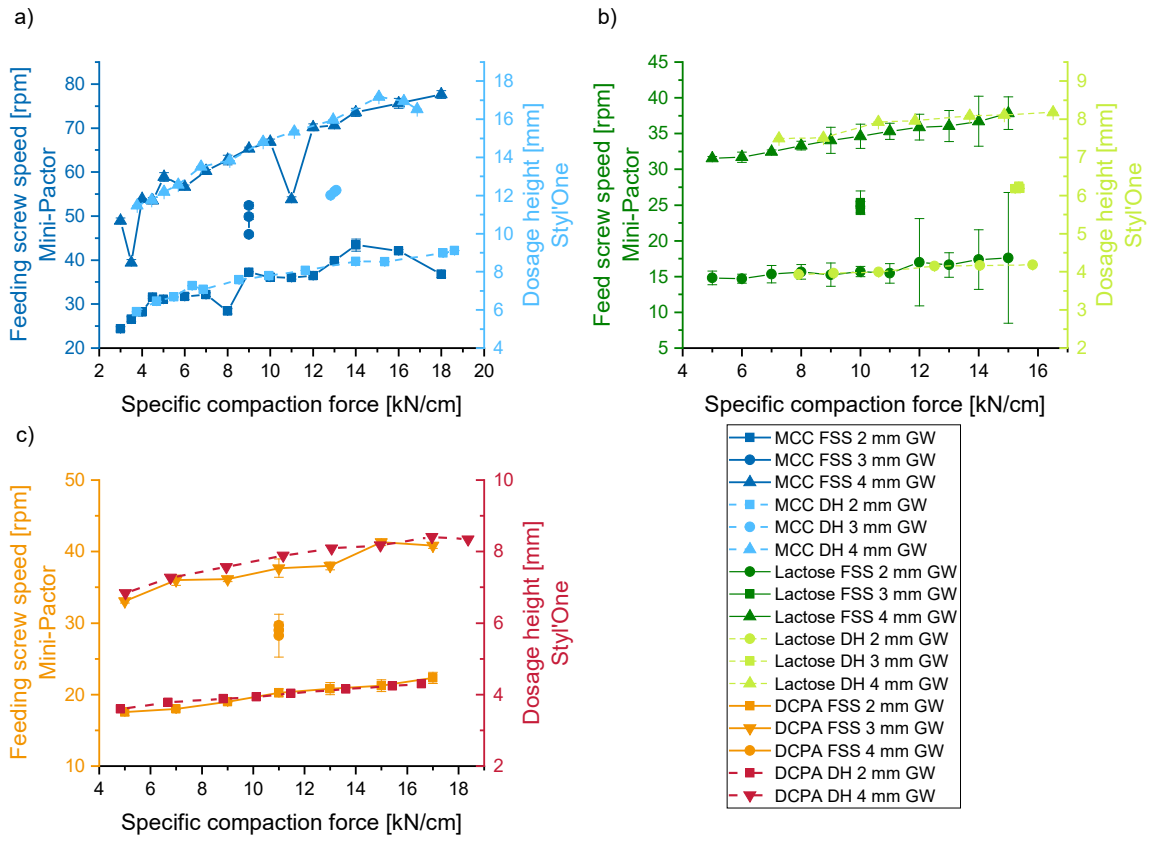

Figure 3.1-19: Correlation between the feeding screw speed (FSS) on the compactor, the dosage height (DH) on the Styl'One and the specific compaction force for a) MCC, b) lactose, c) DCPA; mean ± SD

The feed screw speed increases as well with an increasing gap width, when the specific compaction force is constant, since more material must be dragged between the rolls to fill a bigger gap width. The same trend is visible for the dosage height on the Styl'One: It increases by increasing the mimicked gap width. The feed screw speed and the dosage height are approximately doubled when the gap width is increased from 2 mm to 4 mm.

Comparing the different materials, it is noticeable that the absolute values for the feed screw speed and the dosage height of MCC are higher compared to DCPA and lactose. Furthermore, the increase in speed or dosage height per increase in specific compaction force is higher for MCC than for the other investigated materials. These observations can be explained by differences in the bulk volume and compressibility. MCC has a larger bulk volume than lactose and DCPA. The same mass of powder therefore takes up more space. Added to this is the better compressibility of MCC. As a result, the screw must rotate comparatively faster in order to transport enough powder between the rolls – and transferred to the uniaxial compaction, the dosage height must be higher.

Specific Compaction Force – Compression Pressure

The Styl'One creates a link between the specific compaction force on the roll compactor and the equivalent compression pressure for uniaxial compaction. Figure 3.1-20 depicts this relationship for MCC, lactose and DCPA. It must be mentioned that the compression pressure on the Styl'One might not be the exact same as the roll pressure on the Mini-Pactor. This might be linked to the higher shear stresses in roll compaction compared to uniaxial compaction (Cunningham, 2005). However, it is the compression pressure, which can be used to produce ribblets showing the same solid fraction as real ribbons. The compression pressure increases approximately linearly with an increasing specific compaction force. It should be emphasised that this relationship is material dependent. It differs in the absolute values and as well in the slope of the curves. A compression pressure of 100 MPa at a constant gap width of, e.g., 2 mm leads to a specific compaction force of 9 kN/cm for lactose but to 13.5 kN/cm for MCC and to 10.5 kN/cm for DCPA. And the other way, the same specific compaction force exerted on different materials results in different compression pressures.

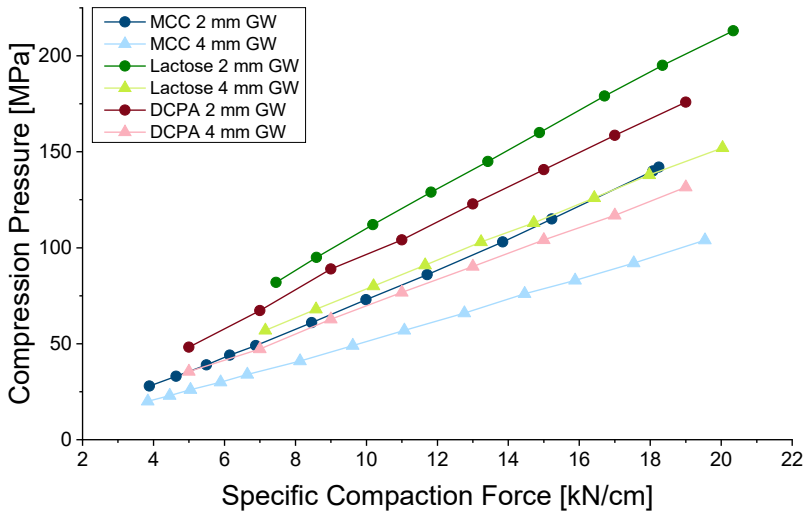

Figure 3.1-20: Compression pressure on the Styl'One in relation to the simulated specific compaction force (Mini-Pactor) for MCC, lactose and DCPA at different gap widths (GW); n ≥ 20, mean

Furthermore, the same specific compaction force at different gap widths leads to different compression pressures. The higher the gap width, the smaller is the resulting pressure on the Styl'One. It must be kept in mind that the dosage height is larger at a higher gap width (Figure 3.1-19). If one considers the reversed relation, a constant compression pressure results in higher specific compaction forces for larger gap widths. For example, 75 MPa compression pressure exerted on MCC result in 10 kN/cm at a 2 mm gap width and in 14 kN/cm at a gap width of 4 mm. These findings explain the observation from above that at a constant specific compaction force the solid fraction is smaller at higher gap widths (Figure 3.1-8). The found relationship between specific compaction force, gap width and compression pressure is in accordance with the findings of Bi et al. (2014). They stated that the maximum roll surface pressure is a result of the roll force and the roll gap. It was found that the pressure increases with an increasing roll force and decreases with an increasing roll gap. It was observed as well by Nesarikar et al. (2012b) that an increased screw speed to roll speed ratio (resulting in an increased gap width) at a constant hydraulic pressure results in a decreased normal stress and thus in ribbons with smaller solid fractions.

Dosage Height – Compression Coefficient – Specific Compaction Force/Compression Pressure

The compression coefficient is the ratio between the dosage height and the mimicked gap width and describes to which extent the powder bed was compacted. Figure 3.1-21 shows the dosage height and the compression coefficient in correlation to the simulated specific compaction force (a, c, e) and the compression pressure (b, d, f) for 2 mm and 4 mm gap widths for MCC, lactose and DCPA. As already mentioned above, the dosage height increases with increasing gap width and specific compaction force.

If the dosage height increases with an increasing specific compaction force at constant gap width, the compression coefficient increases as well with an increasing specific compaction force.

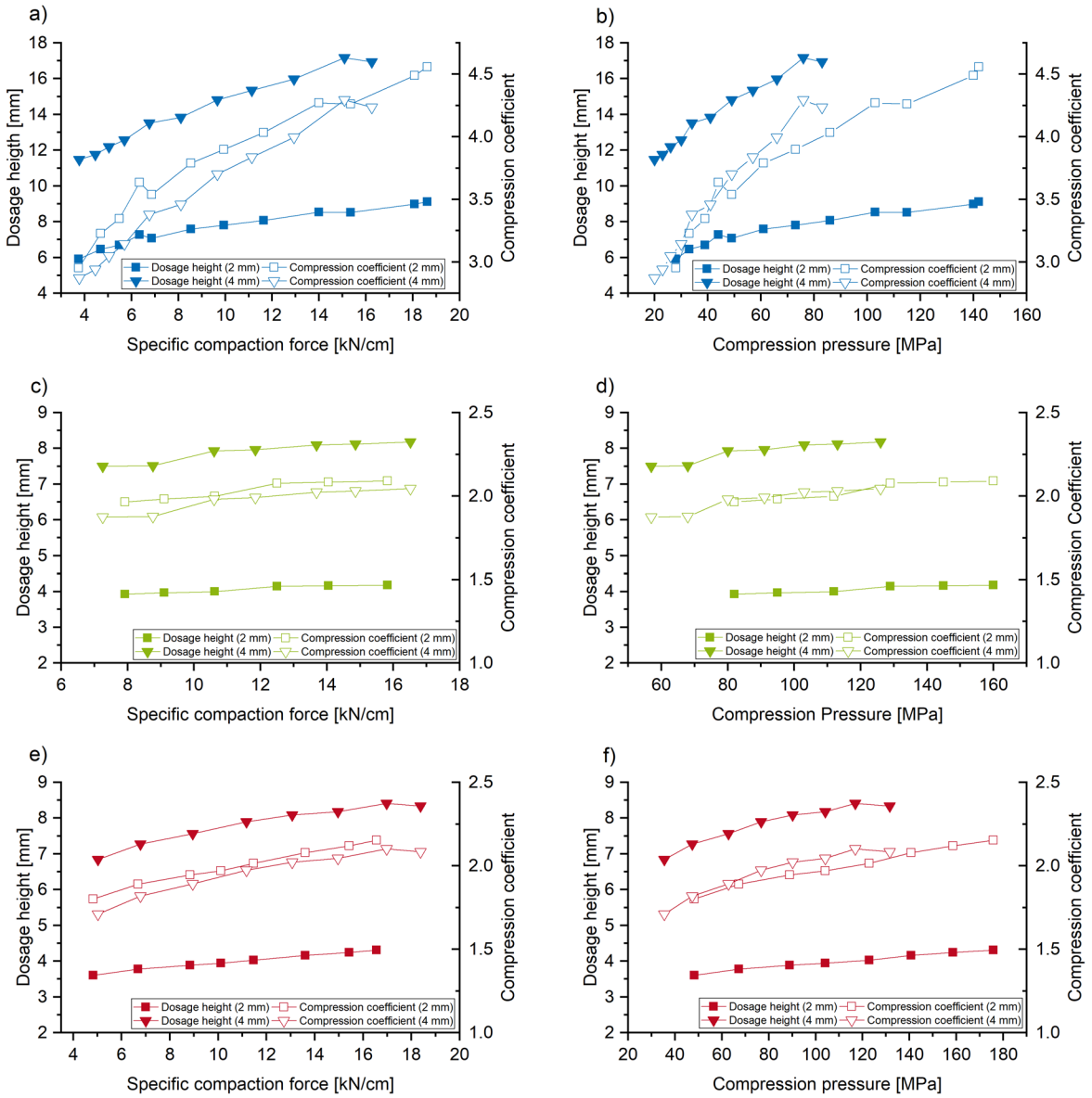

Figure 3.1-21: Compression coefficient and dosage height in dependence of the specific compaction force (a, c, e) and compression pressure (b, d, f) for MCC (a, b), lactose (c, d) and DCPA (e, f) at gap widths of 2 and 4 mm; $n \geq 20$; mean

The compression coefficients for MCC with values between 2.8 and 4.5 are higher than for lactose and DCPA whose compression coefficients range between 1.7 and 2.1. This is mainly due to the higher bulk volume of MCC and its better compressibility compared to the other two materials. Interestingly, the influence of the gap width on the compression coefficient varies between the investigated materials. For MCC, a distinction can be made between the coefficients at the 2 mm and the 4 mm gap width. For

lactose and DCPA, in contrast, the gap width seems to have less influence on the compression coefficient, meaning that the extent of compaction is similar for the 2 and the 4 mm gap width at the same specific compaction force. This may raise the question of why the gap width then influences the solid fraction of ribbons or ribblets. To answer the question conclusively, one must consider several factors which are discussed below.

Solid Fraction – Compression Pressure – Gap Width

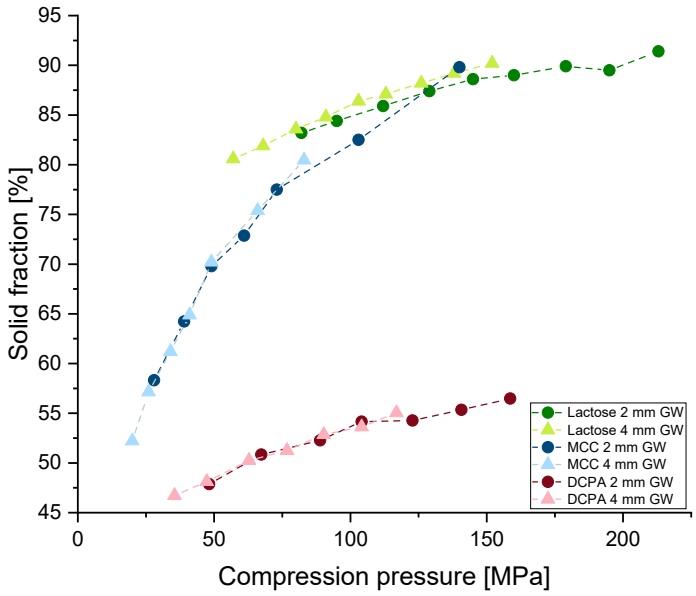

Figure 3.1-22: Correlation between the ribblet solid fraction and the compression pressure for MCC, lactose and DCPA; n = 3 (solid fraction), n ≥ 20 (compression pressure), mean

Figure 3.1-22 shows the correlation between the ribblet solid fraction and the compression pressure on the Styl'One. The solid fraction increases with an increasing compression pressure, like it was observed in the SCF-SF curves. The important difference is that an increase in gap width from 2 to 4 mm at the same compression pressure does not lead to a difference in the solid fraction, but the curves overlap each other. The higher frictional forces at a bigger (simulated) gap width do not seem to be strong enough to have an influence on the solid fraction.

Considering the findings from above, the following comprehensive context can be formulated exemplarily for MCC: A compression pressure of 75 MPa corresponds to a dosage height of approximately 16 mm at a 4 mm gap width and to a dosage height of approximately 8 mm at a 2 mm gap width. The extent of compression, expressed as compression coefficient, is in both cases 4. The resulting ribblet solid fraction is in both cases approximately 77 %, which corresponds to a specific compaction force of 14 kN/cm at a gap width of 4 mm and a specific compaction force of 10 kN/cm at

a 2 mm gap width (Figure 3.1-8). Generally spoken, it was found that for a pair of dosage height and gap width, which results in the same compression coefficient, the same compression pressure is applied, which in turn results in the same solid fraction. The corresponding specific compaction force to this compression pressure, however, is dependent on the gap width. This answers the question from above, why the gap width has an influence on the ribbon and ribblet solid fraction. Applying the same compression pressure on powder beds of different height will result in compacts with the same solid fraction indicating that the gap width is irrelevant. Nevertheless, applying the same specific compaction force at different gap widths will result in compacts with different solid fractions, since the same force acts on a different amount of powder. Hence, the compression pressure might be the parameter which would have to be considered instead of the specific compaction force and the gap width, since it is directly decisive for the solid fraction. However, the actual pressure acting on the powder in a commercial roll compactor is normally not available, unless force transducers are installed in the rolls. Therefore, gap width and specific compaction forces are the machine parameters that can be practically varied to influence the quality of the ribbons. It might be useful to keep the compression pressure constant, rather than the specific compaction force, if one transfers a process from one compactor to another and wants to maintain the same ribbon properties. This hypothesis has to be validated with data from other roll compactors and will be discussed in the following sections.

To summarise, a constant material and process parameter independent Kp factor was determined for the Gerteis Mini-Pactor, whereby the material and process independence only applies to the studied design space. General interrelationships in roll compaction and roll compaction simulation have been formulated. A question is, whether the Kp factor is dependent on the used roll compactor. To answer this question, experiments with other roll compactors were performed.

3.1.3 LB Bohle BRC25

3.1.3.1 Roll Compaction with the BRC25

MCC and lactose were roll compacted on the BRC25 at different specific compaction forces and gap widths following full factorial multilevel experimental plans (Table 3.1-3). The quantitative factor gap width was tested at two levels (2 mm and 4 mm), the specific compaction force was a quantitative multilevel factor. The ribbon solid fraction was again chosen as response since it was the most critical quality attribute for ribbons. The roll speed was kept constant at 2 rpm. Since the single experiments were carried out only once, a centre point was set at 6 kN/cm and 3 mm, which was repeated three times.

This allowed to evaluate the reproducibility for the statistical analysis. The experiments were performed in randomized order.

Table 3.1-3: Full factorial multilevel experimental plans for the roll compaction trials with MCC and lactose on the BRC25

Material	Gap width [mm]	Specific compaction force [kN/cm]
MCC	2	2; 2.5; 3; 3.5; 4; 4.5; 5; 6; 7; 8; 9; 10; 11; 12; 14
	3	6
	4	2; 2.5; 3; 3.5; 4; 4.5; 5; 6; 7; 8; 9; 10; 11; 12; 14
Lactose	2	2; 3; 4; 5; 6; 7; 8; 9; 10; 11
	3	6
	4	2; 3; 4; 5; 6; 7; 8; 9; 10; 11

Table 3.1-4: Powder density of MCC and lactose used for roll compaction on the BRC25; n=3, mean ± SD

Material	Powder density [g/cm³]
MCC	1.5932 ± 0.0032
Lactose	1.5543 ± 0.0024

The powder densities of the used batches of MCC and lactose were determined by helium pycnometry (section 5.2.9.5). The powder densities are listed in Table 3.1-4. Figure 3.1-23 depicts the solid fractions of MCC and lactose ribbons determined with the GeoPyc (section 5.2.10.1) in dependence on the gap width and the applied specific compaction force. For both materials, the solid fraction increases with an increasing specific compaction force, whereas it decreases with an increasing gap width. The total solid fraction values are higher for lactose compared to MCC. The solid fractions of MCC ribbons range from 49 % to 80 % and from 45 % to 76 % for the 2 mm and the 4 mm gap width, respectively. The lactose ribbons show solid fractions between 74 % and 83 % for the 2 mm gap width and between 69 % and 83 % for the 4 mm gap width. The curves can be described by logarithmic fits (Equation (12)). Their correlation coefficients lay between 0.703 (lactose, GW: 2 mm) and 0.994 (MCC, GW: 4 mm). The results for ribbon solid fraction are in accordance with the results from the Mini-Pactor, where similar

trends were observed. The fluctuations in the values for lactose are probably due to irregularities in the process. Multiple compaction was observed occasionally due to material sticking on the rolls, which might lead to higher solid fractions than a single compaction step. The influence of the specific compaction force on the ribbon solid fraction is bigger for MCC than for lactose, as indicated by the higher slope of the SCF-SF curve.

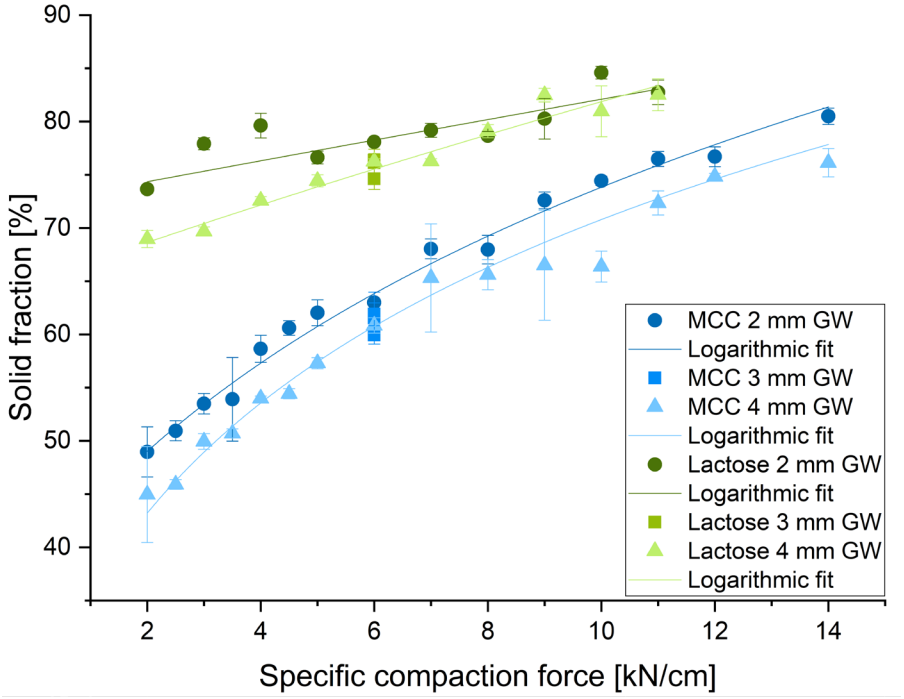

Figure 3.1-23: Solid fraction of MCC and lactose ribbons in dependence on the specific compaction force (SCF) and the gap width (GW); BRC25; n = 3, mean ± SD

Statistical analysis (section 5.2.1) for the experiments with MCC confirmed the above-mentioned observations. A model with high values for the goodness of fit and prediction was built ($R^2 = 0.984$, $Q^2 = 0.980$). The specific compaction force has the biggest influence on the solid fraction as shown in the coefficient plot (Figure 3.1-24). The effect is positive and significant for a confidence interval of 0.95. An increase in the specific compaction force leads to an increased solid fraction. The gap width has a smaller but as well significant effect on the solid fraction. This effect is negative, so that an increase of gap width from 2 mm to 4 mm will result in a decreased solid fraction. A significant negative quadratic effect of the specific compaction force was found, whose magnitude ranges between the specific compaction force and the gap width.

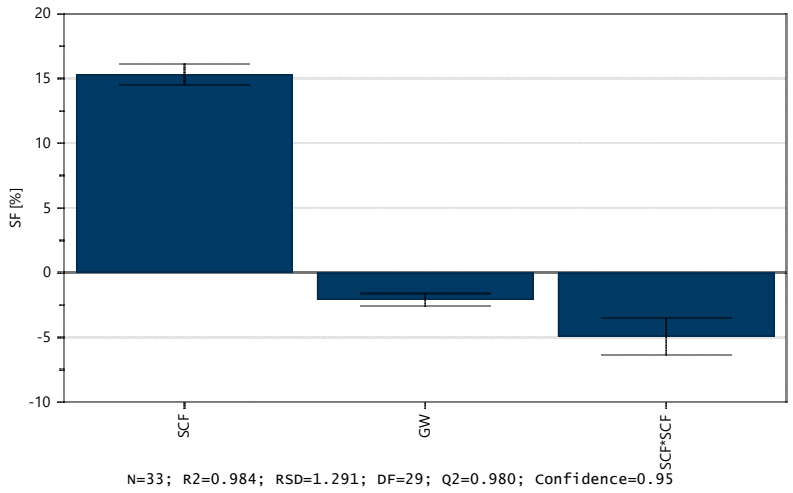

Figure 3.1-24: Coefficient plot for the effects of the specific compaction force (SCF) and the gap width (GW) on the solid fraction of MCC ribbons produced with the BRC25

The SCF-SF curve in Figure 3.1-23 has a high slope at small specific compaction forces. The curve flattens when the specific compaction forces increase. The contour plot (Figure 3.1-25) illustrates the effects on the solid fraction of MCC ribbons. It is obvious that the increase of solid fraction is more pronounced at smaller specific compaction forces: The distance of the lines of equal solid fraction becomes larger at higher specific compaction forces, which is the expression of the negative quadratic effect of the specific compaction force. Furthermore, it is apparent that the gap width has a negative effect on the solid fraction.

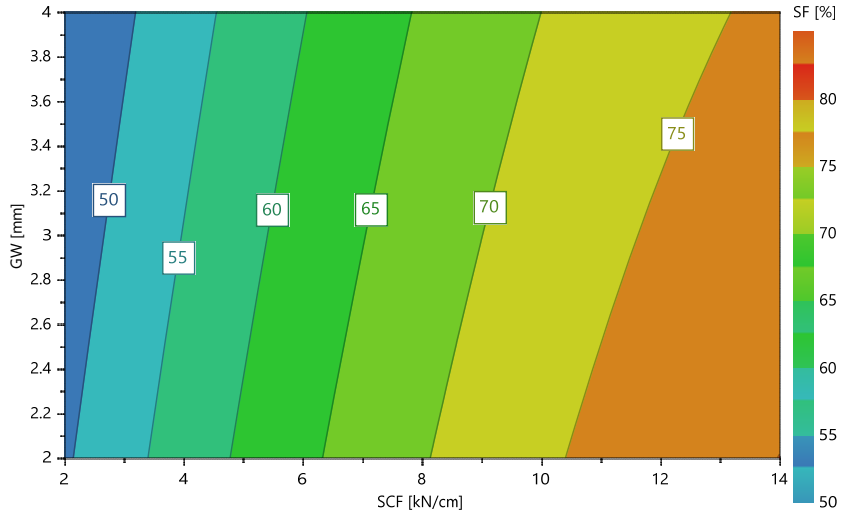

Figure 3.1-25: Contour plot for the solid fraction (SF) of MCC ribbons produced with the BRC25 in dependence on the gap width (GW) and the specific compaction force (SCF)

In contrast to the Mini-Pactor, for lactose, specific compaction forces above 12 kN/cm at 2 mm gap width and 11 kN/cm at 4 mm gap width could not be realised. The process stopped automatically since the safety threshold for the roll torque of the master roll was exceeded.

A regression model was built for lactose with R^2=0.884 and Q^2=0.824. The smaller values for R^2 and Q^2 compared to the model for MCC can be explained by the comparatively poorer raw data and the smaller variability. Like for MCC, the specific compaction force has a positive effect on the solid fraction, the gap width has a negative one (Figure 3.1-26).

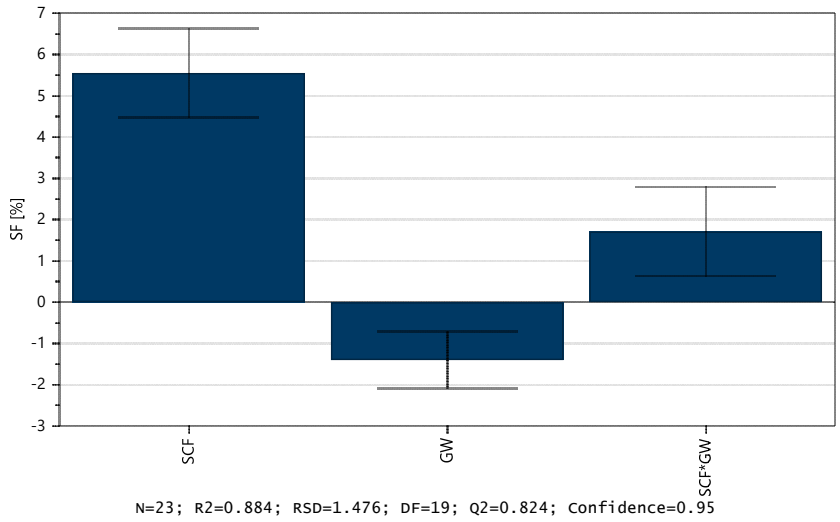

Figure 3.1-26: Coefficient plot for the effects of the specific compaction force (SCF) and the gap width (GW) on the solid fraction of lactose ribbons produced with the BRC25

With an increasing specific compaction force, the solid fraction increases. The extent of this effect is smaller compared to MCC, whereas the negative effect of the gap width on the solid fraction is of similar magnitude. In contrast to MCC, no quadratic effect was found for the specific compaction force. However, a significant positive two-factor interaction was found between the specific compaction force and the gap width. This means, that the two factors must be evaluated together and that they have a multiplicative effect on the solid fraction.

The contour plot (Figure 3.1-27) reveals that the ribbon solid fraction increases more with an increasing specific compaction force at higher gap widths. It is questionable whether this is true or whether it is caused by the comparably high solid fraction values at 3 kN/cm and 4 kN/cm at a gap width of 2 mm (Figure 3.1-23), which flatten the correction curve.

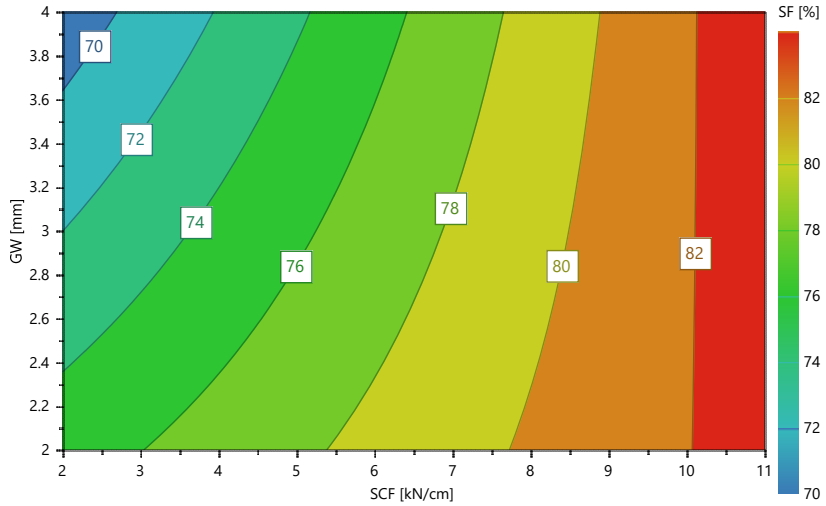

Figure 3.1-27: Contour plot for the solid fraction of lactose ribbons produced with the BRC25 in dependence on the gap width (GW) and the specific compaction force (SCF)

3.1.3.2 Kp Factor Determination for the BRC25

To determine the Kp factor for the BRC25, MCC and lactose ribblets were produced on the Styl'One Evolution following the same experimental plan as for the roll compaction trials (Table 3.1-3). For ribblet production, a default Kp factor of 1 was set. The ribblet solid fraction was determined by powder pycnometry with the GeoPyc (section 5.2.10.1). The same batches of MCC and lactose were used as for the roll compaction experiments. Their powder densities are listed in Table 3.1-4.

In Figure 3.1-28, the ribblet solid fractions are displayed in dependence of the SCF and are compared to the ribbon solid fractions (same data set as shown in Figure 3.1-23). The ribblets produced on the Styl'One show the same general correlations as the ribbons: An increasing specific compaction force leads to an increase in solid fraction, and with an increasing gap width the solid fraction decreases.

Compared to the ribbons, the MCC ribblets show at both gap widths a systematically higher solid fraction (Figure 3.1-28 a). The solid fractions for the 2 mm gap width range from 51.9 % to 86.8 % and from 46.3 % to 78.0 % for the 4 mm gap width. The curves of MCC ribbons and ribblets have similar slopes and seem to be proportionally shifted against each other. This trend of higher ribblet solid fractions was also found for lactose at the 4 mm gap width (Figure 3.1-28 b). The observed solid fractions ranged between 72.2 % and 82.7 %. For the ribblets produced at a gap width of 2 mm, solid fractions were measured between 72.7 % and 85.5 %. For the smaller gap width, the trend of higher ribblet than ribbon solid fraction is only partially correct, and the curves diverge, which could be due to the observed process irregularities during roll compaction.

The aim of the mimicking was to obtain ribbons and ribblets with equal solid fractions. Thus, the simulated specific compaction force or the compaction pressure, which is used on the Styl'One, must be adapted to the roll compactor of interest in order to achieve a good alignment between ribbon and ribblet solid fraction.

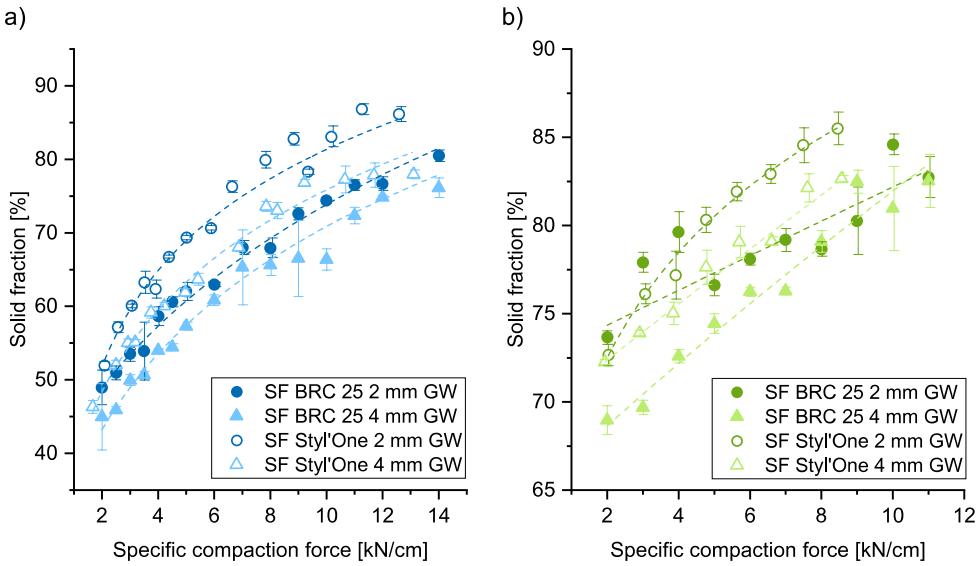

Figure 3.1-28: Solid fraction of ribbons and ribblets in dependence on the specific compaction force (SCF) and the gap width (GW) for a) MCC and b) lactose (Kp factor: 1); BRC25; n=3, mean ± SD

To do so, the Kp factor was determined like described in section 5.2.5.2. The least root mean square errors were calculated to find the Kp factor which leads to the best predictive quality. The root mean square error (RMSE) indicates how much a prediction deviates on average from the actual observed values. The RMSE is an absolute value and has the same unit as the response variable solid fraction. The lower the RMSE is the better is the fit. There is no universal value for the RMSE that indicates a good or a bad fit, since it is dependent on the used data set. In the present case, the fit will be considered as acceptable for RMSE values smaller than 3.0.

First, the Kp factor was calculated for both materials separately to evaluate, whether considerable differences can be found between the materials. A Kp factor of 0.716 was found for MCC, for lactose the factor is 0.693. The differences were considered to be small enough to calculate one single Kp factor for both materials. Finally, a Kp factor of 0.714 was found that leads to the best alignment of ribbon and ribblet solid fraction for both materials at both gap widths.

In Figure 3.1-29, the curves for ribbon and ribblet solid fractions in dependence on the specific compaction force are shown, in which the Kp factor of 0.714 was applied to the mimicked specific compaction forces. The curves of MCC ribbon and ribblet solid fractions (Figure 3.1-29 a) are in good

alignment for the 4 mm gap width. However, slightly increasing deviations can be seen for MCC at higher specific compaction forces for the 2 mm gap width. The curves for lactose ribbon and ribblet solid fractions (Figure 3.1-29 b) at a 4 mm gap width show a good alignment, whereas the curves for the 2 mm gap width deviate more from each other. This could be due to the poor quality of the raw data from roll compaction at small specific compaction forces.

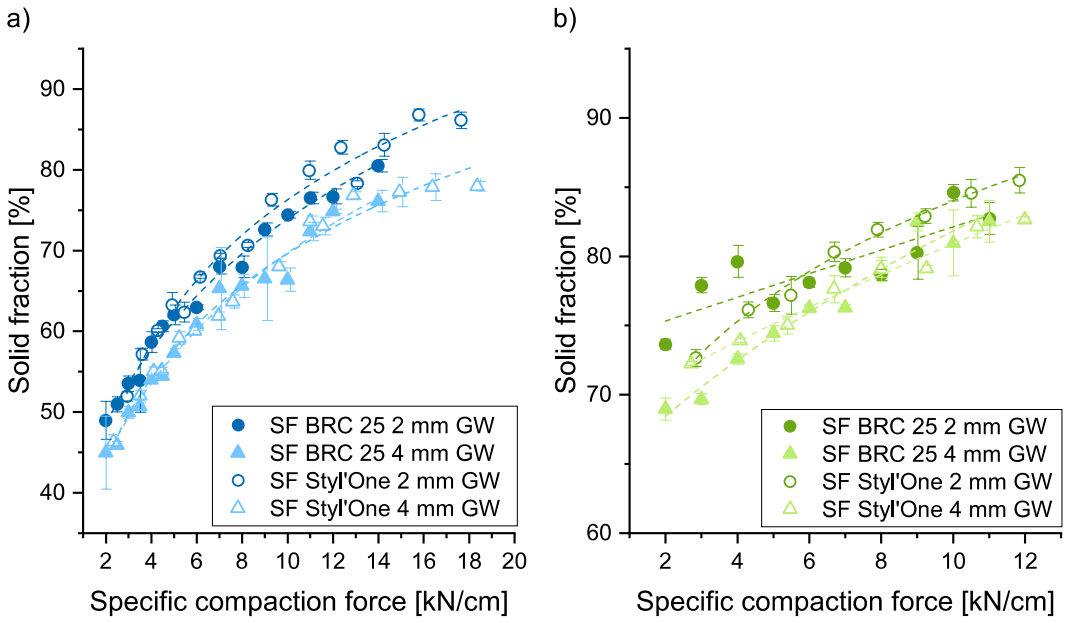

Figure 3.1-29: Solid fraction of ribbons and ribblets in dependence on the specific compaction force (SCF) and the gap width (GW) for a) MCC and b) lactose (Kp factor: 0.714); BRC25; n=3, mean ± SD

The root mean square errors (RMSE) from the Kp factor determination are displayed in Table 3.1-5 and are all below 3.0. The over-all root mean square error is 2.35, when both materials are considered together, which indicates sufficient accuracy. It can be concluded from these results that the factor is independent of the tested materials and the gap widths, at least for the investigated design space. The Kp factor for the BRC25 of 0.714 is similar to the one for the Gerteis Mini-Pactor (0.667). This similarity could be linked to the machine designs, which are identical in their roll width and diameter, and to the similar roll surfaces and sealing systems.

Table 3.1-5: RMSE and Kp factors for the BRC25, for MCC and lactose evaluated individually and together

Material	Gap width [mm]	RMSE	Kp
MCC	2	2.89	/
	4	2.32	/
	2 and 4	2.62	0.716
Lactose	2	2.19	/
	4	1.04	/
	2 and 4	1.71	0.693
MCC & Lactose	2 and 4	2.35	0.714

Figure 3.1-30 depicts the relation between the compression pressure on the Styl'One and the corresponding mimicked specific compaction force. The compression pressure increases almost linearly with an increasing specific compaction force for both materials.

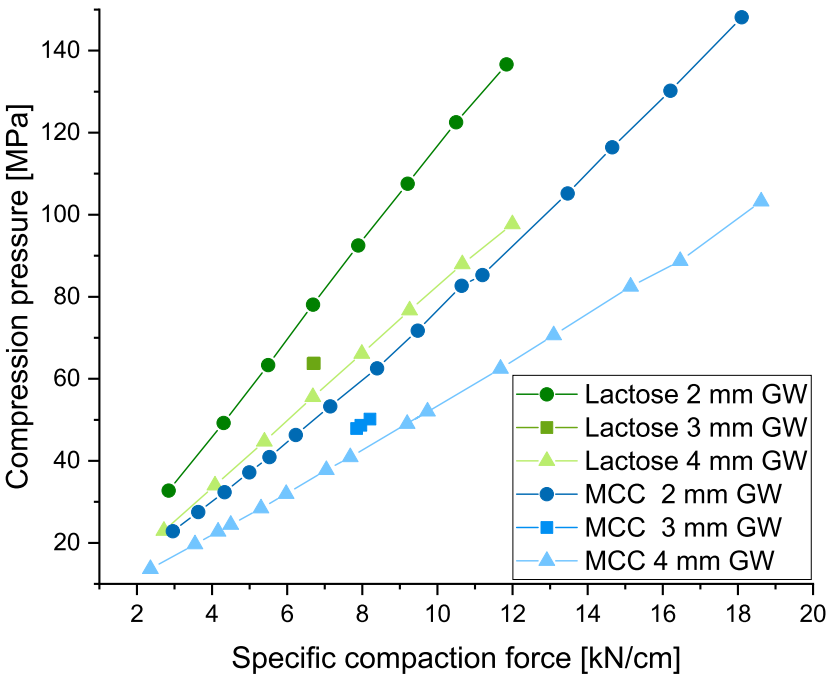

Figure 3.1-30: Compression pressure in relation to simulated specific compaction force (BRC25) for lactose and MCC at different gap widths (GW); n ≥ 20, mean

However, the absolute values differ between the materials: The same specific compaction force at the same gap width corresponds to higher compression pressures for lactose than for MCC. If one considers the reversed relationship: The same compression pressure at the same gap width will result in a higher specific compaction force for MCC than for lactose. An increase in gap width from 2 mm to 4 mm at a constant specific compaction force causes a decrease in compression pressure. This means that one must decrease the compression pressure to maintain the specific compaction force when the gap width is increased. The slopes of the 2 mm curves are steeper compared to the 4 mm curves. Thus, the compression pressure increases more with an increase in specific compaction force at higher gap widths.

The curves (compression pressure – specific compaction force) for the Mini-Pactor and the BRC25 are almost identical. This might be due to the same model input parameters regarding the roll diameter and roll width as well as the similar Kp factor, which connects the simulated with the real specific compaction force. Furthermore, the compactors have a similar feeding system, which conveys the powder by two screws. The findings underline the hypothesis that the roll compactor design has a great influence on the Kp factor.

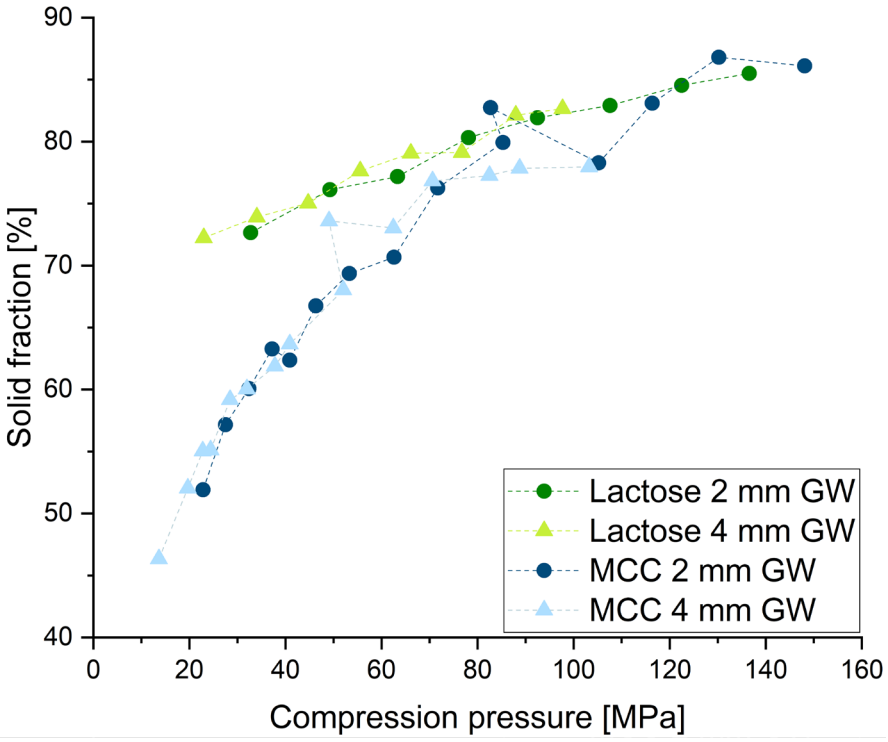

Figure 3.1-31: Correlation between the ribblet solid fraction and the compression pressure for MCC and lactose; n = 3 (solid fraction), n ≥ 20 (compression pressure), mean

The correlation between the compression pressure and the solid fraction of MCC and lactose ribblets is depicted in Figure 3.1-31. Lactose ribblets show predominantly higher solid fractions than MCC at a

constant compression pressure. The curves converge at higher compression pressures. In analogy to the correlation between solid fraction and specific compaction force, the ribblet solid fraction increases with an increasing compression pressure. An increase in gap width from 2 mm to 4 mm at a constant compression pressure, however, does not lead to a change in ribblet solid fraction. These results are in accordance with the ones from simulating the Mini-Pactor (Figure 3.1-22). The fact that the compression pressure seems to be the decisive parameter for ribblet and consequently ribbon solid fraction might be a possibility to facilitate the transfer between different equipment. Further roll compactors with different machine designs compared to the Mini-Pactor and the BRC25 must be investigated to verify this hypothesis.

3.1.4 Alexanderwerk WP120

3.1.4.1 Roll Compaction with the WP120

The two so far described roll compactors in this work are similar in their machine design, which was probably the reason for their similar Kp factors. Thus, roll compactors should be investigated with considerable differences in roll diameter, roll width, roll arrangement and feeding system. The Alexanderwerk WP120 was chosen for this purpose. On the Mini-Pactor and the BRC25 only smooth roll surfaces were used. For the WP120, the factors were extended by the influence of the roll surface (grooved and squared) on the solid fraction. Furthermore, different roll widths of 25 and 40 mm were tested (Figure 3.1-32) in order to evaluate the effect of the roll width on the ribbon solid fraction and to evaluate findings from literature, whether the roll width can be a useful parameter for scale-up (Alleso et al., 2016, Pérez Gago et al., 2018).

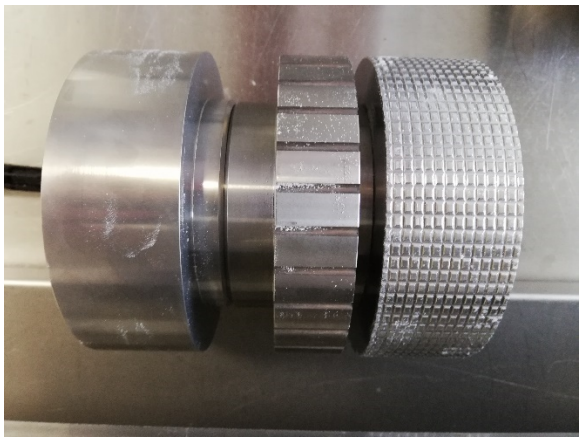

Figure 3.1-32: From left to right rolls with smooth (40 mm), grooved (25 mm) and squared (40 mm) surfaces for the WP120

Another difference between the WP120 and the other investigated roll compactors is the roll diameter, which is 120 mm and thus, smaller than the 250 mm diameter of the BRC25 and the Mini-Pactor. The compactors also differ in their roll arrangement – the WP120 has, in contrast to the inclined and horizontal rolls, vertically positioned rolls. Full factorial multi-level experimental plans were created, which should closely resemble those conducted on the BRC25 and the Mini-Pactor in order to achieve a good comparability. However, some limitations occurred during the experiments. This might be linked to the fact that the chosen parameter settings were not the optimal settings for this compactor. The original and the adapted experimental plans are presented in Table 3.1-6. The smooth rolls could not be used since it was not possible to drag enough material between the rolls to achieve a constant gap. Instead, grooved rolls were used as replacements, which resemble the smooth rolls the most. They were compared to squared rolls, which were expected to have an influence on the nip of the powder. For MCC, the 4 mm gap width could not be realised, since the screw was not able to turn fast enough and thus, it was not possible to transport enough material between the rolls. The experimental plan was adapted, and a 3 mm gap width was chosen instead. Furthermore, not all specific compaction forces could be realised, e.g., for DCPA at a 4 mm gap width. This, again, was due to the limited feeding capacity of the screw at higher specific compaction forces, which did not allow sufficient filling of the gap. The roll speed was kept constant at 4.2 rpm for all experiments. This roll speed was chosen since it is corresponding to the circumferential velocity of the rolls on the Mini-Pactor and the BRC25 (2 rpm). This should assure similar compaction times of the material independent of the used roll compactor.

Table 3.1-6: Experimental plans for the roll compaction trials with MCC and DCPA on the WP120

Factors	**Planned factor levels**	**Performed factor levels**
Roll surface	Smooth, squared	Grooved, squared
Roll width [cm]	2.5; 4	2.5; 4
Material	MCC (Vivapur 102), DCPA (DiCaFos A150)	MCC (Vivapur 102), DCPA (DiCaFos A150)
Roll gap [mm]	2; 3; 4	2; 3
Specific compaction force [kN/cm]	3 - 14	3 - 14

Figure 3.1-33 shows the recorded process parameters specific compaction force, gap width, roll speed, feed screw speed and feed screw capacity for roll compaction of DCPA with 2.5 cm wide squared rolls. Generally, the process was stable within the range of tested specific compaction forces when a gap width of 2 mm was set. The speed of the feeding screw adapted according to the specific compaction force. The screw speed increased with an increase of the force since more material must be transported between the rolls in order to keep the gap width constant. It ranged between 30 rpm and 40 rpm. The screw capacity is a percentage value that indicates the extent to which the possible power of the drive motor is utilised. The screw capacity can also exceed 100 % and serves primarily as orientation for the user. The screw capacity did not change considerably and was nearly constant at 85 % for the different applied forces. An increase of the gap width to 3 mm and 7 kN/cm (centre-point experiment) was associated with a clear increase in screw speed (52 rpm) and capacity (90 %). However, the process was stable over the sampling period. A further increase of the gap width to 4 mm resulted in a further increase in screw speed (60 – 75 rpm) and capacity (> 100 %), combined with distinctly higher fluctuations. The process was stable up to a specific compaction force of 6 kN/cm. At higher forces, the gap width could not be kept constant and the specific compaction force and gap width decreased.

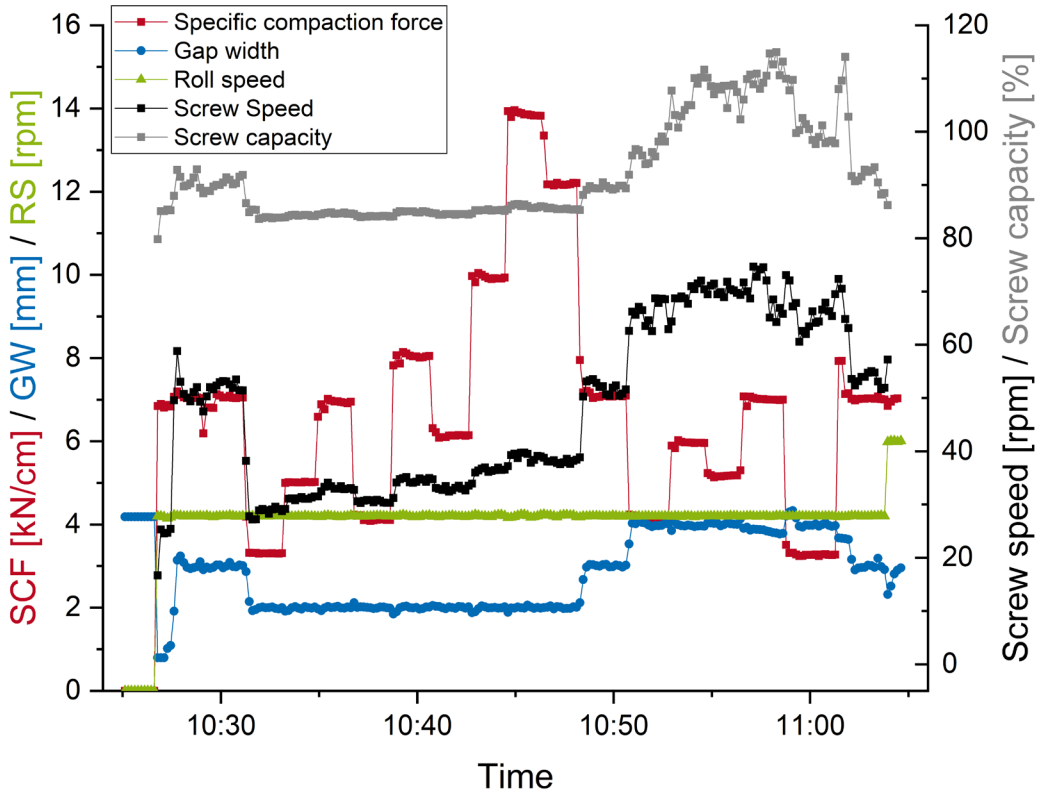

Figure 3.1-33: Process data of DCPA roll compaction on the WP120, 25 mm roll width, squared rolls; SCF: specific compaction force; GW: gap width; RS: roll speed

Figure 3.1-34 depicts the process parameters for compaction of MCC with the WP120, equipped with 25 mm wide squared rolls. It was possible to produce ribbons from 3 kN/cm to 14 kN/cm at a constant 2 mm gap width. The specific compaction force adapted quickly, even for big steps between the settings. The screw speed increased with an increasing specific compaction force so that the gap width could be kept constant. Compared to the compaction of DCPA, the screw speeds were higher for MCC. They ranged from approx. 55 rpm at 3 kN/cm to 80 rpm at 14 kN/cm at a gap width of 2 mm. The 3 mm gap was tested at a specific compaction force of 3 kN/cm, which resulted in screw speeds of appr. 80 rpm. This screw speed was not reached with DCPA, even at a gap width of 4 mm. This might be connected to the higher bulk density of DCPA than for MCC. The same mass MCC takes more volume than DCPA and thus, the screws must turn faster in order to transport the same amount of material between the rolls. Furthermore, the screw speed fluctuated in a bigger extent processing MCC. The screw capacity ranged around 90-95 % for all process settings, which underlines the observations (no data available) that at a gap width of 4 mm the maximum capacity of the feed screw was exceeded.

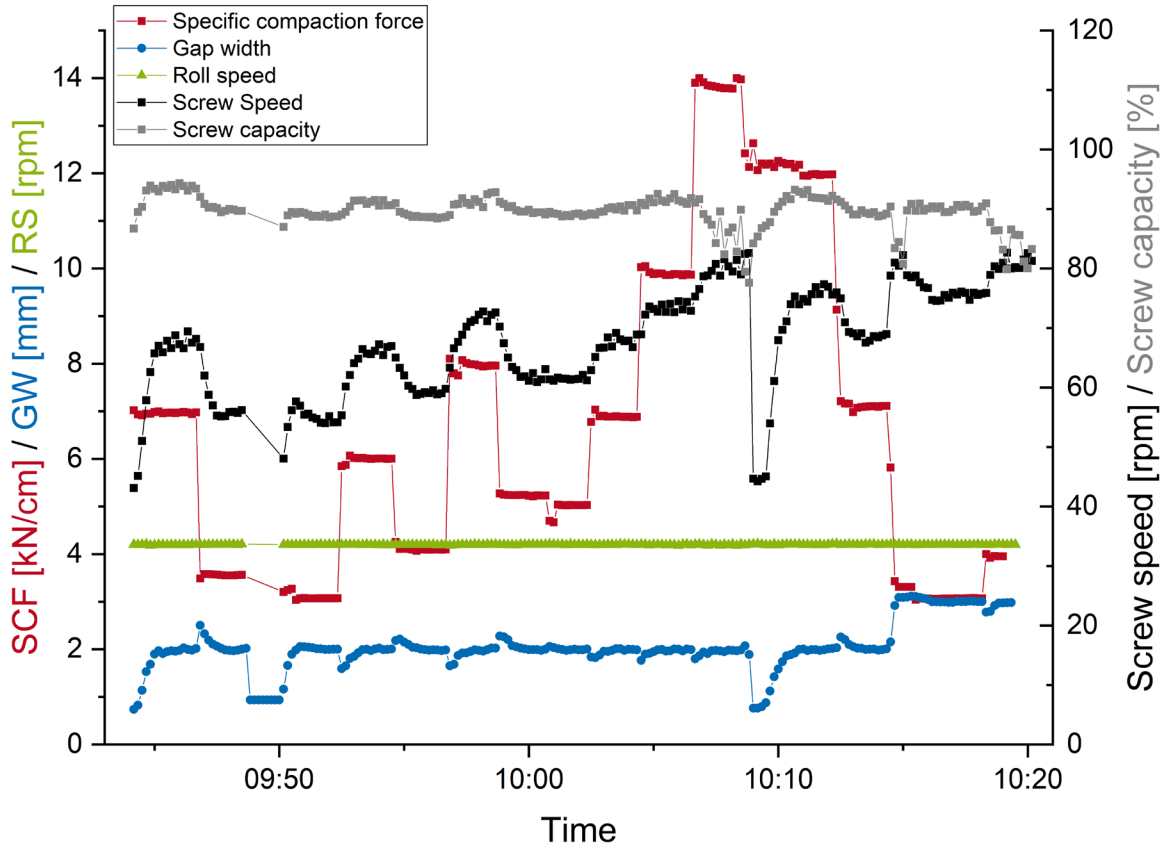

Figure 3.1-34: Process data of MCC roll compaction on the WP120, 25 mm roll width, squared rolls; SCF: specific compaction force; GW: gap width; RS: roll speed

Figure 3.1-33 and Figure 3.1-34 visualise both the capabilities and the limitations of the processes. However, the roll compaction process was reliably stable at smaller gap widths and it was possible to produce ribbons with sufficient strength to handle them and to measure their solid fraction. The powder densities of MCC and DCPA were measured by helium pycnometry (section 5.2.9.5). The powder densities are listed in Table 3.1-7.

Table 3.1-7: Powder density of MCC and DCPA used for roll compaction experiments on the WP120; n=3, mean ± SD

Material	**Powder density [g/cm³]**
MCC	1.6503 ± 0.0090
DCPA	2.9908 ± 0.0341

Ribbon Splitting and Sticking

Ribbon sticking and splitting was observed for almost all experimental settings and roll surfaces. The ribbon adhered on the roll surface and laminated in transverse direction, meaning through the thickness of the ribbon. This phenomenon was also observed by Mahmah et al. (2019), who stated that transversal splitting was linked to powder adhesion on the rolls, which leads - in combination with the residual stresses inside the ribbon – to the formation of cracks. In the present work, it was assumed that there are no relevant differences between the density of the upper and lower part of the laminated ribbon.

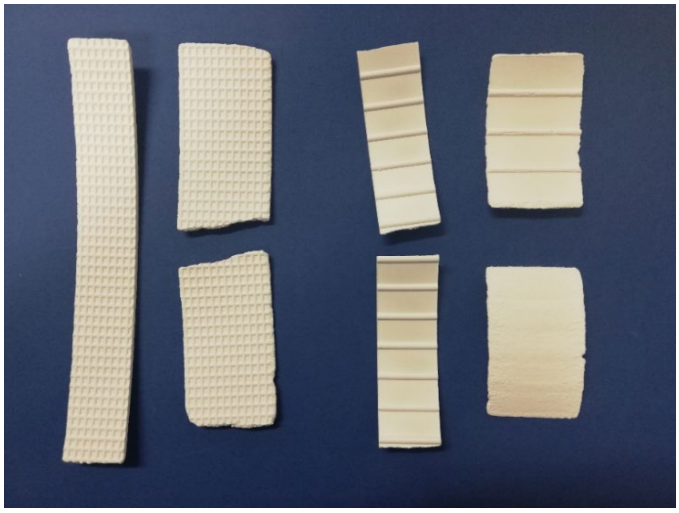

Figure 3.1-35: MCC ribbons produced with squared (left) and grooved (right) rolls with 25 mm and 40 mm roll width

Figure 3.1-35 exemplarily shows MCC ribbons produced with the WP120. In contrast to the ribbons from the Mini-Pactor and the BRC25, the ribbons were almost intact in their width and longer ribbon

fragments were formed, which can be attributed to the cheek plates used as sealing system (Perez-Gandarillas et al., 2016).

Influence of the Specific Compaction Force

The ribbon solid fraction for MCC and DCPA increases with an increasing specific compaction force. This is valid for all tested machine settings and parameters and exemplarily shown in Figure 3.1-36 at a 2 mm gap width and grooved rolls for the 25 mm and 40 mm roll widths (squared rolls in Figure 7.1-1). For the 25 mm roll width, the MCC ribbon solid fraction ranged between 63 % and 85 % and the DCPA ribbon solid fraction ranged from 49 % to 57 %, whereby the increase in solid fraction was greater at lower specific compaction forces than at higher ones.

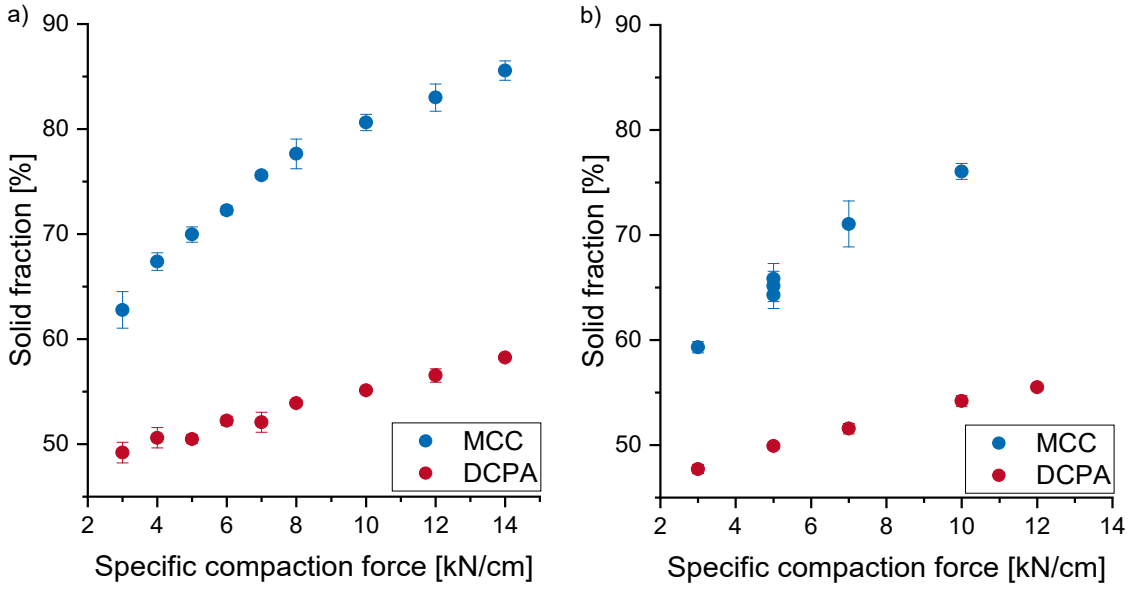

Figure 3.1-36: Solid fraction of MCC and DCPA ribbons in dependence on the specific compaction force for a) 25 mm and b) 40 mm roll width at a gap width of 2 mm, produced with the WP120 with grooved rolls; n=3; mean ± SD

For all experiments carried out, the MCC ribbons are denser compared to the DCPA ribbons using the same process settings. This is in accordance with the results observed on the Mini-Pactor and is linked amongst others to the compressibility of the materials. Regression models were built for MCC (R^2 = 0.97, Q^2 = 0.956) and DCPA (R^2 = 0.972, Q^2 = 0.965), which describe the influence of the factors specific compaction force, gap width, roll width and roll surface on the ribbon solid fraction. The model quality for MCC is smaller compared to the Mini-Pactor and the BRC 25 since not all experiments could be performed as planned. The model for DCPA, in contrast, is of higher quality compared to the one for the Mini-Pactor. The statistical analysis confirms that the specific compaction force has the biggest effect on the ribbon solid fraction as shown in the coefficient plot (Figure 3.1-37). Comparing the two

materials, one can see that the effect of the specific compaction force on MCC is approximately twice as high as on DCPA. For both materials, the specific compaction force has also a negative quadratic effect on the solid fraction, which was partly also found for the Mini-Pactor and the BRC25.

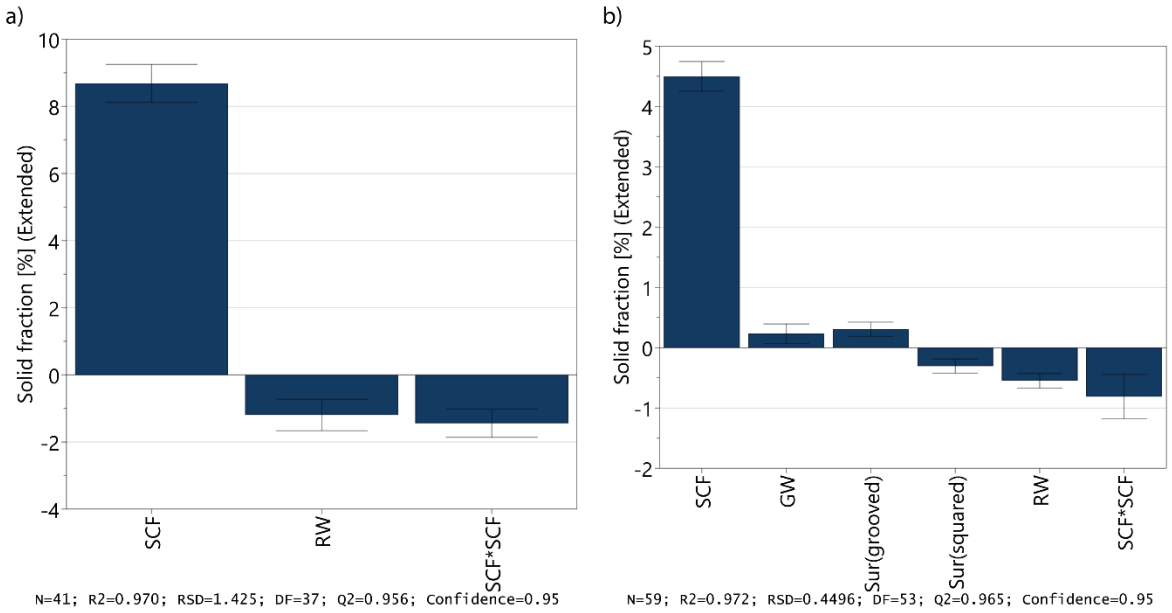

Figure 3.1-37: Coefficient plot for the effects of the specific compaction force (SCF), gap width (GW), roll width (RW), roll surface (Sur) on the solid fraction of ribbons produced with the WP120 for a) MCC and b) DCPA

Influence of the Gap Width

It was generally expected that ribbons produced at higher gap widths would show a smaller solid fraction. However, the effect of the gap width deviated from the observations made on the Mini-Pactor and the BRC25. A smaller gap width did not always lead to denser ribbons. Depending on the material and the process settings this relation was even valid the other way around, so that a higher gap width led to denser ribbons. Figure 3.1-38 illustrates the solid fraction of DCPA and MCC ribbons at different gap widths for both tested rolls surfaces (results for the 40 mm wide rolls in Figure 7.1-2). DCPA ribbons produced with squared rolls showed a trend to denser ribbons at a higher gap width, but the absolute differences between the 2 mm and the 4 mm gap width were small. For the ribbons produced with grooved rolls, the difference in ribbon solid fraction was less and resulted in similar solid fractions for ribbons which were produced at different gap widths. Similar observations were made by Csordas et al. (2018) for MCC and mannitol, which were compacted on a Alexanderwerk BT120. Statistical analysis confirmed a small but significant positive effect of the gap width on the solid fraction for DCPA ribbons.

For MCC ribbons produced with grooved rolls, the solid fraction increased with a decreasing gap width (Figure 3.1-38 d), which is consistent with the results of the Mini-Pactor and the BRC25, but contradicts

the observations made for DCPA. However, only three data-points are available for the 3 mm gap width, so that no definitive conclusion can be drawn from these results. The ribbon solid fraction for the squared rolls was equal for the 2 mm and 3 mm gap width (Figure 3.1-38 c). As with the grooved rolls, the available data is insufficient to draw clear conclusions. The factor gap width was removed from the statistical model for MCC since it resulted in an insignificant effect. This was due to the few data points available for the 3 mm gap width.

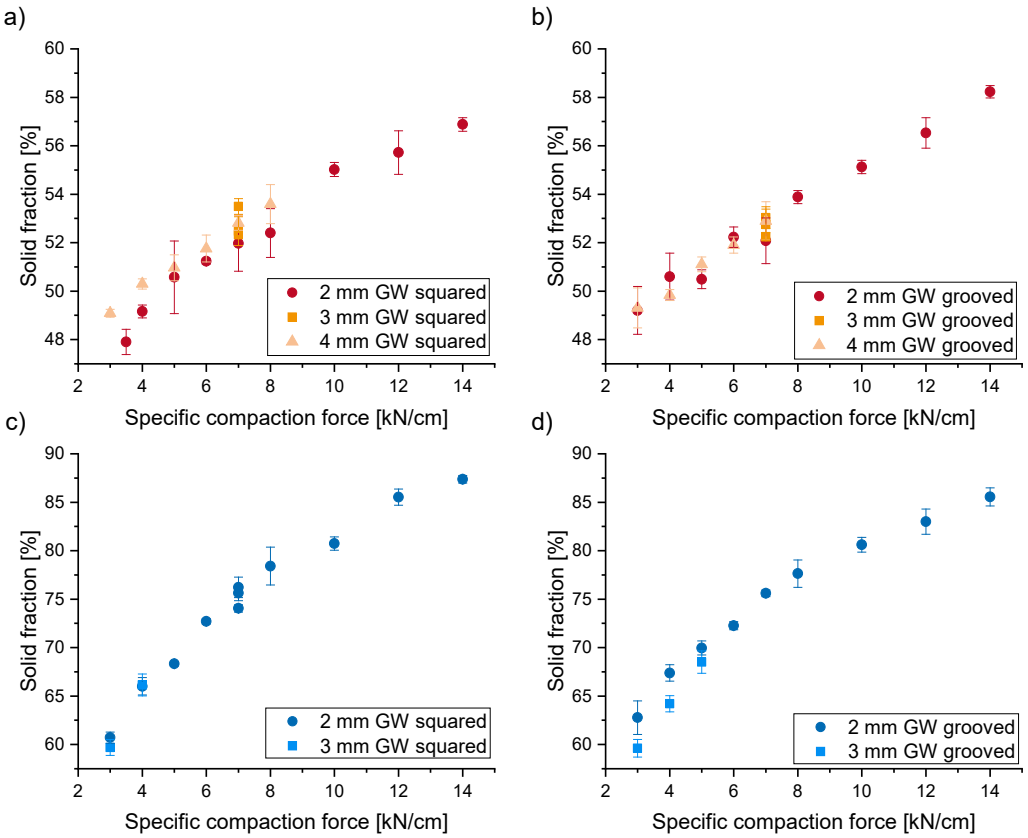

Figure 3.1-38: Solid fraction of MCC and DCPA ribbons in dependence on the gap width (GW) produced with the WP120 with 25 mm wide rolls; a) DCPA, squared rolls; b) DCPA, grooved rolls; c) MCC, squared rolls; d) MCC, grooved rolls; n=3; mean ± SD

Influence of the Roll Surface

It was expected that the squared rolls would lead to ribbons with smaller solid fractions, since the distance between the rolls at the gap width is only from peak to peak 2 mm but higher when measured from plateau to plateau. This was shown by Lim et al. (2011), who used NIR chemical imaging to visualise the density distribution across the ribbon for diamond knurled roll surfaces. However, the influence of the roll surface was found to be small for both investigated materials. This is exemplarily shown for MCC at 2 mm gap width in Figure 3.1-39 a (results for 40 mm roll width in Figure 7.1-3).

The solid fraction of the ribbons produced with grooved rolls was higher at small specific compaction forces (3-5 kN/cm). This trend turned at higher specific compaction forces, at which the squared rolls produced slightly denser ribbons than the grooved ones. For DCPA (Figure 3.1-39 b), a trend of denser ribbons for the grooved roll surface was observed over the whole range of specific compaction forces. However, this trend loses relevance due to the overlapping standard deviations. Overall, the difference between the roll surfaces was only marginal for both materials.

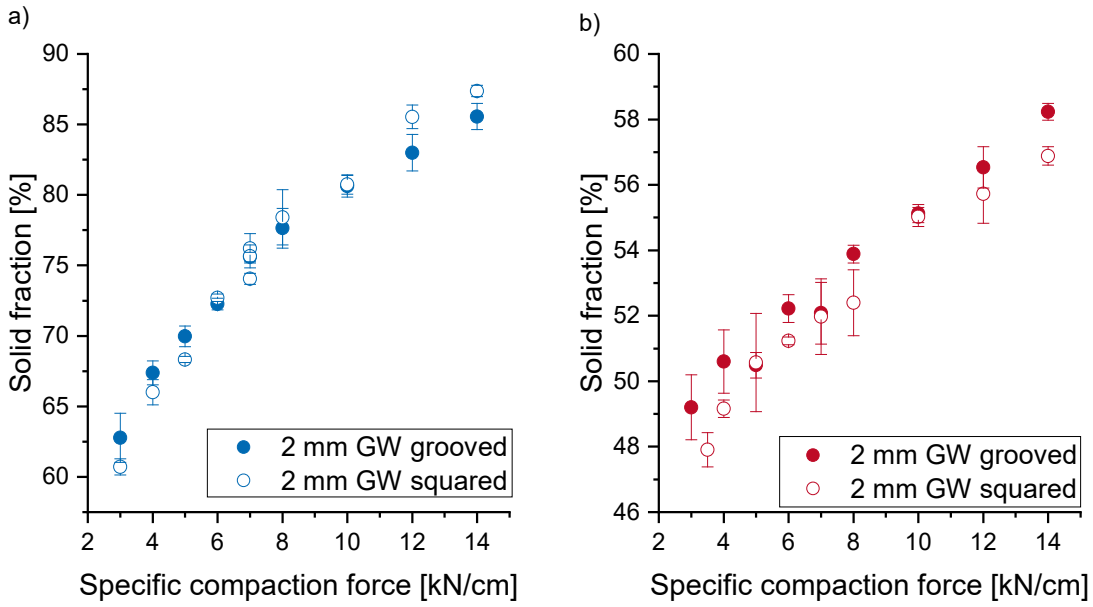

Figure 3.1-39: Solid fraction of a) MCC and b) DCPA ribbons in dependence on the specific compaction force and the roll surface (grooved or squared rolls) at produced with the WP120 at 2 mm gap width (GW) and with 25 mm roll width; n=3, mean ± SD

Statistical analysis confirmed that the effect of the roll surface on the solid fraction was not significant for MCC and was therefore not included in the model. For DCPA on the other hand, the roll surface influences the solid fraction. The grooved rolls have a small but significant positive effect on the ribbon solid fraction, but as already mentioned, this effect might not be relevant considering the overlapping standard deviations in the solid fraction-specific compaction force curve (Figure 3.1-39 b).

Influence of the Roll Width

It was reported in literature that a change in roll width - while maintaining the roll diameter and the process settings - can be used as a simple method to scale up a process (Alleso et al., 2016). In contrast to that, it was found in the present work that the roll width has a significant negative effect on the solid fraction for both tested materials (Figure 3.1-37) – the ribbons produced with 40 mm rolls were less dense than the ribbons produced with 25 mm rolls. This is illustrated for MCC and DCPA in Figure

3.1-40 for the 2 mm gap width and the grooved roll surface (results for squared roll surface in Figure 7.1-4). It was shown by Reynolds et al. (2010) that the maximum roll pressure decreases with an increasing roll width. However, it is not clear, whether the differences in the present study were found only due to the different roll widths or as well due to the different screws, which are used to convey the powder. With the larger screw and the changed screw-to-roll-surface-ratio for the 40 mm wide rolls, there might be less pre-compaction of the powder and ultimately a lower ribbon solid fraction.

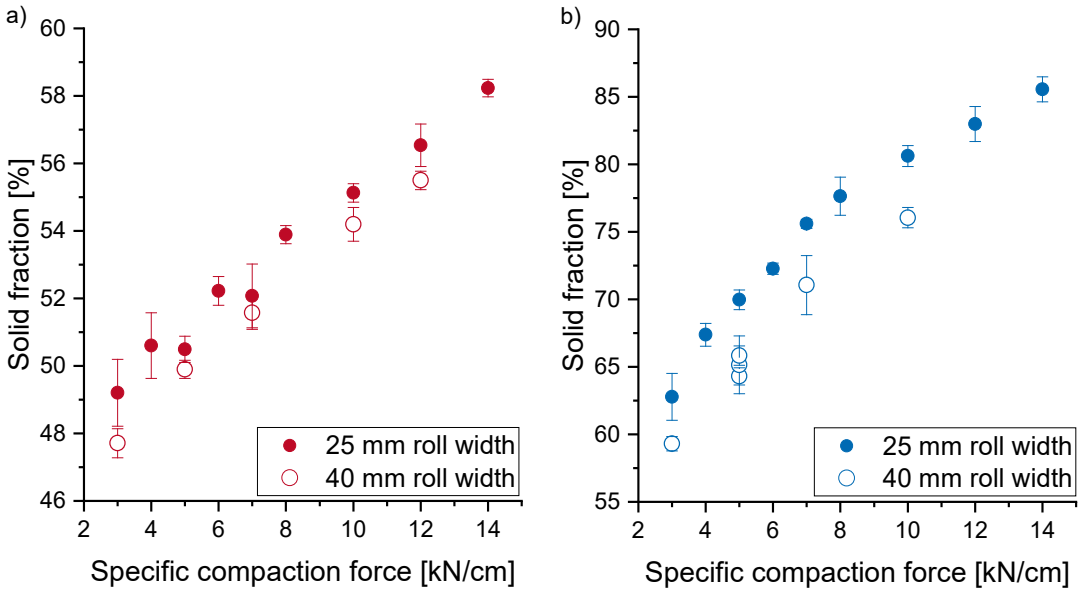

Figure 3.1-40: Solid fraction of a) DCPA and b) MCC ribbons in dependence on the specific compaction force and the roll width (25 mm or 40 mm) produced with the WP120 at 2 mm gap width and grooved rolls; n=3; mean ± SD

Influence of the Screw Torque

As mentioned above, the effects of the gap width and the roll width might be linked to a pre-compaction in the feeding system. In contrast to the Mini-Pactor and the BRC25, the Alexanderwerk compactors work with a single screw feeding system. Yu et al. (2020) used a special side-sealing cheek plate and infrared thermography to monitor the powder temperature inside the feeding and compaction zone of a WP120 and related it to the bulk density of the powder. The powder density increases gradually from the feeding towards the compaction zone. Due to the vertically arranged rolls and the single screw, the powder transport is carried out directly against the rolls, so that a higher pre-compaction may occur, if the powder is not dragged in immediately. The screw torques, which are connected to a higher stress exerted on the powder, were analysed, since they might be a surrogate parameter for the occurring pre-compaction in the feeding-system. Figure 3.1-41 exemplarily illustrates that the screw torque (section 5.2.4.4) increases with an increasing specific compaction force for MCC and DCPA. To increase the

specific compaction force and maintain the gap constant, the screw must transport more material between the rolls and thus, must turn faster. The torques for MCC are generally higher than the ones for DCPA at the same specific compaction forces, which could be linked to the smaller bulk density of MCC. The correlation coefficient for a linear fit of the relation between specific compaction force and screw torque for DCPA is 0.80. A correlation coefficient of 0.43 was determined for MCC. Excluding the outlier at 7 kN/cm, the correlation coefficient for MCC increases to 0.82.

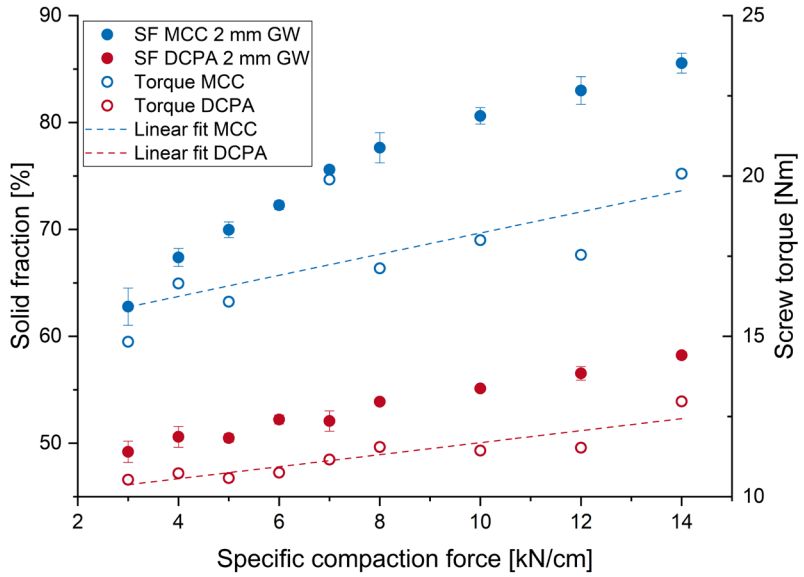

Figure 3.1-41: Screw torque and solid fraction in dependence on the specific compaction force for MCC and DCPA produced with the WP120 at 2 mm gap width (GW) with 25 mm wide grooved rolls; SF: n=3, mean ± SD; Screw torque: n=1

In Figure 3.1-42 b it becomes apparent that the slope of the screw torque – specific compaction force curve is considerably steeper for the larger gap width. To achieve a bigger gap width, the screw must turn faster to increase the material transport towards the rolls. This is linked to a sharp increase in torque, which is also visible for MCC when the gap width is increased from 2 to 3 mm (Figure 3.1-42 a). An additional reason for the increased torque might be a pre-compaction of the powder, which would explain the higher ribbon solid fractions for the larger gap width. Pre-compaction would have the effect that the material already reaches the nip region with higher bulk density and thus becomes more compressed in total.

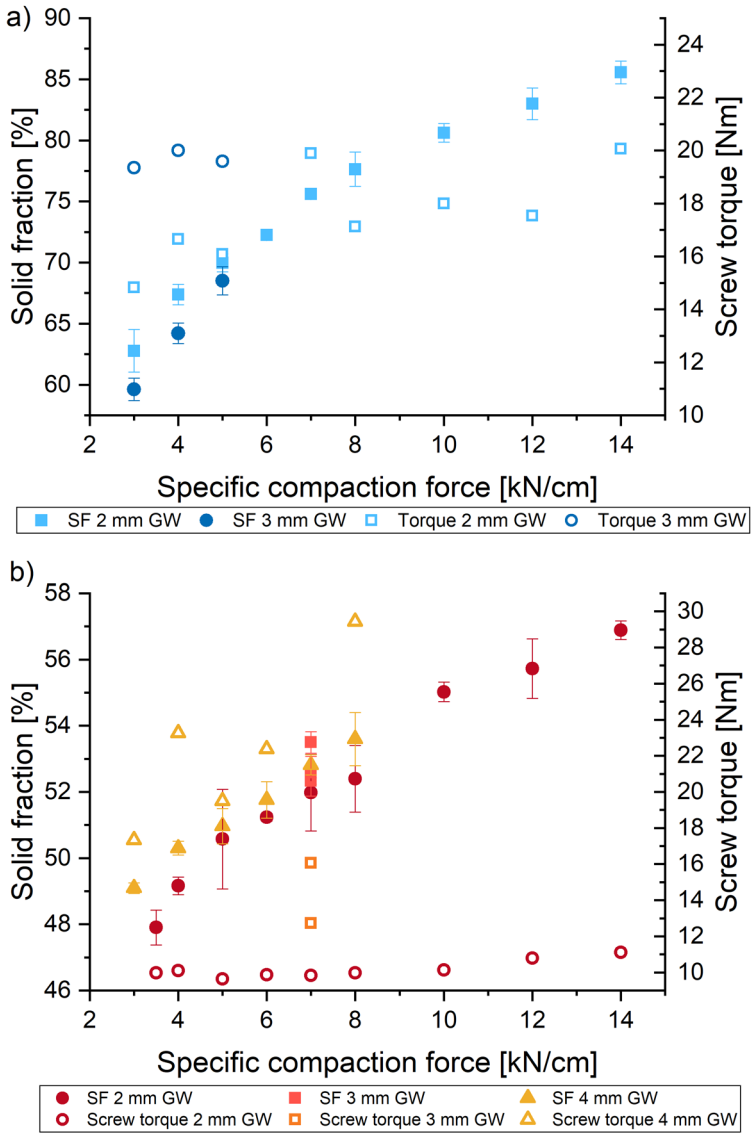

Figure 3.1-42: Correlation between solid fraction (SF), screw torque and specific compaction force; WP120 at different gap widths with 25 mm wide rolls; a) MCC, grooved b) DCPA, squared; SF: n=3, mean ± SD; Screw torque: n=1

The torque of the feeding screw was added as an uncontrolled quantitative factor to the statistical models (Figure 3.1-43) in order to evaluate a possible effect on the ribbon solid fraction. The effect of the screw torque on the ribbon solid fraction was positive but not significant. This might be due to the partially high variations in the recorded values, as these were not averaged over the sampling period but only represent momentary observations at the beginning of a batch with new compaction parameters. The fluctuations in the torque can partially be linked to the randomised order of the experiments. When the specific compaction force was increased to reach the new target force, the screw torques might have been smaller than in the case of a decrease to the new target force, since the torque might still have been high from the setting before.

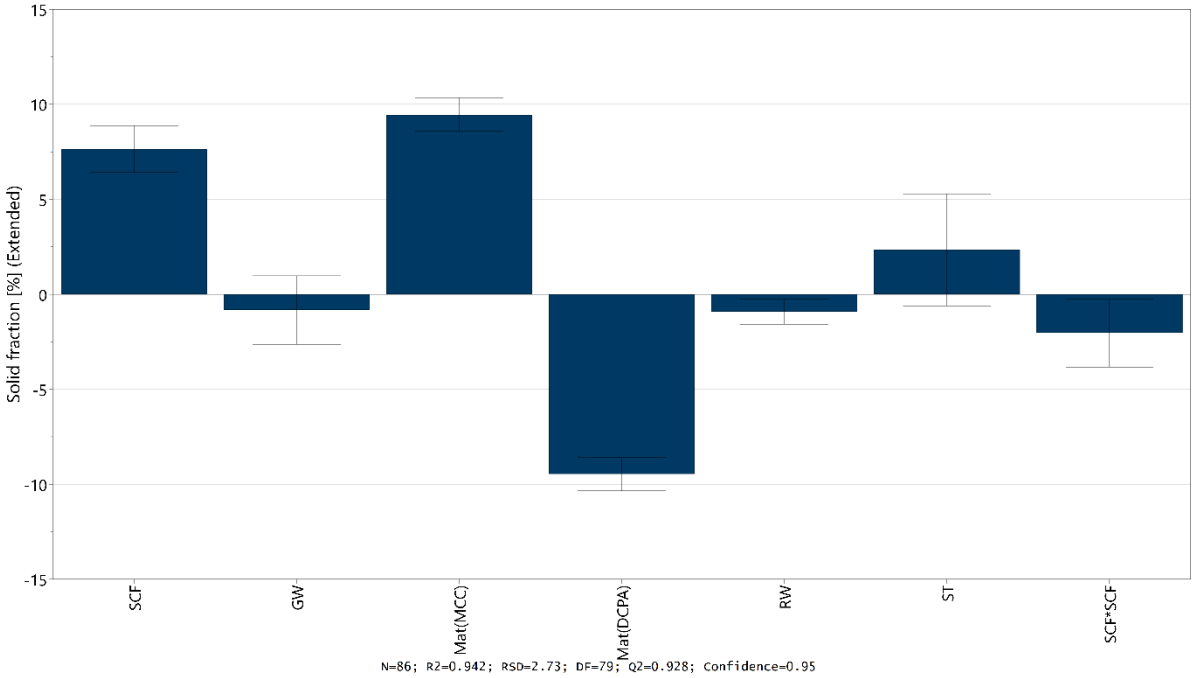

Figure 3.1-43: Coefficient plot for the effects of specific compaction force (SCF), gap width (GW), Material (Mat), roll width (RW), screw torque (ST) on the solid fraction of ribbons produced with the WP120

Nevertheless, the screw torque values give an idea of the pre-compaction inside the feeding system. The results from the statistical analysis strengthen the hypothesis that with larger gap widths, higher screw torques lead to greater pre-compaction of the material in the feeding system. However, further data collection is required to determine exactly how the screw torque affects the ribbon solid fraction.

To conclude, the roll compaction process with the WP120 was investigated for MCC and DCPA regarding the influence of gap width, roll width, specific compaction force and screw torque on the ribbon solid fraction. It must be emphasised that the process performance of the WP120 did not allow to conduct all planned experimental settings, especially higher specific compaction forces at higher gap widths caused problems. The experimental results were statistically analysed, and it was found that the ribbon solid fraction is influenced the most by the specific compaction force. The roll surface was critical for the process performance since a smooth roll surface did not allow sufficient material intake, which might be linked to the horizontal feeding system. The effect of grooved and squared surface was significant for DCPA, where a grooved roll surface leads to higher solid fractions compared to the squared surface. However, this effect was not observed for MCC. The roll width has a significant negative effect on the ribbon solid fraction. A higher roll width caused smaller solid fractions for both investigated materials.

3.1.4.2 Kp Factor Determination for the WP120

The MCC and DCPA ribblets were produced on the Styl'One at the same settings as on the WP120 with a default Kp factor of 1 (section 5.2.5.1). Since flat faced punches were used for the mimicking and one could not distinguish between the two different roll surfaces on the Styl'One, the experiments were performed only once, and the same dataset was used to determine the Kp factor for grooved and squared rolls. The same batches of MCC and DCPA were used as for the roll compaction experiments. Their powder densities are listed in Table 3.1-7. The ribblet solid fraction was determined by powder pycnometry with the GeoPyc (section 5.2.10.1).

In Figure 3.1-44, the solid fractions of MCC ribbons and ribblets in correlation to the specific compaction force for the 25 mm wide rolls are displayed. The figures a and c on the left contain the ribblet data with the default Kp factor of 1. The solid fractions of the ribblets for the 2 mm gap width are higher compared to the ribbons. For the 3 mm gap width, in contrast, the solid fractions of ribbons and ribblets are similar. This is valid for both roll surfaces.

The Kp factors for both materials, roll surfaces and gap widths were calculated separately. According to section 5.2.5.2, the best fit between ribbon and ribblet data was determined by minimising the RMSE. Figures b and d show the graphs with the adapted Kp factors for MCC. The Kp factors for the two roll surfaces at a gap width of 2 mm are identical with a value of 0.82. The Kp factors for the 3 mm gap width are 0.91 and 0.98 for the grooved and squared surfaces, respectively. The four adapted factors are all below 1, since the ribblets are denser than the ribbons and the curves must thus be shifted to the right. The factors are, unlike the factors for the Mini-Pactor and the BRC25, not independent of the gap width. The gap dependence can be explained by the above-mentioned pre-compaction in the feeding system of the WP120, which is not mimicked by the Styl'One. The overestimation of the solid fraction by the Styl'One, which was observed for the Mini-Pactor and the BRC25, was less pronounced for the 3 mm gap width due to the pre-compaction phenomenon and hence, this results in Kp factors closer to 1 for the bigger gap width. The four RMSE for the 25 mm roll width were smaller than 1.21. However, the Kp factors for the 3 mm gap width must be considered with caution as they are based on only 2 and 3 values of the compactor for the squared and grooved surfaces, respectively.

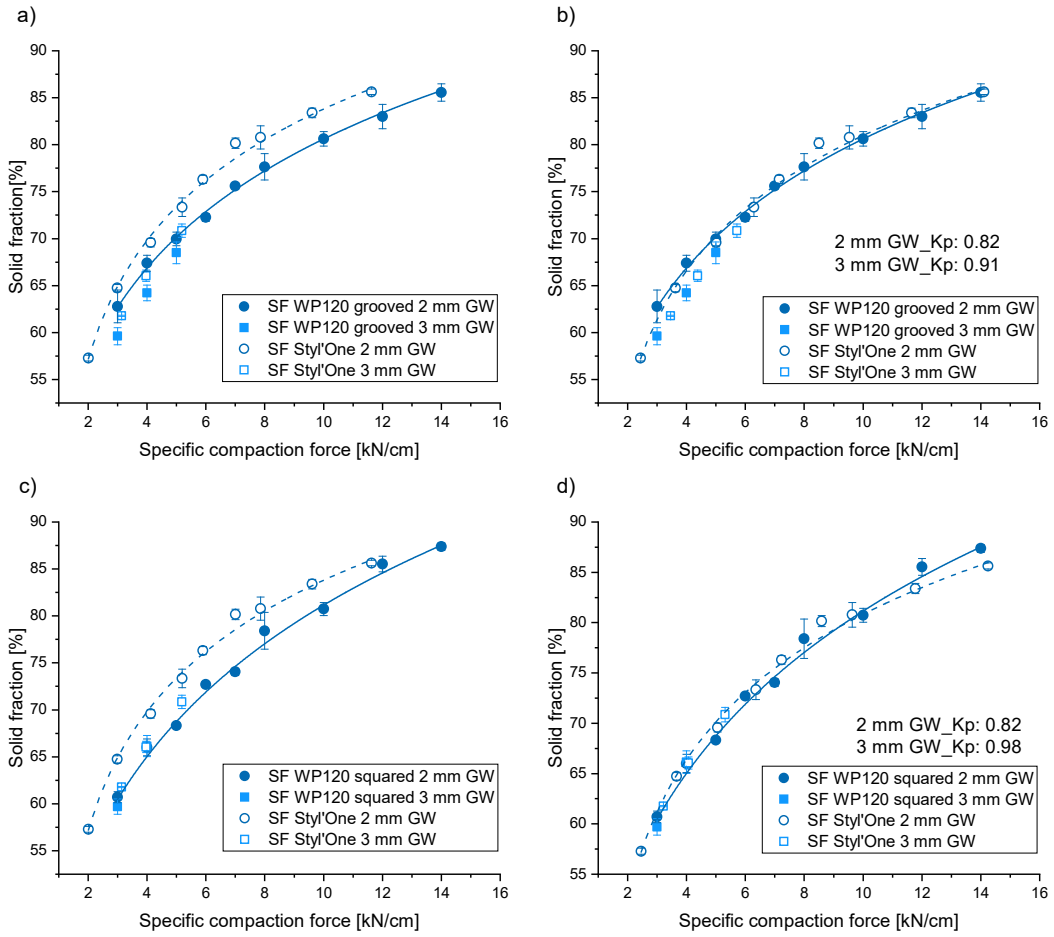

Figure 3.1-44: Solid fraction of MCC ribbons and ribblets in dependence on the specific compaction force (SCF) and the gap width (GW), 25 mm roll width a) grooved, Kp: 1; b) grooved, Kp: x; c) squared, Kp: 1; d) squared, Kp: x; WP120; n = 3; mean ± SD

Figure 3.1-45 displays the DCPA ribblet and ribbon solid fractions for the 25 mm wide rolls for the squared and grooved roll surfaces. The data for the default Kp factor of 1 are depicted in figures a

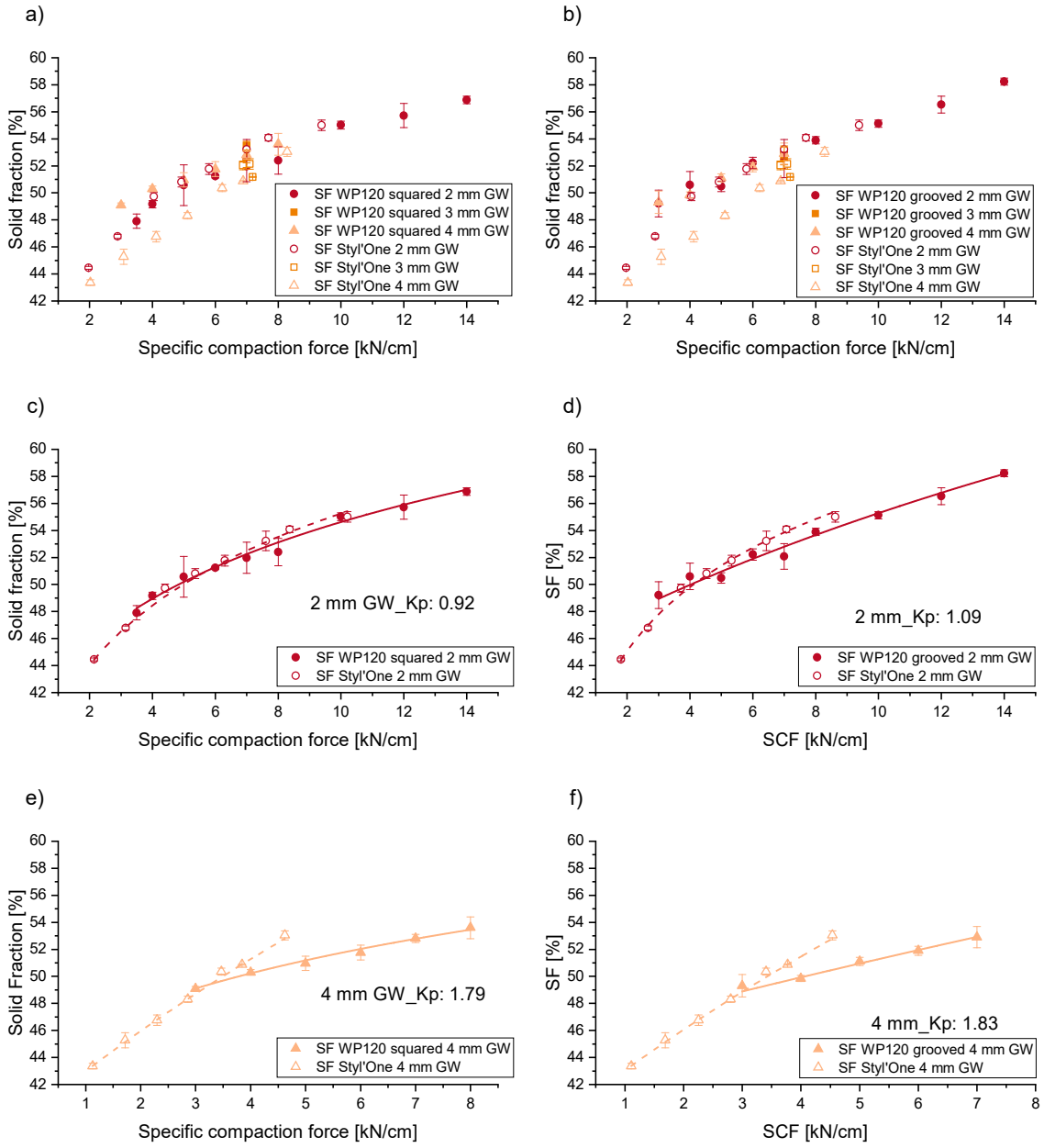

Figure 3.1-45: Solid fraction of DCPA ribbons and ribblets in dependence on the specific compaction force (SCF) and the gap width (GW), 25 mm roll width a) squared, Kp:1; b) grooved, Kp:1; c) squared, 2 mm GW, Kp:x; d) grooved, 2 mm GW, Kp:x; e) squared, 4 mm GW, Kp:x; f) grooved, 4 mm GW, Kp:x; WP120; n = 3; mean ± SD

and b. Here, it is noticeable that the values for the 2 mm gap are close together. Interestingly, for the 4 mm gap the opposite is the case: The Styl'One even underestimates the solid fraction. This results in Kp factors near to or above one. The data for the 2 mm gap width are shown in Figures c and d. Factors of 0.92 and 1.09 were found for the squared and grooved surfaces, respectively. The Kp factors for the 4 mm gap width (Figures e and f) are 1.79 for the squared and 1.83 for the grooved roll surface. The

four RMSE values were smaller than 1.26. The absolute values for the 4 mm gap must be treated with caution, since the overlapping part of the ribbon and ribblet curves is small. However, the values are definitively above 1, since the Styl'One underestimated the solid fraction and the curves must be shifted to the left.

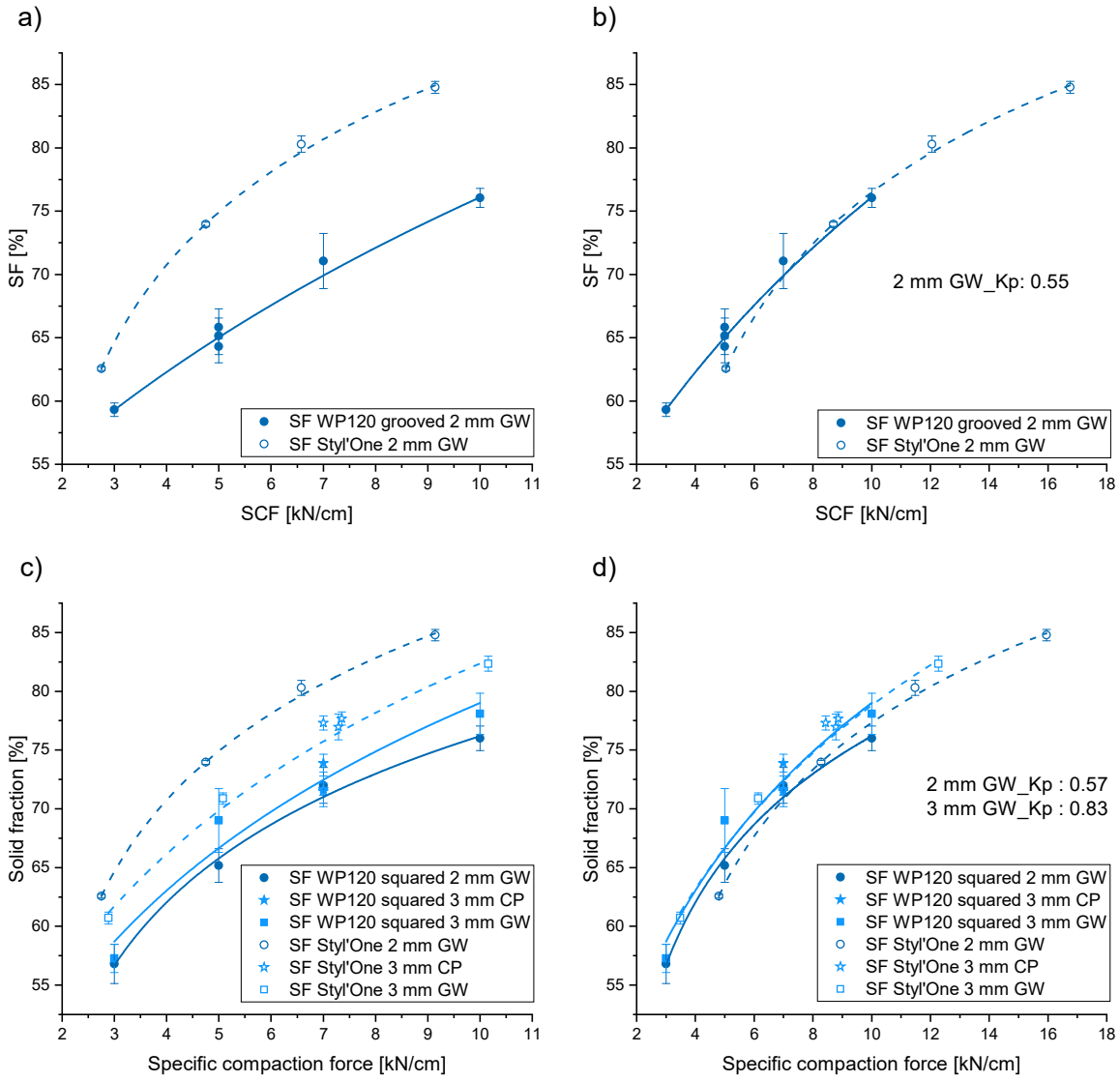

Figure 3.1-46: Solid fraction of MCC ribbons and ribblets in dependence on the specific compaction force and the gap width (GW), 40 mm roll width a) grooved, Kp:1; b) grooved, Kp:0.55; c) squared, Kp:1; d) squared, Kp:0.57 and 0.83; WP120; n = 3; mean ± SD

The results for solid fractions of MCC ribbons and ribblets for the 40 mm wide rolls are depicted in Figure 3.1-46. The Styl'One overestimates the solid fraction for both roll surfaces and gap widths (Figures a and c). The three RMSE values, which were used for the Kp factor calculations, are smaller than 2.19. To align the ribbon and ribblet solid fractions, a Kp factor of 0.55 was applied for the grooved

rolls at the 2 mm gap width (Figure b). A similar factor of 0.57 was found for the squared roll surface and a 2 mm gap width. The Kp factor at the 3 mm gap width for squared rolls was found to be 0.83. The higher Kp factor compared to the 2 mm gap width can be explained by the fact, that the solid fraction for the ribbons was higher at the 3 mm gap and not the other way around as it was expected and observed for the other compactors. Again, this behaviour cannot be mimicked by the Styl'One since the phenomena in the feeding system are not considered.

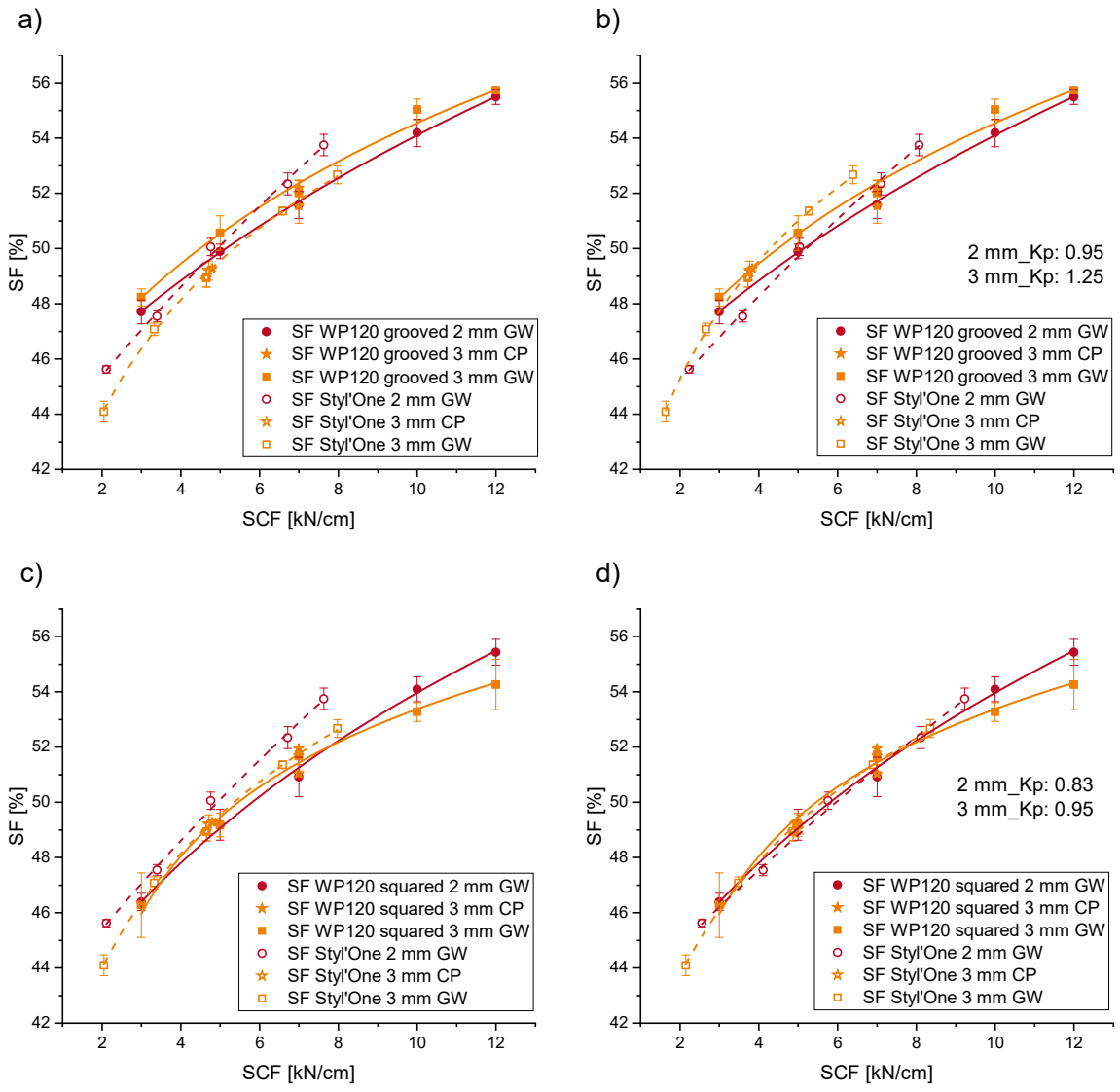

Figure 3.1-47: Solid fraction of DCPA ribbons and ribblets in dependence on the specific compaction force and the gap width (GW), 40 mm roll width a) grooved, Kp:1; b) grooved, Kp:0.95 and 1.25; c) squared, Kp:1; d) squared, Kp:0.83 and 0.95; WP120; n = 3; mean ± SD

The data for the Kp factor determination of DCPA for the 40 mm wide rolls are illustrated in Figure 3.1-47. The curves of ribbon and ribblet solid fraction overlap partially for the default Kp factor of 1.

The Kp factors were again determined by minimising the RMSE. The four RMSE are smaller than 0.54. Looking at the grooved roll surface (Figures a and b), this results in a Kp factor of 0.95, which is near to 1, for the 2 mm gap width and in a Kp factor above 1 of 1.25 for the 3 mm gap width. That one Kp factor is above and one is below 1, can be explained by the inverse correlation of the gap width and the solid fraction on the Styl'One compared to the WP120. The Kp factors for the squared roll surface (Figures c and d) are 0.83 and 0.95 for the 2 and the 3 mm gap width, respectively. Both Kp factors are below but close to 1 as the Styl'One slightly overestimates the solid fraction for both gap widths and the curves must be shifted to the right in order to align ribbon and ribblet solid fractions.

Table 3.1-8: Overview of the Kp factors for the WP120

DCPA	**2 mm GW**	**3 mm GW**	**4 mm GW**
25 mm grooved	1.09	/	1.83
25 mm squared	0.92	/	1.79
40 mm grooved	0.95	1.25	/
40 mm squared	0.83	0.95	/
MCC	**2 mm GW**	**3 mm GW**	**4 mm GW**
25 mm grooved	0.82	0.91	/
25 mm squared	0.82	0.98	/
40 mm grooved	0.55	/	/
40 mm squared	0.57	0.83	/

In contrast to the BRC25 and the Mini-Pactor, it was not possible to find a single Kp factor, which is valid for both tested materials, the process parameters and machine settings. Table 3.1-8 summarises the calculated Kp factors for the WP120. Although the factors differ in their absolute values and some must be treated with caution, they can be divided into groups and some trends can be identified. The Kp factors for DCPA are higher compared to MCC. They are closer to 1 or even above one, whereas the Kp factors for MCC are below 1. For both materials, a higher gap width leads to a higher Kp factor, which indicates that the ribbon solid fraction is influenced by pre-compaction in the feeding system to a higher

extent for the larger gap width as it was assumed above. For DCPA, the grooved roll surface results in higher Kp factors, whereas for MCC both roll surfaces show similar factors. This is due to the smaller effect of the roll surface on the ribbon solid fraction for MCC compared to DCPA. The Kp factors are for both materials smaller for the 40 mm than for the 25 mm wide rolls. This is in accordance with the statistical findings about the negative effect of the roll width on the solid fraction. For future improvement of the mimicking process, it might be possible to reduce the number of Kp factors by using a punch tooling that mimics the roll surface, e.g., squared instead of smooth, or to calculate an average gap width considering the geometry of the roll surface.

The Styl'One experiments allow to connect the compression pressure, which is applied on the powder bed during uniaxial compaction, with the corresponding specific compaction force for the WP120. Figure 3.1-48 depicts this correlation for the 25 mm roll width and grooved roll surface for MCC and DCPA. The compression pressure increases approximately linearly with an increasing specific compaction force.

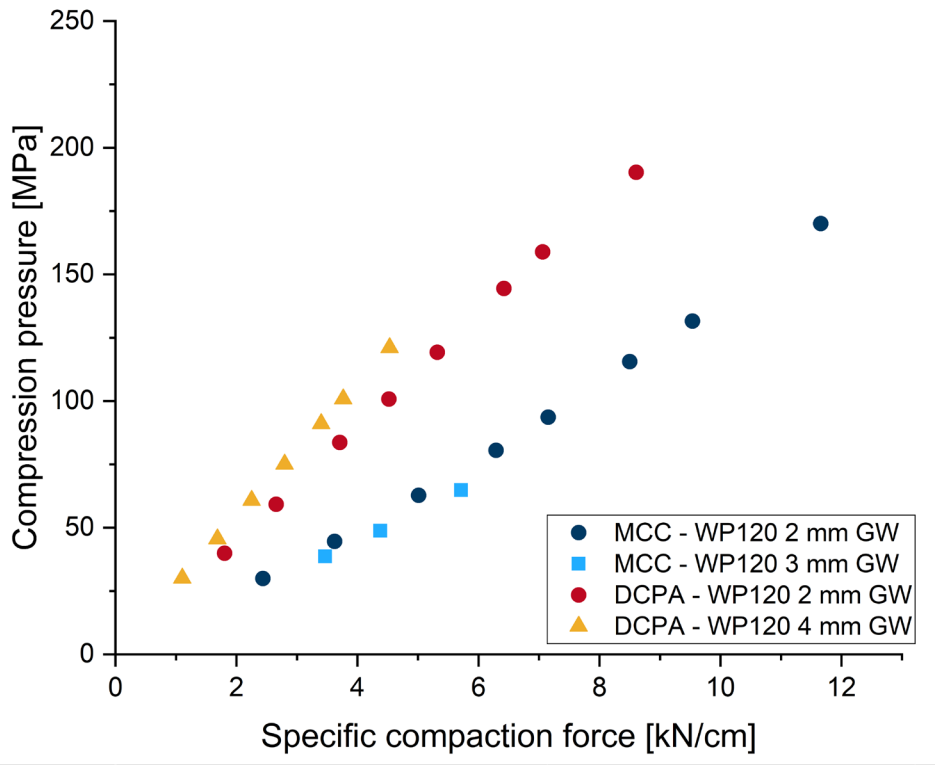

Figure 3.1-48: Correlation between the compression pressure and the simulated specific compaction force (WP120 with 25 mm wide grooved rolls) for MCC and DCPA at different gap widths (GW); n = 30, mean

One can see again that this correlation is material dependent and that it differs in the absolute values as well as in the slope of the curves. For DCPA a slight difference is visible between values for the 2 and the 4 mm gap width, whereas for MCC there are no clear differences between the 2 and the 3 mm gap

width. As stated in section 3.1.2.3, applying the same compression pressure results in ribbons with the same solid fraction. This underlines the observation that roll compaction of MCC at gap widths of 2 mm and 3 mm leads to similar ribbon solid fractions. In the case of the WP120, however, the compression pressure is not only generated by the compaction between the rolls but also includes the compaction in the feeding system. It is noticeable that the compression pressures for DCPA are higher for the larger gap width than for the 2 mm gap width at the same specific compaction force.

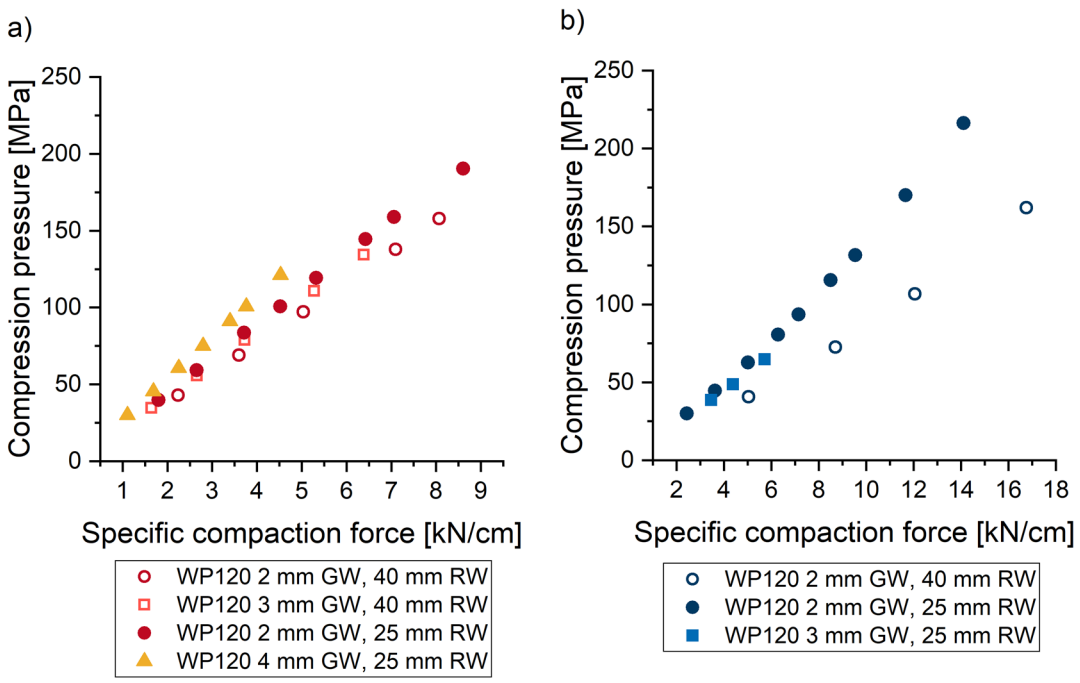

Figure 3.1-49: Compression pressure in relation to the simulated specific compaction force (WP120 grooved rolls) at different gap widths (GW) and roll widths (RW) for a) DCPA and b) MCC; n ≥ 20, mean

The correlation between the compression pressure and the simulated specific compaction force for 25 mm and 40 mm wide rolls are compared in Figure 3.1-49. For both materials, the correlations for the wider 40 mm rolls show smaller slopes compared to the 25 mm roll width. The same compression pressure results for the 25 mm wide rolls in smaller specific compaction forces than for the 40 mm wide rolls. In other words, if a specific compaction force of e.g., 9 kN/cm is set on the roll compactor equipped with 25 mm wide rolls the resulting pressure, which is exerted on the MCC powder, corresponds to appr. 115 MPa and if it is equipped with 40 mm wide rolls the same specific compaction force corresponds to appr. 72 MPa. This confirms the observations from above, that a higher roll width leads to ribbons with a smaller solid fraction.

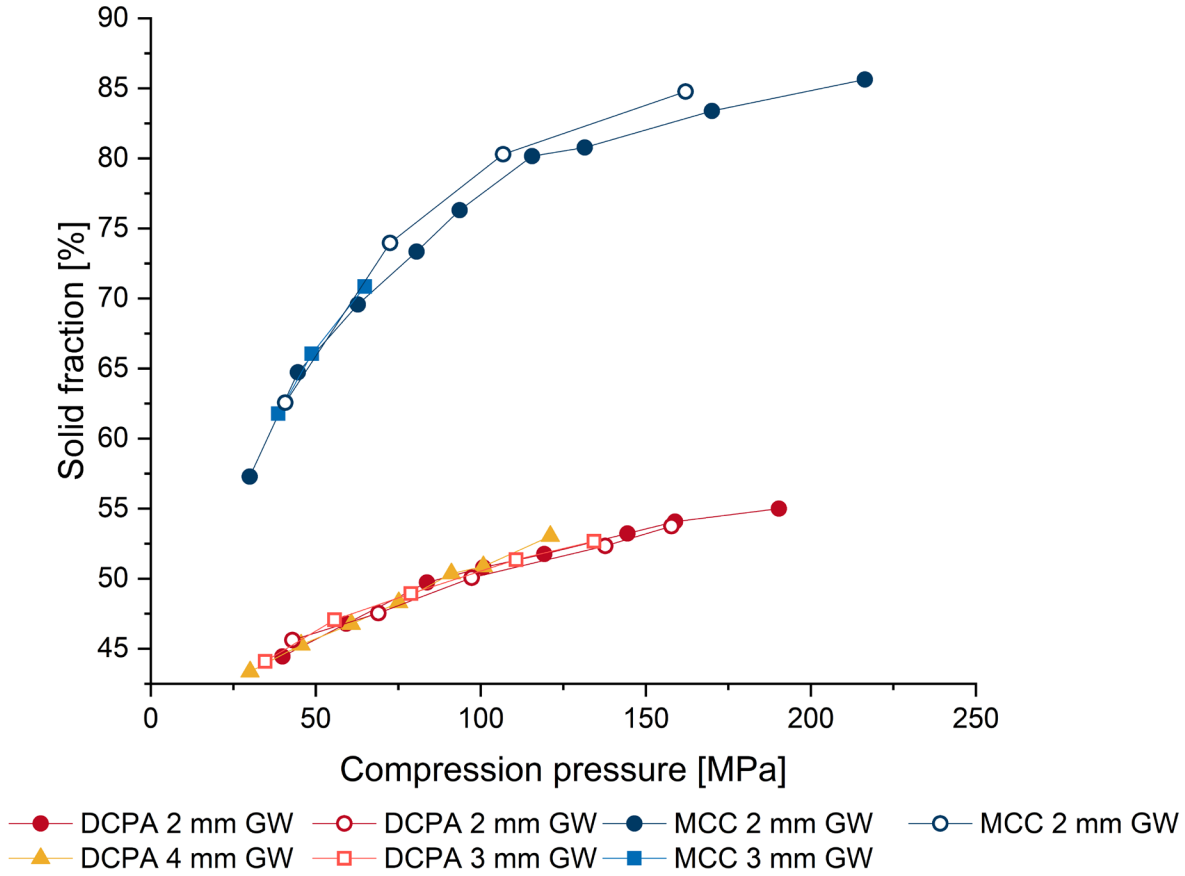

Figure 3.1-50: Correlation between the ribblet solid fraction and the compression pressure for MCC and DCPA at different gap widths; simulated WP120: 25 mm roll width (full symbols), 40 mm roll width (empty symbols); n = 3 (solid fraction), n ≥ 20 (compression pressure), mean

The correlation between the compression pressure on the Styl'One and the solid fraction of DCPA and MCC ribblets is shown in Figure 3.1-50. As already observed for the simulation of the Mini-Pactor and the BRC25, the solid fraction increases with an increasing compression pressure, whereas an increase in gap width or different roll widths at a constant compression pressure have no impact on the ribblet solid fraction. Since a flat faced pair of punches was used for the mimicking experiments and the differences between roll surfaces were modelled by adjusting the Kp factor, only one data set per material and gap width is shown in the figure. If one considers the results from the previous chapters about the Mini-Pactor (section 3.1.2.3) and the BRC25 (section 3.1.3.2), these similarities might be used for process transfer between equipment if the Kp factors for the compactors are available.

To conclude, the Kp factor determination for the WP120 for MCC and DCPA with varying roll widths and roll surfaces was performed. Interestingly, no single Kp factor was found but individual Kp factors for each material, roll width, roll surface and gap width.

3.1.5 Alexanderwerk WP200

3.1.5.1 Roll Compaction with the WP200

The roll compaction on the WP200 (section 5.2.4.5) was performed with MCC and DCPA. The full factorial multi-level experimental plan is shown in Table 3.1-9. The WP200 was equipped with rolls which have a diameter of 200 mm, a width of 75 mm and a squared surface. The specific compaction force was varied between 3 and 12 kN/cm. In contrast to the experiments on the WP120, the gap width was not part of the experimental plan and was kept constant at 3 mm. Instead, the effect of the roll speed was investigated.

Table 3.1-9: Full factorial multi-level experimental plan for the roll compaction of MCC and DCPA on the WP200

Factor	Level
Material	MCC, DCPA
Roll speed [rpm]	2.5, 5.2 (CP), 8
Specific compaction force [kN/cm]	3, 8, 12, (16)

The circumferential speed that corresponds to the speeds of the other roll compactors would be 2.5 rpm. However, the roll speed of 2.5 rpm was too small and exceeded the lower limit of the screw engine, when MCC was processed. Typical roll speeds in production are higher than the investigated 8 rpm. The manufacturer states that the maximum roll speed is 38 rpm. Since the material consumption would increase considerably at higher roll speeds, it was decided to work at low roll speeds even though they do not represent real production conditions.

The process data for the roll compaction of MCC is presented in Figure 3.1-51. During operation, unrealistically high values for the specific compaction force were repeatedly returned from the inverters to the controller. However, these were not real specific compaction force values but errors in the recording. The figure shows how the screw speed responds to changes in the specific compaction force and the roll speed. At higher roll speeds and higher specific compaction forces the screw must turn faster to transport enough material. At a roll speed of 2.5 rpm, the screw speed fluctuated strongly, and it was not possible to stabilise the gap. The motor is not designed for such a low roll speed since it does not correspond to the normal production settings. At higher roll speeds of 5.2 and 8 rpm, the process ran smoothly. The screw capacity remained in a low range of appr. 30 % during the whole process.

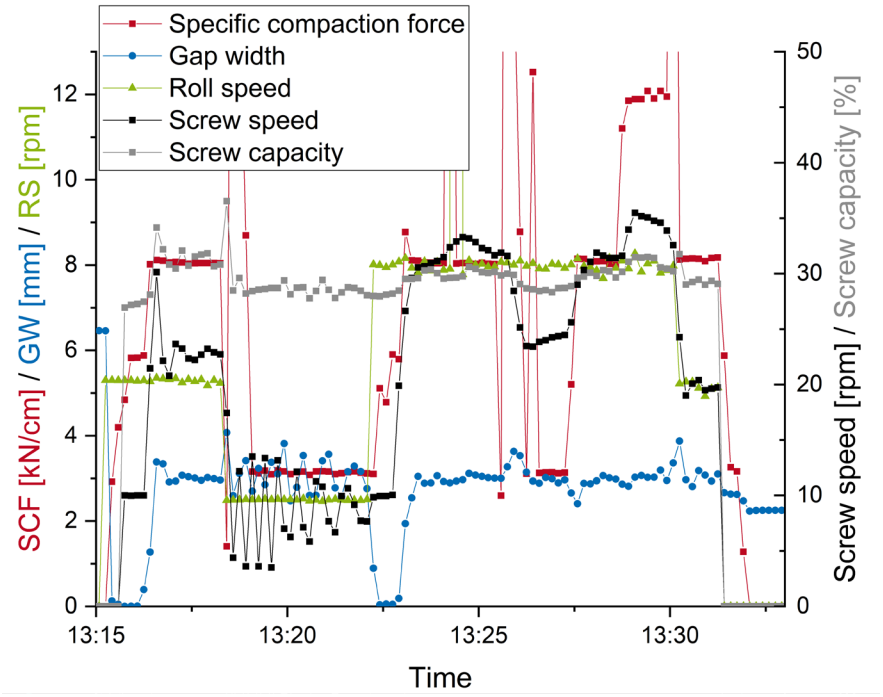

Figure 3.1-51: Process data of MCC roll compaction on the WP200; specific compaction force, gap width, roll speed, screw capacity and screw speed

Figure 3.1-52 shows the process data for the roll compaction of DCPA. In contrast to MCC, constant values for force and gap were quickly reached and were stable at the three investigated roll speeds.

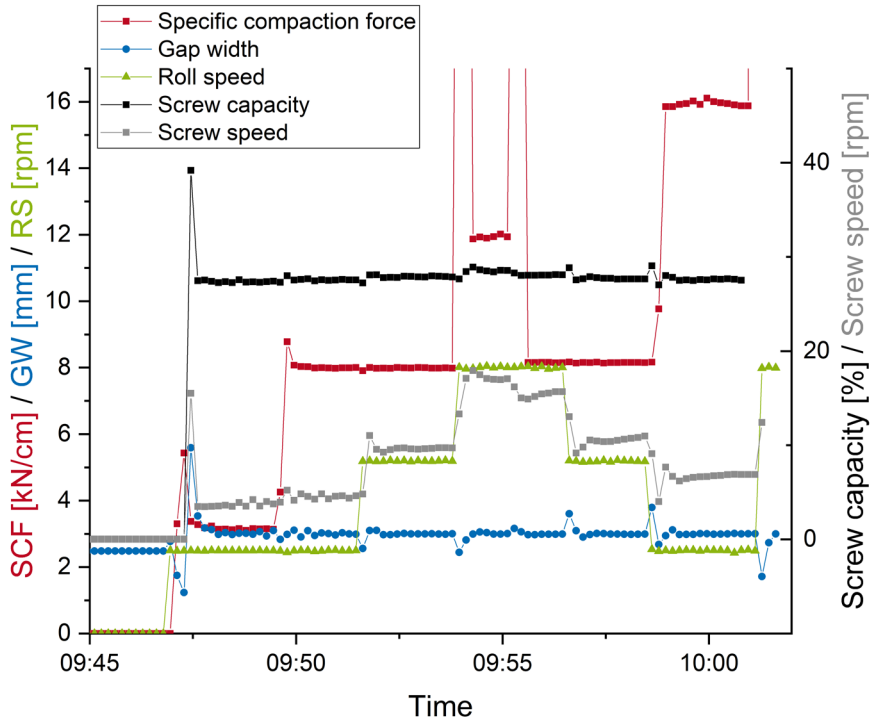

Figure 3.1-52: Process data of DCPA roll compaction on the WP200; specific compaction force, gap width, roll speed, screw capacity and screw speed

The screw speed increased with an increase in roll speed and specific compaction force since more material must be delivered to maintain the gap constant. The screw speed increased as well with an increasing specific compaction force, while the screw capacity remained constant around 30 % independent on the set parameter. The experimental plan was extended by the point 16 kN/cm at 2.5 rpm to explore the capabilities of the process. The ribbon solid fraction was measured by powder pycnometry according to section 5.2.10.1. The same batches of MCC and DCPA were used as for the roll compaction experiments on the WP120. Their powder densities are listed in Table 3.1-7.

Figure 3.1-53 illustrates the correlation between the solid fraction of MCC ribbons and the applied specific compaction force, produced at different roll speeds. As mentioned above, the 2.5 rpm roll speed could not be realised and only the roll speeds 5.2 and 8 rpm were evaluated. The ribbons were denser at higher specific compaction forces and the solid fraction ranged between 49 and 72 %. The ribbons at 8 kN/cm and 5.2 rpm roll speed had a smaller solid fraction than the ones produced at 8 rpm. This was an unexpected result, since a smaller roll speed should lead to prolonged compaction times and thus to a higher extent of compaction, especially for plastically deforming materials.

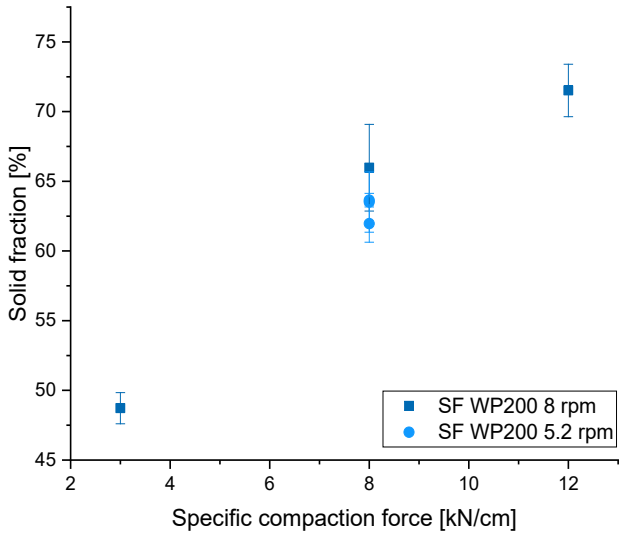

Figure 3.1-53: Solid fraction for MCC ribbons in dependence of the specific compaction force produced with the WP200 at two rolls speeds and a gap width of 3 mm; n=3, mean ± SD

Figure 3.1-54 depicts the ribbon solid fraction for DCPA produced at different roll speeds and specific compaction forces. The ribbon solid fraction increased with an increasing specific compaction force and ranged between 44 and 54 %. A clear conclusion concerning the effect of the roll speed on the solid fraction cannot be drawn due to the overlapping standard deviations. However, a trend can be seen that

the ribbons produced at a smaller roll speed have a higher solid fraction, which was contrary to the results for MCC ribbons.

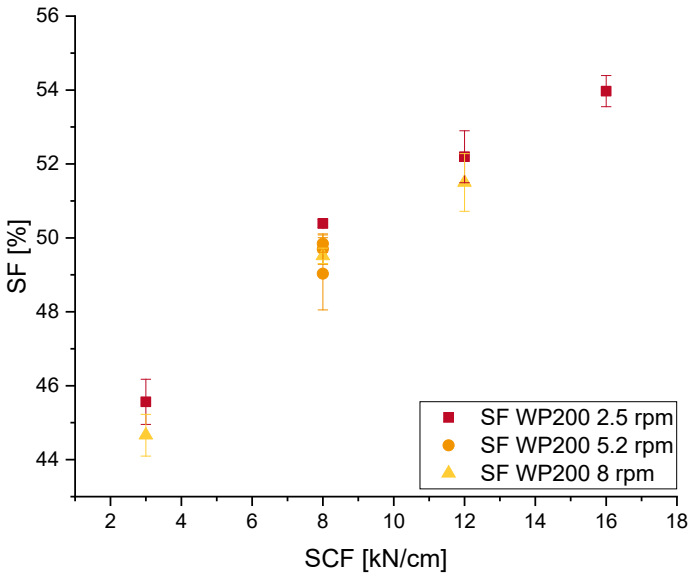

Figure 3.1-54: Solid fraction for DCPA ribbons in dependence of the specific compaction force produced with the WP200 at different rolls speeds and a gap width of 3 mm; n=3, mean ± SD

3.1.5.2 Kp Factor Determination for the WP200

The production of MCC and DCPA ribblets on the Styl'One was performed based on the experimental plan that was used for the WP200. The default Kp factor of 1 was used for the experiments. The ribblet solid fraction was determined by powder pycnometry (section 5.2.10.1). The same batches of MCC and DCPA were used as for the roll compaction experiments on the WP200. Their powder densities are listed in Table 3.1-7.

The differences in design between the two Alexanderwerk compactors are reflected in the punch displacement profiles used in the Styl'One software (Figure 3.1-55). The die filling phase is the same for both profiles, but the differences between the simulated roll compactors become visible in the punch movements of the subsequent compaction phase. Compared to the WP120, the punch displacement profile of the WP200 has a wider compaction zone at the same circumferential speed. This corresponds to the different roll diameters of 120 mm and 200 mm, respectively.

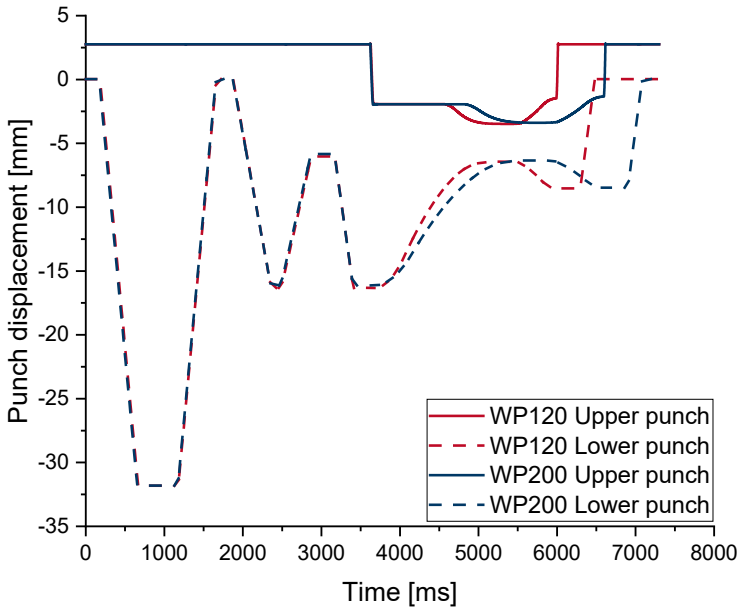

Figure 3.1-55: Punch displacement profiles of WP120 and WP200

In Figure 3.1-56 a, the MCC ribbon and ribblet solid fractions at 8 rpm are depicted with a Kp factor of 1. The ribblets show a higher solid fraction at the same specific compaction force. Thus, the Styl'One overestimates the solid fraction and the values must be shifted to the right to achieve an alignment. The Kp factor was calculated according to section 5.2.5.2 and in Figure 3.1-56 b the adapted curves are shown with the determined Kp factor of 0.63.

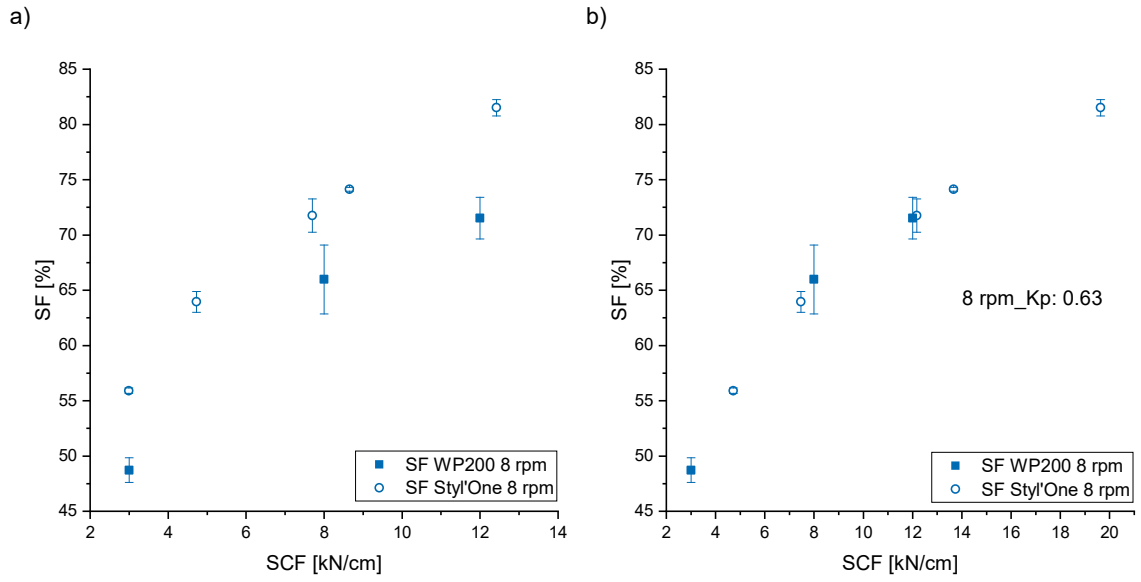

Figure 3.1-56: Solid fraction of MCC ribbons and ribblets in dependence on the specific compaction force and the roll speed; WP200, 75 mm roll width and squared roll surface; a) Kp:1; b) Kp:0.63; n = 3; mean ± SD

Figure 3.1-57 depicts the DCPA ribbon and ribblet solid fraction in dependence on the specific compaction force. Figures a and b give an overview and figures c-f show the data for 2.5 rpm and 8 rpm separately. The solid fractions of ribblets at a roll speed of 2.5 rpm are similar to the ribbon solid fractions. This results in a Kp factor of 0.97, which is close to 1. For the 8 rpm roll speed, the Styl'One slightly overestimates the solid fraction. A Kp factor of 0.87 was determined. However, the factors for both roll speeds must be treated with caution, since the underlying amount of data is small.

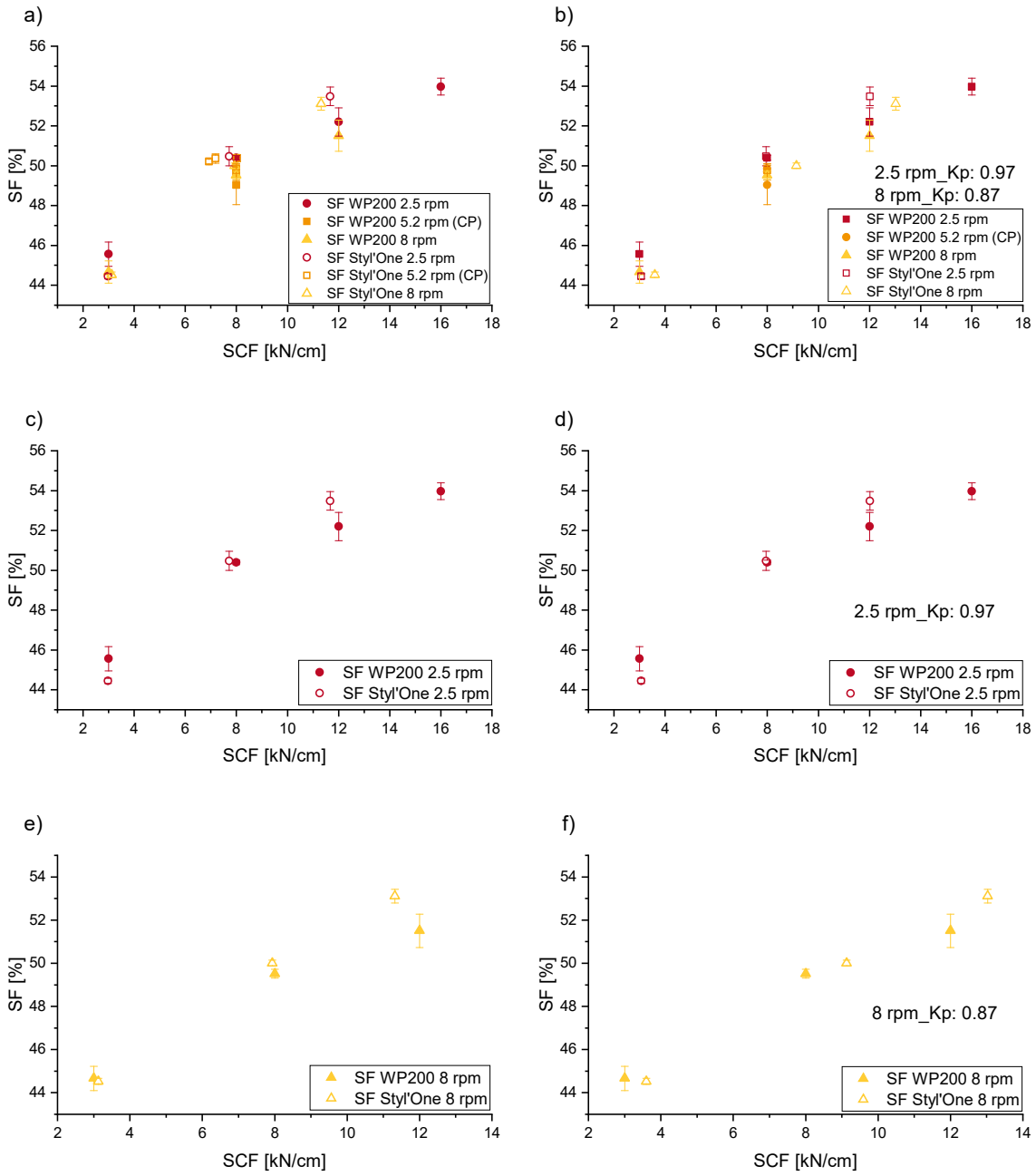

Figure 3.1-57: Solid fraction of DCPA ribbons and ribblets in dependence on the specific compaction force and the roll speed; WP200, 75 mm roll width and squared roll surface; a) Kp:1; b) Kp:0.97 and 0.87; c) 2.5 rpm, Kp:1; d) 2.5 rpm, Kp: 0.97; e) 8 rpm, Kp:1; f) 8 rpm, Kp:0.87

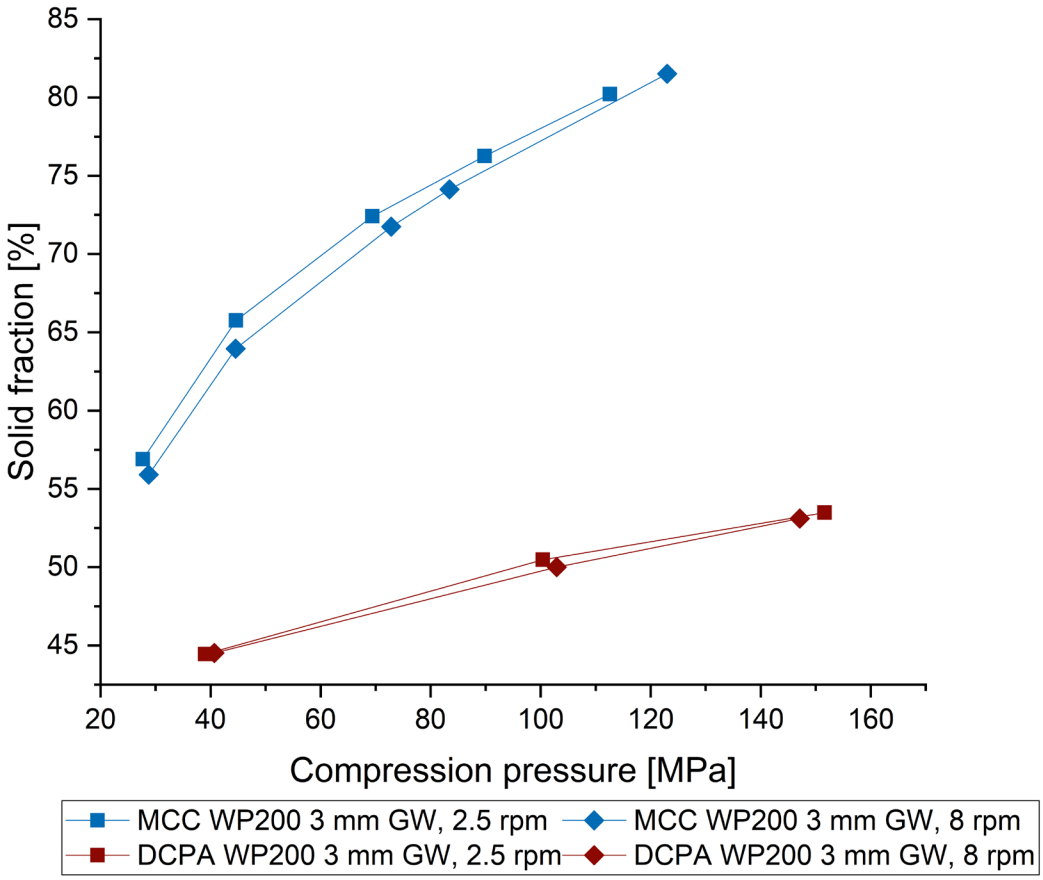

Figure 3.1-58: Correlation between the ribblet solid fraction and the compression pressure for MCC and DCPA at different roll speeds; WP200; n=3 (solid fraction), n ≥ 20 (compression pressure), mean

The correlation between the compression pressure on the Styl'One and the solid fraction of MCC and DCPA ribblets is shown in Figure 3.1-58. The experiments for MCC at a roll speed of 2.5 rpm could not be performed on the roll compactor due to technical limitations but were nevertheless carried out on the Styl'One. As observed in the simulations of the other roll compactors, the solid fraction increases with an increasing compression pressure. The change in roll speed from 2.5 to 8 rpm does not have a relevant influence on the ribblet solid fraction. However, a slight trend towards higher solid fractions at the lower roll speed can be observed for MCC ribblets.

To conclude, the Kp factors for roll compaction of MCC and DCPA on the WP200 were determined at different roll speeds. For MCC, however, only data with the roll speed of 8 rpm could be used for the Kp factor determination since the experimental plan could not be realised as planned due to the parameters being set unfavourably for the machine. It was found that the Kp factor is dependent on the compacted material as well as on the roll speed. It should be noted, however, that the Kp factors were determined based on very small amounts of data and must therefore be treated with caution. So far,

hybrid modelling cannot be used for the WP200 as a material-saving way of determining the required process parameters since a new calibration would be necessary for each formulation or material. Apparently, the model does not cover all relevant factors, which have an influence on the ribbon solid fraction.

3.1.6 Comparison of the Roll Compactors Mini-Pactor, BRC25, WP120 and WP200

Four roll compactors were evaluated regarding their process performance. Hybrid simulation of the roll compaction process was performed with the Styl'One. Some similarities and some differences were found between the compactors, which are highlighted in the following.

Regarding process performance, it was noticeable that not all process parameter settings could be carried out with all compactors. The range of feasible specific compaction forces and gap widths was larger for the BRC25 and the Mini-Pactor compared to the WP120. Furthermore, the feeding was found to be problematic for the WP120. This is probably related to the vertical arrangement of the rolls and the single-screw feeding system of the WP120, which cannot transport the material as well as the BRC25 and the Mini-Pactor, which are equipped with two screws and horizontally or inclined arranged rolls. Additionally, it must be considered that the experimental plan, which was used for the experiments on the WP120, was designed closely to the ones of the Mini-Pactor and the BRC25 and thus, might not have represented normal settings for this compactor. Nevertheless, it was possible to produce ribbons on the WP120 with the desired solid fraction.

The WP120 is a machine which is typically used for research and development or in small scale production, whereas the bigger WP200 is used for large scale production purpose. Figure 3.1-59 compares the solid fractions of DCPA ribbons produced with the same circumferential speed on the small- and the large-scale compactor. The ribbons from the WP200 have a smaller solid fraction compared to the ribbons produced on the WP120. The circumferential roll speed was the same for both roll compactor types, so that differences in solid fraction due to varying "dwell times" should be excluded. WP120 and WP200 differ geometrically mainly in their roll diameter and roll width, but also the feeding screws are of different sizes. Reynolds et al. (2010) showed that an increasing roll diameter and an increasing roll width result in a decreased maximum pressure on the rolls. The different sized screws lead to a different powder transport in the feeding system, which might relate to varying degrees of pre-densification. Taken together, this results in a smaller ribbon solid fraction for the WP200 compared to the WP120.

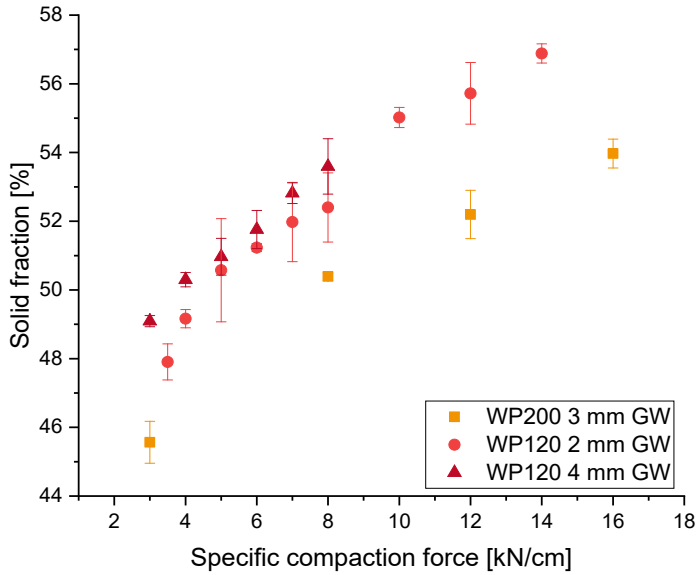

Figure 3.1-59: Solid fraction for DCPA ribbons produced at the same circumferential speed at various gap widths (GW) on the WP120 (squared roll surface, 25 mm roll width) and WP200 (squared roll surface, 75 mm roll width, 2.5 rpm); n=3; mean ± SD

In Figure 3.1-60, the solid fractions of MCC ribbons produced on different roll compactors – BRC25, Mini-Pactor and WP120 - are displayed. To be able to compare the compactors with each other, settings were chosen which were as similar as possible – a 2 mm gap width, equal circumferential speed, 25 mm roll width and smooth or grooved roll surfaces.

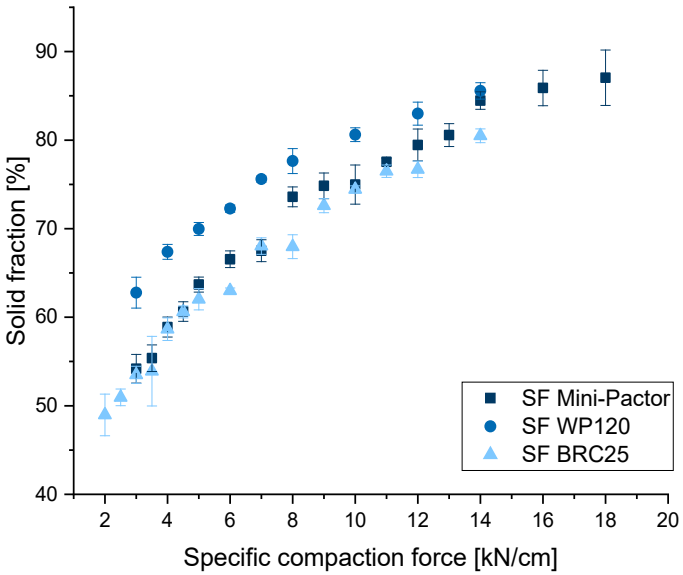

Figure 3.1-60: Solid fraction of MCC ribbons in dependence on the specific compaction force at a gap width of 2 mm compacted with smooth rolls and rim roll sealing system on the BRC25 and the Mini-Pactor and with grooved rolls and cheek plate sealing system on the WP120, 25 mm roll width; n=3, mean ± SD

The results obtained for the Mini-Pactor and the BRC25 are similar. Interestingly, on the WP120 the same ribbon solid fractions are obtained at smaller specific compaction forces compared to the other compactors. This difference is more pronounced at small specific compaction forces and decreases at higher forces, where the curves are converging. There are several explanations for the observed differences in solid fraction. The WP120 appeared to have relevant pre-compaction in the feeding system so that the material arrives at the rolls in an already denser bulk state. Furthermore, the WP120 was equipped with a vacuum de-aeration system to improve the powder transport towards the rolls, which increases the powder bulk density as well. In addition, the sealing systems differ between the investigated compactors. The BRC25 and the Mini-Pactor were equipped with rimmed rolls whereas cheek plates were used on the WP120. It is known that cheek plates result in an overall higher solid fraction compared to rimmed rolls (Csordas et al., 2018). Besides the feeding system, the arrangement of the rolls and the sealing system, the compactors differ also in their roll diameter. The BRC25 and the Mini-Pactor both have roll diameters of 250 mm, whereas the rolls of the WP120 are smaller with a diameter of 120 mm. Since the circumferential speed was kept constant for the compactors, the differences in solid fraction cannot be linked to different compression times. This supports the assumption that the roll diameter influences the ribbon solid fraction.

The relation between the compression pressure and the simulated specific compaction force for the investigated roll compactors is compared in Figure 3.1-61. The Kp factor defines the relationship between the compression pressure on the Styl'One and the specific compaction force on the corresponding roll compactor. This relationship is different for different gap widths. The same specific compaction force at different gap widths results in different compression pressures. And the same compression pressure corresponds to different specific compaction forces depending on the chosen gap width. Furthermore, the relationship between compression pressure and specific compaction force is different for different materials. The same compression pressure at the same gap width corresponds to different specific compaction forces depending on the processed material.

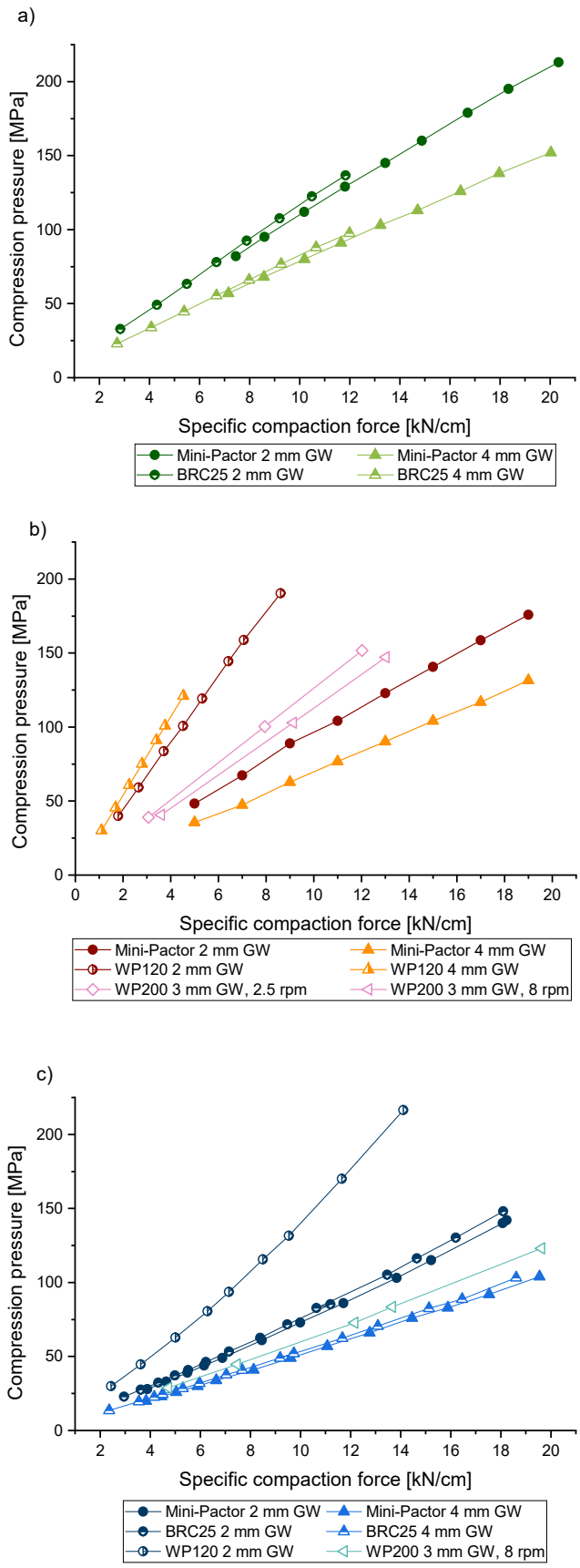

Figure 3.1-61: Correlation between the compression pressure and the simulated specific compaction force for a) lactose, b) DCPA, c) MCC; simulated WP120: grooved rolls, 25 mm roll width; mean, n ≥ 20

Differences but also similarities between the compactors can be seen in the figure. The SCF-CP correlations are similar for the BRC25 and the Mini-Pactor. This is valid for MCC and lactose in figures a and c, respectively. The WP120 and the WP200, in contrast, deviate considerably in their relationship compared to the other roll compactors. The relationships for the WP120 show higher slopes and from figures b and c it can be seen that smaller specific compaction forces are assigned to larger compression pressures compared to the Mini-Pactor. For DCPA (figure b), the compression pressure values for the 4 mm gap width are bigger than for the 2 mm gap width, which is opposite to the other roll compactors and might be linked to the pre-compaction in the feeding system of the WP120. These results mirror which was observed comparing the ribbon solid fractions: The WP120 produces ribbons with higher density than the Mini-Pactor and the BRC25 at the same specific compaction force. The WP200, as well, shows a higher slope in the SCF-CP correlation compared to the Mini-Pactor and the BRC25. The values for DCPA rank between those of the WP120 and the Mini-Pactor. The MCC curve (3 mm GW) lies between the 2 and the 4 mm GW curve of the Mini-Pactor and the BRC25.

In figure b (DCPA), it is noticeable that the roll diameters increase from the left to the right – from the WP120 (12 cm diameter), over the WP200 (20 cm diameter) to the BRC25 and the Mini-Pactor, which both have a roll diameter of 25 cm. The same trend can be observed in figure c (MCC), except the WP200 curve (3 mm GW). The smaller roll diameters, the possible pre-compaction and the cheekplate sealing system for the WP120 and WP200 compared to the other compactors apparently lead to a higher maximum roll pressure at the same specific compaction force – and the increased maximum roll pressure in turn is decisive for the higher ribbon solid fraction. However, for the WP200 the factors roll width and roll diameter are mixed so that their effects cannot be clearly distinguished.

The equivalent compression pressure to a certain specific compaction force is the smaller the bigger the gap width, the roll width and the roll diameter. Similar findings are reported by Hilden et al. (2011). In their work, however, the influence of the gap width is not considered.

The curves of all investigated compactors, showing the relationship between compression pressure and ribblet solid fraction for MCC, DCPA and lactose, are summarised in Figure 3.1-62. The ribblet solid fractions rank in a similar range for the respective materials, independent on the simulated roll compactor. The curves are also similar in their shape and slope. As already observed and described in the respective chapters for the different roll compactors, the correlation between the compression pressure and the ribblet solid fraction is not dependent on the gap width.

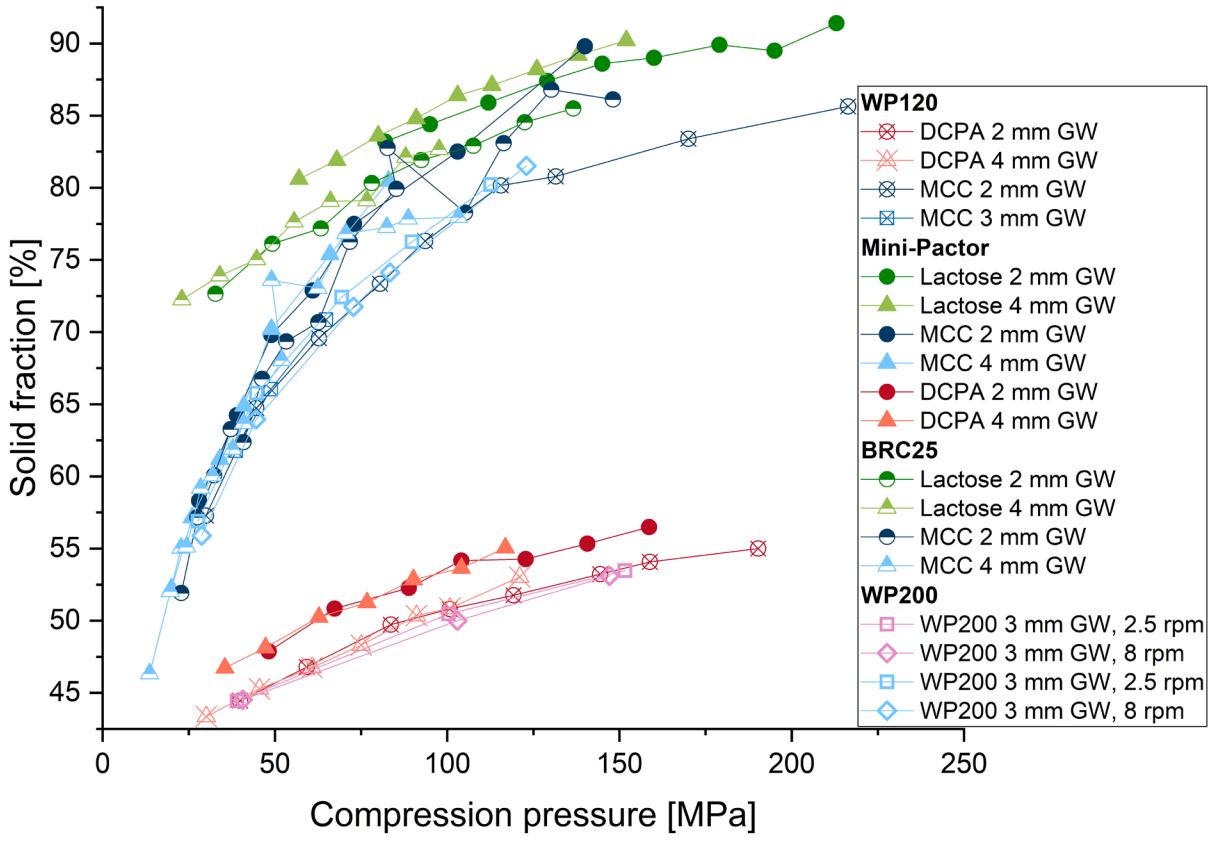

Figure 3.1-62: Correlation between the ribblet solid fraction and the compression pressure for WP120, Mini-Pactor, BRC25 and WP200; n ≥ 20, mean

Slightly differences between the compactors, e.g., in the solid fraction of DCPA ribblets, can be explained by different powder densities of the initial batches (Table 3.1-2, Table 3.1-4, Table 3.1-7). It becomes clear that a constant compression pressure results in ribblets with the same solid fraction for the respective materials. This and the knowledge about the relationship between specific compaction force and compression pressure (illustrated in Figure 3.1-61) allow that the required compression pressure can be determined based on the desired ribbon solid fraction. Based on the determined compression pressure, the required specific compaction force at a certain gap width for each compactor can be derived, provided that the Kp factor for the compactor is known.

The upscaling from the WP120 to the WP200 by maintaining the ribbon solid fraction constant can be explained using the example of DCPA. From Figure 3.1-62 it becomes clear that a compression pressure of 100 MPa will result in a ribblet solid fraction of appr. 51 %. From hybrid modelling, the correlation between the specific compaction force and the compression pressure is known for both roll compactors (Figure 3.1-61). With this knowledge, one can easily determine the specific compaction force corresponding to the compression pressure of 100 MPa: 4.5 kN/cm and 8 kN/cm for the WP120 and

WP200, respectively. The SCF-SF curve (Figure 3.1-59) for DCPA ribbons from WP120 and WP200 shows that these simulated specific compaction forces correspond very well with the ones on the compactors. However, no general Kp factor could be found for the Alexanderwerk compactor, so that this might be of small relevance in practice.

The following example for MCC from Figure 3.1-61 c shall illustrate the interrelationships also between the other compactors: A compression pressure of 75 MPa corresponds to a specific compaction force of 6 kN/cm for the WP120 at a gap width of 2 mm. The same compression pressure, in contrast, results in a specific compaction force of 10 kN/cm at gap width of 2 mm for the BRC25 and the Mini-Pactor. The WP200 experiments were performed at a gap width of 3 mm and in this case the compression pressure of 75 MPa is connected to a specific compaction force of 12 kN/cm. For the BRC25 and the Mini-Pactor at a 4 mm GW, the compression pressure of 75 MPa corresponds to a specific compaction force of 14 kN/cm. From the curves (Figure 3.1-62) describing the correlation between the compression pressure and the ribblet solid fraction, it can be seen that a compression pressure of 75 MPa results in similar ribblet solid fractions for all compactors regardless of the gap width. So, instead of using the specific compaction force as the comparative parameter between different roll compactors, it could be much more senseful to directly choose the compression pressure or maximum roll pressure for comparison, since it is the decisive factor for the ribblet or ribbon solid fraction. Unfortunately, the maximum roll pressure is often not known since force transducers on the roll surface are not the standard equipment of a roll compactor. However, hybrid modelling with the Styl'One can provide the important information, which specific compaction force corresponds to which compression pressure. This makes the transfer of a process to another equipment considerably easier and is a valuable support for the development of processes in early project phases as well as for upscaling issues.

3.1.7 Summary

Roll compaction experiments were performed with four different roll compactors – Mini-Pactor, BRC25, WP120, WP200 - to gain a deeper understanding of the roll compaction process and to investigate the influence of process and machine variables on the ribbon quality. The ribbon solid fraction was chosen as the critical quality attribute since it is crucial for the properties of the intermediate and final products resulting from the ribbons. In addition to the process parameters specific compaction force, gap width and roll speed, the influence of the roll compactor design was also evaluated regarding the roll surface, roll width and roll diameter.

The roll compaction process was simulated by the hybrid modelling approach using the compaction simulator Styl'One Evolution with the aim to establish a time- and material- saving method to determine the required roll compaction parameter settings to obtain ribbons with the desired solid fraction. The hybrid modelling approach was validated with the four above mentioned roll compactors, which differ in their machine design. The Kp correction factors, which are used to adjust the simulated specific compaction force for the Styl'One, were determined for the roll compactors. It was aimed to produce ribblets with the Styl'One, which show the same solid fractions as real ribbons from the roll compactors. It was investigated whether there is a single Kp factor for all roll compactors or whether the factor must be determined anew for each compactor. In addition, it was examined whether the Kp factor is dependent on the material properties and process parameters by considering different materials with varying compaction behaviour and a wide range of process parameter settings.

Ribbons were produced and the ribbon solid fraction was determined by powder pycnometry. It was confirmed that the specific compaction force has the greatest influence on the solid fraction of the ribbons. For all compactors, the solid fraction increases with increasing specific compacting force. The relationship between the specific compaction force and the solid fraction can be described by logarithm functions as shown in section 3.1.2.1. In addition, a quadratic negative effect of the specific compaction force was found, which is evident from the fact that the increase in the solid fraction is smaller at higher specific compaction forces. The investigation of the factor gap width showed for the BRC25 and the Mini-Pactor compactors that larger gap widths lead to lower solid fractions at the same specific compaction force. For the WP120, on the other hand, it was found that larger gap widths can result in ribbons with higher relative density. However, this could also be related to pre-compaction processes in the single screw feeding system. The roll width, which was investigated with the WP120 at 25 and 40 mm wide rolls, has a negative influence on the solid fraction. This means that a larger roll width results in ribbons with a smaller solid fraction. Furthermore, a small but significant influence of the roll surface on the solid fraction of the ribbons was observed, with squared rolls resulting in lower solid fractions than grooved rolls. Roll compaction with the BRC25 and the Mini-Pactor resulted in ribbons with similar solid fractions, whereas the ribbon solid fraction for the WP120 was generally higher compared to the other compactors. This can be attributed to several factors like the different sealing systems (rimmed rolls for the BRC25 and the Mini-Pactor and cheek plates for the WP120), the different roll diameters (Mini-Pactor and BRC25 have a 250 mm roll diameter, the WP200 has a roll diameter of

200 mm and the WP120 of 120 mm), the different feeding systems (one screw or two screws) and the partially smaller roll widths of the BRC25 and the Mini-Pactor compared to the WP120 and WP200.

The roll compactors were compared regarding their performance. It was found that they differ in some parts considerably in their process performance regarding the feasible parameter settings. While all planned settings could be carried out on the Mini-Pactor and the BRC25 (beside one setting at a high specific compaction force), stable processes could not be achieved on the WP120 for all intended settings, e.g., at the larger gap widths and at higher specific compaction forces. This is probably due to the limited powder transport capacity of the WP120's feeding system. It must be noted that the WP120 was probably not in its optimal working range due to the chosen process parameters.

The validation of the hybrid modelling and the determination of the Kp factors for the Gerteis Mini-Pactor and the LB Bohle BRC25 were successfully performed. Kp factors of 0.667 and 0.714 were determined for the Mini-Pactor and the BRC25, respectively. It was found that the Kp correction factor is material independent (tested with MCC, lactose and DCPA) and valid for different gap widths in the investigated design space. Once the Kp factors are determined, it is possible to produce ribblets with the same average solid fraction as ribbons from roll compaction. Due to the material- and process-parameter-independent Kp factors in the investigated design space, it is reasonable to assume that the hybrid modelling approach can also be extended to formulations that are composed of several components (section 3.4).

The determination of the Kp factor for the WP120 was performed with two materials, MCC and DCPA, considering beside the gap width and the specific compaction force also varying roll widths and roll surfaces. It was found that there is not only one Kp factor for the WP120, but that a separate Kp factor must be determined for each material, each roll width, each roll surface and each gap width. This eliminates the advantage of the hybrid modelling approach that the correct process settings can be found with little material input as it was possible for the Mini-Pactor and the BRC25. This variability of Kp factors was attributed amongst others to the fact that a pre-compaction in the feeding system occurred, which was not observed for the Mini-Pactor and the BRC25. The hybrid modelling approach does not cover this pre-compaction phenomenon and would have to be extended to achieve accurate predictive results for the Alexanderwerk compactors. It might be possible that the influence of the roll surface could be mimicked by working with punch tools with different surfaces corresponding to the roll

surfaces e.g., with squared punches. However, it would probably not be possible to simulate the influence of the roll surface on the powder intake.

The Kp factors for roll compaction of MCC and DCPA on the WP200 were determined at different roll speeds at several specific compaction forces and a constant gap width. For MCC, however, only data with the roll speed of 8 rpm could be used for the Kp factor determination since the smaller roll speeds were not typical production settings and thus not feasible on the machine. It was found again, like for the WP120, that the Kp factor is dependent on the compacted material and, additionally, on the roll speed. However, the observed influence of the roll speed must be treated with caution since the standard deviations of the ribbon solid fraction overlap with each other and the amount of data, which is used to calculate the Kp factor is small. It was not tested in the present thesis, if the roll speed has an influence on the Kp factors of the BRC25 and the Mini-Pactor, but it is assumed that the influence would be small due to the feeding systems with two screws. Apparently, the Kp factor cannot not cover all relevant factors, which have an influence on the ribbon solid fraction so that hybrid modelling for WP200 is at the moment not a material-saving way of determining the required roll compaction process parameters.

Relations between the ribbon/ribblet solid fraction, the compression pressure and the simulated specific compaction force were established for the investigated materials. It was found that this relationship is material dependent regarding absolute values and slopes. The same specific compaction force does not lead to the same compression pressure when different gap widths are used. However, independent of the gap width and independent on the simulated compactor, the same solid fraction resulted when the same compression pressures were applied to the same material. This leads to the assumption that it is not the specific compaction force but the resulting maximum roll pressure which is the decisive factor for the ribbon solid fraction. The specific compaction force seems to be dependent on the gap width and the material which is compacted. Interestingly, the curves (compression pressure – specific compaction force) for the Mini-Pactor and the BRC25 are almost identical. This might be due to the same model input parameters regarding the roll diameter and roll width. Furthermore, the compactors have a similar feeding system, which conveys the powder by two screws. The compactors WP120 and WP200, in contrast, showed considerable differences. Higher slopes cause that smaller specific compaction forces are assigned to larger compression pressures compared to the Mini-Pactor and the BRC25. Additionally, the roll compactors can be ranked regarding the relation between compression pressure and (simulated) specific compaction force according to their roll diameter. These findings underline the hypothesis that the roll compactor design has a great influence on the Kp factor and the ribbon quality.

It could not be conclusively clarified which influences exactly form the Kp factor. The feeding system, the roll width and the roll diameter seem to have an influence. This is also indicated by the fact that the Kp factors for the compactors, which are closest in their construction design, are similar. Furthermore, the differences in powder compaction between the roll compaction process and the die compression process like the non-uniform powder transport between the rolls could contribute to the Kp factor.

3.2 Solid Fraction Prediction – Elastic Recovery[2]

3.2.1 Introduction and Objectives

For the hybrid modelling approach, it was shown that it is possible to produce ribblets with the same average SF as ribbons from roll compaction (section 3.1). The simulation and mimicking with a uniaxial system are thus considered suitable to correctly mirror the roll compaction process. However, the prediction accuracy for the SF was not sufficient for the tested materials. The predicted ribblet SFs were often higher than the actual ones, especially for microcrystalline cellulose. It was assumed that the lack of prediction accuracy was due to the elastic recovery of the compacts, because the resulting volume expansion was not included into the hybrid modelling calculations (Reimer and Kleinebudde, 2019).

Elastic recovery is a well-known and widely investigated phenomenon in the field of tableting. According to Train (1956), the tableting process on the particle level can be divided into four stages. After forming a denser powder bed by slipping of the particles (stage 1) and the formation of temporary columns and vaults (stage 2), structural failure of the material occurs under fragmentation or plastic flow (stage 3). In stage 4, the voids of the porous compact further decrease and a structure of sufficient strength is formed. In the decompression phase, the tablet volume increases due to elastic recovery, which continues after ejection. Depending on material properties like the yield pressure, the indentation hardness and the elasticity, pharmaceutical powders show a predominant compression behaviour of fragmentation, plastic flow and/or elastic deformation (Roberts and Rowe, 1987). Antikainen and Yliruusi (2003) state that all materials show a more or less pronounced plastic and elastic part during compression, differing in their extent. Elastic recovery can be divided into two parts, the fast in-die elastic recovery and the slow out-of-die elastic recovery. For some materials, the elastic recovery can continue even for several hours or days after compaction (Picker, 2001). Several materials were tested and the in-die and out-of-die elastic recovery of the tablets at varying solid fractions was compared. The different extent of elastic recovery and the observed time dependencies were linked to material properties. Maarschalk et al. (1997) stated that stress relaxation of tablets after compression can manifest itself as tablet expansion and/or capping. A direct relation between the stored energy within the tablet and the volume expansion was found. High bonding capacities of powder combined with a high stored energy and a high ejection friction coefficient favour capping of the tablets. On the other hand, low bonding strengths combined with low ejection friction coefficients lead to tablets with low resistance

[2] Parts of this chapter were published in the article: **Keizer, H. L. and P. Kleinebudde**, 2020. Elastic Recovery in Roll Compaction Simulation. International Journal of Pharmaceutics 573, 118810. (List of Publications)

towards an increase in compact volume and thus an increase in porosity. Mazel et al. (2013) implemented a method to link the elastic moduli with the total elastic recovery of the compacts. Nevertheless, an instrumented die to measure the radial stresses is necessary. Katz et al. (2013) developed a method to characterise a material regarding its compression behaviour including the (visco-)elastic recovery in-die and out-of-die with only one compression cycle. It was assumed first, that the elastic recovery after decompression is equal to the increase in SF during the elastic deformation under pressure and second, that the elastic recovery is independent of the maximum pressure applied. Antikainen and Yliruusi (2003) on the opposite showed that there is a pressure dependency of the elastic recovery. They established an elasticity factor to characterise the elastic recovery in the decompression phase and implemented a method to quantify the pressure dependency of elastic recovery. Paronen and Juslin (1983) used the differences between in-die and out-of-die Heckel plots to characterise the fast and slow elastic behaviour of starches. Ilic et al. (2013) compared the deformation behaviour of pharmaceutical powders using in-die and out-of-die methods based on the Heckel and Walker equations. It was found that the in-die analysis falsely suggests higher compressibility than the out-of-die methods, since the elastic deformation is not considered in the in-die analysis. Furthermore, they suggested to use out-of-die methods, since they provide a more realistic picture of the properties of the final tablets.

The phenomenon of elastic recovery can be transferred from die compression to roll compaction. When ribbons exit the gap between the rolls, they undergo an elastic recovery. This results in ribbons thicker than the set gap width what is accompanied by a reduction in the ribbon SF compared to the powder under load (Patel et al., 2010). Mahmah et al. (2019) investigated the phenomenon of longitudinal and transverse ribbon splitting in roll compaction and linked it with the elastic recovery of the ribbons. A splitting index was introduced in analogy to the capping index for tableting (Akseli et al., 2013), that correlates the elastic recovery at a certain maximum roll stress with the ribbon tensile strength. Nkansah et al. (2008) introduced a method for the estimation of ribbon solid fraction by using the compaction throughput and included a correction factor that compensates for the relaxation after compaction.

Several approaches to mimic the roll compaction process have been introduced over time (section 1.3.2), but the number of literature taking into account the elastic recovery of the ribbons is limited. 2D finite element modelling was used by several authors (Cunningham, 2005, Dec et al., 2003, Michrafy et al., 2011b, Muliadi et al., 2012). In all studies, the ribbon density was calculated at the gap, but the extrusion zone and elastic recovery of the ribbons were not part of the modelling. Nesarikar et al. (2012b) used instrumented rolls to measure the normal roll stresses and developed statistical models to link the mean

ribbon density with the maximum normal stress and the gap width using out-of-die porosity – compression pressure profiles obtained by analysis of the pre-blend on a compaction simulator. In a further study (Nesarikar et al., 2012a), a placebo model was calibrated based on the Johanson equation to predict ribbon density for an API containing formulation and to facilitate the scale-up process. The approaches result in good prediction of ribbon relative density but instrumented rolls, which are necessary for the model calibration, are not always available. Reynolds et al. (2010) highlighted the importance of the roll compaction model input parameters material compressibility and the pre-consolidation relative density for the outcome of the prediction. Values estimated from the roll compaction process itself were compared with those from uniaxial compaction. The differences were attributed to the elastic recovery, which is considered in the measurements of the ribbon relative density after roll compaction, but not in the in-die measurements of the uniaxial compaction. It was concluded that the parameters estimated by uniaxial compaction would over-predict the ribbon density and model input data were taken from the roll compaction experiments. This led to an accurate ribbon density prediction but with the drawback of high material consumption for the preliminary roll compaction experiments. Toson et al. (2019) predicted the throughput and the final ribbon solid fraction with an in-silico DoE considering the elastic recovery. Nevertheless, compared to other modelling approaches the material consumption for the preliminary roll compaction experiments is relatively high.

In this chapter the evaluation of the elastic recovery of different materials after compaction is presented. The extent of elastic recovery - in-die and out-of-die - was measured regarding its dependence on the compression pressure, compression speed and powder bed thickness/gap width. The aim of this part of the work was to consider the elastic recovery inside and outside of the die in the hybrid modelling approach to allow not only the production of ribbons and ribblets with equal solid fraction but also to accurately predict the final ribblet and ribbon solid fraction.

3.2.2 Minimum Height Method

In section 3.1 it was shown that it is possible to produce ribblets which show the same solid fraction as real ribbons from roll compaction. In addition to this, the hybrid modelling approach allows a prediction of the ribblet solid fraction. The originally used approach is the minimum height method, which is described in more detail in section 5.2.5.3. Only two input information are needed for the calculations: the powder density of the starting material and the ribblet mass. Additionally, the envelope volume of the ribblet is necessary, which is calculated by the die dimension and the minimum distance between

upper and lower punch at maximum pressure. The dimensions of the die are constant and the distance between the punches is recorded by the displacement transducers of the Styl'One.

Figure 3.2-1 compares the ribbon and ribblet solid fraction determined by powder pycnometry with the predicted ribblet solid fraction in dependence on the specific compaction force. It was already shown in section 3.1 that the values for ribbons and ribblets overlap well. Analysing the predictions, a systematic overestimation of the solid fraction of MCC and lactose ribblets compared to the one measured by powder pycnometry can be noticed (Reimer and Kleinebudde, 2019). This overestimation is considerably more pronounced for MCC than for lactose. These findings are in accordance with the literature. Recently, Wünsch et al. (2019) compared the in-die and out-of-die compressibility of lactose, MCC and DCPA and found that the in-die compressibility curves lead to smaller porosity values / higher solid fractions than the out-of-die analysis.

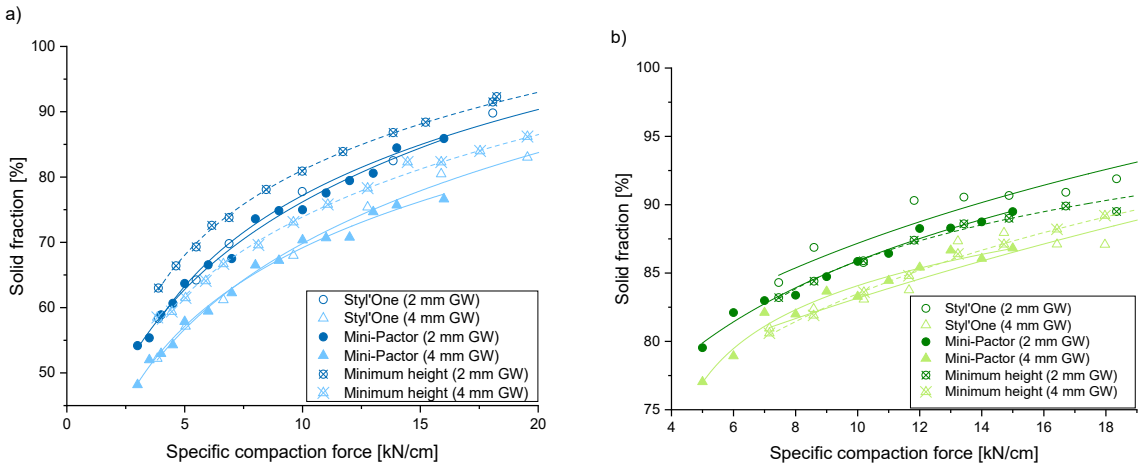

Figure 3.2-1: Measured solid fraction of ribbons (Mini-Pactor), ribblets and predicted ribblet solid fraction in dependence of the specific compaction force for a) MCC and b) lactose; powder densities listed in Table 3.1-2

The reason for the observed overestimation in the ribblet solid fraction prediction lays in the calculation approach (section 5.2.5.3). The lack in prediction accuracy of the minimum height method can be explained by two main weaknesses. First, the minimum distance between the punches does not represent the final thickness of the compacts after ejection since it does not consider the elastic recovery of the compacts. Second, the automatic learning phase is performed at a default force of 51 kN (255 MPa) and not the finally used one so that the pressure dependency of the elastic recovery cannot be considered. The ribblet solid fraction calculated by the minimum height method is an in-die solid fraction under maximum pressure whereas the solid fraction determined with powder pycnometry is an out-of-die

value, which includes the elastic recovery of the ribblets. It is therefore a natural consequence that differences between the predictions and the measurements were found.

For tablets, it was stated by Ilic et al. (2013) that out-of-die measurements of solid fraction are more realistic compared to in-die measurements and should therefore be preferred. This statement can be transferred to roll compaction. Since the ribbons undergo elastic recovery before they are milled to granules, the out-of-gap solid fraction is the more decisive factor for the downstream process than the value at the minimum gap width.

3.2.3 In-die Elastic Recovery

3.2.3.1 In-die Elastic Recovery of Different Materials

The raw materials used in this chapter were characterised regarding their powder density (section 5.2.9.5) and residual moisture (section 5.2.9.1). The results are listed in Table 3.2-1.

*Table 3.2-1: Material characteristics powder density and residual moisture (n=3, mean ± SD) * mean of different batches*

Material	Powder density [g/cm³]	Residual moisture [%]
MCC	1.5513 ± 0.305*	4.75 ± 0.36
DCPA	2.8555 ± 0.317	0.89 ± 0.17
Lactose	1.5439 ± 0.227	0.68 ± 0.12
Carrageenan	1.7332 ± 0.215	12.56 ± 0.48
HPMC	1.3017 ± 0.203	3.32 ± 0.67

In a first step, the fast in-die elastic recovery of ribblets was investigated. This is the elastic recovery which takes place inside the die, as soon as the upper punch upward movement starts, and pressure is released from the compacted powder bed. The fast in-die elastic recovery was evaluated regarding its dependency on the material, the compression pressure, the simulated gap width and dosage height. Furthermore, the influences of the dwell-time and the simulated roll speed were investigated. The in-die elastic recovery of MCC, HPMC, carrageenan, lactose and DCPA ribblets was determined at varying gap widths and specific compaction forces according to Armstrong and Haines-Nutt (1974) as described in section 5.2.11.2.

The results of the in-die elastic recovery evaluation are depicted in Figure 3.2-2. The mimicked specific compaction forces are displayed in the corresponding compression pressures in MPa to allow a better comparability between the different materials, since the specific compaction force-compression pressure-relationship differs between the materials as described in section 3.1.2.3. An in-die elastic recovery could be observed for all investigated materials, but to a different extent for each material.

The highest in-die elastic recovery can be observed for carrageenan with 5.0 % - 8.3 %, followed by the celluloses HPMC (4.4 % - 5.4 %) and MCC (2.2 % - 3.8 %). In contrast to that, DCPA and lactose undergo a smaller in-die elastic recovery of 1.1 % - 2.2 % and 0.7 % - 1.6 %, respectively. Carrageenan has distinct viscoelastic compression behaviour (Picker, 1999), which corresponds well with the high elastic recovery. The extent of elastic recovery is higher for the predominantly plastically deforming materials MCC and HPMC than for the brittle materials lactose and DCPA.

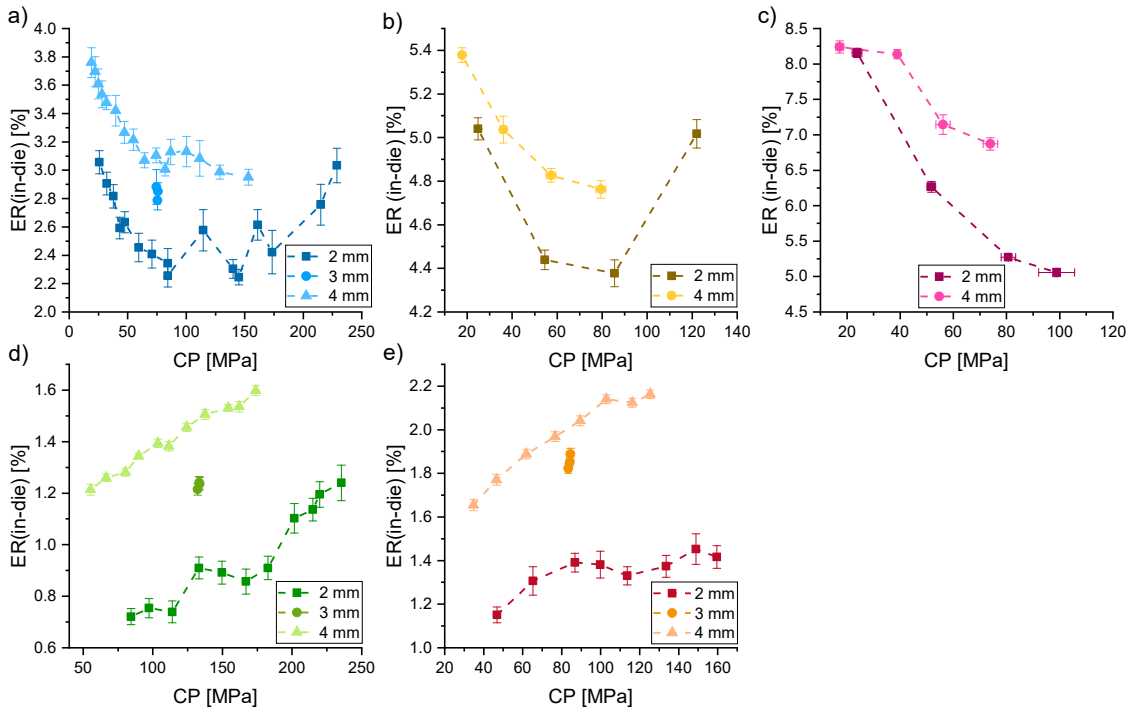

Figure 3.2-2: In-die elastic recovery in correlation with the compression pressure at different gap widths for a) MCC, b) HPMC, c) carrageenan, d) lactose, e) DCPA; n ≥ 20, mean ± SD

The in-die elastic recovery is dependent on the applied compression pressure. The elastic recovery of lactose and DCPA is increasing with an increasing compression pressure, which is in accordance with literature (Antikainen and Yliruusi, 2003). In contrast, for MCC, HPMC and carrageenan, the elastic recovery is decreasing when the compression pressure is increased. At higher pressures, HPMC and MCC show a reverse development, so that the elastic recovery increases again with an increasing

pressure (Mazel et al., 2013). Antikainen and Yliruusi (2003) associated the different behaviour at low and high pressures with air trapped in the powder bed. The more brittle materials lactose and DCPA mainly deform under fragmentation. A higher portion of the new particles created by fragmentation might be under stress at higher compression pressures, which results in an increasing elastic recovery with an increasing compression pressure (Ilic et al., 2013).

The mimicked gap width has as well a distinct influence on the elastic recovery. An increased simulated gap width leads to a higher elastic recovery for all tested materials regardless the applied compression pressure. It is important to keep in mind that the dosage height, which is the equivalent to the feeding screw speed on the roll compactor, increases with an increasing compression pressure and that the dosage height is approximately doubled comparing a 2 mm with a 4 mm gap width (Figure 3.1-19). Thus, under a constant compression pressure and a higher simulated gap width a bigger amount of material is compressed. Due to the increasing shear and frictional forces, which are exerted on the thicker powder bed inside the die, the material undergoes less plastic or brittle but more elastic deformation. The elastic deformation is reversible and the release of the stored elastic energy results in an increased elastic recovery for big gap widths compared to small gap widths.

Based on these observations, it is reasonable that an implementation of the in-die elastic recovery in the simulation can lead to an improved predictive accuracy, since a better prediction of the final ribblet volume would allow a more accurate calculation of the ribblet solid fraction out of the die.

Dependence of the Elastic Recovery of MCC on the Dwell Time and the Roll Speed

Dwell time is defined as the period, in which the maximum force on upper and lower punch is held constant (section 5.2.11.2). The influence of the dwell time on the in-die elastic recovery of MCC was investigated and the results are displayed in Figure 3.2-3a. The powder was compressed at 17.5 MPa, the dosage height was 10 mm. A decrease of the in-die elastic recovery was observed with an increasing dwell time from 1.4 % at 600 ms to 0.8 % at 3000 ms. An increased dwell time gives the MCC particles more time to deform plastically under pressure. The extent of plastic deformation becomes bigger which leads to a less pronounced relaxation after the pressure is released from the powder (Anuar and Briscoe, 2009). Haware et al. (2010) investigated the influence of the dwell time on different materials. It was shown that the dwell time effects the elastic recovery of elastically deforming materials the most, followed by plastically deforming materials whereas no influence on fragmentating materials was observed.

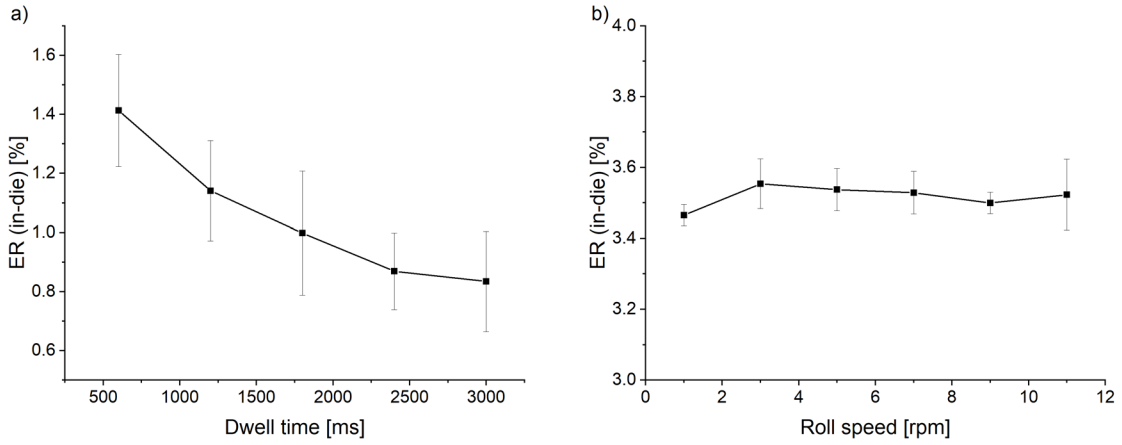

Figure 3.2-3: In-die elastic recovery in dependence of a) dwell time and b) roll speed for MCC; mimicked roll compactor: Mini-Pactor; n=10, mean ± SD

The effect of the dwell time cannot be directly transferred to roll compaction since the rolls do not stop to move for a certain time, but the movement is a continuous rotation. However, altering roll speed could affect the deformation of the particles due to different residence times between the rolls. The influence of the roll speed on the in-die elastic recovery was investigated on the Styl'One by mimicking roll speeds between 3 and 11 rpm at 6 kN/cm (32 MPa). No relevant change could be observed, the values fluctuated around 3.5 % (Figure 3.2-3). From Anuar and Briscoe (2009) it is known that starch tablets show a compression velocity dependent elastic recovery. However, it was stated as well that the speed of industrial rotary die tablet presses is too high to observe this phenomenon in practice. The same can be assumed for the mimicked roll speeds which are too high to observe a reduction in elastic recovery of the MCC compacts with a decreasing velocity. Furthermore, MCC shows a smaller extent of time dependent plastic deformation than starch (David and Augsburger, 1977) which may impede an observation of the phenomenon.

3.2.3.2 Zero Force Method

The findings concerning the fast in-die elastic recovery described in the previous chapter have been incorporated into the software and the zero force method was developed, which is described in more detail in section 5.2.5.3. It should improve the solid fraction prediction accuracy of the hybrid modelling approach. As described in section 5.2.11.2, the elastic recovery can be measured in-die. Armstrong and Haines-Nutt (1974) introduced this method but at the time the accuracy of the used equipment was not able to measure elastic recovery values of less than 2 %. However, the Styl'One provides sensors, which can detect in-die elastic recovery with better accuracy, so that the calculation of the ribblet volume can be adapted. Instead of using the minimum distance between upper and lower punch at maximum force,

the distance between the punches is taken, when the force at the upper punch decreases to zero during its upward movement after the compression. The predictive capability of the zero force method was tested using MCC and lactose which were compacted at three different simulated specific compaction forces and two gap widths.

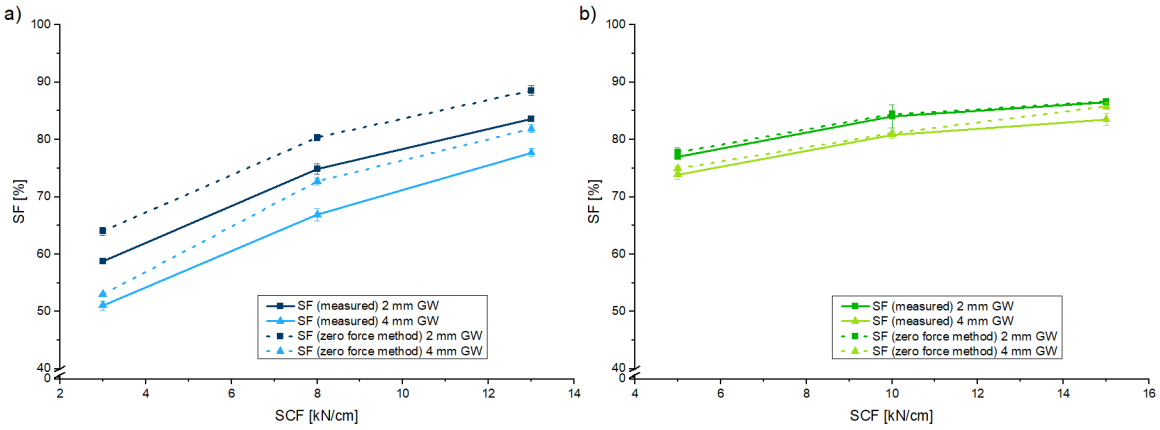

Figure 3.2-4: Comparison of the solid fraction measured by powder pycnometry with the solid fraction predicted by the zero force method for a) MCC and b) lactose in dependence of the specific compaction force (SCF) at two gap widths (GW); n ≥ 3, mean ± SD

Figure 3.2-4 shows the measured MCC and lactose ribblet solid fraction compared to the values, which were predicted with the zero force method. The powder densities of MCC and lactose used in this experiment are listed in Table 3.2-2.

Table 3.2-2: Powder density of MCC and lactose used for evaluation of the zero force method; n=3, mean ± SD

Material	Powder density [g/cm³]
MCC	1.5194 ± 0.0053
lactose	1.5467 ± 0.0020

For MCC, the predicted solid fractions are higher than the measured ones for the tested specific compaction forces and for both gap widths. The differences between prediction and measurement range from 2 to 6 % in solid fraction. Compared to the minimum height method, the prediction accuracy was improved but the solid fraction is still over-estimated. MCC shows as well a slow out-of-die elastic recovery (Picker, 2001). This would lead to a further increase in volume and thus, the solid fraction further decreases outside the die. For lactose in contrast, the predicted solid fractions match the measured ones accurately. The differences between the predicted and the measured values are smaller than 2 % solid fraction. It is reported that the out-of-die elastic recovery of lactose is small (Maarschalk et al.,

1997). This would explain the smaller deviations between the prediction and the measurements compared to MCC.

These findings lead to the question, how the materials differ in terms of their slow out-of-die elastic recovery, and if the consideration of the relaxation events outside the die can improve the prediction accuracy for materials like MCC.

3.2.4 Out-of-Die Elastic Recovery

3.2.4.1 Chromatic Confocal Measurement of the Axial Elastic Recovery

Following the findings in the previous section about the fast in-die elastic recovery, the slow out-of-die elastic recovery of pure MCC, lactose and carrageenan should be further investigated. The gain in height of the ribblets, which were produced at a mimicked gap width of 4 mm and at pressures between 50 and 250 MPa on the Styl'One, was monitored contactless with a chromatic confocal probe (CHRocodile E, Precitec Optronik GmbH) over a period of 30 minutes after ejection (section 5.2.11.3). The results are depicted in Figure 3.2-5.

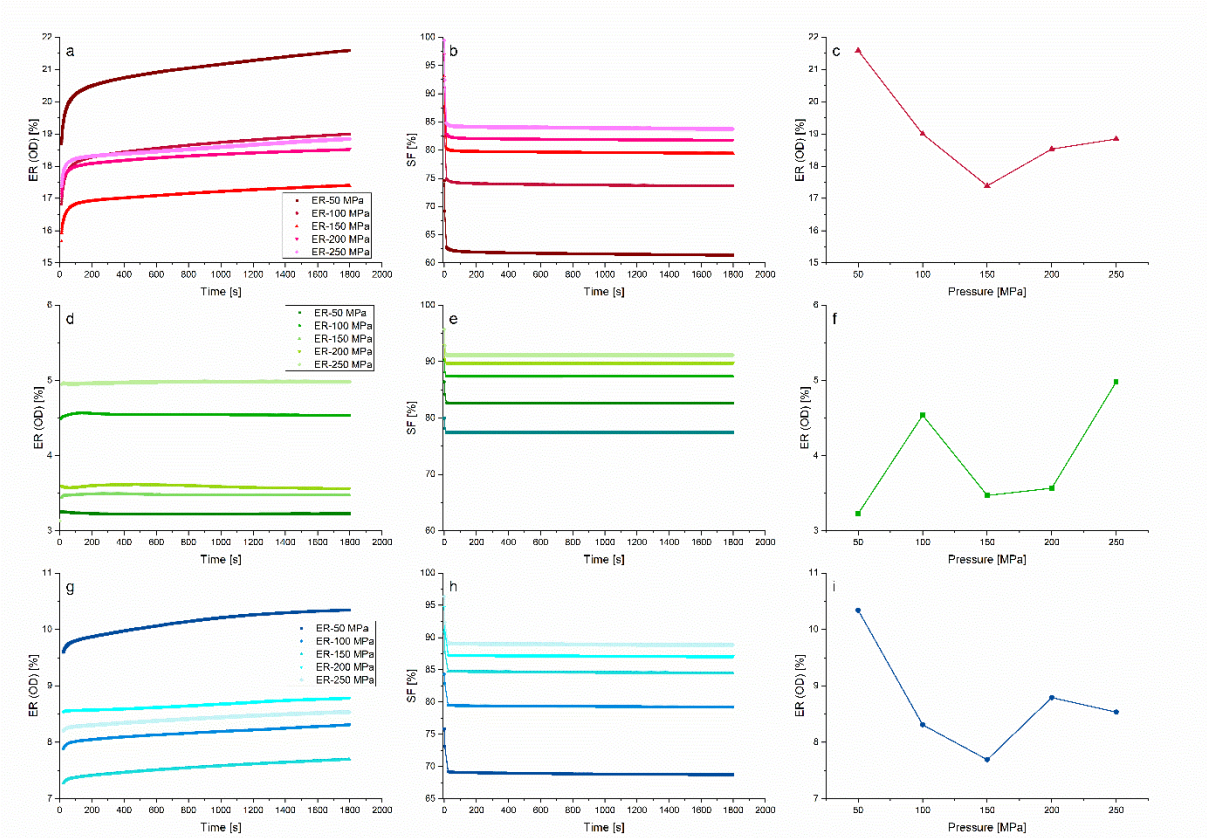

Figure 3.2-5: Axial out of die elastic recovery of carrageenan (a, b), lactose (d, e) and MCC (g, h) ribblets over 30 min; elastic recovery after 30 minutes (c, f, i); n = 2, mean

Carrageenan, which has distinct elastic compaction behaviour, shows the largest elastic recovery after ejection (17 % - 22 %), followed by the plastically deforming MCC (7 % - 10 %) and the predominantly brittle deforming lactose (3 % - 5 %). For lactose compacts, the elastic recovery is comparatively small and seems already to be completed only seconds after the ejection. After the first seconds, no further change in tablet height was detected. This smaller and faster elastic recovery was observed as well for DCPA by Haware et al. (2010), who attributed this behaviour to the particle fragmentation under load. The compacts containing of lactose showed capping at the edges, which is in accordance with the findings of Maarschalk et al. (1997). They stated that plastic materials like MCC can release the stored energy in volume extension whereas the stress release in compacts containing brittle materials like lactose leads to capping issues because they are not able to undergo enough elastic recovery.

The extent of the out-of-die elastic recovery is dependent on the applied compression pressure, which confirms the findings of Ilic et al. (2013). However, there is no linear relationship between pressure and the elastic recovery after 30 minutes (Figure 3.2-5 c, f, i). The elastic recovery of MCC compacts decreases at compression pressures between 50 and 150 MPa before it increases again at 200 MPa, which is in accordance with the observed in-die effects (section 3.2.3). The elastic recovery of carrageenan compacts decreases as well at low pressures and increases between 150 MPa and 250 MPa. The elastic recovery of lactose compacts was small and fluctuated between 3 and 5 % in the considered pressure range showing no clear trend.

The change in solid fraction (section 5.2.10.3) due to the out-of-die elastic recovery is most pronounced in the first seconds because the speed of relaxation is highest at the beginning and decreases with the time. Carrageenan shows the highest decrease in solid fraction of up to 15 % due to volume increase. The solid fraction of MCC compacts decreases by around 5 % whereas the solid fraction of lactose decreases by less than 2.5 %. This further decrease in solid fraction outside the die confirms the observed discrepancies between the prediction based on the in-die method and the measured values out-of-die presented in Figure 3.2-4.

3.2.4.2 Long-term Axial Elastic Recovery

The two materials showing the lowest and the highest elastic recovery, lactose and carrageenan, were chosen to monitor the axial elastic recovery in long-term. The thickness of the ribblets produced at 50, 150 and 250 MPa was determined with a calliper for further 9 days after production (section 5.2.11.4). The results are shown in Figure 3.2-6.

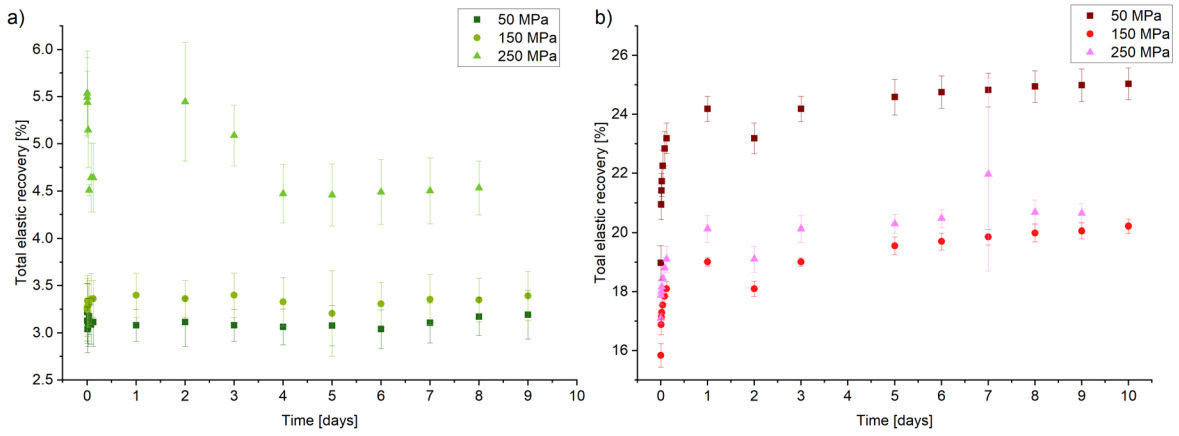

Figure 3.2-6: Total axial elastic recovery of lactose (a) and carrageenan (b) ribblets; n = 10, mean ± SD

The elastic recovery of carrageenan (16 % - 25 %) is much more pronounced compared to lactose (3 % - 5.5 %). The total elastic recovery increases with an increasing compression pressure for lactose, whereas it decreases from 50 MPa to 150 MPa and slightly increases again at 250 MPa for carrageenan. These results are consistent with those described in the previous sections 3.2.3 and 3.2.4.1. For lactose, the changes of the total elastic recovery are the most pronounced in the first minutes after ejection. The elastic recovery of the lactose ribblets produced at 250 MPa decreases by one percentage point from 5.5 % to 4.5 %, which indicates that the compacts were shrinking. The initial changes in elastic recovery of the ribblets produced at 50 MPa and 100 MPa is smaller than 0.5 percentage points. For the 250 MPa ribblets, the initial decrease is followed by an increase up to the starting value of 5.5 %. Afterwards, the elastic recovery decreases to the starting value of 4.5 % and remains constant at this level. The higher fluctuations in the total elastic recovery of lactose ribblets at 250 MPa could be related to invisible cracks inside the compacts. The elastic recovery of carrageenan increases most in the first minutes after ejection. 80 % of the elastic recovery is already completed within 5 minutes after ejection. 90 % of the final elastic recovery is reached after 1-2 hours at tableting pressures of 50 MPa and 250 MPa and after approximately 3 hours at 150 MPa. In contrast to lactose, the increase in height of carrageenan compacts continues over six days and the elastic recovery finally reaches values of 20 % for the 150 MPa ribblets, 21 % for the 250 MPa ribblets and 25 % for the 50 MPa ribblets.

The pronounced time-dependent elastic recovery for carrageenan was also observed by York and Baily (1977) and Picker (2001). The high standard deviation for the total elastic recovery of carrageenan at 250 MPa after 7 days may be due to person related measurement errors, since the other standard deviations are all smaller.

In roll compaction, not the pure excipients but powder mixtures are used so that it can be expected that the elastic recovery will be lower compared to the extreme example carrageenan. The axial elastic recovery is most pronounced in the first minute after ejection. Hence, this period is the most critical in terms of the resulting accuracy of the solid fraction prediction, which will be further discussed in section 3.2.4.4.

3.2.4.3 Radial Elastic Recovery

It should be evaluated whether the radial elastic recovery must be considered to improve solid fraction prediction. The radial elastic recovery of MCC, lactose and carrageenan ribblets was evaluated after a storage time of one week (section 5.2.11.5). The results are shown in Figure 3.2-7. The elastic recovery in radial direction was 6 to 20 times less pronounced than in the axial direction, which confirmed findings from literature (Picker, 2001). Rippie and Danielson (1981) reported that materials like MCC and lactose behave like Kelvin bodies under distortion. After the pressure is released, the body partly returns to its original state due to the Hook element. The higher axial expansion can be explained by the fact that the compression pressure during tableting is applied in axial direction onto the powder bed. The stress release takes place in the opposite direction to the one of the original applied force. Moreover, the elastic recovery in radial direction can only occur after the compact has been ejected (Haware et al., 2010, Train, 1956), since the powder inside the die is confined by the die wall.

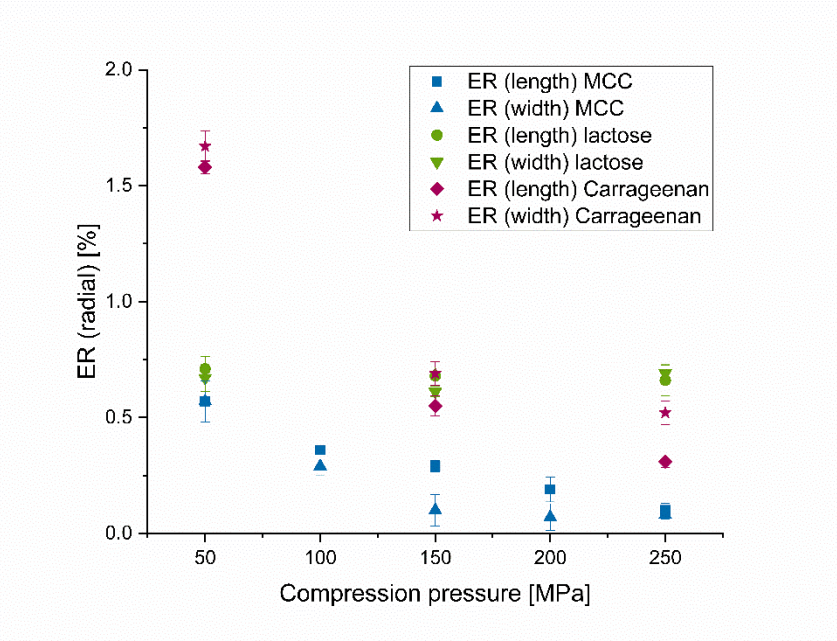

Figure 3.2-7: Radial elastic recovery of MCC, lactose and carrageenan ribblets; n = 10, mean ± SD

The elastic recovery in width and length was smaller than 0.8 % except for carrageenan that showed an elastic recovery of up to 1.6 % at 50 MPa compression pressure. For MCC and carrageenan, the radial elastic recovery decreased with an increasing compression pressure. The radial elastic recovery of lactose compacts ranged around 0.7 % for the three tested compression pressures.

To summarise, the radial elastic recovery is relatively small compared to the axial one so that it had no relevant impact on the change in solid fraction. It was hence decided to ignore the radial elastic recovery in the solid fraction prediction calculations, also for the purpose of simplicity.

3.2.4.4 Out-of-Die Method

Based on the findings presented in the previous chapters (3.2.4.1 - 3.2.4.3), an out-of-die method was developed. In contrast to the zero force method (3.2.3.2) it should allow a solid fraction prediction considering as well the out-of-die axial elastic recovery of the ribblets. It was shown that 80 % of the axial elastic recovery is completed within a few seconds to minutes after ejection so that the ribblet SF will not change considerably afterwards (section 3.2.4.2). The elastic recovery in radial direction is smaller than 1.6 % for the tested materials and can thus be neglected in the calculations of the SF.

To better target the ribblet solid fraction after ejection, an additional learning step was implemented after the automatic learning. Due to the non-linear pressure dependency of the elastic recovery, this additional learning phase is performed not at 51 kN (255 MPa) as it was done in the automatic learning but at the compression pressure, which corresponds to the desired specific compaction force. The height of the learning compact is measured with a digital calliper one minute after ejection. This time period of one minute is a recommendation but can be adapted individually depending on the elastic properties of the investigated materials. The height of the compact together with the dimensions of the rectangular punch (10 mm x 20 mm) are then used to calculate the out-of-die volume of the compact. The additional learning phase was tested with MCC (powder density: Table 3.1-4). The aim was to determine the SCF to produce ribblets with solid fractions of 60 and 80 %, which is the recommended solid fraction range with regard to further processing (Zinchuk et al., 2004). Gap widths of 2 mm and 4 mm and a roll speed of 2 rpm were chosen. The ribblet solid fraction was measured according to section 5.2.10.2 with a calliper. The measurement results were compared with the target values and the relative deviations from the target value were calculated as described in section 5.2.5.3. The results are summarized in Table 3.2-3.

Table 3.2-3: Specific compaction forces and prediction errors of ribblet solid fraction for MCC ribblets using the out of die method (n = 20)

Predicted ribblet solid fraction [%]	Gap width [mm]	Specific compaction force [kN/cm]	Compression pressure [MPa]	Measured ribblet solid fraction[%]	Relative deviation from target SF [%]
60	2	4.3	30.4	61.0	1.7
60	4	5.8	29.1	59.8	- 0.3
80	2	12.9	94.3	80.4	0.5
80	4	20.0	104.8	81.3	1.6

The relative deviations from the target solid range between - 0.3 and 1.7 % and the highest total deviation was 1.3 percentage points (80 % SF, 4 mm GW). The predicted specific compaction forces to achieve the target solid fraction of 60 % were 4.3 kN/cm and 5.8 kN/cm at a gap width of 2 mm and 4 mm, respectively. The specific compaction forces correspond to compression pressures of 30.4 MPa and 29.1 MPa, respectively. The specific compaction forces necessary for a ribblet solid fraction of 80 % were found to be 12.9 kN/cm at a 2 mm gap width and 20.0 kN/cm at a 4 mm gap width. The specific compaction forces correspond to compression pressures of 94.3 MPa and 104.8 MPa, respectively. These results confirm the trends of increasing specific compaction forces with increasing gap widths for constant solid fractions and underline the findings that the applying same compression pressure results in ribblets with the same solid fraction (presented in section 3.1.2.2 and Figure 3.1-17). The additional learning phase considering the out-of-die elastic recovery of the ribblets improved the solid fraction prediction considerably. This makes it now possible not only to mimic a certain specific compaction force at a certain gap width and to measure the solid fraction afterwards but to determine the specific compaction force to achieve the desired solid fraction and to transfer the determined settings directly to the roll compactor without extensive experimental effort. Only a very small amount of material is needed to predict the correct settings: three ribblets for the automatic learning and one ribblet for the advanced learning. Even with five further ribblets to confirm the settings only approximately 5 grams (filling by hand) - depending on the material properties - are sufficient, once the Kp factor for the roll compactor of interest is established. This is a great improvement compared to other methods which require 150 g (Nesarikar et al., 2012a) or more and are more laborious regarding the analytic methods.

Comparing the different methods of solid fraction calculation (Figure 3.2-8), it can be seen that the new learning phases led to a considerable improvement in prediction accuracy. The methods were compared

by compacting MCC ribblets at three different specific compaction forces and two gap widths. The comparative parameter was the error in prediction. The minimum height method predicted the ribblet solid fraction "at gap" and led to the highest errors in prediction since neither in-die nor out-of-die elastic recovery were considered. It is noticeable hat the errors become smaller with increasing specific compaction forces, which is in accordance with the findings that, for MCC, the elastic recovery decreases with increasing specific compaction forces/compression pressures.

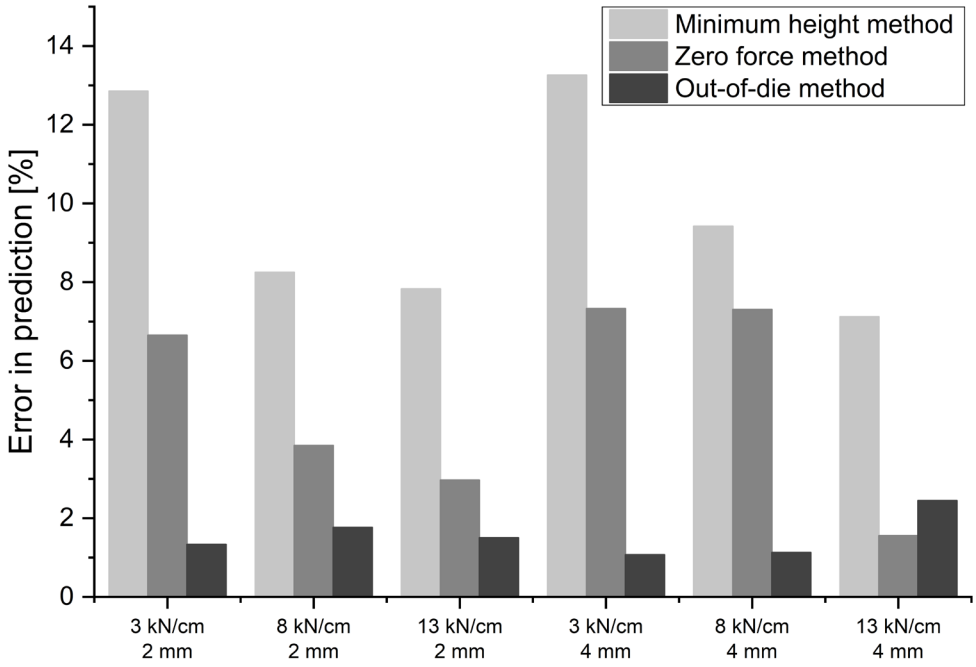

Figure 3.2-8: Comparison of the errors in prediction of the methods – minimum height method, zero force method, out-of-die method - for the solid fraction prediction of MCC ribblets at three simulated specific compaction forces and two gap widths

The first step was to implement the in-die elastic recovery (zero force method), which led to a decrease of the maximum prediction errors from 13 to 7 %. By accounting as well for the elastic recovery that occurs outside the die during the first minute after ejection, considerably higher prediction precision of the solid fraction could be achieved and the $errors_{ribblet}$ could be reduced to values below 2.5 % (out-of-die method). These small errors further support the assumptions that the elastic recovery is responsible for the lack in prediction and that the radial elastic recovery can be neglected due to its minimal influence on the ribblet solid fraction.

3.2.5 Summary

The predicted ribblet solid fractions were compared with the measured ribblet solid fractions to evaluate whether the hybrid modelling approach allows not only to produce ribblets with the same solid fraction as ribbons but also to predict the correct ribblet/ribbon solid fraction. It was found that the Styl'One systematically overestimates the ribblet solid fraction in its predictions. This overestimation was more pronounced for MCC than for lactose. It was hypothesised that this overestimation was due to the elastic recovery that occurs as soon as the punch pressure starts to decrease again after the compression.

To verify this hypothesis, the in-die elastic recovery of ribblets made from different materials was investigated regarding its dependence on the compression pressure and the gap width. For this purpose, a method was developed in which the height of the ribblet is determined at the moment when the upper punch force decreases to zero during its upward movement. It was observed that the extent of the in-die elastic recovery is strongly dependent on the material which is compressed. The elastic recovery is highest for carrageenan, followed by HPMC and MCC, while lactose and DCPA show only little elastic recovery. Furthermore, the compression pressure and the gap width have an influence on the elastic recovery. Depending on the material, the elastic recovery either increases or decreases with an increasing compression pressure. All investigated materials had in common that the elastic recovery increases with an increasing gap width. These findings underlined the assumption that the elastic recovery is responsible for the systematic overestimation of the ribblet solid fraction. Therefore, the so called zero force method, which allows to consider the in-die elastic recovery for the solid fraction calculations, was implemented in the hybrid modelling approach. This considerably reduced the prediction errors for the ribblet solid fraction.

As a next step, the out-of-die elastic recovery was investigated for different materials to evaluate whether it should be considered to further improve the solid fraction prediction. Using a chromatic confocal measurement technique, it was possible to observe the ribblet height over time. The elastic recovery of ribblets continues after ejection to different extents depending on the material and the applied compression pressure. Out-of-die elastic recovery shows the same general relationships as observed for the in-die elastic recovery. The gain in height is the highest at the beginning and decreases with time. Most of the elastic recovery was finished after approximately 1 minute. A long-term monitoring of the ribblet height was carried out for carrageenan and lactose ribblets to evaluate how long the elastic recovery continues. The elastic recovery for lactose ribblets was mainly finished after some minutes whereas the elastic recovery for carrageenan ribblets continued for several days. However, 80 % of the

elastic recovery were completed after seconds to minutes and 90 % were completed after three hours, at the latest. In addition to that, the radial elastic recovery of ribblets was investigated in width and length to assess its magnitude compared to axial elastic recovery. The elastic recovery in radial direction was found to be smaller than 0.8 % except for carrageenan, which showed values of up to 1.6 % for a pressure of 50 MPa. The radial elastic recovery is small, compared to the axial elastic recovery, and can therefore be ignored for the solid fraction calculations.

Based on these observations made in measuring elastic recovery outside the die, the out-of-die method was developed. The most important improvements in this method are that during the advanced learning step the ribblet is not compressed with the maximum force but with a force already adjusted to the target force and that afterwards, after a recommended period of one minute, the height of the ribblet is measured by means of a calliper. This allows the calculation of the ribblet volume after out-of-die elastic recovery and thus a more precise determination of the ribblet solid fraction. The method was tested with MCC and the relative deviations from the target solid fraction were between -0.3 and 1.7 %, which is a strong increase in prediction accuracy compared to the minimum height- and the zero force-methods. With this improvement, it is now possible to define the ribblet solid fraction at a certain gap width as a target value and to directly obtain the specific compaction force, which must be set on the compactor to achieve this. The great advantage of the hybrid modelling approach considering in-die and out-of-die elastic recovery is that with only a few grams (appr. 5 g) of material the necessary parameter settings can be predicted, once the Kp factor has been determined for the roll compactor.

3.3 Nip Angle Estimation

3.3.1 Introduction and Objectives

The space between the rolls of a roll compactor is divided into a slip, a compaction and a release zone (Figure 1.2-1). The angle at the transition from the slip to the compaction zone is called the nip angle α (Johanson, 1965). The slip region is characterised by a higher roll speed compared to the speed of the powder. It slips on the roll surface. At the nip angle, the speed of the rolls and the powder at the roll surface is equal, so that the powder is dragged towards the gap. The nip angle is an important parameter for the process understanding since it represents the start of the main powder compaction and is decisive for the degree of compaction.

There are several methods to determine the nip angle – either experimentally or by simulation approaches – leading to different results. Johanson (1965) stated in his rolling theory that the nip angle is independent of the roll speed and that it increases with increasing compressibility of the powder. Muliadi et al. (2012) determined the nip angle by a 2D finite element method. This approach was compared to the model of Johanson. The discrepancies found between the two methods were explained by the one-dimensional approach of Johanson versus the 2D approach of the finite element method, which can consider the velocity gradients of the powder, that is ignored by Johanson. Nesarikar et al. (2012a) determined the nip angle of different blends calculating the intersection of the two tangents on the ascending and descending part of the pressure profile obtained by instrumented roll data. They found a linear relationship between nip angle, gap width and specific compaction force. Bi et al. (2014) used a similar approach and predicted the nip angle by calculating the intersection between the roll pressure gradients of the slip and non-slip area. It was stated that the nip angle was almost independent of the specific compaction force and gap width. Furthermore, they found that the nip angle increased with an increasing effective angle of wall friction and decreased with an increasing internal angle of friction and an increasing compressibility constant. Al-Asady et al. (2016) introduced an experimental method for the nip angle determination of MCC by indentation of the pre-compacted powder. They investigated the influence of the roll speed, the hydraulic pressure and the gap width on the nip angle. A modification of the rolls from a smooth to serrated surface alters the friction between powder and roll. It was shown that an increase in the wall friction coefficient leads to an increasing nip angle and peak pressure (Guigon et al., 2007). Tan et al. (2016) compared different methods of nip angle determination and established an approach to determine the nip angle for serrated rolls by using mass balance calculations in the nip region. The serrated geometry was considered by transformation into an average roll gap. Furthermore,

uniaxial compaction was used to estimate the powder density at the beginning of the nip angle. Mahmah et al. (2019) investigated the influence of the roll surface on different roll compaction parameters like the maximum roll pressure and the nip angle. Johanson's theory was used for the calculation of the nip angle, so that the absolute values might not be correct. Nevertheless, a trend can be seen that suggests higher nip angles for a serrated roll surface than for a smooth roll surface.

The above-mentioned methods have in common that they are laborious or require high computational effort. The aim of this part of the work was to establish a simple method to estimate the nip angle using the uniaxial compaction simulator Styl'One Evolution (Medelpharm). The influence of the specific compaction force, the gap width and the roll speed as well as the material properties on the nip angle of different excipients should be evaluated.

3.3.2 Example Calculation of Nip Angle

The method to calculate the nip angle is described in detail in section 5.2.6. In the following an example is given for the calculation of the nip angle α. The mimicked roll compactor is a Gerteis Mini-Pactor with a roll diameter D of 250 mm, the tested material is MCC, the roll speed is 2 rpm and the simulated specific compaction force is 13 kN/cm. The thicknesses T_0 and T_1, which are necessary for the calculation of the nip angle, are obtained from the recorded compression data of the Styl'One.

$$\alpha = arccos\left(1 + \frac{(T_1 - T_0)}{D}\right) \tag{14}$$

The deaeration thickness T_0, which represents the thickness at which a first significant increase in force is detected, is 6.89 mm and the minimum thickness under load T_1 is 1.95 mm. This results in

$$\alpha = arccos\left(1 + \frac{(1.95\ mm - 6.89 mm)}{250\ mm}\right) \tag{15}$$

$$\alpha = arccos(0.9802)$$

$$\alpha = 11.4\ °$$

a nip angle of 11.4 °. From the equation it is clear that changes of T_0 and T_1 will lead to different nip angles. These thickness values are connected to the material properties, the mimicked gap width, the roll speed and the specific compaction force, whose influences are discussed in section 3.3.3.

3.3.3 Nip Angle in Dependence on Process Parameters and Material Properties

The three investigated materials MCC, lactose and DCPA differ in their nip angles (Figure 3.3-1 a). For all tested materials, the nip angles increase when the specific compaction force increases and as well with an increasing gap width an increase in nip angle is observed. MCC shows the highest nip angles between 9 – 15 ° whereas lactose and DCPA both have smaller nip angles in a range of approximately 6 to 10 °. When the nip angle is correlated to the compression pressure (Figure 3.3-1 b) the same relationship can be observed as with the specific compaction force.

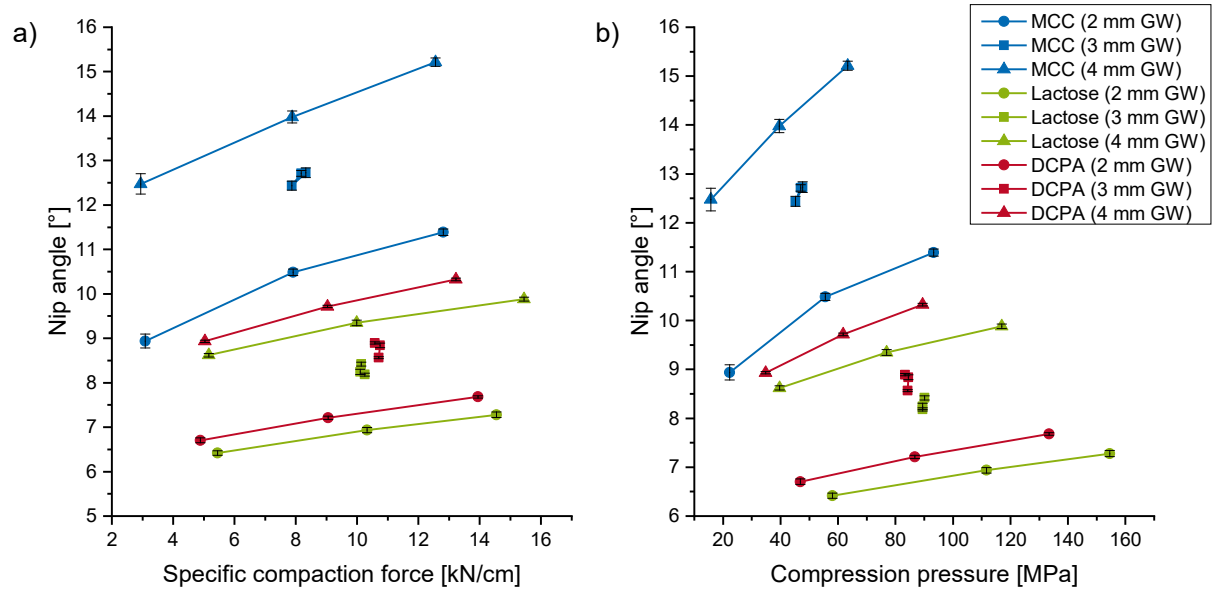

Figure 3.3-1: Nip angles of MCC, lactose and DCPA in dependence of the a) specific compaction force and b) compression pressure at gap widths of 2 and 4 mm, centre point at 3 mm gap width; $n \geq 20$, mean ± SD

The specific compaction force or compression pressure have a significant positive effect on the nip angle for all tested materials, which is illustrated in the coefficient plot (Figure 3.3-2). In order to work at a higher specific compaction force and to maintain the gap width constant at the same time, it is necessary to transport more material between the rolls which is then compressed to the same thickness. This means that the nip of the powder between the rolls must start at a higher angular position to assure the required densification.

By 2D finite element method, as well, a positive correlation of an increasing specific compaction force and the nip angle was found (Michrafy et al., 2011b). For MCC, nip angles between 7.4 and 12.4 ° were predicted for roll pressures between 16 and 120 MPa. Muliadi et al. (2012) used 2D finite element method as well to model the roll compaction of MCC with an Alexanderwerk WP120. The nip angle ranged between 15 and 20 ° depending on the chosen input parameters (roll-powder friction, effective

angle of friction and compressibility). The effect of the specific compaction force on the nip angle was also experimentally confirmed (Al-Asady et al., 2016) for MCC on an Alexanderwerk WP120. At low hydraulic pressures, a nip angle of 6.8 ° was determined, which increased at higher pressures (100-250 MPa) to angles between 26 and 30 °. Looking at it the other way around, Mazor et al. (2018) found in their study by a combined DEM/FEM-approach that a higher nip angle due to an increased powder feed leads to a higher specific compaction force and ribbon density.

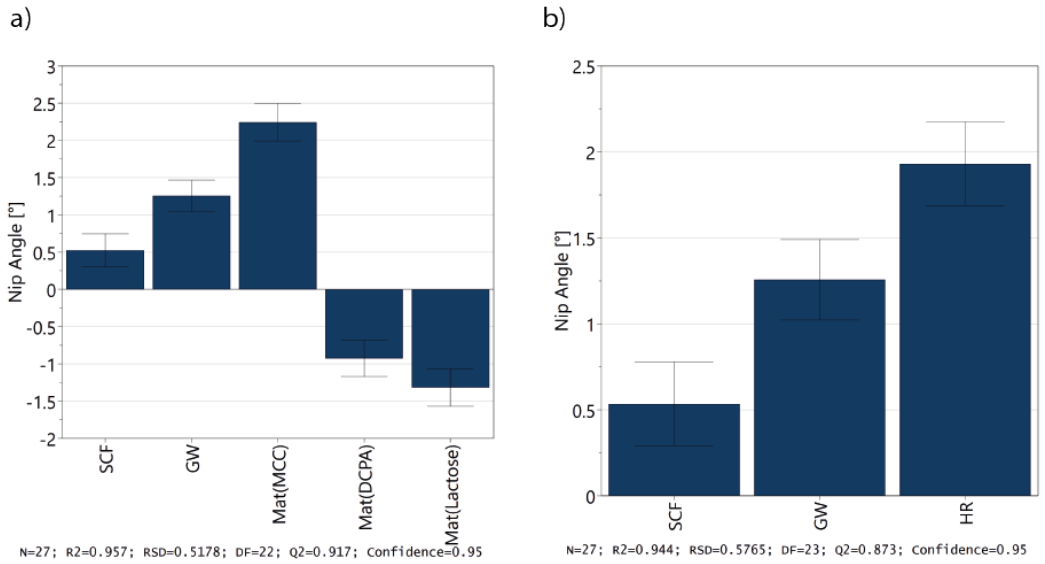

Figure 3.3-2: Coefficient plots for the effects of the specific compaction force (SCF), the gap width (GW) and a) the materials (Mat) as qualitative factors and b) the Hausner ratio (HR) as quantitative factor on the nip angle

A doubling of the gap width from 2 to 4 mm at a constant specific compaction force results in an increasing nip angle for the three tested materials (Figure 3.3-1). This is valid over the whole range of tested specific compaction forces and in accordance with recent literature (Bindhumadhavan et al., 2005, Mansa et al., 2008), whereas Johanson (1965) stated that the nip angle is independent of the gap width. Bindhumadhavan et al. (2005) found nip angles for MCC from 9 to 11 ° at gap widths between 0.9 and 2 mm. They stated that the gap width has no big influence on the nip angle, but the investigated gap widths were relatively small.

An increase in the gap width from 2 to 4 mm while maintaining the same specific compaction force is accompanied by a higher screw speed and thus an increased material feed on the roll compactor. On the compaction simulator, this is reflected by an increased dosage height as shown in section 3.1.2.3. The amount of material that must be dragged between the rolls to achieve a higher gap width is bigger and this leads to an earlier transition from slip to nip region. In the studied factor space, the effect of the gap

width on the nip angle is bigger compared to the one of the specific compaction force as depicted in the coefficient plots (Figure 3.3-2).

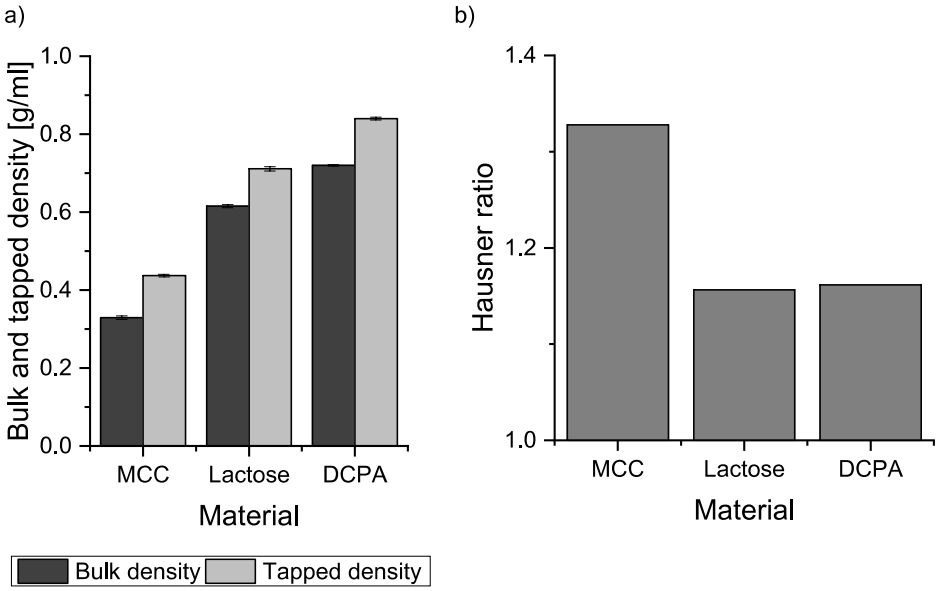

Figure 3.3-3: a) Bulk and tapped densities, n = 3, mean ± SD and b) Hausner ratios of MCC, lactose and DCPA

The investigated materials were analysed regarding their bulk and tapped density (section 5.2.9.3) and the Hausner ratio was calculated (section 5.2.9.4), the results are listed in Table 3.3-1 and visualised in Figure 3.3-3. Statistical analysis revealed as well that the differences in nip angle for the tested materials can be linked amongst others to their Hausner ratios (Figure 3.3-2 b). Since the effect of the Hausner ratio and the materials are directly connected, they must be considered separately from each other. The lower the compaction tendency of the material, the lower is the nip angle. MCC has a Hausner ratio of 1.33, DCPA and lactose of 1.16. For materials with a high Hausner ratio, the volume of the material that must be compacted to a certain thickness is bigger than for those with a small factor, since a higher Hausner ratio is linked to a smaller bulk density (Tan et al., 2016). So, the nip angle is correlated with the compression coefficient. If the material has a low starting solid fraction, a higher compression coefficient is needed, which in return results in a higher nip angle. The findings confirm as well the results of Mansa et al. (2008), in which the Hausner ratios of MCC and DCPA were linked to the nip angle.

Table 3.3-1: Bulk and tapped density and Hausner ratio of MCC, lactose and DCPA (n=3; mean ± SD)

Material	Bulk density [g/cm³]	Tapped density [g/cm³]	Hausner ratio
MCC	0.329 ± 0.005	0.437 ± 0.004	1.328 ± 0.029
Lactose	0.615 ± 0.004	0.711 ± 0.005	1.156 ± 0.001
DCPA	0.725 ± 0.003	0.841 ± 0.003	1.161 ± 0.010

The nip angle of MCC reacts the most sensible to changes in the specific compaction force and the gap width, whereas the absolute changes for lactose and DCPA are smaller. These differences are linked to the compressibility of the materials. The better compressible a material (and the smaller its compressibility constant) the more powder must be drawn between the rolls to achieve the same gap width compared to a less compressible excipient. Thus, materials with good compressibility have higher nip angles (Bi et al., 2014, Johanson, 1965, Yu et al., 2012). Tan et al. (2016) compared experimentally the nip angles of MCC, lactose and DCPA mixtures and found that the nip angles decrease with increasing amounts of the less compressible materials lactose and DCPA. The nip angle of MCC ranged around 13 ° depending on the method of determination, for lactose an angle of around 6 ° was found and a mixture of 90 % DCPA and 10 % MCC had a nip angle around 7 °.

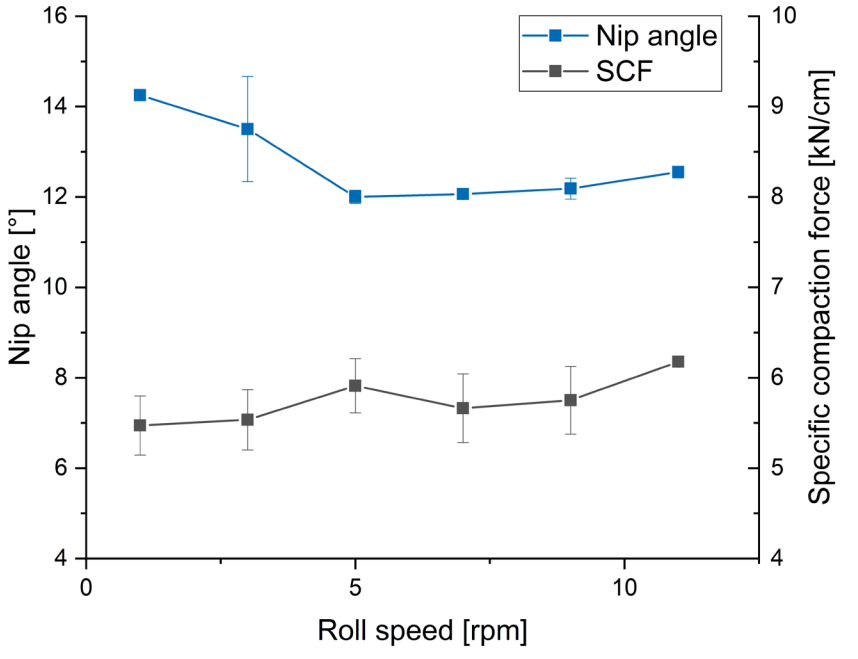

Figure 3.3-4: Nip angle of MCC in dependence on the roll speed n=10; mean ± SD

Figure 3.3-4 illustrates the influence of the roll speed on the nip angle of MCC. The specific compaction force should be kept constant at 6 kN/cm but some fluctuations were observed. However, the effect of the specific compaction force is not significant (Figure 3.3-5). The nip angle decreases from 14.2 to 12.0 ° with an increasing roll speed from 1 to 5 rpm. The negative effect of the roll speed on the nip angle is significant. This was reported as well by Mansa et al. (2008), who linked the roll speed to the nip angle by intelligent software. A slight increase from 12.0 to 12.6 ° is observed at roll speeds higher than 5 rpm. Additionally, a quadratic positive effect of the roll speed was found, which models the curve minimum at 5 rpm. In total, the influence of the roll speed on the nip angle of MCC is small (Patel et al., 2010) – the difference between the minimum and the maximum angle was 2.3 °.

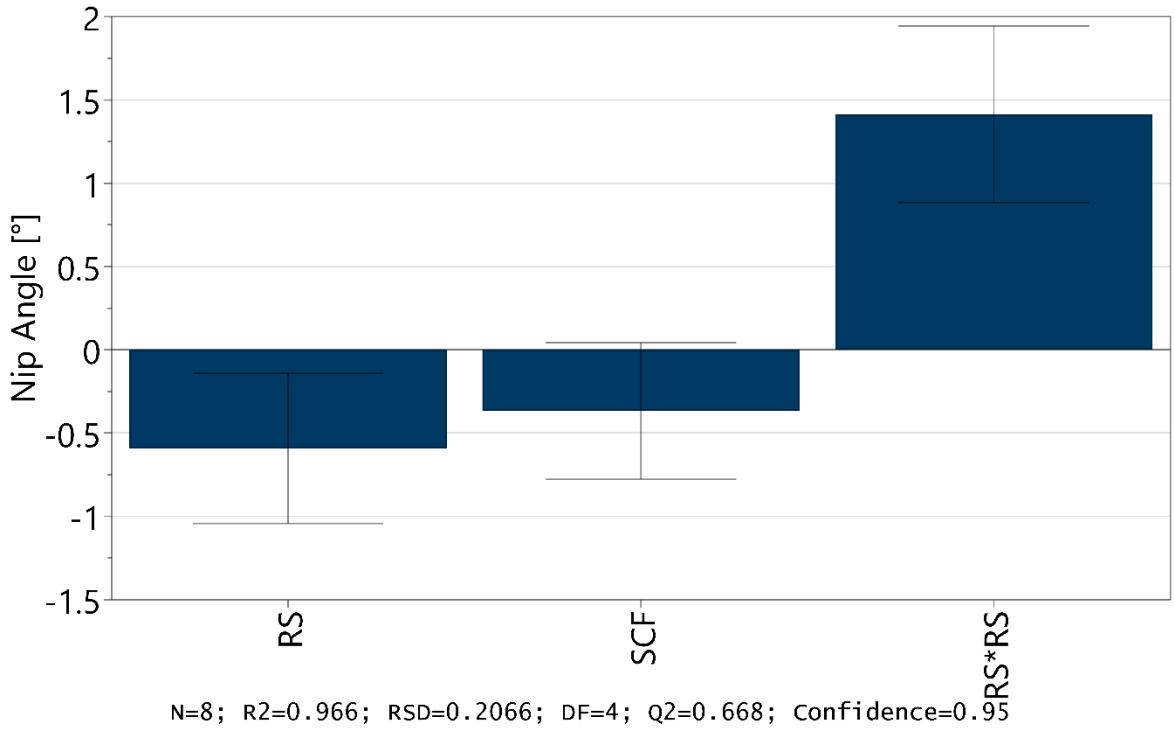

Figure 3.3-5: Coefficient plot for the effects of specific compaction force (SCF) and roll speed (RS) on the nip angle of MCC

Al-Asady et al. (2016) experimentally showed as well that the nip angle of MCC decreases with an increase in roll speed from 25 ° at 3 rpm and finally ends in a plateau of around 10 ° between 6 and 7 rpm. The decrease was much more pronounced than in the present work. This could be linked to a higher pre-compression by the screw in the feeding system, which was observed in experiments on the Alexanderwerk WP120 roll compactor (section 3.1.4). To summarise, no clear conclusion can be drawn from the experiment and additional experiments would have to be carried out in order to verify the influence of the roll speed on the nip angle.

3.3.4 Summary

The uniaxial compaction simulator Styl'One was used to estimate the nip angle on the Mini-Pactor for several materials in dependence on the specific compaction force, the gap width and the roll speed. The determined nip angles for MCC, DCPA and lactose were comparable to values from literature. The nip angles differed between the materials tested. MCC showed the highest nip angles followed by DCPA and lactose. It was confirmed that the better compressible a material is, the bigger is its nip angle. The differences between the materials were linked to the material characteristics bulk and tapped density. A higher Hausner ratio led to higher nip angles since for those materials the volume of powder that must be transported between the rolls to achieve the desired gap width is higher than for those with a smaller Hausner ratio. Furthermore, statistical analysis revealed significant positive effects of the gap width and the specific compaction force on the nip angle, with the influence of the gap width being higher than that of the specific compaction force. A small influence of the roll speed on the nip angle was observed. With increasing roll speed, the nip angle decreases and entered a plateau at higher velocities. The developed method for the estimation of the nip angle by uniaxial compaction simulation is a promising and simple approach. So far, a possible pre-compression in the feeding system and the influence of the roll surface cannot be mimicked by this method. The latter could be integrated to the calculation by using the average roll gap as proposed by Tan et al. (2016) or by using punches with a modified surface. However, the here presented approach provides results that are consistent with literature. It gives an estimation of the general product properties and the behaviour during roll compaction with only small experimental and computational effort compared to already existing approaches. A next step would be to experimentally confirm the estimated nip angles on the mimicked roll compactor, e.g., by using instrumented rolls.

3.4 Mimicking the Downstream Process

3.4.1 Introduction and Objectives

The downstream process from a raw powder mixture, through the ribbons and granules to the finished tablets should be mimicked. The results obtained with pure excipients (section 3.1) and the changes in solid fraction calculation, which were derived from the insights on elastic recovery in roll compaction (section 3.2), were applied on the mimicking of the downstream process for an API containing mixture. Haeffler et al. (2019) stated that it is not enough for roll compaction scale-up or change of equipment to keep the solid fraction constant, since this approach does not result in granules with identical properties. However, this could be mainly due to the different types of granulation units used by the different roll compactor suppliers. Using the solid fraction is still a useful approach to get an indication for the optimal process parameters.

By simulating and mimicking the roll compaction process with the hybrid modelling approach on the Styl'One Evolution (sections 5.2.5.4), the optimal process parameters, which result in ribbons with the desired quality attributes, should be identified. This would allow to use only a small amount of material and could omit extensive roll compaction experiments. In a next step, the process parameters found by mimicking should be applied to the roll compactor to assess how accurate the mimicking is. The quality attribute solid fraction was chosen for comparison of ribbons and ribblets. Both, ribbons and ribblets should subsequently be milled to granules in the oscillating granulation unit of the roll compactor (section 5.2.7). The granule size distribution (section 5.2.12) was compared to evaluate whether granulation of ribbons and ribblets leads to granules of different quality. The obtained granules were compacted to tablets with the Styl'One Evolution (section 5.2.8). The quality attributes tensile strength, mass uniformity and disintegration time were the basis for comparing the tablets (section 5.2.13).

The question was whether hybrid modelling can simulate roll compaction not only for pure excipients but also for a powder mixture containing hydrochlorothiazide (HCT) as active pharmaceutical ingredient. In addition to HCT, the model formulation was composed of lactose, MCC, copovidone and crospovidone. The functions and mass fractions of the ingredients are listed in Table 3.4-1.

The model drug hydrochlorothiazide is a frequently used drug with a diuretic and antihypertensive effect. It is administered either alone or in combination with other APIs in doses between 12.5 and 50 mg. In doses of 12.5 and 25 mg, it is used for the treatment of arterial hypertonia. In higher doses of 25 and 50 mg, cardiac, hepatic or renal oedema can be treated. Doses of 12.5, 25 and 50 mg are available

on the German market (Jurasovic and Bouvier, 2021). The highest daily dose for treatment of adults is 100 mg (Langendorf and Krug, 2020). Pedersen et al. (2018) have published a study, in which they pointed out that hydrochlorothiazide increases the risk of nonmelanoma skin cancer. They recommend that "the use should be carefully considered". As a result, a red-hand-letter was published by the pharmaceutical manufacturers in coordination with the EMA and the BfArM to inform about this (BfArM, 2018). However, hydrochlorothiazide was chosen as model drug in the present work due to its poor compaction properties and its difficult handling (Meier et al., 2017).

Herting et al. (2007) investigated roll compaction dry granulation with subsequent tableting of a hydrochlorothiazide containing formulation with a drug load of 7 % to compare the properties of different dry binders. In the present work, a higher drug load of 25 % (m/m) was chosen to depict the highest realistic dose and a worst-case scenario with regard to the poor flow, handling and compaction properties of the micronised hydrochlorothiazide. Sun and Kleinebudde (2016) recommended in their review to choose excipients of different compaction behaviour for a roll compaction formulation. The mixture of the excipients combines the advantages and reduces the disadvantages of the single materials. MCC and lactose were chosen as the main binders/fillers of the formulation. MCC is known to deform predominantly plastically, whereas lactose shows a more brittle behaviour. Kollidon VA64 was used as dry binder. Arndt and Kleinebudde (2018a) showed that the particle size has a distinct influence on the binding capacity of the dry binder. The finest particles led to tablets with the highest tensile strength. However, all tested copovidone qualities showed good dry binding properties. For the present study, Kollidon CL-SF was chosen as disintegration aid to assure appropriate disintegration times according to the specifications of the European Pharmacopoeia for uncoated tablets. Also, for MCC 102 and copovidone short disintegration times were found (Arndt and Kleinebudde, 2018a), so that the combination should result in an acceptable tablet disintegration. The mean particle sizes of the starting powders measured by dynamic image analysis (section 5.2.9.2) range between 16.5 and 118.3 µm and are shown in Table 3.4-1. Due to the small particle size of HCT, its adhesive behaviour and the high fraction of 25 % in the formulation, the powder mixture was not applicable for direct compression and it required a granulation step before tableting.

Table 3.4-1: Composition and mean particle sizes of ingredients

Material	Type of material	Function	% [w/w]	Mean particle size [µm] (n=3, ±SD)
Hydrochlorothiazide	HCT Micro II	API	25	16.5 ± 0.5
Lactose	Granulac 200	Filler	50	54.5 ± 4.2
Microcrystalline cellulose	Vivapur 102	Filler/Binder	15	118.3 ± 1.7
Copovidone	Kollidon VA64	Binder	5	99.3 ± 1.0
Crospovidone	Kollidon CL-SF	Disintegrant	5	29.9 ± 0.6

There were three main questions for this study. First, is it enough to use only the ribbon solid fraction as comparative parameter or must further properties be considered to develop a well-functioning process? Second, do the intermediates - ribblets, ribbons, granules - show different properties? And third, do roll compaction and roll compaction simulation result in tablets of comparable quality?

3.4.2 Hybrid Modelling and Roll Compaction

The roll compaction process was mimicked using the hybrid modelling approach according to section 5.2.5.4. The question was, which specific compaction force must be set on the roll compactor, the Gerteis Mini-Pactor, for a certain gap width to achieve ribbons with the desired solid fractions. The powder density, which must be entered to the software of the Styl'One to calculate the solid fraction, was determined by helium pycnometry (section 5.2.9.5) and was 1.5235 g/cm³. Based on a 2^2 full-factorial experimental design, the relation between the two factors solid fraction and gap width and the specific compaction force was investigated with the Styl'One. The two levels for the factor solid fraction were 70 % and 80 %, for the gap width 2 mm and 4 mm. 75 % solid fraction at 3 mm gap width was the centre point (Table 3.4-2).

The results of section 3.2.4.4 have shown that the developed out-of-die method can make reliable predictions about the solid fraction of the ribblets, since it considers the elastic-recovery. In-die and out-of-die elastic recovery of the ribblets were previously the reason that the solid fraction could not be used as a target parameter for the hybrid modelling. With the improvements made, now, it should be possible to determine the specific compaction force necessary to obtain ribblets - and consequently ribbons – with the desired solid fraction at a certain gap width.

Table 3.4-2: Full-factorial 2² experimental design

Experiment	Gap width		Solid fraction	
N	**Level**	**[mm]**	**Level**	**[%]**
1	-1	2	-1	70
2	1	4	-1	70
3	-1	2	1	80
4	1	4	1	80
5	0	3	0	75
6	0	3	0	75
7	0	3	0	75

The compression behaviour of the blend at three different dosage heights and maximum pressure of 250 MPa was evaluated in the first learning process. As described in section 5.2.5.3, the values for the various factor level combinations were entered in the recipe. The dosage height and the compression pressure were adapted automatically by the software based on the first learnings and the given values for solid fraction and gap width. The calculation of the target compression pressure was refined by the advanced learning step. The conversion of compression pressure into the specific compaction force is done by the software (section 3.1.1).

The predicted specific compaction forces for the target solid fractions at various gap widths ranged between 3.51 kN/cm for 70 % solid fraction at 2 mm gap width and 11.79 kN/cm at 4 mm gap width for 80 % solid fraction (Table 3.4-3). The same trends as for pure excipients (section 3.1.2.2 *Specific Compaction force – Compression pressure)* were observed for the complete formulation: At a larger gap width, a higher specific compaction force must be applied to the powder to achieve the same solid fraction than at a smaller gap width. For each setting, ten ribblets were produced, which were analysed regarding their solid fraction after elastic recovery (section 5.2.10.2).

Table 3.4-3 Predicted specific compaction forces for the different gap width-solid fraction combinations and the specific compaction forces used on the roll compactor

Target SF [%]	GW [mm]	Predicted SCF [kN/cm]	SCF (Mini-Pactor) [kN/cm]
70	2	3.51	3.5
70	4	4.88	5.0
75	3	6.62	6.5
80	2	8.57	8.5
80	4	11.79	12.0

The results (Table 3.4-3) obtained by the simulation were transferred to the Mini-Pactor. Ribbons for each setting were produced with smooth rolls, rim roll sealing system and a tamping to feeding screw speed ratio of 2:1. The run order was randomised, and samples were collected as soon as the process reached steady state conditions. The roll compaction process data shown in Figure 3.4-1 is an excerpt from the raw data, only the sampling periods are depicted. The process data for experiment N1 (3.5 kN/cm, 2 mm) are not displayed due to a data transmission error.

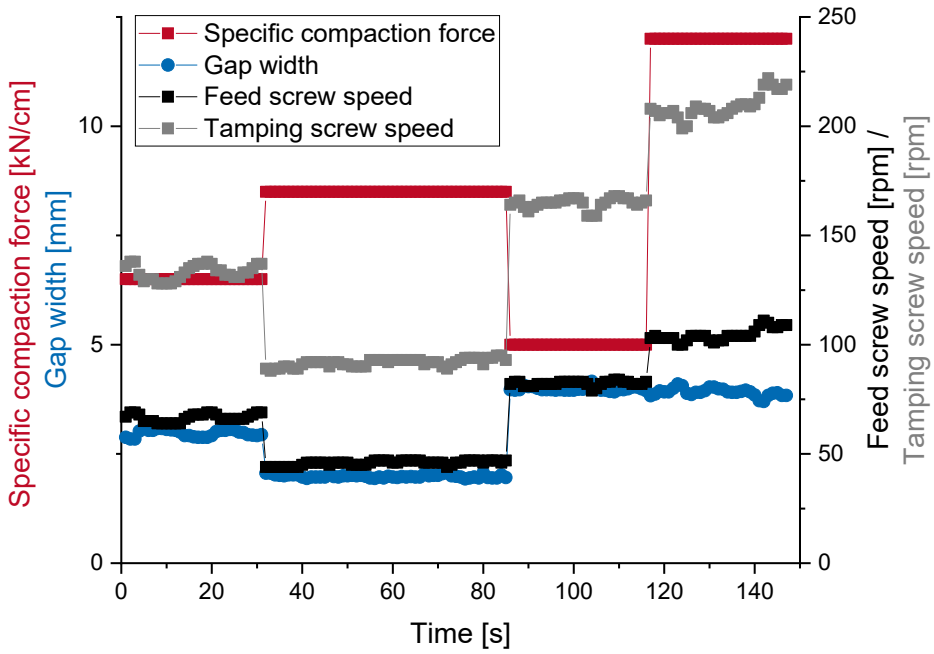

Figure 3.4-1: Roll compaction process parameter specific compaction force (kN/cm), gap width (mm), feed and tamping screw speed (rpm); data shown from the sampling periods only

The roll compactor operates with nested control loops, in which the specific compaction force has the highest priority and is the first parameter to be kept constant. Figure 3.4-1 shows that the specific compaction force remained steady at the target force value during the sampling times. The gap width exhibited some variations but was still within an acceptable range around the respective target gap width. The fluctuations in the gap width are reflected in the screw speed data since the gap width is controlled by varying the screw speeds. A time offset between maximum screw speed and maximum gap width can be observed, since the extra powder conveyed at higher screw speeds must first reach the gap before it can increase. Overall, the processing of the powder mixture was successful in spite of some difficulties, which may be related to the properties of HCT. Yu et al. (2012) compared roll compaction of free-flowing and cohesive powders and reported that an increasing flowability is advantageous for the feeding efficiency, especially for roll compactors which are gravity fed. In case of the Mini-Pactor, screws are used for the feeding and the powder flowability may have less influence.

The ribbon solid fraction was measured via powder pycnometry (section 5.2.10.1) to evaluate, whether the desired solid fractions were achieved. Due to the limited sample numbers, the ribblet dimensions were measured with a calliper for the solid fraction calculations (section 5.2.10.2). It was shown by Zinchuk et al. (2004) that the two methods provide equivalent results. The measured ribbon and ribblet solid fractions and the respective deviations from the target values are listed in Table 3.4-4. It is noticeable that the ribbons and ribblets have a similar solid fraction. The differences between the solid fraction of ribbons and ribblets for the same setting range between 0.1 and 1.2 %. These differences are smaller than the measuring accuracy of the powder pycnometer, so that the ribbons and ribblets can be considered equal regarding their solid fraction. All measured solid fractions are below the respective target values. The deviations from the target values for the ribblets range between 1.6 and 4.6 % and between 2.0 and 4.6 % for the ribbons. The highest absolute deviation from the target solid fraction was 3.3 % SF. As reported in section 3.2, the elastic recovery of the compacts was responsible for the deviations from predicted and actual solid fraction values. The fast in-die elastic recovery as well as the out-of-die elastic recovery after one minute were considered in the learning phases. The period of one minute, however, might have been too short for this formulation and caused errors in the learning, which eventually resulted in solid fractions that were lower than the target solid fraction. The small deviations between ribbon and ribblet solid fraction underline the hypothesised material independence of the Kp factor for the Mini-Pactor.

Table 3.4-4: Target solid fraction and real solid fraction and the corresponding deviations from the target values for ribbons and ribblets

Target SF [%]	GW [mm]	Ribblets			Ribbons	
		SF [%]	Deviation from target [%]	$\lvert SF_{ribbon} - SF_{ribblet} \rvert$ [%]	SF [%]	Deviation from target [%]
70	**2**	67.5	3.6	0.1	67.4	3.7
70	**4**	66.8	4.6	0.1	66.7	4.6
75	**3**	73.9	1.5	1.1	72.8	2.9
75	**3**	74.0	1.3	1.1	72.9	2.8
75	**3**	73.6	1.8	1.2	72.4	3.4
80	**2**	78.2	2.3	0.2	78.4	2.0
80	**4**	77.6	3.1	0.6	78.2	2.2

Figure 3.4-2 displays the correlation between the simulated specific compaction force and the corresponding compression pressure on the Styl'One. Ribblets with the same target solid fraction at different gap widths were compressed with different specific compaction forces but with similar compression pressures.

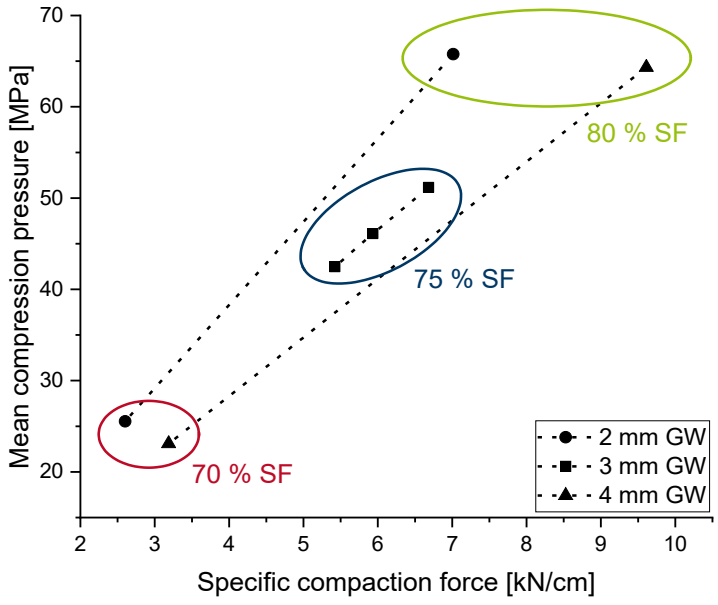

Figure 3.4-2: Correlation between the simulated specific compaction force and the mean compression pressure on the Styl'One for the different gap widths grouped according to the target solid fraction

To achieve a solid fraction of 80 % at gap widths of 2 and 4 mm, similar mean compression pressures of 65.8 and 64.3 MPa were needed, respectively. These compression pressures correspond to a specific

compaction force of 7.0 kN/cm at a 2 mm gap width but 9.6 kN/cm at a gap width of 4 mm. These findings are in accordance with the results found with pure excipients (section 3.1.2). The deviations in the specific compaction force – compression pressure correlation for a target solid fraction of 75 % (data points marked blue in Figure 3.4-2) might be due to the poor flow properties, which resulted in a fluctuating die filling and consequently in different compression pressures. However, ribbons and ribblets with similar solid fractions close to the target solid fractions were obtained, which was the main objective of this part of the study.

3.4.3 Granulation

The ribbons and ribblets with a target solid fraction of 75 % and a 3 mm gap width were chosen for granulation and tableting. This solid fraction was chosen to obtain ribbons/ribblets with a sufficient mechanical stability, which favors a low fraction of fines during granulation, and at the same time to obtain granules with sufficient tabletability by applying a preferably low compression pressure during roll compaction/simulation (Sun and Kleinebudde, 2016).

Both, ribbons and ribblets were stored for one day before they were milled into granules in the oscillating granulation unit of the Mini-Pactor (section 5.2.7). Ribbons and ribblets were granulated in portions of approximately 150 g. This corresponds to the actual ribbon throughput of 160 g/min at 3 rpm, 6.5 kN/cm and 3 mm gap width. After two minutes, the granulation was stopped. At that time roughly 90 % of the ribbons and ribblets were granulated.

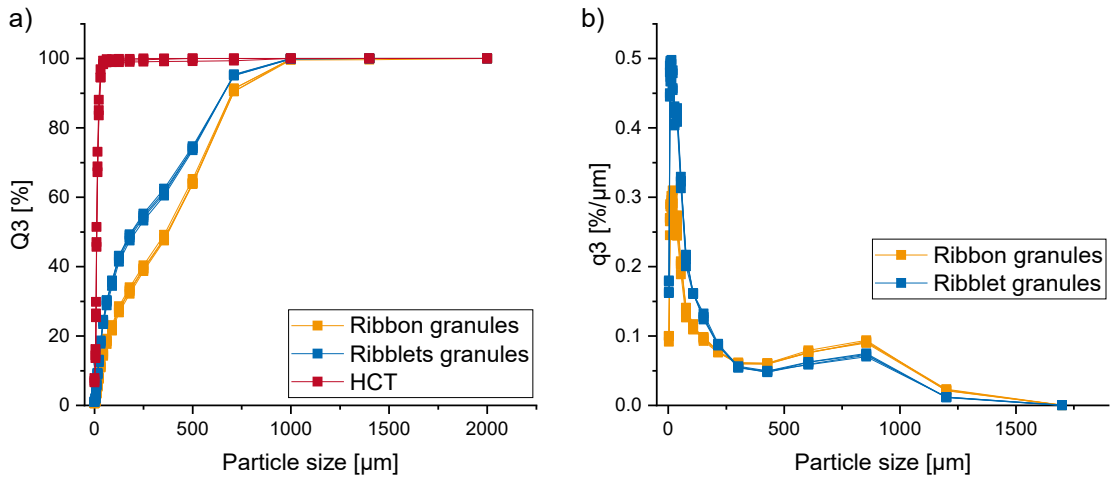

Figure 3.4-3: a) cumulative particle size distribution (Q3) for ribbon and ribblet granules and uncompacted HCT powder; b) density distribution (q3) of ribbon and ribblet granules; n=4

The particle size distribution of the ribbon and ribblet granules was measured with dynamic image analysis (section 5.2.12). The granulation resulted in a mean particle size of 528 µm for the ribbon

granules and of 272 µm for the ribblet granules (Table 3.4-5). Figure 3.4-3 a compares the granule size distributions with the particle size distribution of the uncompacted hydrochlorothiazide, which is the component with the smallest mean particle size. It is visible that the dry granulation process had the desired effect of increasing the particle size for ribbon and ribblet granules.

The density distributions (q3) of ribbon and ribblet granules are compared in Figure 3.4-3 b. Both granule types show bimodal distributions, which are typical for the roll compaction dry granulation process (Arndt, 2018, Haeffler et al., 2019, Inghelbrecht and Remon, 1998a, Perez-Gandarillas et al., 2016, Perez Gago and Kleinebudde, 2017, Reynolds, 2010). The granulation in the granulation unit of the Mini-Pactor led to a similar particle size distribution for both types of granules. Nevertheless, differences in the fraction of fines were observed. The $D_{10\%}$ of ribbon granules was 40.0 µm, whereas 10 % of the ribblet granules were smaller than 25.1 µm (Table 3.4-5). Since the granulation parameters, the type of granulator, residence time in the granulator and the amount of material were the same for ribbons and ribblets, these factors could not explain the differences. However, the different shapes of the ribbons and ribblets could be linked to the fraction of fines.

Table 3.4-5: Quantiles (D 10 %, 50 %, 90 %) of ribbon and ribblet granule size distribution; n = 4, mean ± SD

Quantiles	**Ribbon granules [µm]**	**Ribblet granules [µm]**
$D_{10\%}$	40.0 ± 1.3	25.1 ± 0.6
$D_{50\%}$	527.6 ± 10.6	272.9 ± 13.8
$D_{90\ \%}$	987.8 ± 5.7	920.2 ± 1.5

From tablet friability testing it is known that friability is not only related to the tablet tensile strength but also to the shape of the tablet and the existence of sharp edges or corners (Osei-Yeboah and Sun, 2015). The ribbons have an irregular shape whereas the ribblets have a defined cuboid one. Schiano et al. (2016) used ribbon friability as a tool to evaluate the behaviour of ribbons during the milling step. They state that the formation of fines may be mainly due to abrasion during the milling step. In the present study, the sharp edges of the ribblets may have led to a higher fraction of fines, because the shear and collision forces at the edges of the ribblets are more pronounced than for the more rounded ribbons. Additionally, the ribblets may have had a longer residence time in the granulator compared to the

ribbons, since the ribblets had all the same size whereas the ribbon sample consisted of smaller and bigger compacts resulting in a more variable residence time.

It must be noticed that the granulation step was more material consuming (150 g/run) than the simulation of the roll compaction (≈ 5 g/setting). A transfer to a small-scale mill, which could provide granule size distributions like the granulation unit of the Mini-Pactor, would be beneficial. Vendola and Hancock (2008) investigated the influence of different types of mills and the milling conditions on the particle size distribution. It was found that similar particle size distributions can be achieved with some experimental effort to find the correct milling process conditions for the different mill geometries. However, the hybrid modelling approach is still less material and time consuming than the conventional trial and error methods. To summarise, beside the observed differences in the fraction of fines granulation of ribbons and ribblets led to comparable granule size distributions.

3.4.4 Tableting

The uncompacted powder blend and the granules obtained of ribbons and ribblets were compressed to tablets on the Styl'One Evolution (section 5.2.8). The tablet target mass was 200 mg, resulting in a drug content of 50 mg per tablet. The powder blend was weighed in for each tablet and was filled into the die by hand due to its poor flowability. In contrast to that, it was possible to use a force feed shoe for the granules, which indicates an improved flowability. However, an over-fill of the die was necessary to assure a uniform die filling. The over-fill for the ribbon granules was set at 2 mm, whereas the over-fill for the ribblet granules had to be increased to 4 mm. This might be linked to the higher fraction of fines for the ribblet granules. Small particles have a higher specific surface area, which leads to higher inter-particle bonding and thus to a reduced flowability. The adhesive forces outweigh the gravity forces so that the die filling is negatively affected (Schiano et al., 2018, Xie and Puri, 2012).

Table 3.4-6: Experimental design for tableting

Factor	**Level**
Starting material	Ribbon granules, ribblet granules, uncompacted powder
Compression pressure [MPa]	50, 100, 150, 200, 250

Compression pressures in a range between 50 and 250 MPa were used to produce the tablets. Hence, the resulting full-factorial experimental plan consists of the qualitative factor starting material and the

quantitative factor compression pressure (Table 3.4-6). The target criteria mass uniformity, tensile strength and disintegration time were analysed.

3.4.4.1 Mass Uniformity

The mass uniformity of the tablets was evaluated according to section 5.2.13.1. The coefficient of variation of the tablet weight is shown in Figure 3.4-4 a. The maximum deviation from the mean weight was plotted for the different tablet batches in Figure 3.4-4 b. The results do not show a correlation between the compression pressure and the mass uniformity of the tablets, but differences between the tablet types were observed. The tableting of granules was repeated twice at 150 MPa, since this setting was the centre point of the chosen design of experiment, whereas the direct compression of the powder blend was performed only once.

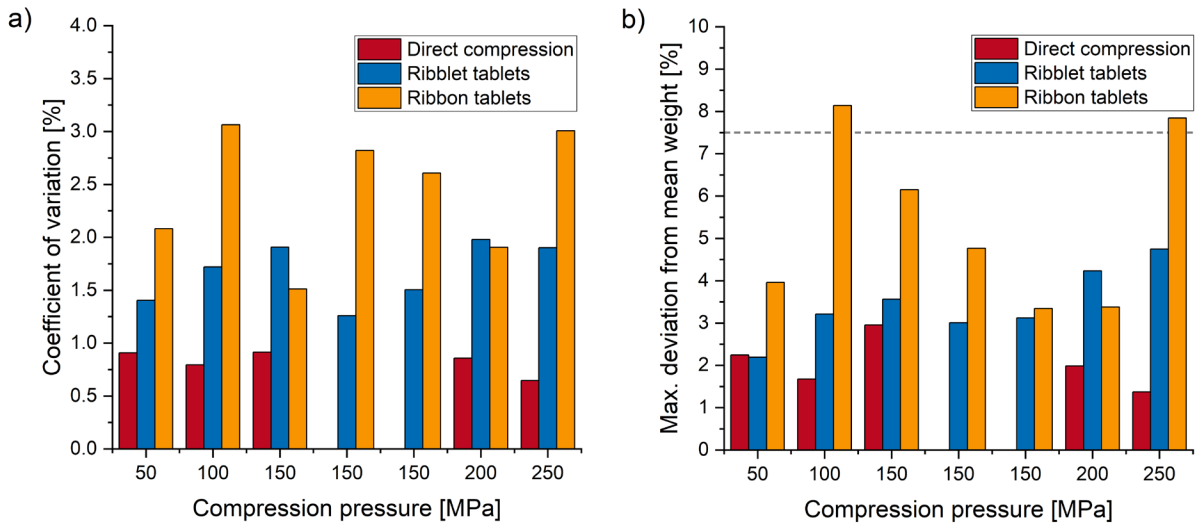

Figure 3.4-4: a) Coefficient of variation of the tablet weight b) Percentage maximum deviation of a single tablet from the mean weight of 20 tablets for the different compression pressures and types of tablets, grey line at 7.5 % represents the limit according to the European Pharmacopoeia; n=20, mean

The tablets of the unprocessed powder blend matched the test criteria of the European Pharmacopoeia the best with values below 3 % maximum deviation from the mean weight and with coefficients of variation smaller than 1 %. However, this result is misleading since the tablets of the unprocessed powder blend had to be weighed in manually and the die was filled by hand due to the poor flowability. The manual execution allowed an exact weighing to the target weight.

Ribbon and ribblet granules in contrast, could be compressed to tablets using the force feed shoe, because the flowability was improved by roll compaction/dry granulation. This is in accordance with the findings of Schiano et al. (2018), who showed that dry granulation positively influences the die filling in tableting due to the increased particle size. In the present study, ribbon and ribblet granules

resulted in tablets with an acceptable mass uniformity. Only the ribbon tablets showed at 100 and 250 MPa one tablet out of twenty with a maximum deviation from the mean above 7.5 % but below 15 %, so that the criteria of the European Pharmacopoeia for the mass uniformity of single dosed units (monograph 2.9.5) were still met.

The higher mass deviations could be attributed to a non-uniform filling of the die, which was favoured by the relatively high fraction of fines in the granules. Contradictory was that the ribblet granules possessed a greater fraction of fines than the ribbon granules but resulted in tablets with smaller mass variation. An explanation for this could be a non-uniform distribution of the fines within the ribbon granules in the feed shoe (Guo et al., 2011b). Another reason might be the different over-fill settings for ribbon and ribblet granules (section 5.2.8). The ribbon granules were tableted with an over-fill of 2 mm whereas the ribblet granules were compressed with an over-fill of 4 mm. The higher over-fill resulted in a more uniform filling of the die.

3.4.4.2 Solid Fraction and Tensile Strength

The weight, the dimensions and the hardness of direct compressed, ribblet and ribbon tablets were measured with a semi-automatic tablet testing system and the tensile strength was calculated according to Fell and Newton (1970) (section 5.2.13.2). The tensile strengths are compared in Figure 3.4-5. A value of 2 MPa was considered to be the threshold for a sufficient tensile strength that allows good handling of the tablets (Osei-Yeboah and Sun, 2015, Paul and Sun, 2017, Sun et al., 2009). The tensile strength increases with an increasing compression pressure. The tensile strength of the direct compressed tablets ranged between 0.43 at the lowest and 4.3 MPa at the highest investigated compression pressure. Ribbon and ribblet tablets showed tensile strengths from 0.26 to 3.5 MPa and from 0.25 to 3.5 MPa, respectively. For the three types of tablets, the aimed tensile strength of 2 MPa (dashed line) could be reached – for direct compressed tablets between 125 and 150 MPa and for ribbon and ribblet tablets between 150 and 175 MPa.

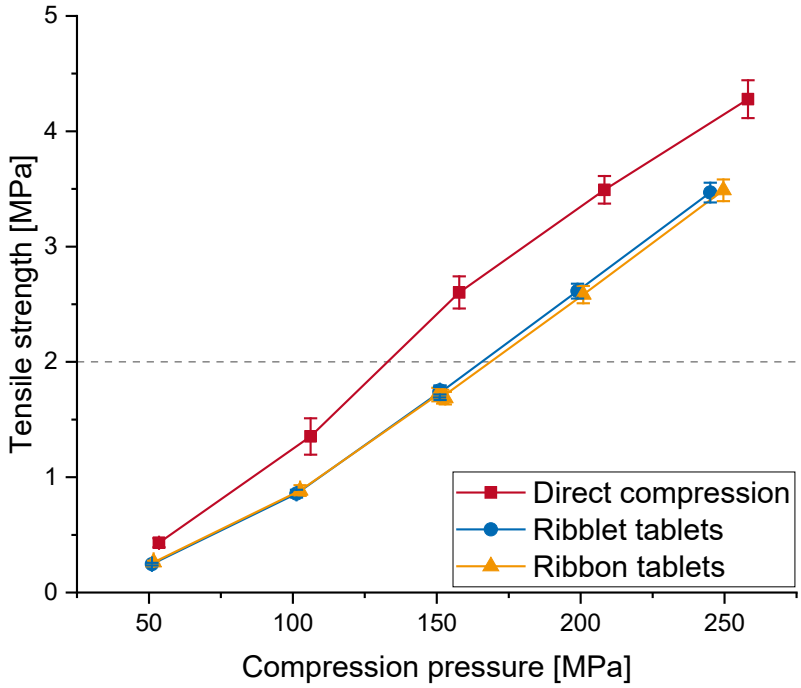

Figure 3.4-5: Tablet tensile strength as a function of the compression pressure (tabletability) for ribbon tablets, ribblet tablets and direct compressed tablets, dashed line: 2 MPa; n=20, mean ± SD

The compression pressure – tensile strength curves for ribbon and ribblet tablets in Figure 3.4-5 overlap at all measured points, whereas the direct compressed tablets show a systematically higher tensile strength. This can be explained by the loss in tabletability after (mimicked) roll compaction/dry granulation. A reduced tabletability in case of a recompression is an often described phenomenon in literature (Freitag and Kleinebudde, 2003, Kochhar et al., 1994, Kochhar et al., 1995, Sun and Himmelspach, 2006). Malkowska and Khan (1983) found that the higher the applied pressure during the first compression was, the more pronounced the reduction in tensile strength of the final tablets was. Various mechanisms were discussed in literature to be responsible for the loss in tabletability. Sun and Kleinebudde (2016) stated that both, particle size enlargement and granule-hardening are the main factors leading to the reduced tensile strength of tablets after roll compaction.

In Figure 3.4-6, the compactibility (solid fraction - tensile strength), compressibility (compression pressure - solid fraction) and tabletability (compression pressure - tensile strength) of the different tablets are compared. Tablet tensile strength increases with an increasing solid fraction for the three investigated types of tablets. It is visible, that besides the tabletability also the compactibility of ribbon and ribblet tablets is reduced: they reach the same tensile strength only at higher solid fractions than the direct compressed tablets. The different fraction of fines in the ribbon and ribblet granules (section 3.4.3) did not affect the tablet tensile strength, which was reported as well by Yohannes et al. (2015).

The compressibility for all three types of tablets is similar. Even though the granules have already been exposed to pressure during the roll compaction step, they resulted in tablets with the same solid fraction when they were exposed to the same compression pressure as the uncompacted powder mixture, which is in accordance with results described in literature (Herting and Kleinebudde, 2007). Farber et al. (2008) suggested that powder compaction is a cumulative process and developed a unified compaction curve which combines the compaction of a powder in roll compaction and subsequent tableting with direct compression.

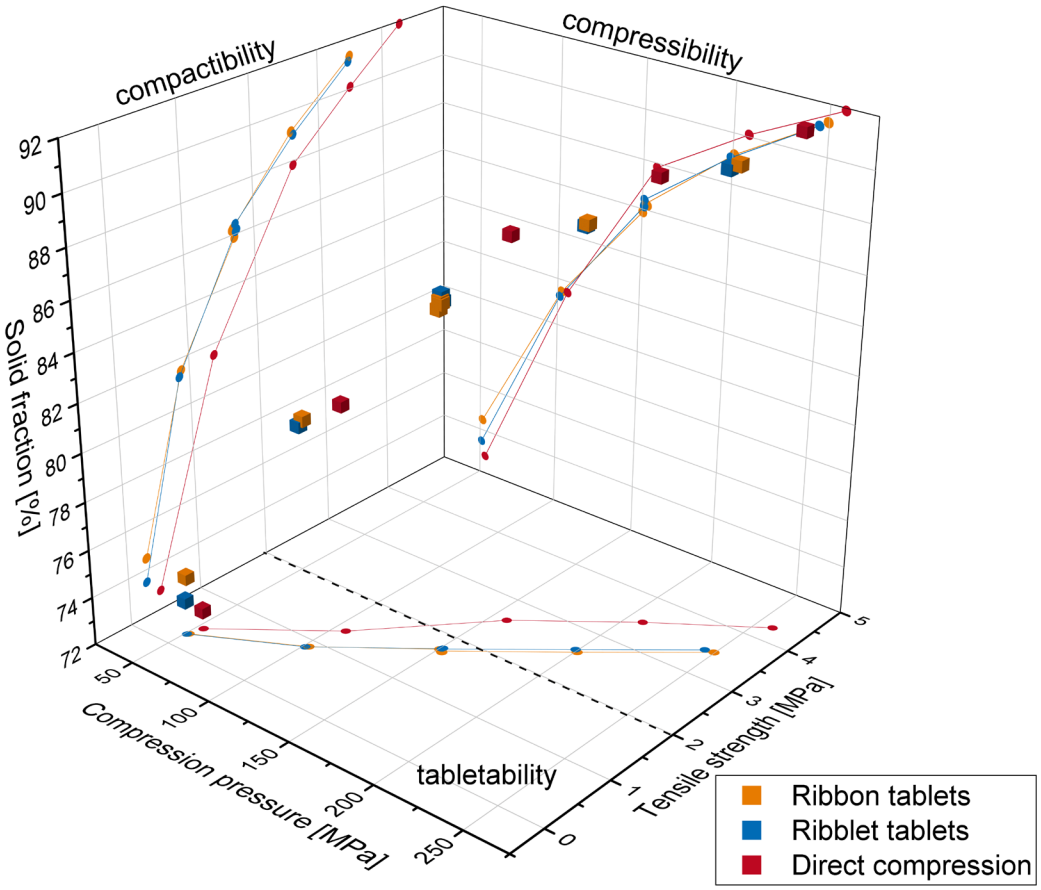

Figure 3.4-6: Compactibility, compressibility and tabletability of ribbon tablets, ribblet tablets and direct compressed tablets, n=20, mean

The similar solid fractions and tensile strengths of the tablets produced with ribbon- and ribblet-granules indicate that the compression pressure on the Styl'One corresponds well to the applied specific compaction force on the Mini-Pactor. The results support the findings for the ribbon and ribblet solid fraction. They show that mimicking ribbons by producing compacts with the same solid fraction is a reasonable approach to reproduce the downstream process with little material input.

3.4.4.3 Disintegration

The disintegration time was determined as described in section 5.2.13.3 to evaluate if the tablets fulfil the criteria of the European pharmacopoeia and if differences between directly compressed, ribbon- and ribblet-tablets can be observed. Figure 3.4-7 depicts the individual and mean disintegration times as a function of the compression pressure.

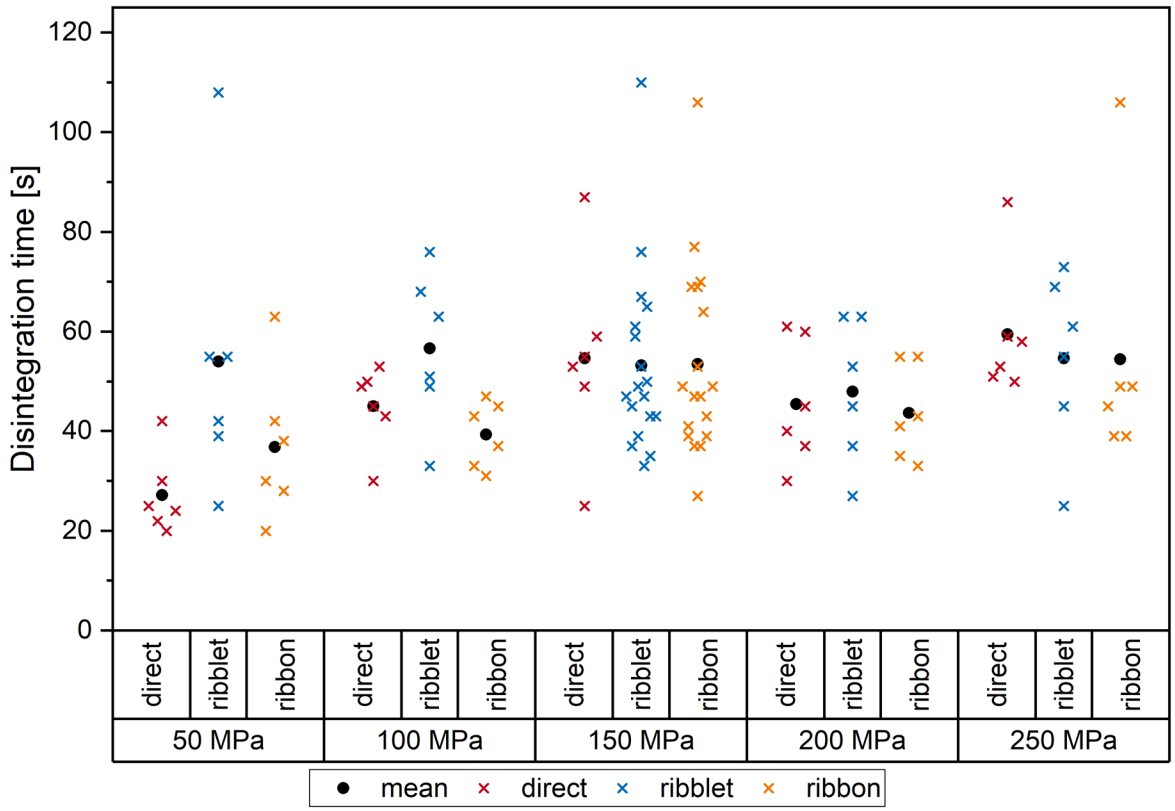

Figure 3.4-7: Disintegration time in dependence on the compression pressure for ribbon tablets, ribblet tablets and direct compressed tablets; individual data points and mean values, n≥6

The disintegration times show high variations within one group of tablets and compression pressure. All tablets disintegrated between 20 and 110 seconds, so that they fulfilled the disintegration criteria (< 15 min) of the European Pharmacopoeia for immediate-release formulations.

For crospovidone it is stated that the main mechanism responsible for its ability to work as disintegrant is the strain recovery (Desai et al., 2016, Markl and Zeitler, 2017, Quodbach and Kleinebudde, 2016). Strain recovery was described as the ability of a material to memorise its original shape and to recover up to a certain level to this shape after a strain (Lendlein and Kelch, 2002). The effect of compression pressure during tableting on the swelling when a compact containing crospovidone comes to contact with a liquid was investigated amongst others by Quodbach and Kleinebudde (2016). The uni-

directional expansion is strongly pressure dependent. Therefore, it was expected for the present study that the disintegration times would decrease with increasing compression pressure.

The results within the group of direct compressed tablets were contradictory to the expectations - a slight trend to higher disintegration times with increasing compression pressure was observed. However, due to the high variations this effect is not conclusive. It must be considered, that the fraction of the disintegration agent crospovidone of 5 % (m/m) is comparably high and the disintegration times are all noticeably short. This may have overshadowed the effect of the compression pressure on the disintegration time within the group of direct compressed tablets.

For the disintegration time of ribbon- and ribblet-tablets in dependence on the compression pressure, no trend was observed. Berkenkemper (2019) hypothesised that the programming of the crospovidone is already completed during the roll compaction step. After granulation, the particles are randomly oriented and so they are in the final tablets. The compression pressure applied during the tableting step has no clear effect on the performance of the disintegrant, because the programming of the chains was already done during roll compaction. Since the shape recovery of polymer chains is in the opposite direction of the programming but their orientation in the tablet is randomly, the resulting shape recovery of the tablet is omni-dimensional.

It was stated that the omni-dimensional shape recovery is less effective than the unidimensional one of directly compressed tablets (Berkenkemper, 2019), but this was not observed in the present case. Overall, there were no relevant differences in disintegration times between the three groups of tablets. This could be linked to the similar tablet porosities (Figure 3.4-6). Tablets showing the same porosity have similar disintegration times even if they differ in their tensile strength due to different pressures applied during roll compaction (Rajkumar et al., 2016). Another reason could be again the high fraction of crospovidone in the formulation resulting in short disintegration times. In terms of a formulation optimisation, it might be possible to reduce the proportion of the disintegration aid, save costs and still meet the criteria of the European Pharmacopoeia for immediate-release formulations.

3.4.5 Summary

The downstream process was mimicked with a formulation containing HCT as API to test whether the hybrid modelling approach can be extended from the so far tested pure excipients to formulations with multiple ingredients. It was evaluated whether it is enough to consider the critical quality attribute ribbon solid fraction to determine the process parameters. It was investigated whether the quality attributes of

the intermediates - ribbons/ribblets and granules – are similar comparing the roll compaction and the roll compaction simulation. Furthermore, it was investigated whether roll compaction and roll compaction simulation with the hybrid modelling approach result also in tablets with comparable quality attributes.

The process parameters to obtain ribblets with a solid fraction of 60 and 80 % at a 2 mm and 4 mm gap width were identified with the Styl'One and these parameters were transferred to the roll compactor. The production of ribblets and ribbons with a target solid fraction was successful, the deviations between target and measured solid fraction were smaller than 4.6 % (corresponds to a highest total deviation of 3.3 % SF) and the differences between ribbon and ribblet solid fractions were smaller than 1.2 %. The milling of ribbons and ribblets led to similar granule size distributions but the ribblet granules had a higher fraction of fines (D10% ribblets: 25 µm; D10% ribbons: 40 µm). However, this difference had no relevant influence on the tableting step and the resulting tablet properties. Tablets from ribbons and ribblets produced at five different compression pressures from 50 to 250 MPa have similar properties, whereas the properties of the tablets produced by direct compression at the same compression pressures differed in some parts. Roll compaction and roll compaction simulation led to a reduced tabletability compared to direct compression. Nevertheless, it was possible to produce tablets with tensile strengths above 2 MPa. The mass uniformity was acceptable for the three groups of tablets. However, the flowability was improved by granulation, which allowed a filling by the feed shoe for the granules instead the filling by hand for the powder blend. It was expected that differences in disintegration times would occur between the granules and the powder blend, but this was not confirmed by the experiments. Instead, similar disintegration times were obtained for all three groups of tablets at all pressures investigated. Nevertheless, all tablets fulfilled with disintegration times smaller than two minutes the requirements of the European Pharmacopoeia which demands disintegration times below 15 minutes.

To conclude, it was shown for the first time that only approximately 5 g of material are necessary to find the correct settings for the roll compaction step by hybrid modelling for a formulation containing an API and several excipients. The downstream process from the starting powder to the final tablet was successfully realised with sufficient accuracy, which can considerably save time and costs in the formulation development.

4 Summary

RC/DG has gained in importance in the production of solid dosage forms containing heat or moisture sensitive excipients or APIs. Simulating the process is of specific interest during formulation development since often only small amounts of the materials are available at this early point. It was aimed in this work to develop a time and material saving method to mimic and simulate the roll compaction process by uniaxial compaction with the compaction simulator Styl'One Evolution. In the hybrid modelling approach, the critical quality attribute solid fraction is used to compare the quality of real ribbons from roll compaction with the one of the mimicked compacts (ribblets). Besides some information about the compactor design (roll diameter, roll width), the modelling approach only needs the powder density of the starting material as input parameter. The rolls are represented by rectangular flat faced punches, the gap width is mimicked by the minimum distance between upper and lower punch, the roll diameter and roll speed are represented by the U-shaped punch movement profile. First, learning steps are carried out, in which a few tablets are produced to evaluate the compression behaviour at different filling heights. Then, the compression pressure on the tablet press can be converted into the specific compaction force on the roll compactor needed to obtain ribblets and consequently ribbons with the desired solid fraction.

In a first step, the hybrid modelling approach was verified with data from roll compaction experiments. Roll compaction was performed on the Gerteis Mini-Pactor with three materials showing different compaction behaviour - MCC, lactose and DCPA - in a wide range of specific compaction forces and at different gap widths. Statistical models were established, which describe the factors that have significant linear and quadratic effects on the ribbon solid fraction. Then, mimicking was performed with the Styl'One. The solid fraction at a certain specific compaction force was initially overestimated. After establishing a correction factor (Kp factor), it was possible to produce ribblets showing the same solid fraction as ribbons from roll compaction. The hybrid modelling approach was successfully calibrated and a material and process parameter independent Kp factor of 0.667 was determined. General relationships linking the gap width and the specific compaction force with the compression pressure acting on the powder were found. The same specific compaction force leads to different compression pressures depending on the material and the gap width. Applying the same specific compaction force at different gap widths leads to different ribblet solid fraction but applying the same compression pressure at different gap width results in the same ribblet solid fraction. Hence, the specific compaction force is a result of the compression pressure, the materials compressibility and the gap width. In a next step, the

investigations were extended to the BRC25, a roll compactor which resembles the Mini-Pactor in many parts of the machine design like the roll width, roll diameter and feeding system, to evaluate whether the Kp factor is independent of the used roll compactor. Roll compaction and mimicking were performed with MCC and lactose. A Kp factor of 0.714 similar to the one of the Mini-Pactor was found and again, it was possible to produce ribblets with the same solid fraction as ribbons from roll compaction. The WP120 was chosen for further investigations regarding the influence of the machine design on the Kp factor since it differs considerable from the so far used roll compactors in the feeding system, the roll arrangement, the sealing system, the roll diameter, and the roll width. The circumferential roll speed was adapted to the Mini-Pactor and the BRC25. Roll compaction was performed with MCC and DCPA. Two roll widths and two roll surfaces were included in the experiments. Besides the specific compaction force and the gap width, both factors had a small but significant effect on the ribbon solid fraction. It was assumed, based on screw torque data, that pre-compaction occurred in the feeding system and that this is the cause of the partially contradictory effects of the gap width on the ribbon solid fraction. It was not possible to determine one single Kp factor for all materials and settings, since roll width and diameter as well as the roll surface seem the cause changes which cannot be mimicked by the Styl'One. Roll compaction of MCC and DCPA was also performed on the WP200 so that a further roll compactor with different roll width and diameter was included to the experiments. As for the WP120, it was not possible to find a uniform Kp factor for the WP200. It was dependent on the material and the roll speed, whereby the latter must be considered with caution due to the small amount of underlying data. For both compactors, WP120 and WP200, this material dependence was mainly attributed to the fact that hybrid modelling cannot consider the processes in the feeding system. Comparing the compactors, ribbons produced by the WP120 show a higher solid fraction compared to the BRC25 and the Mini-Pactor at the same specific compaction force, which is caused amongst others by the pre-compaction in the feeding system, the smaller roll diameter and the different sealing system. The compactors differ in their process performance: the WP120 showed limitations in the feasible process parameter settings, especially at higher gap widths and specific compaction forces. The WP120 might not have been in its optimal working range due to the chosen experimental plan, which was designed closely to the ones for the BRC25 and the Mini-Pactor. However, the desired ribbon solid fractions could be produced. From the obtained results, it cannot be clearly deduced, on which influencing factors exactly the Kp factor depends. However, the feeding system, the roll width and the roll diameter seem to be relevant. This is also supported by the fact that compactors, which are similar in their machine design, have similar Kp factors. Additionally, the differences in powder compaction between the roll compaction process and

the die compression process like the non-uniform powder transport between the rolls could contribute to the Kp factor.

Although ribblets with the same solid fraction as ribbons could be obtained, deficiencies in the prediction of the ribblet solid fraction were observed. This lack in prediction accuracy was attributed to the elastic recovery of the ribblets after compression which was not considered by the solid fraction calculations. In the second part of this work, a method to measure the axial in-die elastic recovery was developed and several materials were evaluated regarding their in-die elastic recovery. A dependence on the gap width and the compression pressure was observed for the magnitude of the elastic recovery. For some materials, the elastic recovery increased with increasing compression pressure, for others it decreased. The in-die elastic recovery measurement was implemented to the simulations and the zero force method was established. It was possible to reduce the errors in solid fraction prediction, but some deviations were remaining. Therefore, the out-of-die elastic recovery was studied by confocal chromatic measurements. The material recovers quicker in the beginning and that the elastic recovery slows down until a final ribblet height is reached. Additionally, the out-of-die elastic recovery in radial direction was investigated, which is considerably smaller compared to the elastic recovery in axial recovery and was therefore not included in the solid fraction calculation. An out-of-die method for solid fraction prediction with an additional learning step was established considering the elastic recovery after one minute and the prediction errors could be reduced considerably to values smaller than 2.5 % for MCC. It is now possible not only to produce ribblets with the same solid fraction as ribbons but also to preselect the desired ribblet/ribbon solid fraction at a certain gap width and the Styl'One returns the specific compaction force that must be set on the compactor for this purpose. When the die is filled by hand, only approximately 5 g of material are needed to find the required specific compaction force, which is a noticeably smaller amount compared to other simulation methods.

In the third part of this thesis, a method was developed to estimate nip angles for the Mini-Pactor by uniaxial compression. The nip angle is the angle, at which the material feed between the rolls starts and the powder at the roll surface has the same speed as the rolls. The influence of the gap width, the specific compaction force and the roll speed on the nip angle was investigated for MCC, lactose and DCPA and evaluated by statistical analysis. The nip angle was found to be dependent on the Hausner ratio, the gap width, and the specific compaction force as well as on the roll speed. The method provides only estimated values, but the obtained results are near to values reported in literature. The method was

implemented to the simulation software. As a next step, a practical verification of the estimations on a roll compactor would have to be carried out.

Finally, after successfully mimicking the roll compaction process with pure excipients, the hybrid modelling approach was extended to a formulation containing multiple ingredients. With this HCT containing formulation, the whole downstream process - powder blend preparation, roll compaction, dry granulation and tableting - was mimicked. The desired process parameters to obtain ribbons with certain solid fractions were determined with the Styl'One and transferred to the roll compactor. The solid fractions of the produced ribbons and ribblets were in good agreement with each other and as well with the pre-set target solid fraction on the Styl'One. The ribbons and ribblets from the centre point settings were granulated in the granulation unit of the Mini-Pactor, the PSD was determined and both types of granules showed the typical bimodal PSD. However, the ribblet granules had a higher fraction of fines, which was attributed to the rectangular shape of the ribblets resulting in a higher friability during granulation. The granules and the uncompacted powder blend were pressed to tablets at different compression pressures and the tablets were analysed regarding their properties. The expected loss in tabletability was observed for the tablets made from granules compared to the directly compressed tablets. Tablets made from ribbon and ribblet granules possessed almost identical porosity, tensile strength and disintegration time. It was shown for the first time that it is possible to predict and mimic the roll compaction process for a formulation containing multiple ingredients by the hybrid modelling approach with a considerably low time and material consumption. Furthermore, the whole downstream process could be mimicked successfully by only using the ribbon/ribblet solid fraction as critical quality attribute.

5 Experimental Part

5.1 Materials

The materials used in the present work are listed in Table 5.1-1.

Table 5.1-1: List of used materials

Substance	Name/grade	Source of supply
Microcrystalline cellulose	Vivapur 102	J. Rettenmaier & Söhne
Lactose monohydrate	Tablettose 80	MEGGLE
Lactose monohydrate	Granulac 200	MEGGLE
Dibasic calcium phosphate anhydrate	DiCaFos A150	Chemische Fabrik Budenheim
κ-Carrageenan	Gelcarin GP 812	FMC Biopolymer
Hydroxypropylmethylcellulose	Pharmacoat 603, 3 mPa*s, substitution type 2910	Shin Etsu
Magnesium stearate	Ligamed MF-2-V	Peter Greven
Hydrochlorothiazide micronized	HCT Micro II	Abic (Teva Group)
Copovidone	Kollidon VA64	BASF
Crospovidone	Kollidon CL-SF	BASF

5.2 Methods

5.2.1 Design of Experiments

The experimental plans were created with the help of the software MODDE 12 (Sartorius Stedim Biotech), which was also used to statistically analyse the results. Full factorial multilevel experimental plans were generated to investigate the effects of various influencing factors on the target response. The experiments were performed in randomised order to avoid systematic errors. If settings were found to be technically not feasible, the points were left out and/or the experimental design was adapted. The individual experimental settings were generally carried out only in one single run. These single runs were extended by a centre point, which is carried out three times. The settings at the centre point result

from the factor levels of the chosen experimental design and are in their centre. The centre point allows for statements about the reproducibility of the experiment, which would not be possible with a single execution. All statistical models shown in this work are built upon a significance level of 0.95.

To interpret the quality of a regression model, several parameters can be used. The coefficient of determination R^2 describes the goodness of fit, meaning how well the regression model can fit the raw data. R^2 can take values between 0 and 1, where 1 means a perfect model and 0 no fit at all. The parameter Q^2 complements R^2 and describes the goodness of prediction. It expresses how good the prediction quality of the regression model is. It can take values from minus infinity to 1, where 1 means again a perfect model. The difference between R^2 and Q^2 should be smaller than 0.2-0.3. The third parameter is the model validity, which is a statistic value based on ANOVA evaluation. It is obtained from the lack of fit test and describes, e.g., whether the chosen model (linear, interaction, quadratic, …) is appropriate. The higher the value the better the model validity, where values above 0.25 indicate a valid model. Another parameter, which can be considered to evaluate the model quality, is the reproducibility. It describes the variability of replicates. If the variability is small, the reproducibility takes high numerical values. In contrast, if the reproducibility takes small numerical values below 0.5, the variability is high, which can be an indicator for a poor control of the experimental setup. (Eriksson et al., 2008)

Model optimisation to improve its prediction capability was carried out using coefficient plots. The coefficient plot displays the scaled and centred coefficients and their confidence intervals for the response of interest. If the confidence intervals include the value 0, the respective coefficient can be considered as non-significant. In this case, the non-significant coefficients were excluded from the model. This exclusion should result in a simpler model with an increased Q^2.

5.2.2 Storage of Materials and Samples

The used materials and blends were stored under controlled temperature and humidity conditions (21 °C, 45 % RH) for at least 72 h before the conduction of the experiment to allow equilibration with the surrounding. The collected samples were as well stored at the above-mentioned conditions before they were analysed to avoid effects of temperature and humidity on the results.

5.2.3 Powder Blend Preparation

The components of the blends were sieved through an analytical sieve with a mesh size of 355 µm to destroy any existing agglomerates. They were weighed individually on an analytical balance. The blends were produced using free-fall mixers. A Turbula® mixer (T2C, W.A. Bachhofen, Switzerland) was used

to blend batches smaller than 1 kg. The ingredients were blended for 20 minutes. A LM40 mixer (L.B. Bohle, Germany) was used for the blending process of batches bigger than 1 kg up to 5 kg. The ingredients were mixed for 20 minutes at a rotation speed of 30 rpm.

5.2.4 Roll Compaction

5.2.4.1 General

The production of ribbons by roll compaction was performed on four different types of compactors: Mini-Pactor (Gerteis, Switzerland), BRC25 (L.B. Bohle, Germany), WP120 and WP200 (Alexanderwerk AG, Germany). The experiments on the Mini-Pactor and the BRC25 were conducted under controlled temperature and humidity conditions of 21 °C and 45 % RH. The conditions for the experiments on the WP120 and WP 200 were not controlled but monitored. The temperature ranged between 16.9 and 25.4 °C and the relative humidity between 34.8 and 59.1 % RH.

The compactors were equipped with a system of control loops that keep the specific compaction force constant. The gap width was kept constant by dynamic adjustment of the feeding screw speed. The experimental designs included the parameters gap width, specific compaction force, roll width and roll speed as quantitative factors. Materials and roll surfaces were treated as qualitative factors. The runs were performed in randomised order and ribbon samples were collected for each parameter setting after the steady state conditions for gap width (± 0.1 mm) and specific compaction force (± 0.1 kN/cm) were reached. Each parameter setting from the experimental design (section 5.2.1) was carried out once. The centre point setting was conducted in triplicate to be able to assess the reproducibility of the process.

5.2.4.2 Gerteis Mini-Pactor

The Mini-Pactor was equipped with rolls with a smooth surface, a diameter of 250 mm and a width of 25 mm. The rolls had an inclined position of a 30° angle. A rimmed roll sealing system was mounted to keep the quantity of fines as low as possible. Two screws – a horizontal arranged feeding and a inclined arranged tamping screw - transport the powder from the hopper towards the rolls. The tamping to feeding screw speed ratio can be adjusted according to the material properties to assure a smooth powder transport. Roll speeds of 2 and 3 rpm and gap widths between 2 and 4 mm were set. The specific compaction forces ranged between 3 and 19 kN/cm. The process data was recorded with a frequency of 1 Hz. The detailed settings are shown in section 3.1.2 and 3.4.2.

5.2.4.3 Bohle BRC25

The BRC25 has horizontally arranged rolls with a smooth surface, which had a diameter of 250 mm and a roll width of 25 mm. A rimmed roll sealing system was mounted. Two screws – a horizontal arranged feeding and a vertical arranged tamping screw - convey the powder from the hopper towards the rolls. Specific compaction forces between 3.5 and 14 kN/cm were applied. The roll speed was kept constant at 2 rpm for all experiments and the gap width was varied between 2 and 4 mm. The granulation unit was not used. The acquisition of the process data for the specific compaction force, gap width, tamping and feeding screw speed and torque as well as the roll speed was performed with a frequency of 0.1 Hz. Due to a data error, the process data is only available for preliminary experiments with lactose and not for the experiments performed for the Kp factor determination. The detailed settings are shown in section 3.1.3 (Table 3.1-3).

5.2.4.4 Alexanderwerk WP120

The vertically arranged rolls had a diameter of 120 mm. Two roll surfaces – grooved and squared - were used as well as two different roll widths – 25 and 40 mm. A cheek plate sealing system was mounted. The powder is conveyed from the hopper to the rolls by a single horizontal screw. The screw size varies between the 25 and the 40 mm roll width. The granulation unit was not mounted for the conducted experiments. Gap widths from 2 to 4 mm and specific compaction forces from 3 to 14 kN/cm were applied at a constant roll speed of 4.2 rpm, which corresponds to the circumferential speed of the Mini-Pactor and the BRC25. The detailed settings are shown in section 3.1.4. For each parameter combination, a new batch was started. The acquisition of the process data for the specific compaction force, gap width, screw speed, screw capacity and roll speed was performed with a frequency of 0.1 Hz. The parameter screw torque, in contrast, was tracked batch wise. It is not an average value over the batch but a momentary record at the time of the switch of parameters for the new batch. The detailed settings are shown in section 3.1.4.1 (Table 3.1-6).

5.2.4.5 Alexanderwerk WP200

The vertically arranged rolls had a diameter of 200 mm, a roll width of 75 mm and a squared roll surface. The powder is conveyed from the hopper to the rolls by one single horizontally arranged screw. A cheek plate sealing system was mounted. As for the WP120, the granulation unit was not used since only the production of ribbons was relevant for the experiments. Roll speeds of 2.5, 5.2 and 8 rpm were set at a constant gap width of 3 mm. Specific compaction forces between 3 and 16 kN/cm were applied. The acquisition of the process data for the specific compaction force, gap width, screw speed, screw capacity

and roll speed was performed with a frequency of 0.1 Hz. The detailed settings are shown in section 3.1.5.1 (Table 3.1-9).

5.2.5 Roll Compaction Simulation

5.2.5.1 Hybrid modelling

The tableting instrument Styl'One Evolution (Medelpharm, France) was used for the hybrid modelling of the roll compaction process. The machine was controlled by the dedicated ANALIS software. Due to the improvements made to the model and their implementation to the software, there were repeated software updates throughout the work. The flow chart (Figure 5.2-1) provides an overview of the hybrid modelling process with the Styl'One, the learnings steps and the required input data to determine the specific compaction force to obtain ribbons with a desired solid fraction.

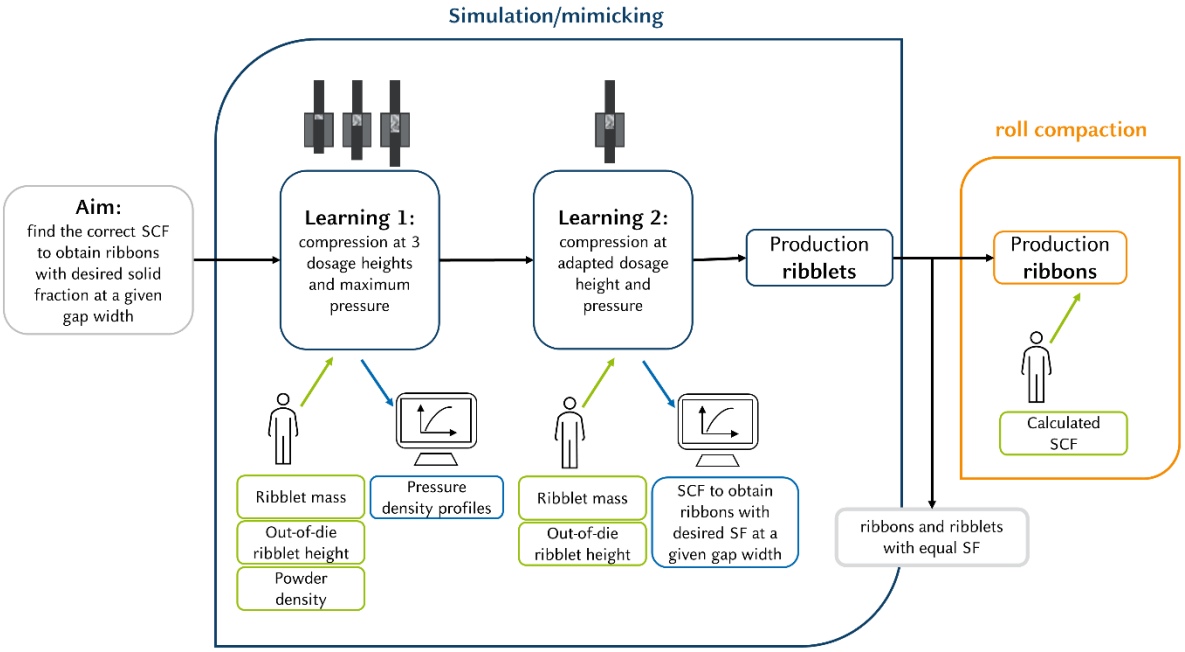

Figure 5.2-1: Flow chart of the simulation/mimicking process to determine the SCF needed to obtain ribbons with the desired solid fraction at a given gap width

The uniaxial compaction simulator was equipped with a pair of rectangular (20 mm x 10 mm) flat faced Euro D punches, which mimic the roll surface. The punch deformation was measured by pressing the upper and the lower punch directly against each other and was stored in the punch property file. The position of upper and lower punch was tared before each experiment and in regular intervals during the experiments using a metal gauge block of 1 mm thickness.

The data acquisition frequency for punch displacement and force sensors was set at 2000 Hz. The die was either filled manually by hand or by the force driven feed shoe. Depending on the flowability of the

used materials, two different paddles could be chosen for the feed shoe. One had thicker spokes and is used for acceptably flowing powders, the other had thinner spokes and is used for cohesive and poorly flowing powders. The paddle rotated at 20 % of the maximum speed.

The external lubrication unit was used for some experiments to avoid too high ejection forces. Magnesium stearate powder was dispersed by pressured air (3-4 bar) and was sprayed automatically onto the punches and into the die for 500 ms before each tableting cycle. The external lubrication is available during the production cycles as well as for the learning steps.

The value of powder density (section 5.2.10.1) was entered into the software, since is necessary for calculating and predicting the solid fraction of the ribblet. The type of roll compactor, which should be mimicked, was chosen in the software. For each roll compactor profile, data were available on the roll diameter, roll width, maximum and minimum speed, gap width and specific compaction force, which were included in the calculations. The roll speed, which should be mimicked, could be chosen in the range of speed that is technically feasible on the roll compactor.

At the beginning of an experiment, the software guided through different learning steps to gain information about the compaction behaviour of the material. At first, three ribblets were made at the maximum force of 51 kN (255 MPa) at different dosage heights. The dosage height expressed in mm is the position of the lower punch during the filling phase of the tableting cycle and determines the amount of powder, which can be filled into the die. If the punch is at its highest possible position, the dosage height is 0 mm. The default dosage heights in the learning were 5, 10 and 15 mm but they can be adapted if necessary. The alternative dosage heights were 3, 6 and 9 mm, which were used for materials showing too high ejection forces to avoid exceeding the safety threshold. The mass of each learning ribblet was measured with an analytical balance (AC1215, Sartorius) and was entered to the software. The ribblets had to be validated in the learning window before proceeding to the next dosage height. The production of the first learning ribblet was repeated until the die was evenly filled and a constant mass was reached.

A recipe is created, in which the desired parameters – dosage height, compression pressure (in MPa), solid fraction and gap width - can be defined. Two parameters can be chosen at a time and the others are calculated by the software based on the learnings. One can choose either the gap width and the target pressure, the gap width and the solid fraction, the gap width and the dosage height or the dosage height and the target pressure. To get reliable results for the compression pressure–specific compaction force relation, the Kp correction factor for the roll compactor of interest must be determined (section 5.2.5.2)

and entered to the recipe. The chosen target compression pressure is converted into the specific compaction force (kN/cm), which is then shown in the recipe.

Afterwards, a so-called advanced learning was performed, in which another ribblet was produced. This second learning was used to refine the recipe for the target dosage height and specific compaction force. The modification of the advanced learning was part of the thesis and the different approaches are described in more detail in section 3.2. After the recipe has been saved, a third learning was recommended to complete the knowledge about the compaction behaviour of the material. One ribblet was produced at a force, which corresponds to the one chosen in the recipe, and the software created a force-displacement profile.

The compression cycle considers the chosen gap width, which is represented by the minimum distance between the upper and the lower punch during compression. The compression speed and the sine shaped displacement mimic the roll dimensions and the roll movement. The desired amount of ribblets to be produced can be chosen as well as the compression cycles that should be saved. The option to save all cycles was chosen. After the production was completed, the process data were saved in an Excel sheet. Data for one single compression cycle can be exported manually.

5.2.5.2 Kp Factor Determination

The Kp correction factor must be determined experimentally for the roll compactor, which should be simulated. It compensates for hardly imitable parameters and adjusts the simulated specific compaction force so that it corresponds to the actual specific compaction force on the roll compactor. The corrected specific compaction force ($SCF_{corrected}$) is calculated according to equation (16),

$$SCF_{corrected} = \frac{SCF_{default}}{Kp} \tag{16}$$

where $SCF_{default}$ is the specific compaction force determined with the default *Kp* correction factor of 1.

To determine the Kp factor for the roll compactors, pure excipients were compacted on the roll compactor and on the Styl'One Evolution, where the default *Kp* factor of 1 was used. A wide range of specific compaction forces and gap widths between 2 and 4 mm were used. The ribbons and ribblets were analysed regarding their solid fraction according to section 5.2.10.

Visually

The *Kp* factor for the Mini-Pactor was determined visually. MCC, lactose and DCPA were compacted to evaluate whether the factor is material independent. The specific compaction force – solid fraction curves of ribbons and ribblets were plotted and fitted with a logarithmic function. The specific compaction force was changed by adjusting the Kp factor manually until the best visual alignment was achieved for both gap width curves.

Calculation (Excel, Solver Add-in)

The Kp factors for the BRC25 and the Alexanderwerk compactors were determined using the least square method with the "Solver" Add-In in Excel. The BRC25 Kp factor was determined using MCC and lactose as model substances. On the Alexanderwerk compactors WP120 and WP200, MCC and DCPA were used.

The specific compaction force of the roll compactor was plotted against the solid fraction of the ribbons. The data were fitted with logarithmic functions. The simulated specific compaction force of the Styl'One was plotted against the solid fraction of the ribblets and was fitted as well. A cell for the Kp factor was created, which was set at 1. The values in the column [A] of the simulated specific compaction forces were divided by the Kp factor (SCF/Kp).

A column [B] was created, in which the equation of the roll compactors fitting curve was solved by inserting the SCF/Kp values for the x-variable. Another column [C] was created, in which the least square errors between the columns [A] and [B] were calculated. A cell [D] was created, which contains the root mean square error (RMSE) resulting of the column [C]. Generally, the RMSE is calculated according to Equation (17) by dividing the sum of the squared differences between the predicted and the observed values by the sample size of the data set and taking the square root.

$$RMSE = \sqrt{\frac{\sum_{i=1}^{n}(P_i - O_i)^2}{n}} \tag{17}$$

where P_i is the predicted value and O_i is the observed value and n is the sample size of the data set.

The Solver Add-In for Excel can optimise variables in a cell to minimise or maximise the value in a target cell. The Kp factor cell was chosen as the variable. The cell [D] was chosen to be the target cell, that should be minimised. With an evolutionary algorithm the Kp value, that led to the smallest RMSE, was determined.

5.2.5.3 Solid Fraction Prediction

The solid fraction of the ribblets should be the same as the solid fraction of the real ribbons from the roll compactor. The predicted solid fraction is displayed in the recipe. The method of prediction in the advanced learning step was optimised in the context of this work and the different methods are described below.

Minimum Height Method

The minimum height method was the originally used method for the solid fraction prediction. The parameters, which should be chosen by the operator, were gap width and specific compaction force. The compression pressure was changed in the recipe until the desired specific compaction force was displayed. Afterwards, the learning ribblet was produced at the calculated dosage height based on the first learning step at a compression force of 51 kN (255 MPa). A pressure-density curve was recorded. The mass of the ribblet was determined on an analytical balance and entered to the software. The compression pressure changed automatically based on the performed learning and must be adjusted again until the correct specific compaction force was displayed. The predicted solid fraction $SF_{ribblet}$ was displayed in the recipe. It is calculated according to equation (18),

$$SF_{ribblet}[\%] = \frac{m}{\frac{h_{min} \times l \times w}{\rho_{powder}}} \times 100 \qquad (18)$$

where l and w are the punch dimension (20 mm x 10 mm), m the mass of the ribblet and h_{min} the minimum distance between the punches during compression. ρ_{powder} is the powder density of the starting material.

Zero Force Method

The zero force method should consider the fast in-die elastic recovery of the ribblets and as well its pressure dependence to achieve a more accurate solid fraction prediction. The principle of measuring the elastic recovery in-die is described in more detail in section 5.2.11.2. The advanced learning is conducted at the adapted dosage height. It is not performed at the maximum force of 51 kN (255 MPa) but at the one, which is calculated from the initial learning and should be finally used for ribblet production. A safety margin of 20 % is included in the learning pressure to ensure that the target pressure for production is within the investigated pressure range because the pressure-density curve cannot be extrapolated to higher pressures. The mass of the learning ribblet was measured on an analytical balance

(AC1215, Sartorius) and was entered into the software. The solid fraction of the learning ribblet ($SF_{ribblet}$) is calculated according to equation (19),

$$SF_{ribblet}[\%] = \frac{m}{\frac{h_{ZF} \times l \times w}{\rho_{powder}}} \times 100 \quad (19)$$

where m is the mass of the ribblet, h_{ZF} the distance between upper and lower punch when the force on the upper punch decreases to zero during its upward movement. l and w are the length and the width of the die dimensions (20 mm x 10 mm) and ρ_{powder} is the powder density of the starting material.

Out-of-Die Method

The elastic recovery is not finished inside the die but continuous after ejection. For the out-of-die method, the slow out-of-die elastic recovery was implemented to the learning phases. The first learning step is performed at 51 kN (255 MPa) as described in section 5.2.5.1. In addition to the mass of the learning ribblets, their height was also determined with a digital calliper (Mitutoyo, Japan) one minute after production. The desired settings were defined in the recipe. The additional learning phase was performed at the adapted dosage height and the adapted compression pressure to consider the pressure dependent elastic recovery. The mass of the learning ribblet was determined with an analytical balance (AC1215, Sartorius) and was entered to the software. The height of this second learning ribblet was measured with a digital calliper one minute after ejection and was saved in the software. This time period can be adapted according to the extent of elastic recovery of the used materials. The solid fraction can be calculated according to equation (20),

$$SF_{ribblet}[\%] = \frac{m}{\frac{h_{out-of-die} \times l \times w}{\rho_{powder}}} \times 100 \quad (20)$$

where m is the mass of the ribblet and $h_{out\text{-}of\text{-}die}$ the height of the learning ribblet, which was measured out of die with the digital calliper. l and w are the length and the width of the die dimensions (20 mm x 10 mm) and ρ_{powder} is the powder density of the starting material.

With this improved prediction method, it is also possible to get accurate results using the mode, in which the gap width and the desired solid fraction are chosen and the other parameters – SCF and dosage height - are calculated since it considers the elastic recovery of the compacts after compression.

Deviation from target solid fraction

The deviation of the measured ribblet or ribbon solid fraction after elastic recovery from the targeted solid fraction is calculated according to equations (21) and (22), respectively.

$$deviation\ from\ target_{ribblet}[\%] = \frac{|SF_t - SF_{ribblet}|}{SF_t} \times 100 \quad (21)$$

$$deviation\ from\ target_{ribbon}[\%] = \frac{|SF_t - SF_{ribbon}|}{SF_t} \times 100 \quad (22)$$

where SF_t is the target solid fraction, $SF_{ribblet}$ the measured ribblet solid fraction and SF_{ribbon} the measured ribbon solid fraction.

Error in solid fraction prediction

The deviation of the measured ribblet solid fraction after elastic recovery from the predicted solid fraction is called the error in solid fraction prediction and is calculated following equation (23).

$$error_{ribblet}[\%] = \frac{|SF_{pred} - SF_{ribblet}|}{SF_{pred}} \times 100 \quad (23)$$

where SF_{pred} is the predicted solid fraction and $SF_{ribblet}$ the measured ribblet solid fraction after elastic recovery.

5.2.5.4 Mimicking of an API Containing Formulation

A hydrochlorothiazide containing powder blend (composition of the mixture described in section 3.4.1) was compacted and granulated on the Gerteis Mini-Pactor. The granules were compressed to tablets. To save material and time in process development, the roll compaction process shall be mimicked using the out of die method (section 5.2.5.3). The process was simulated on the Styl'One Evolution at a roll speed of 3 rpm. Ribblets with solid fractions between 60 % and 80 % were simulated and produced. Due to the poor handling of the ribblets with a solid fraction smaller than 70 %, it was decided to produce ribblets and ribbons with target solid fractions of 70, 75 and 80 %. The ribbons were produced at the specific compaction forces, which were determined by the simulation on the Styl'One (Table 3.4-3). Ribbons and ribblets were characterised regarding their solid fraction to determine the prediction accuracy.

Ribbons and ribblets with the centre point solid fraction of 75 % were chosen to be granulated (section 5.2.7) and subsequently compressed to tablets (section 5.2.8). The granule size distribution (section 5.2.12) of ribbon and ribblet granules was compared. The tablet properties (section 5.2.13) tensile strength, uniformity of mass and disintegration time were investigated as well to evaluate if the mimicking of the whole downstream process is possible and accurate.

5.2.6 Nip Angle Estimation

The nip angle α is defined as the angle between the beginning and the end of the compaction zone. Figure 5.2-2 illustrates how the nip angle is estimated by roll compaction simulation on the Styl'One.

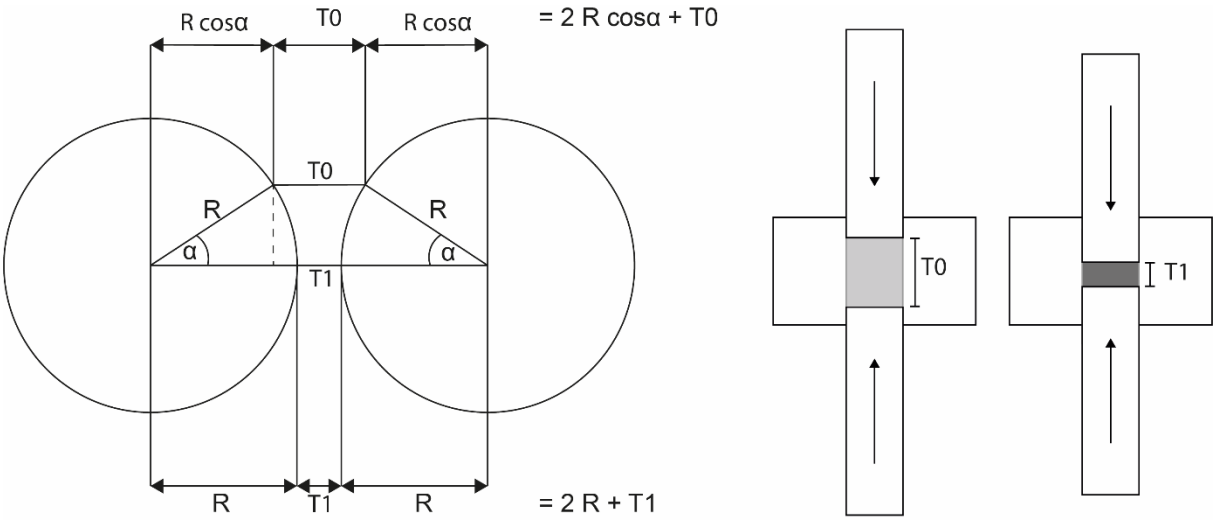

Figure 5.2-2: Principle of nip angle calculation with uniaxial compaction

On the roll compactor, T_0 is the distance between the rolls at the transition between the feeding and the compaction zone. On the Styl'One Evolution, this distance T_0 corresponds to the powder bed thickness, at which the force on the upper punch begins to increase significantly. This point is automatically determined by the ANALIS software, which analyses the force-displacement curve with an algorithm for a strong change in its slope.

T_1 is the minimum gap width on the roll compactor. This corresponds to the minimum distance between the upper and lower punch during compression on the Styl'One Evolution.

Two ways to mathematically describe the distance between the centres of the rolls are shown in equation (24). By equating the two terms and solving the equation for α, the nip angle can be calculated according to equation (25),

$$2 \times R \times \cos\alpha + T_0 = 2 \times R + T_1 \qquad (24)$$

$$\alpha = arccos\left(1 + \frac{(T_1 - T_0)}{D}\right) \quad (25)$$

where R is the radius and D the diameter of the rolls.

The influence of the mimicked specific compaction force and the gap width on the nip angle of MCC, lactose and DCPA was investigated. Furthermore, the Hausner ratio (section 5.2.9.4) of the excipients and the nip angle were correlated. The influence of the roll speed (3 – 11 rpm) on the nip angle was evaluated for MCC.

5.2.7 Granulation of Ribbons and Ribblets

Before further processing, ribbons and ribblets were stored for one day under controlled conditions (21 °C, 45 % RH). They were grained in the oscillating mill of the Mini-Pactor (Gerteis, Switzerland), which was equipped with a star rotor. A sieve with a mesh size of 1.0 mm was used. The distance between the sieve and the rotor was set at 1.0 mm. The star rotor rotated 120 ° clockwise at a rotational speed of 40 rpm and 180 ° counterclockwise at a rotational speed of 60 rpm. 150 g of the ribbons or ribblets were poured into the granulator unit and grained for 2 minutes. The obtained granules were collected in plastic bags. The fines, that adhered to the compactor were added to the granule samples. The granulation unit was cleaned between two batches. The yield was measured with a balance. The granules were stored under controlled conditions (21 °C, 45 % RH) for one day before they were further processed.

5.2.8 Tableting

The Styl'One Evolution (Medelpharm, France) was used for the tableting experiments. Euro B punches with a diameter of 8 mm were mounted. The punch deformation was determined by a direct punch to punch compression at a pressure of 255 MPa. At the beginning of each experimental day and after cleaning the punch from powder stuck on the punch surface during the experiments, a tare of the displacement sensors was performed using a metal gauge block of 1 mm thickness.

The die-filling for the tableting of the powder blend was performed manually by hand due to the bad flowability of the blend. Per tablet, 200 mg ± 5 mg were weighed on an analytical balance (AC1215, Sartorius) and filled into the die manually. For each parameter setting 32 tablets were produced.

The die-filling for the tableting of the granules was performed by a force driven hopper. It was equipped with a paddle, which is designed for bad flowing powder. The speed of the hopper was set at 10 %. The tablets were produced at five different compression pressures between 50 and 250 MPa. The target tablet mass of 200 mg was set by a learning phase. The dosage height was adjusted until the mass of 200 mg was achieved. 50 tablets were produced per parameter setting.

The over-fill is a possibility to achieve a more uniform die filling. The position of the lower punch (dosage height) determines the cavity for the powder necessary to achieve the desired tablet mass, assuming that the die is completely filled with powder. But for bad flowing powders, the die may not be entirely filled so that the tablet mass is smaller than the target. Using over-fill, the punch position is lower by a set distance than necessary during the die filling. The lower punch then moves upwards to the set dosage height so that any excess powder can be removed by the scraper of the fill shoe and the target tablet mass is reached. The over-fill was set at 2 mm for tableting the ribbon granules and at 4 mm for the ribblet granules.

The external lubrication unit was used to reduce the ejection forces. Magnesium stearate powder was sprayed onto the punches and into the die by compressed air. The pressure was set between 3 and 4 bar. The spray time was set at 500 ms. On the dosing unit, the minimum quantity of powder to be sprayed into the die was set.

The “One compression” profile of the Styl’One was used. It is characterised by a V-shaped displacement-time curve. The experiments were conducted in force mode. In the force mode, the upper punch compresses the powder until the set force is reached. To ensure an accurate detection (data collection frequency of 2000 Hz) of the tableting force, the tableting speed was set at 15 % of the maximum speed.

A full factorial experimental design was created. The compression pressure was set as an uncontrolled quantitative factor to consider process related fluctuations of the compression pressure. The type of powder/granule was set as a qualitative factor. Tablet mass (n=20), tensile strength (n=20) and disintegration time (n=6) were chosen as responses. The tablet characterisation is described in section 5.2.13.

5.2.9 Characterisation of Raw Materials

5.2.9.1 Residual Moisture

The residual moisture was determined with an infrared balance (MA 10D, Sartorius, Germany). The samples were dried at a temperature of 105 °C. The measurement was terminated as soon as the balance detected a change in residual moisture less than 0.1 %/min. The experiments were performed in triplicate and the mean was taken.

5.2.9.2 Particle Size Distribution

The particle size distribution of the raw materials was determined by dynamic image analysis with the CamSizer XT (Retsch, Germany), which was equipped with the X-Jet module. The size classes were chosen according to the European Pharmacopoeia in the range from 6 µm to 2000 µm. Approximately 25 g sample powder were filled to the funnel and the powder was transported to the measuring chamber via the vibration chute. The width of the nozzle was 4 mm and the distance between funnel and vibration chute was set at 4 mm. The samples were dispersed with an air pressure of 80 kPa to avoid agglomeration and wrong particle detection. A minimum of 1.5 million particles was analysed. The size parameter x_{min}, which provides similar results to an analytical sieving, was chosen for analysis. The measurements were performed in triplicate and the mean was taken.

5.2.9.3 Bulk and Tapped Density

Bulk and tapped density were determined with a tamping volumeter (J. Engelsmann AG Apparatebau, Germany) following the procedure of the European Pharmacopoeia (Council of Europe, 2020a). Bulk and tapped density are the ratio of the sample mass and the bulk or tap volume, respectively. To determine the bulk volume, 100.0 g or 60.0 g (depending on the bulk volume) of material were filled into the graduated cylinder (250 ml) without consolidating it and the bulk volume V_0 was recorded. To determine the tapped volume, the graduated cylinder was tapped 10, 500 and 1250 times until a change in volume less than 2 ml was detected. The final tapped volume V_f was recorded. The measurements were performed in triplicate. The bulk density and tapped density were calculated by equation (26) and (27) and the mean was taken.

$$\rho_{bulk}\left[\frac{g}{cm^3}\right] = \frac{m}{V_0} \tag{26}$$

$$\rho_{tapped}\left[\frac{g}{cm^3}\right] = \frac{m}{V_f} \tag{27}$$

5.2.9.4 Hausner Ratio

The Hausner ratio (*HR*) provides information about the flow and compaction properties of a material. It can be calculated by forming the ratio between bulk volume V_0 and final tapped volume V_f as shown in equation (28).

$$HR = \frac{V_0}{V_f} \tag{28}$$

5.2.9.5 Powder Density

The powder density ρ_{powder} was determined with the helium pycnometer AccuPyc 1330 (Micromeritics, USA). A sample chamber of 3.5 cm³ volume was used. A verification of the sample chamber volume and of a metallic sphere of known volume was performed at the beginning of each measurement day. About half of the sample chamber was filled with powder and the sample mass was determined with an analytical balance (MC 210 P, Sartorius). Ten purge cycles and five measurement cycles were performed per run. The temperature was kept constant at 25 °C ± 1 °C. The powder density was determined in triplicate and the mean was taken.

5.2.10 Solid Fraction

5.2.10.1 Powder Pycnometry

A powder pycnometer (GeoPyc 1360, Micromeritics, USA) was used to determine the ribbon and ribblet envelope density. The fines in the ribbon samples were removed by sieving the sample through a 2000 µm mesh size sieve. The ribblets were cleaned from dust with a brush. The method is described in detail by Zinchuk et al. (2004). Figure 5.2-3 shows schematically the measurement principle. Ribbon sample mass was determined by an analytical balance (CP 224 S, Sartorius / Type 1702, Sartorius). A sample volume of 15 % ± 5 % was targeted. DryFlo powder was filled into the measurement chamber, which had a diameter of 25.4 mm. The default conversion factor was set at 0.5153 cm³/cm. Three blank cycles were performed to determine the DryFlo volume at a consolidation force of 51 kN. The sample was added to the measurement chamber assuring that it was well surrounded by the DryFlo powder. Three sample cycles were performed at a consolidation force of 51 kN to determine the envelope volume $V_{envelope}$ of the sample. The relative density or solid fraction $SF_{compact}$ can be calculated by equation (29), where $\rho_{envelope}$ is the envelope density of the compact and ρ_{powder} is the powder density of the raw material, which is determined by helium pycnometry (section 5.2.9.5).

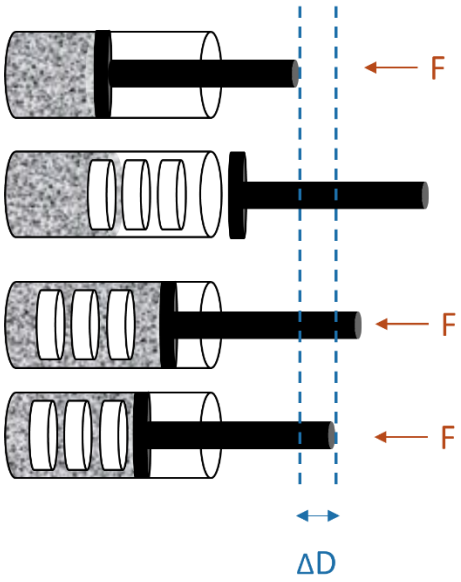

Figure 5.2-3:Principle of powder pycnometry measurements; F: consolidation force; ΔD: difference in punch position

The envelope density is calculated from the sample mass m and $V_{envelope}$. The measurements were performed at least in triplicate and the mean was taken. If the absolute standard deviation exceeded 2.5 %, another three samples were measured.

$$SF_{compact}[\%] = \frac{\rho_{envelope}}{\rho_{powder}} \times 100 = \frac{\frac{m}{V_{envelope}}}{\rho_{powder}} \times 100 \quad (29)$$

5.2.10.2 Micrometre Screw / Digital Calliper

Due to their regular shape, the ribblet envelope volume $V_{ribblet}$ can also be determined with a micrometre screw (Mitutoyo, Japan) or a digital calliper (Mitutoyo, Japan) by measuring the length, width and height of the ribblet (n=10). A prerequisite for this is that the ribblets are free of defects, e.g., from capping or sticking. The envelope density was obtained by forming the ratio of the sample mass, measured on an analytical balance (Sartorius Type 1702), and the envelope volume. The SF is the ratio between the envelope density and the powder density determined by helium pycnometry (section 5.2.9.1). It can be calculated using equation (30).

$$SF_{ribblet}[\%] = \frac{\rho_{envelope}}{\rho_{powder}} \times 100 = \frac{\frac{m}{l \times w \times h}}{\rho_{powder}} \times 100 \quad (30)$$

5.2.10.3 Chromatic Confocal Measurements

For the solid fraction calculation in section 3.2.4.1, the length and the width of the ribblets were assumed to be constant, 20 and 10 mm respectively. The change in height (axial direction) was detected by a chromatic confocal sensor (CHRocodile E, Precitec Optronik GmbH). Thus, the ribblet volume can be calculated. The ribblet mass was determined with an analytical balance (AC1215, Sartorius). The solid fraction can be calculated for each time point *t* according to equation (31),

$$SF_{ribblet}[\%] = \frac{\rho_{envelope}}{\rho_{powder}} \times 100 = \frac{\frac{m}{1\ cm \times 2\ cm \times h_{con}}}{\rho_{powder}} \cdot 100 \qquad (31)$$

where h_{con}, is the ribblet height at a time point t measured by the chromatic confocal probe (section 5.2.11.3).

5.2.11 Elastic Recovery

5.2.11.1 General

The elastic recovery of ribblets after compaction can be divided into the fast in-die elastic recovery and the slow out-of-die elastic recovery. Furthermore, a distinction is made between elastic recovery in axial and in radial direction.

5.2.11.2 In-die Axial Elastic Recovery

The fast in-die axial elastic recovery of different pharmaceutical excipients was evaluated regarding its dependency on various parameters with the Styl'One Evolution (Medelpharm, France). The occurring forces and the punch positions during the compression cycle were monitored by piezo electric force sensors and displacement transducers, which have a resolution of 1 µm and an accuracy of ± 5 µm (values provided by the supplier). The in-die elastic recovery ($ER_{in\text{-}die}$) is defined as the difference between the upper punch position at the minimum punch distance under load (h_{min}) and the upper punch position when the force decreases to zero in the upward movement after compression (h_{ZF}) divided by the minimum punch distance (h_{min}). Figure 5.2-4 a depicts schematically the punch positions for calculating the elastic recovery. It is calculated according to equation (32), which is modified after Armstrong and Haines-Nutt (1974).

$$ER_{in-die}[\%] = \frac{h_{ZF} - h_{min}}{h_{min}} \times 100 \qquad (32)$$

Figure 5.2-4 b shows exemplarily one compression cycle, in which the relevant heights are marked.

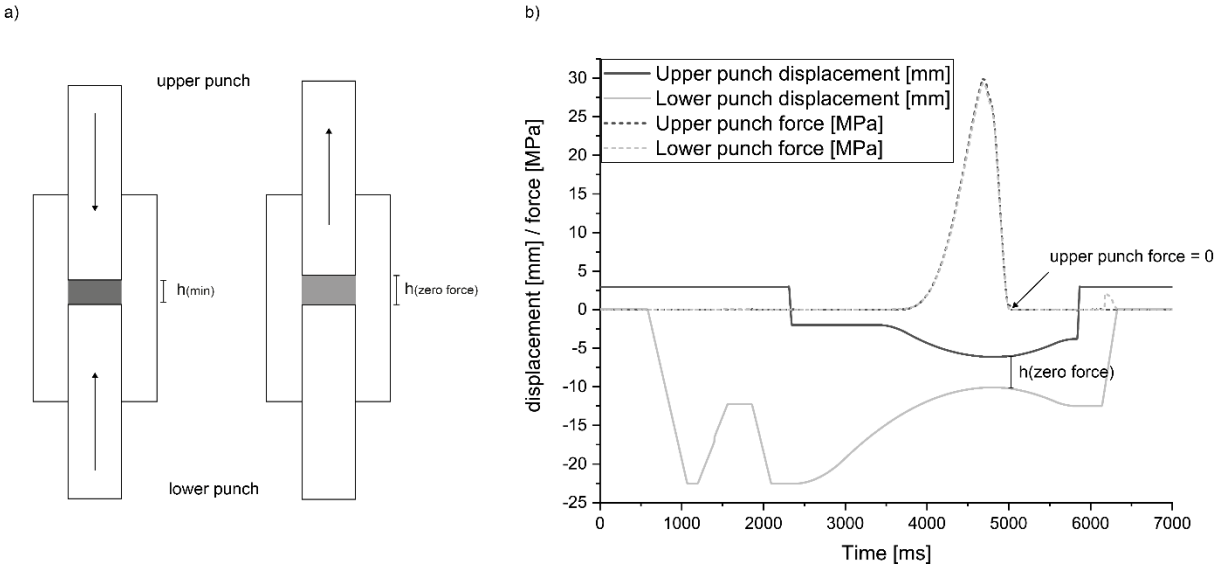

Figure 5.2-4: Zero force measurement of in-die elastic recovery

Compression Pressure and Gap Width

The in-die elastic recovery of MCC, lactose, DCPA, carrageenan and HPMC was determined at varying mimicked specific compaction forces and gap widths at a constant roll speed of 2 rpm using the Gerteis Mini-Pactor profile. To achieve a better comparability between the different excipients, the simulated specific compaction forces were given in the corresponding compression pressure in MPa. At least twenty ribblets were produced per setting.

Mimicked Roll Speed

The dependence of the in-die elastic recovery of MCC on the mimicked roll speed was evaluated at roll speeds between 3 and 11 rpm (3, 5, 7, 9, 11 rpm) at a constant gap width of 3 mm and a constant specific compaction force of 6 kN/cm. That corresponds to a compression pressure of 32 MPa. Ten ribblets were produced per roll speed setting.

Dwell Time

Dwell time is defined as the period, in which the maximum force on upper and lower punch is held constant. The punch positions changed slightly under maximum force due to the occurring material creep. The influence of the dwell time was investigated using the “extended dwell time” tableting cycle of the Styl’One Evolution. Dwell times in a range between 600 and 3000 ms were tested. The compression height was set at 3 mm. The resulting force was 3.5 kN (17.5 MPa) at its peak. Ten ribblets were produced for each dwell time setting.

5.2.11.3 Out-of-Die Axial Elastic Recovery with Chromatic Confocal Measurement

Ribblets of MCC, lactose and carrageenan were produced with the Styl'One Evolution. Compression pressures between 50 and 250 MPa were applied. The powder was filled into the die manually. The ribblets were compacted to an initial height of 4 mm. The external lubrication unit, which sprayed magnesium stearate powder onto the punches and into the die, was used for lactose ribblets to avoid too high ejection forces. The slow out-of-die elastic recovery in axial direction after the ejection of the ribblet was measured over a time period of 30 minutes with a chromatic confocal probe (CHRocodile E, Precitec Optronik GmbH). Ribblets were placed underneath the probe approximately 10 seconds after ejection. Two ribblets were analysed per compression pressure setting. Figure 5.2-5 schematically shows the experimental setup for the chromatic confocal measurements.

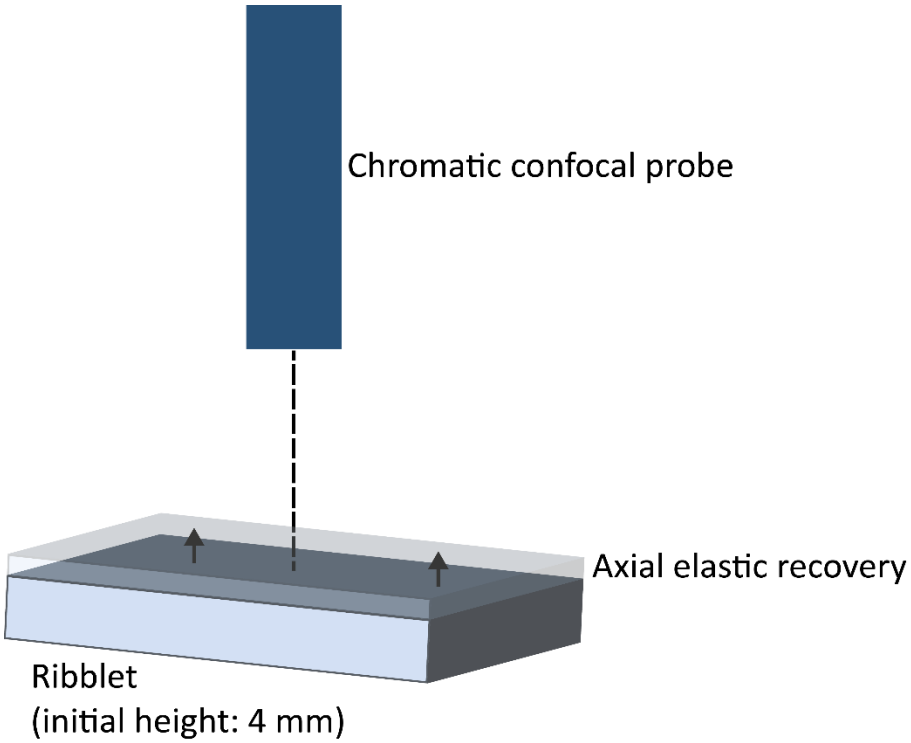

Figure 5.2-5: Schematic illustration of the chromatic confocal measurement of the ribblet hight

The chromatic confocal probe uses a white light source. The light is directed to the optical probe, which creates a full spectrum of light. Only one wavelength at a time is focused on the sample surface. The reflection of the light allows an accurate measurement of the distance between the probe and the sample surface (Figure 5.2-6). The acquisition frequency was 100 Hz and the mean of ten values was taken.

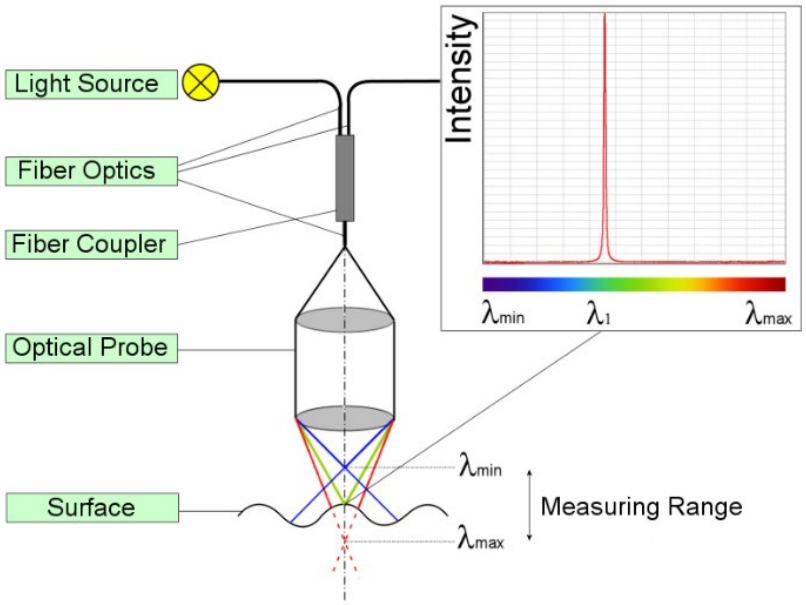

Figure 5.2-6: Principle of chromatic confocal measurement (by courtesy of Precitec Optronik GmbH, Germany)

The distance between the probe and the sample surface decreased over time due to the elastic recovery of the ribblet. Using equation (33), the out-of-die elastic recovery ($ER_{out\text{-}of\text{-}die}$) can be calculated.

$$ER_{out-of-die}[\%] = \frac{h_{con} - h_{min}}{h_{min}} \times 100 \qquad (33)$$

where h_{con} is the height of the ribblet at a time point t and h_{min} the minimum distance between upper and lower punch during compression. Thus, the out-of-die elastic recovery is composed of the in-die elastic recovery and the elastic recovery, which takes place after ejection and is measured by the chromatic confocal probe.

5.2.11.4 Long-term Out-of-die Axial Elastic Recovery

The two materials that show the lowest and the highest elastic recovery – lactose and carrageenan – were selected for the long-term investigation of the phenomenon. It should be evaluated when the elastic recovery is completed. The ribblets (n=10) were produced at 50, 150 and 250 MPa using the "one compression cycle" of the Styl'One Evolution. The ribblet height was monitored over a time period of 10 days (0, 5, 10, 15, 30, 60, 120, 180 minutes and daily for 9 further days) with a digital calliper (Mitutoyo, Japan). The ribblet height was measured in triplicate and the mean was taken. The total axial elastic recovery (ER_{total}) can be calculated by equation (34),

$$ER_{total}[\%] = \frac{h_t - h_{min}}{h_{min}} \times 100 \qquad (34)$$

where h_t is the ribblet height at a certain time point t and h_{min} the minimum distance between the upper and the lower punch under load.

5.2.11.5 Radial Elastic Recovery

The elastic recovery of MCC, lactose and carrageenan ribblets in radial direction was evaluated. The ribblets (n=10) were produced at compression pressures between 50 MPa and 250 MPa with the Styl'One Evolution. The length and the width of the ribblets was measured with a digital calliper (Mitutoyo, Japan) directly after ejection and after seven days of storage. The radial elastic recovery is divided into the one of the ribblet length (ER_{length}) and of the ribblet width (ER_{width}). They are calculated according to equation (35) and (36), respectively.

$$ER_{length}[\%] = \frac{l_t - l_{die}}{l_{die}} \times 100 \quad (35)$$

$$ER_{width}[\%] = \frac{w_t - w_{die}}{w_{die}} \times 100 \quad (36)$$

where l_t and w_t are the length and the width of the ribblet at a timepoint t and l_{die} and w_{die} the length and the width of the rectangular punch.

5.2.12 Particle Size Distribution of Granules

Prior to analysis, the sample was divided into three equal quantities in a rotary sample divider (PT 100, Retsch, Germany). The particle size distribution of the granules was determined via dynamic image analysis with the CamSizer XT (Retsch, Germany). The X-Jet module was mounted, and the funnel position was set at 4 mm. The dispersion pressure was adjusted at 30 kPa to avoid breakage of the granules during the analysis. A minimum of 1.5 million particles was analysed and the x_{min} value was chosen as shape parameter. The measurements were performed four times (n=4).

5.2.13 Characterisation of Tablets

5.2.13.1 Uniformity of Mass

The uniformity of mass was evaluated following the procedure 2.9.34 of the European Pharmacopoeia (Council of Europe, 2020e) summarised in the following. Twenty tablets were weighed individually with a semi-automatic tablet testing system (SmartTest50, Sotax, Switzerland). The average mass was determined. The target tablet mass was 200 mg and therefore the tablets are classified in the category

between 80 and 250 mg. Thus, no more than two of the individual masses may deviate from the average mass by more than 7.5 % and none of them may deviate by more than 15 %.

5.2.13.2 Tensile Strength

The tablet tensile strength σ was calculated after Fell and Newton (1970) as shown in equation (37), where P is the applied load until failure, D the tablet diameter and h the tablet height.

$$\sigma\,[MPa] = \frac{2 \times P}{\pi \times D \times h} \qquad (37)$$

The load until failure, diameter and height of twenty tablets were determined with a semi-automatic tablet testing system (SmartTest50, Sotax, Switzerland). The tablet tensile strength should be higher than 2 MPa to ensure a good handling for the patient and a sufficient resistance against damage during coating, packaging, transport or storage.

5.2.13.3 Disintegration

The disintegration time of six tablets was tested with a PTZ Auto (PharmaTest) following the European Pharmacopoeia procedure 2.9.1. Disintegration of tablets and capsules (Council of Europe, 2020b). Water was used as the liquid medium. The temperature was maintained constant at 37 °C ± 2 °C. The uncoated tablets comply with the test if they disintegrate completely within 15 minutes. The completion of the disintegration was detected automatically by modified discs. The threshold value for detection was set at 700.

6 References

Akseli, I., S. Iyer, H. P. Lee and A. M. Cuitino, 2011. A Quantitative Correlation of the Effect of Density Distributions in Roller-Compacted Ribbons on the Mechanical Properties of Tablets Using Ultrasonics and X-Ray Tomography. AAPS PharmSciTech 12, 834-853. https://doi.org/10.1208/s12249-011-9640-z.

Akseli, I., N. Ladyzhynsky, J. Katz and X. R. He, 2013. Development of Predictive Tools to Assess Capping Tendency of Tablet Formulations. Powder Technology 236, 139-148. https://doi.org/10.1016/j.powtec.2012.04.026.

Al-Asady, R. B., R. M. Dhenge, M. J. Hounslow and A. D. Salman, 2016. Roller Compactor: Determining the Nip Angle and Powder Compaction Progress by Indentation of the Pre-Compacted Body. Powder Technology 300, 107-119. https://doi.org/10.1016/j.powtec.2016.02.039.

Alleso, M., R. Holm and P. Holm, 2016. Roller Compaction Scale-up Using Roll Width as Scale Factor and Laser-Based Determined Ribbon Porosity as Critical Material Attribute. European journal of pharmaceutical sciences 87, 69-78. https://doi.org/10.1016/j.ejps.2015.11.001.

Almaya, A. and A. Aburub, 2008. Effect of Particle Size on Compaction of Materials with Different Deformation Mechanisms with and without Lubricants. AAPS PharmSciTech 9, 414-418. https://doi.org/10.1208/s12249-008-9059-3.

Antikainen, O. and J. Yliruusi, 2003. Determining the Compression Behaviour of Pharmaceutical Powders from the Force-Distance Compression Profile. International journal of pharmaceutics 252, 253-261. https://doi.org/10.1016/S0378-5173(02)00665-8.

Anuar, M. S. and B. J. Briscoe, 2009. The Elastic Relaxation of Starch Tablets During Ejection. Powder Technology 195, 96-104. https://doi.org/10.1016/j.powtec.2009.05.019.

Armstrong, N. A., 1989. Time-Dependent Factors Involved in Powder Compression and Tablet Manufacture. International journal of pharmaceutics 49, 1-13. https://doi.org/10.1016/0378-5173(89)90146-4.

Armstrong, N. A. and R. F. Haines-Nutt, 1974. Elastic Recovery and Surface Area Changes in Compacted Powder Systems. Powder Technology 9, 287-290. https://doi.org/10.1016/0032-5910(74)80054-9.

Arndt, O.-R., R. Baggio, A. K. Adam, J. Harting, E. Franceschinis and P. Kleinebudde, 2018. Impact of Different Dry and Wet Granulation Techniques on Granule and Tablet Properties: A Comparative Study. Journal of Pharmaceutical Sciences 107, 3143-3152. https://doi.org/10.1016/j.xphs.2018.09.006.

Arndt, O. R., 2018. Einfluss von Trockenbindemitteln auf die Granulierung und Tablettierung. Doctoral Thesis, Heinrich Heine University Düsseldorf.

Arndt, O. R. and P. Kleinebudde, 2018a. Influence of Binder Properties on Dry Granules and Tablets. Powder Technology 337, 68-77. https://doi.org/10.1016/j.powtec.2017.04.054.

Arndt, O. R. and P. Kleinebudde, 2018b. Roll Compaction and Tableting of High Loaded Metformin Formulations Using Efficient Binders. AAPS PharmSciTech 19, 2068-2076. https://doi.org/10.1208/s12249-018-1012-5.

Arndt, O. R. and P. Kleinebudde, 2018c. Towards a Better Understanding of Dry Binder Functionality. International journal of pharmaceutics 552, 258-264. https://doi.org/10.1016/j.ijpharm.2018.10.007.

Berkenkemper, S., 2019. Funktionalität von Zerfallsbeschleunigern mit unterschiedlichen Mechanismen nach Walzenkompaktierung. Diploma Thesis, Martin-Luther Universität Halle-Wittenberg.

BfArM, 2018. Rote-Hand-Brief zu Hydrochlorothiazid (Hct): Risiko von nichtmelanozytärem Hautkrebs [Basalzellkarzinom (Basaliom); Plattenepithelkarzinom der Haut (Spinaliom)]. Available at: https://www.bfarm.de/SharedDocs/Risikoinformationen/Pharmakovigilanz/DE/RHB/2018/rhb-hydrochlorothiazid.html (Accessed: 07/03/2021).

Bi, M. D., F. Alvarez-Nunez and F. Alvarez, 2014. Evaluating and Modifying Johanson's Rolling Model to Improve Its Predictability. Journal of Pharmaceutical Sciences 103, 2062-2071. https://doi.org/10.1002/jps.24012.

Bindhumadhavan, G., J. P. K. Seville, M. J. Adams, R. W. Greenwood and S. Fitzpatrick, 2005. Roll Compaction of a Pharmaceutical Excipient: Experimental Validation of Rolling Theory for Granular Solids. Chemical Engineering Science 60, 3891-3897. https://doi.org/10.1016/j.ces.2005.02.022.

Boersen, N., D. Belair, G. E. Peck and R. Pinal, 2016. A Dimensionless Variable for the Scale up and Transfer of a Roller Compaction Formulation. Drug Dev. Ind. Pharm. 42, 60-69. https://doi.org/10.3109/03639045.2015.1029937.

Boersen, N., M. T. Carvajal, K. R. Morris, G. E. Peck and R. Pinal, 2015. The Influence of API Concentration on the Roller Compaction Process: Modeling and Prediction of the Post Compacted Ribbon, Granule and Tablet Properties Using Multivariate Data Analysis. Drug Dev. Ind. Pharm. 41, 1470-1478. https://doi.org/10.3109/03639045.2014.958754.

Cantor, S. L. A., L.L.; Hoag, S.W., 2008. Pharmaceutical Granulation Processes, Mechanism, and the Use of Binders in Pharmaceutical Dosage Forms - Tablets. Informa Healthcare USA, 261-301.

Council of Europe, 2020a. Bulk and Tapped Density of Powders in European Pharmacopoeia. Council of Europe: European Directorate for the Quality of Medicines and Healthcare, Strasbourg, 10.0, 10.0/2.09.34.00.

Council of Europe, 2020b. Disintegration of Tablets and Capsules in European Pharmacopoeia. Council of Europe: European Directorate for the Quality of Medicines and Healthcare, Strasbourg, 10.0, 10.0/2.09.01.00.

Council of Europe, 2020c. Granules in European Pharmacopoeia. Council of Europe: European Directorate for the Quality of Medicines and Healthcare, Strasbourg, 10.0, 10.0/0499.

Council of Europe, 2020d. Tablets in European Pharmacopoeia. Council of Europe: European Directorate for the Quality of Medicines and Healthcare, Strasbourg, 10.0, 10.0/0478.

Council of Europe, 2020e. Uniformity of Mass of Single-Dose Preparations in European Pharmacopoeia. Council of Europe: European Directorate for the Quality of Medicines and Healthcare, Strasbourg, 10.0, 10.0/2.09.05.00.

Csordas, K. and P. Kleinebudde, 2018. Evaluation of the Performance of Different Types of Roll Compactors. Powder Technology 337, 84-91. https://doi.org/10.1016/j.powtec.2017.04.009.

Csordas, K., R. Wiedey and P. Kleinebudde, 2018. Impact of Roll Compaction Design, Process Parameters, and Material Deformation Behaviour on Ribbon Relative Density. Drug Development and Industrial Pharmacy 44, 1295-1306. https://doi.org/10.1080/03639045.2018.1446444.

Cunningham, J. C., 2005. Experimental Studies and Modeling of the Roller Compaction of Pharmaceutical Powders. Doctoral Thesis, Drexel University.

Cunningham, J. C., D. Winstead and A. Zavaliangos, 2010. Understanding Variation in Roller Compaction through Finite Element-Based Process Modeling. Computers & Chemical Engineering 34, 1058-1071. https://doi.org/10.1016/j.compchemeng.2010.04.008.

David, S. T. and L. L. Augsburger, 1977. Plastic-Flow During Compression of Directly Compressible Fillers and Its Effect on Tablet Strength. Journal of Pharmaceutical Sciences 66, 155-159. https://doi.org/10.1002/jps.2600660205.

Dec, R. T., A. Zavaliangos and J. C. Cunningham, 2003. Comparison of Various Modeling Methods for Analysis of Powder Compaction in Roller Press. Powder Technology 130, 265-271. https://doi.org/10.1016/s0032-5910(02)00203-6.

Desai, P. M., C. V. Liew and P. W. S. Heng, 2016. Review of Disintegrants and the Disintegration Phenomena. Journal of Pharmaceutical Sciences 105, 2545-2555. https://doi.org/10.1016/j.xphs.2015.12.019.

Ende, M. T. A., S. K. Moses, A. J. Carella, R. A. Gadkari, T. W. Graul, A. L. Otano and R. J. Timpano, 2007. Improving the Content Uniformity of a Low-Dose Tablet Formulation through Roller Compaction Optimization. Pharmaceutical Development and Technology 12, 391-404. https://doi.org/10.1080/10837450701369253.

Ennis, B. J., 2005. Theory of Granulation: An Engineering Perspective in Handbook of Pharmaceutical Granulation Technology, 2nd Edition ed. Taylor & Francis Group, 7-78.

Eriksson, L., E. Johansson, N. Kettaneh-Wold, C. Wikström and S. Wold, 2008. Analysis of Factorial Design in Design of Experiments: Principles and Applications, 76-82.

Farber, L., K. P. Hapgood, J. N. Michaels, X. Y. Fu, R. Meyer, M. A. Johnson and F. Li, 2008. Unified Compaction Curve Model for Tensile Strength of Tablets Made by Roller Compaction and Direct Compression. International journal of pharmaceutics 346, 17-24. https://doi.org/10.1016/j.ijpharm.2007.06.022.

Fassihi, A. R. and I. Kanfer, 1986. Effect of Compressibility and Powder Flow Properties on Tablet Weight Variation. Drug Development and Industrial Pharmacy 12, 1947-1966. https://doi.org/10.3109/03639048609042619.

Faure, A., P. York and R. C. Rowe, 2001. Process Control and Scale-up of Pharmaceutical Wet Granulation Processes: A Review. European Journal of Pharmaceutics and Biopharmaceutics 52, 269-277. https://doi.org/10.1016/S0939-6411(01)00184-9.

Fell, J. T. and J. M. Newton, 1970. Determination of Tablet Strength by Diametral-Compression Test. Journal of Pharmaceutical Sciences 59, 688-691. https://doi.org/10.1002/jps.2600590523.

Freitag, F. and P. Kleinebudde, 2003. How Do Roll Compaction/Dry Granulation Affect the Tableting Behaviour of Inorganic Materials? Comparison of Four Magnesium Carbonates. European Journal of Pharmaceutical Sciences 19, 281-289. https://doi.org/10.1016/S0928-0987(03)00133-7.

Fu, J. S., Y. S. Cheong, G. K. Reynolds, M. J. Adams, A. D. Salman and M. J. Hounslow, 2004. An Experimental Study of the Variability in the Properties and Quality of Wet Granules. Powder Technology 140, 209-216. https://doi.org/10.1016/j.powtec.2004.01.019.

Funakoshi, Y., T. Asogawa and E. Satake, 1977. Use of a Novel Roller Compactor with a Concave-Convex Roller Pair to Obtain Uniform Compacting Pressure. Drug Development and Industrial Pharmacy 3, 555-573. https://doi.org/10.3109/03639047709055633.

Gamble, J. F., M. Tobyn, A. B. Dennis and T. Shah, 2010. Roller Compaction: Application of an in-Gap Ribbon Porosity Calculation for the Optimization of Downstream Granule Flow and Compactability Characteristics. Pharmaceutical Development and Technology 15, 223-229. https://doi.org/10.3109/10837450903095342.

Grote, S. and P. Kleinebudde, 2018. Roll Compaction/Dry Granulation of Dibasic Calcium Phosphate Anhydrous-Does the Morphology of the Raw Material Influence the Tabletability of Dry Granules? Journal of Pharmaceutical Sciences 107, 1104-1111. https://doi.org/10.1016/j.xphs.2017.12.003.

Guigon, P. and O. Simon, 2003. Roll Press Design—Influence of Force Feed Systems on Compaction. Powder Technology 130, 41-48. https://doi.org/10.1016/s0032-5910(02)00223-1.

Guigon, P., O. Simon, K. Saleh, G. Bindhumadhavan, M. J. Adams and J. P. K. Seville, 2007. Chapter 5 Roll Pressing in Handbook of Powder Technology. Elsevier Science B.V., 255-288.

Guo, Y., C. Y. Wu, K. D. Kafui and C. Thornton, 2011a. 3D DEM/CFD Analysis of Size-Induced Segregation During Die Filling. Powder Technology 206, 177-188. https://doi.org/10.1016/j.powtec.2010.05.029.

Guo, Y., C. Y. Wu and C. Thornton, 2011b. The Effects of Air and Particle Density Difference on Segregation of Powder Mixtures During Die Filling. Chemical Engineering Science 66, 661-673. https://doi.org/10.1016/j.ces.2010.11.017.

Haeffler, G., L. Schmidt, S. Lakio, G. Reynolds, J. Odman and P. Tajarobi, 2019. A Systematic Study of the Impact of Changes of Roller Compactor Equipment on Granule and Tablet Properties. Powder Technology 341, 11-22. https://doi.org/10.1016/j.powtec.2018.09.002.

Hancock, B. C., S.-D. Clas and K. Christensen, 2000. Micro-Scale Measurement of the Mechanical Properties of Compressed Pharmaceutical Powders. 1: The Elasticity and Fracture Behavior of Microcrystalline Cellulose. International journal of pharmaceutics 209, 27-35. http://dx.doi.org/10.1016/S0378-5173(00)00541-X.

Hancock, B. C., J. T. Colvin, M. Mullarney and A. V. Zinchuk, 2003. The Relative Densities of Pharmaceutical Powders, Blends, Dry Granulations, and Immediate-Release Tablets. Pharmaceutical Technology 27, 64-80.

Hancock, B. C., C. R. Dalton and S.-D. Clas, 2001. Micro-Scale Measurement of the Mechanical Properties of Compressed Pharmaceutical Powders. 2: The Dynamic Moduli of Microcrystalline Cellulose. International journal of pharmaceutics 228, 139-145. http://dx.doi.org/10.1016/S0378-5173(01)00833-X.

Hausman, D. S., 2004. Comparison of Low Shear, High Shear, and Fluid Bed Granulation During Low Dose Tablet Process Development. Drug Development and Industrial Pharmacy 30, 259-266. https://doi.org/10.1081/Ddc-120030419.

Hausman, D. S., R. T. Cambron and A. Sakr, 2005. Application of Raman Spectroscopy for on-Line Monitoring of Low Dose Blend Uniformity. International journal of pharmaceutics 298, 80-90. https://doi.org/10.1016/j.ijpharm.2005.04.011.

Haware, R. V., I. Tho and A. Bauer-Brandl, 2010. Evaluation of a Rapid Approximation Method for the Elastic Recovery of Tablets. Powder Technology 202, 71-77. https://doi.org/10.1016/j.powtec.2010.04.012.

Hein, S., K. M. Picker-Freyer and J. Langridge, 2008. Simulation of Roller Compaction with Subsequent Tableting and Characterization of Lactose and Microcrystalline Cellulose. Pharmaceutical development and technology 13, 523-532. https://doi.org/10.1080/10837450802288972.

Herting, M. G. and P. Kleinebudde, 2007. Roll Compaction/Dry Granulation: Effect of Raw Material Particle Size on Granule and Tablet Properties. International journal of pharmaceutics 338, 110-118. https://doi.org/10.1016/j.ijpharm.2007.01.035.

Herting, M. G., K. Klose and P. Kleinebudde, 2007. Comparison of Different Dry Binders for Roll Compaction/Dry Granulation. Pharmaceutical Development and Technology 12, 525-532. https://doi.org/10.1080/10837450701557303.

Hervieu, P., F. Dehont, E. Jerome, A. Delacourte and J. C. Guyot, 1994. Granulation of Pharmaceutical Powders by Compaction an Experimental Study. Drug Development and Industrial Pharmacy 20, 65-74. https://doi.org/10.3109/03639049409047214.

Hildebrandt, C., S. R. Gopireddy, R. Scherliess and N. A. Urbanetz, 2019. Investigation of Powder Flow within a Pharmaceutical Tablet Press Force Feeder - a DEM Approach. Powder Technology 345, 616-632. https://doi.org/10.1016/j.powtec.2019.01.040.

Hilden, J., G. Earle and E. L. Co, 2011. Prediction of Roller Compacted Ribbon Solid Fraction for Quality by Design Development. Powder Technology 213, 1-13. https://doi.org/10.1016/j.powtec.2011.05.025.

Ilic, I., B. Govedarica, R. Sibanc, R. Dreu and S. Srcic, 2013. Deformation Properties of Pharmaceutical Excipients Determined Using an in-Die and out-Die Method. International journal of pharmaceutics 446, 6-15. https://doi.org/10.1016/j.ijpharm.2013.02.001.

Inghelbrecht, S. and J. P. Remon, 1998a. Reducing Dust and Improving Granule and Tablet Quality in the Roller Compaction Process. International journal of pharmaceutics 171, 195-206. http://dx.doi.org/10.1016/S0378-5173(98)00195-1.

Inghelbrecht, S. and J. P. Remon, 1998b. Roller Compaction and Tableting of Microcrystalline Cellulose/Drug Mixtures. International journal of pharmaceutics 161, 215-224. http://dx.doi.org/10.1016/S0378-5173(97)00356-6.

Inghelbrecht, S. and J. P. Remon, 1998c. The Roller Compaction of Different Types of Lactose. International journal of pharmaceutics 166, 135-144. http://dx.doi.org/10.1016/S0378-5173(98)00022-2.

Jaminet, F. and H. Hess, 1966. Untersuchung Über Kompaktierung Und Trockengranulierung. Pharmaceutica Acta Helvetiae 41, 39-58.

Johanson, J. R., 1965. A Rolling Theory for Granular Solids. Journal of Applied Mechanics 32, 842-848. https://doi.org/10.1115/1.3627325.

Jurasovic, M. and V. Bouvier, 2021. ATC C03AA03 - Hydrochlorothiazid. Gelbe Liste Online, Available at: https://www.gelbe-liste.de/atc/Hydrochlorothiazid_C03AA03 (Accessed: 07/03/2021).

Katashinskii, V. P., 1966. Analytical Determination of Specific Pressure During the Rolling of Metal Powders. Soviet Powder Metallurgy and Metal Ceramics 5, 765-772. https://doi.org/10.1007/bf00776244.

Katz, J. M., R. Roopwani and I. S. Buckner, 2013. A Material-Sparing Method for Assessment of Powder Deformation Characteristics Using Data Collected During a Single Compression–Decompression Cycle. Journal of Pharmaceutical Sciences 102, 3687-3693. https://doi.org/10.1002/jps.23676.

Keizer, H. L. and P. Kleinebudde, 2020. Elastic Recovery in Roll Compaction Simulation. International journal of pharmaceutics 573, 118810. https://doi.org/10.1016/j.ijpharm.2019.118810.

Khorasani, M., J. M. Amigo, P. Bertelsen, C. C. Sun and J. Rantanen, 2016. Process Optimization of Dry Granulation Based Tableting Line: Extracting Physical Material Characteristics from Granules, Ribbons and

Tablets Using near-IR (NIR) Spectroscopic Measurement. Powder Technology 300, 120-125. https://doi.org/10.1016/j.powtec.2016.03.004.

Kleinebudde, P., 2004. Roll Compaction/Dry Granulation: Pharmaceutical Applications. European Journal of Pharmaceutics and Biopharmaceutics 58, 317-326. https://doi.org/10.1016/j.ejpb.2004.04.014.

Kochhar, S. K., M. H. Rubinstein and D. Barnes, 1994. Slugging and Recompression Characterisation of Some Blends of Pharmaceutical Excipients. International journal of pharmaceutics 112, 225-231. https://doi.org/10.1016/0378-5173(94)90358-1.

Kochhar, S. K., M. H. Rubinstein and D. Barnes, 1995. The Effects of Slugging and Recompression on Pharmaceutical Excipients. International journal of pharmaceutics 115, 35-43. https://doi.org/10.1016/0378-5173(94)00250-9.

Kristensen, H. G. and T. Schaefer, 1987. Granulation: A Review on Pharmaceutical Wet-Granulation. Drug Development and Industrial Pharmacy 13, 803-872. https://doi.org/10.3109/03639048709105217.

Langendorf, M. and P. Krug, 2020. Fachinformation HCT AbZ 25 mg Tabletten. Fachinformationsverzeichnis Deutschland, Available at: https://www.fachinfo.de/suche/fi/012261 (Accessed: 07/03/2021).

Leane, M., K. Pitt and G. Reynolds, 2015. A Proposal for a Drug Product Manufacturing Classification System (MCS) for Oral Solid Dosage Forms. Pharmaceutical Development and Technology 20, 12-21. https://doi.org/10.3109/10837450.2014.954728.

Lendlein, A. and S. Kelch, 2002. Shape-Memory Polymers. Angewandte Chemie International Edition 41, 2034-2057. https://doi.org/10.1002/1521-3773(20020617)41:12<2034::aid-anie2034>3.0.co;2-m.

Leuenberger, H., 2001. New Trends in the Production of Pharmaceutical Granules: Batch Versus Continuous Processing. European Journal of Pharmaceutics and Biopharmaceutics 52, 289-296. http://dx.doi.org/10.1016/S0939-6411(01)00199-0.

Li, Z., X. Lin, L. Shen, Y. L. Hong and Y. Feng, 2017. Composite Particles Based on Particle Engineering for Direct Compaction. International journal of pharmaceutics 519, 272-286. https://doi.org/10.1016/j.ijpharm.2017.01.030.

Lim, H., V. S. Dave, L. Kidder, E. Neil Lewis, R. Fahmy and S. W. Hoag, 2011. Assessment of the Critical Factors Affecting the Porosity of Roller Compacted Ribbons and the Feasibility of Using NIR Chemical Imaging to Evaluate the Porosity Distribution. International journal of pharmaceutics 410, 1-8. https://doi.org/10.1016/j.ijpharm.2011.02.028.

Liu, Y. and C. Wassgren, 2016. Modifications to Johanson's Roll Compaction Model for Improved Relative Density Predictions. Powder Technology 297, 294-302. https://doi.org/10.1016/j.powtec.2016.04.017.

Liu, Z., M. J. Bruwer, J. F. MacGregor, S. S. S. Rathore, D. E. Reed and M. J. Champagne, 2011. Scale-up of a Pharmaceutical Roller Compaction Process Using a Joint-Y Partial Least Squares Model. Industrial & Engineering Chemistry Research 50, 10696-10706. https://doi.org/10.1021/ie102316b.

Long, W. M. and J. R. Alderton, 1960. The Displacement of Gas from Powders During Compaction. Powder Metallurgy 3, 52-72. https://doi.org/10.1179/pom.1960.3.6.004.

Maarschalk, K. V. D. V., K. Zuurman, H. Vromans, G. K. Bolhuis and C. F. Lerk, 1997. Stress Relaxation of Compacts Produced from Viscoelastic Materials. International journal of pharmaceutics 151, 27-34. https://doi.org/10.1016/S0378-5173(97)04889-8.

Mahmah, O., M. J. Adams, C. S. Omar, B. Gururajan and A. D. Salman, 2019. Roller Compaction: Ribbon Splitting and Sticking. International journal of pharmaceutics 559, 156-172. https://doi.org/10.1016/j.ijpharm.2019.01.031.

Malkowska, S. and K. A. Khan, 1983. Effect of Re-Compression on the Properties of Tablets Prepared by Dry Granulation. Drug Development and Industrial Pharmacy 9, 331-347. https://doi.org/10.3109/03639048309044678.

Mangal, H., 2018. Implementierung Der Trockengranulation in Eine Kontinuierliche Produktionsanlage Für Feste Arzneiformen. Doctoral Thesis, Heinrich Heine University Düsseldorf.

Mangal, H. and P. Kleinebudde, 2018. Is the Adjustment of the Impeller Speed a Reliable Attempt to Influence Granule Size in Continuous Dry Granulation? Advanced Powder Technology 29, 1339-1347. https://doi.org/10.1016/j.apt.2018.02.029.

Mansa, R. F., R. H. Bridson, R. W. Greenwood, H. Barker and J. P. K. Seville, 2008. Using Intelligent Software to Predict the Effects of Formulation and Processing Parameters on Roller Compaction. Powder Technology 181, 217-225. https://doi.org/10.1016/j.powtec.2007.02.011.

Markl, D. and J. A. Zeitler, 2017. A Review of Disintegration Mechanisms and Measurement Techniques. Pharmaceutical Research 34, 890-917. https://doi.org/10.1007/s11095-017-2129-z.

Mazel, V., V. Busignies, H. Diarra and P. Tchoreloff, 2013. On the Links between Elastic Constants and Effective Elastic Behavior of Pharmaceutical Compacts: Importance of Poisson's Ratio and Use of Bulk Modulus. Journal of Pharmaceutical Sciences 102, 4009-4014. https://doi.org/10.1002/jps.23710.

Mazel, V., V. Busignies, H. Diarra and P. Tchoreloff, 2015. Lamination of Pharmaceutical Tablets Due to Air Entrapment: Direct Visualization and Influence of the Compact Thickness. International journal of pharmaceutics 478, 702-704. https://doi.org/10.1016/j.ijpharm.2014.12.023.

Mazor, A., L. Orefice, A. Michrafy, A. de Ryck and J. G. Khinast, 2018. A Combined DEM & FEM Approach for Modelling Roll Compaction Process. Powder Technology 337, 3-16. https://doi.org/10.1016/j.powtec.2017.04.053.

Medelpharm, 2020. Styl'one Evolution R&D, Scale-up and Production Support, Information Leaflet.

Mehrotra, A., B. Chaudhuri, A. Faqih, M. S. Tomassone and F. J. Muzzio, 2009. A Modeling Approach for Understanding Effects of Powder Flow Properties on Tablet Weight Variability. Powder Technology 188, 295-300. https://doi.org/10.1016/j.powtec.2008.05.016.

Meier, R., K. P. Moll, M. Krumme and P. Kleinebudde, 2017. Simplified, High Drug-Loaded Formulations Containing Hydrochlorothiazide for Twin-Screw Granulation. Chemie Ingenieur Technik 89, 1025-1033. https://doi.org/10.1002/cite.201600134.

Michrafy, A., E. Diarra, J. A. Dodds and M. Michrafy, 2011a. Experimental and Numerical Analyses of Homogeneity over Strip Width in Roll Compaction. Powder Technology 206, 154-160. https://doi.org/10.1016/j.powtec.2010.04.030.

Michrafy, A., H. Diarra, J. A. Dodds, M. Michrafy and L. Penazzi, 2011b. Analysis of Strain Stress State in Roller Compaction Process. Powder Technology 208, 417-422. https://doi.org/10.1016/j.powtec.2010.08.037.

Miguelez-Moran, A. M., C. Y. Wu and J. P. Seville, 2008. The Effect of Lubrication on Density Distributions of Roller Compacted Ribbons. International journal of pharmaceutics 362, 52-59. https://doi.org/10.1016/j.ijpharm.2008.06.009.

Miller, R. W., 2005. Roller Compaction Technology in Handbook of Pharmaceutical Granulation Technology. Taylor & Francis Group, 159-188.

Moroney, K. M., P. Cronin, O. A. Adeleye, B. E. Schaller, M. A. Howard, B. Castro-Dominguez, R. Ramachandran and G. M. Walker, 2020. An Evaluation of the Johanson Model for Roller Compaction Process Development for a High Dose API. Powder Technology 366, 82-95. https://doi.org/10.1016/j.powtec.2020.02.058.

Mosig, J. and P. Kleinebudde, 2015. Critical Evaluation of Root Causes of the Reduced Compactability after Roll Compaction/Dry Granulation. Journal of Pharmaceutical Sciences 104, 1108-1118. https://doi.org/10.1002/jps.24321.

Muliadi, A. R., J. D. Litster and C. R. Wassgren, 2012. Modeling the Powder Roll Compaction Process: Comparison of 2-D Finite Element Method and the Rolling Theory for Granular Solids (Johanson's Model). Powder Technology 221, 90-100. https://doi.org/10.1016/j.powtec.2011.12.001.

Muliadi, A. R., J. D. Litster and C. R. Wassgren, 2013. Validation of 3-D Finite Element Analysis for Predicting the Density Distribution of Roll Compacted Pharmaceutical Powder. Powder Technology 237, 386-399. https://doi.org/10.1016/j.powtec.2012.12.023.

Nesarikar, V. V., C. Patel, W. Early, N. Vatsaraj, O. Sprockel and R. Jerzweski, 2012a. Roller Compaction Process Development and Scale up Using Johanson Model Calibrated with Instrumented Roll Data. International journal of pharmaceutics 436, 486-507. https://doi.org/10.1016/j.ijpharm.2012.06.027.

Nesarikar, V. V., N. Vatsaraj, C. Patel, W. Early, P. Pandey, O. Sprockel, Z. Gao, R. Jerzewski, R. Miller and M. Levin, 2012b. Instrumented Roll Technology for the Design Space Development of Roller Compaction Process. International journal of pharmaceutics 426, 116-131. https://doi.org/10.1016/j.ijpharm.2012.01.032.

Nkansah, P., S. J. Wu, S. Sobotka, K. Yamamoto and Z. J. Shao, 2008. A Novel Method for Estimating Solid Fraction of Roller-Compacted Ribbons. Drug Development and Industrial Pharmacy 34, 142-148. https://doi.org/10.1080/03639040701484387.

Omar, C. S., R. M. Dhenge, J. D. Osborne, T. O. Althaus, S. Palzer, M. J. Hounslow and A. D. Salman, 2015. Roller Compaction: Effect of Morphology and Amorphous Content of Lactose Powder on Product Quality. International journal of pharmaceutics 496, 63-74. http://dx.doi.org/10.1016/j.ijpharm.2015.06.032.

Osei-Yeboah, F. and C. C. Sun, 2015. Validation and Applications of an Expedited Tablet Friability Method. International journal of pharmaceutics 484, 146-155. https://doi.org/10.1016/j.ijpharm.2015.02.061.

Parikh, D. M., 2005. Introduction in Handbook of Pharmaceutical Granulation Technology, 2nd Edition ed. Taylor & Francis Group.

Park, S. Y., S. C. Galbraith, H. L. Liu, H. Lee, B. Cha, Z. R. Huang, T. O'Connor, S. Lee and S. Yoon, 2018. Prediction of Critical Quality Attributes and Optimization of Continuous Dry Granulation Process Via Flowsheet Modeling and Experimental Validation. Powder Technology 330, 461-470. https://doi.org/10.1016/j.powtec.2018.02.042.

Paronen, P. and M. Juslin, 1983. Compressional Characteristics of 4 Starches. Journal of Pharmacy and Pharmacology 35, 627-635. https://doi.org/10.1111/j.2042-7158.1983.tb02855.x.

Parrott, E. L., 1981. Densification of Powders by Concavo-Convex Roller Compactor. Journal of Pharmaceutical Sciences 70, 288-291. https://doi.org/10.1002/jps.2600700316.

Patel, B. A., M. J. Adams, N. Turnbull, A. C. Bentham and C. Y. Wu, 2010. Predicting the Pressure Distribution During Roll Compaction from Uniaxial Compaction Measurements. Chemical Engineering Journal 164, 410-417. https://doi.org/10.1016/j.cej.2009.12.022.

Paul, S. and C. C. Sun, 2017. Dependence of Friability on Tablet Mechanical Properties and a Predictive Approach for Binary Mixtures. Pharmaceutical Research 34, 2901-2909. https://doi.org/10.1007/s11095-017-2273-5.

Paul, S. and C. C. Sun, 2018. Systematic Evaluation of Common Lubricants for Optimal Use in Tablet Formulation. European Journal of Pharmaceutical Sciences 117, 118-127. https://doi.org/10.1016/j.ejps.2018.02.013.

Peck, G. E. S., J.L.P.; Morris, K.R., 2008. Dry Granulation in Pharmaceutical Dosage Forms - Tablets. Informa Healthcare USA.

Pedersen, S. A., D. Gaist, S. A. J. Schmidt, L. R. Holmich, S. Friis and A. Pottegard, 2018. Hydrochlorothiazide Use and Risk of Nonmelanoma Skin Cancer: A Nationwide Case-Control Study from Denmark. Journal of the American Academy of Dermatology 78, 673-681. https://doi.org/10.1016/j.jaad.2017.11.042.

Perez-Gandarillas, L., A. Perez-Gago, A. Mazor, P. Kleinebudde, O. Lecoq and A. Michrafy, 2016. Effect of Roll-Compaction and Milling Conditions on Granules and Tablet Properties. European Journal of Pharmaceutics and Biopharmaceutics 106, 38-49. https://doi.org/10.1016/j.ejpb.2016.05.020.

Perez Gago, A. and P. Kleinebudde, 2017. MCC-Mannitol Mixtures after Roll Compaction/Dry Granulation: Percolation Thresholds for Ribbon Microhardness and Granule Size Distribution. Pharmaceutical development and technology 22, 764-774. https://doi.org/10.3109/10837450.2016.1163388.

Pérez Gago, A., G. Reynolds and P. Kleinebudde, 2018. Impact of Roll Compactor Scale on Ribbon Density. Powder Technology 337, 92-103. https://doi.org/10.1016/j.powtec.2017.02.045.

Peter, S., R. F. Lammens and K.-J. Steffens, 2010. Roller Compaction/Dry Granulation: Use of the Thin Layer Model for Predicting Densities and Forces During Roller Compaction. Powder Technology 199, 165-175. https://doi.org/10.1016/j.powtec.2010.01.002.

Picker, K. M., 1999. Matrix Tablets of Carrageenans. I. A Compaction Study. Drug Development and Industrial Pharmacy 25, 329-337. https://doi.org/10.1081/Ddc-100102178.

Picker, K. M., 2001. Time Dependence of Elastic Recovery for Characterization of Tableting Materials. Pharmaceutical Development and Technology 6, 61-70. https://doi.org/10.1081/PDT-100000014.

Pishnamazi, M., S. Casilagan, C. Clancy, S. Shirazian, J. Iqbal, D. Egan, C. Edlin, D. M. Croker, G. M. Walker and M. N. Collins, 2019. Microcrystalline Cellulose, Lactose and Lignin Blends: Process Mapping of Dry Granulation via Roll Compaction. Powder Technology 341, 38-50. https://doi.org/10.1016/j.powtec.2018.07.003.

Quodbach, J. and P. Kleinebudde, 2016. A Critical Review on Tablet Disintegration. Pharmaceutical Development and Technology 21, 763-774. https://doi.org/10.3109/10837450.2015.1045618.

Railkar, A. M. and J. B. Schwartz, 2000. Evaluation and Comparison of a Moist Granulation Technique to Conventional Methods. Drug Development and Industrial Pharmacy 26, 885-889. https://doi.org/10.1081/Ddc-100101313.

Rajkumar, A. D., G. K. Reynolds, D. Wilson, S. Wren, M. J. Hounslow and A. D. Salman, 2016. Investigating the Effect of Processing Parameters on Pharmaceutical Tablet Disintegration Using a Real-Time Particle Imaging Approach. European Journal of Pharmaceutics and Biopharmaceutics 106, 88-96. https://doi.org/10.1016/j.ejpb.2016.06.005.

Rees, J. E. and P. J. Rue, 1978. Time-Dependent Deformation of Some Direct Compression Excipients*. Journal of Pharmacy and Pharmacology 30, 601-607. https://doi.org/10.1111/j.2042-7158.1978.tb13340.x.

Reimer, H. L. and P. Kleinebudde, 2019. Hybrid Modeling of Roll Compaction Processes with the Styl'One Evolution. Powder Technology 341, 66-74. https://doi.org/10.1016/j.powtec.2018.02.052.

Reynolds, G., R. Ingale, R. Roberts, S. Kothari and B. Gururajan, 2010. Practical Application of Roller Compaction Process Modeling. Computers & Chemical Engineering 34, 1049-1057. https://doi.org/10.1016/j.compchemeng.2010.03.004.

Reynolds, G. K., 2010. Modelling of Pharmaceutical Granule Size Reduction in a Conical Screen Mill. Chemical Engineering Journal 164, 383-392. https://doi.org/10.1016/j.cej.2010.03.041.

Riepma, K. A., H. Vromans, K. Zuurman and C. F. Lerk, 1993. The Effect of Dry Granulation on the Consolidation and Compaction of Crystalline Lactose. International journal of pharmaceutics 97, 29-38. https://doi.org/10.1016/0378-5173(93)90123-W.

Rippie, E. G. and D. W. Danielson, 1981. Viscoelastic Stress/Strain Behavior of Pharmaceutical Tablets: Analysis During Unloading and Postcompression Periods. Journal of Pharmaceutical Sciences 70, 476-482. https://doi.org/10.1002/jps.2600700503.

Roberts, R. J. and R. C. Rowe, 1987. The Compaction of Pharmaceutical and Other Model Materials - a Pragmatic Approach. Chemical Engineering Science 42, 903-911. https://doi.org/10.1016/0009-2509(87)80048-9.

Rowe, J. M., J. R. Crison, T. J. Carragher, N. Vatsaraj, R. J. McCann and F. Nikfar, 2013. Mechanistic Insights into the Scale-up of the Roller Compaction Process: A Practical and Dimensionless Approach. Journal of Pharmaceutical Sciences 102, 3586-3595. http://dx.doi.org/10.1002/jps.23659.

Rumpf, H., 1958a. Grundlagen Und Methoden Des Granulierens. Chemie Ingenieur Technik 30, 144-158. https://doi.org/10.1002/cite.330300307.

Rumpf, H., 1958b. Grundlagen Und Methoden Des Granulierens. 3. Teil: Überblick Über Die Technischen Granulierverfahren. Chemie Ingenieur Technik 30, 329-336. https://doi.org/10.1002/cite.330300510.

Sajjia, M., S. Shirazian, D. Egan, J. Iqbal, A. B. Albadarin, M. Southern and G. Walker, 2017. Mechanistic Modelling of Industrial-Scale Roller Compactor 'Freund TF-MINI Model'. Computers & Chemical Engineering 104, 141-150. https://doi.org/10.1016/j.compchemeng.2017.04.018.

Schiano, S., L. Chen and C. Y. Wu, 2018. The Effect of Dry Granulation on Flow Behaviour of Pharmaceutical Powders During Die Filling. Powder Technology 337, 78-83. https://doi.org/10.1016/j.powtec.2017.08.064.

Schiano, S., C. Y. Wu, A. Mirtic and G. Reynolds, 2016. A Novel Use of Friability Testing for Characterising Ribbon Milling Behaviour. European Journal of Pharmaceutics and Biopharmaceutics 104, 82-88. https://doi.org/10.1016/j.ejpb.2016.03.034.

Schönert, K. and U. Sander, 2002. Shear Stresses and Material Slip in High Pressure Roller Mills. Powder Technology 122, 136-144. https://doi.org/10.1016/S0032-5910(01)00409-0.

Seem, T. C., N. A. Rowson, A. Ingram, Z. Y. Huang, S. Yu, M. de Matas, I. Gabbott and G. K. Reynolds, 2015. Twin Screw Granulation - a Literature Review. Powder Technology 276, 89-102. https://doi.org/10.1016/j.powtec.2015.01.075.

Shlieout, G., R. F. Lammens, P. Kleinebudde and M. Bultmann, 2002. Dry Granulation with a Roller Compactor Part II: Evaluation and Operation Modes. Pharmaceutical Technology Europe 14, 32. http://search.ebscohost.com/login.aspx?direct=true&db=buh&AN=7541607&site=ehost-live

Simon, O. and P. Guigon, 2000. Interaction between Feeding and Compaction During Lactose Compaction in a Laboratory Roll Press. KONA Powder and Particle Journal 18, 131-138. https://doi.org/10.14356/kona.2000019.

Simon, O. and P. Guigon, 2003. Correlation between Powder-Packing Properties and Roll Press Compact Heterogeneity. Powder Technology 130, 257-264. http://dx.doi.org/10.1016/S0032-5910(02)00202-4.

Soh, J. L. P., F. Wang, N. Boersen, R. Pinal, G. E. Peck, M. T. Carvajal, J. Cheney, H. Valthorsson and J. Pazdan, 2008. Utility of Multivariate Analysis in Modeling the Effects of Raw Material Properties and Operating Parameters on Granule and Ribbon Properties Prepared in Roller Compaction. Drug Development and Industrial Pharmacy 34, 1022-1035. https://doi.org/10.1080/03639040801925990.

Sommer, K. and G. Hauser, 2003. Flow and Compression Properties of Feed Solids for Roll-Type Presses and Extrusion Presses. Powder Technology 130, 272-276. https://doi.org/10.1016/S0032-5910(02)00204-8.

Souihi, N., M. Dumarey, H. Wikstrom, P. Tajarobi, M. Fransson, O. Svensson, M. Josefson and J. Trygg, 2013a. A Quality by Design Approach to Investigate the Effect of Mannitol and Dicalcium Phosphate Qualities on Roll Compaction. International journal of pharmaceutics 447, 47-61. https://doi.org/10.1016/j.ijpharm.2013.02.036.

Souihi, N., M. Josefson, P. Tajarobi, B. Gururajan and J. Trygg, 2013b. Design Space Estimation of the Roller Compaction Process. Industrial & Engineering Chemistry Research 52, 12408-12419. https://doi.org/10.1021/ie303580y.

Souihi, N., G. Reynolds, P. Tajarobi, H. Wikstrom, G. Haeffler, M. Josefson and J. Trygg, 2015. Roll Compaction Process Modeling: Transfer between Equipment and Impact of Process Parameters. International journal of pharmaceutics 484, 192-206. https://doi.org/10.1016/j.ijpharm.2015.02.042.

Sun, C. C. and P. Kleinebudde, 2016. Mini Review: Mechanisms to the Loss of Tabletability by Dry Granulation. European Journal of Pharmaceutics and Biopharmaceutics 106, 9-14. https://doi.org/10.1016/j.ejpb.2016.04.003.

Sun, C. Q. and M. W. Himmelspach, 2006. Reduced Tabletability of Roller Compacted Granules as a Result of Granule Size Enlargement. Journal of Pharmaceutical Sciences 95, 200-206. https://doi.org/10.1002/jps.20531.

Sun, C. Q. C., H. Hou, P. Gao, C. Ma, C. Medina and F. J. Alvarez, 2009. Development of a High Drug Load Tablet Formulation Based on Assessment of Powder Manufacturability: Moving Towards Quality by Design. Journal of Pharmaceutical Sciences 98, 239-247. https://doi.org/10.1002/jps.21422.

Tan, B. M., L. W. Chan and P. W. Heng, 2016. Determination of the Nip Angle in Roller Compactors with Serrated Rolls. Journal of Pharmaceutical Sciences 105, 1967-1975. https://doi.org/10.1016/j.xphs.2016.04.008.

Thapa, P., J. Tripathi and S. H. Jeong, 2019. Recent Trends and Future Perspective of Pharmaceutical Wet Granulation for Better Process Understanding and Product Development. Powder Technology 344, 864-882. https://doi.org/10.1016/j.powtec.2018.12.080.

Toson, P., D. G. Lopes, R. Paus, A. Kumar, J. Geens, S. Stibale, J. Quodbach, P. Kleinebudde, W.-K. Hsiao and J. Khinast, 2019. Model-Based Approach to the Design of Pharmaceutical Roller-Compaction Processes. International Journal of Pharmaceutics: X 1, 100005. https://doi.org/10.1016/j.ijpx.2019.100005.

Train, D., 1956. An Investigation into the Compaction of Powders. Journal of Pharmacy and Pharmacology 8, 745-760. https://doi.org/10.1111/j.2042-7158.1956.tb12206.x.

United States Pharmacopeial Convention, 2021. Oral Drug Products - Product Quality Tests, 2. https://online.uspnf.com/uspnf/document/1_GUID-DA161518-EC27-4647-AACD-29D28F2A4E92_5_en-US.

Vendola, T. A. and B. C. Hancock, 2008. The Effect of Mill Type. Pharmaceutical Technology 32, 72-86. https://www.scopus.com/inward/record.uri?eid=2-s2.0-59449101935&partnerID=40&md5=ff06fe295bcd702adb80e9b0e4187dfa

Vervaet, C. and J. P. Remon, 2005. Continuous Granulation in the Pharmaceutical Industry. Chemical Engineering Science 60, 3949-3957. https://doi.org/10.1016/j.ces.2005.02.028.

Wagner, C. M., M. Pein and J. Breitkreutz, 2013. Roll Compaction of Mannitol: Compactability Study of Crystalline and Spray-Dried Grades. International journal of pharmaceutics 453, 416-422. https://doi.org/10.1016/j.ijpharm.2013.05.024.

Wennerstrum, S., 2000. Ten Things You Need to Consider When Choosing and Installing a Roller Press System. Powder and Bulk Engineering 14, 37-62.

Wiedey, R. and P. Kleinebudde, 2017. The Density Distribution in Ribbons From roll compaction. Chemie-Ingenieur-Technik 89, 1017-1024. https://doi.org/10.1002/cite.201600143.

Wiedey, R. and P. Kleinebudde, 2018. Infrared Thermography - a New Approach for in-Line Density Measurement of Ribbons Produced from Roll Compaction. Powder Technology 337, 17-24. https://doi.org/10.1016/j.powtec.2017.01.052.

Wiedey, R., R. Sibanc, A. Wilms and P. Kleinebudde, 2018. How Relevant Is Ribbon Homogeneity in Roll Compaction/Dry Granulation and Can It Be Influenced? European Journal of Pharmaceutics and Biopharmaceutics 133, 232-239. https://doi.org/10.1016/j.ejpb.2018.10.021.

Wünsch, I., J. H. Finke, E. John, M. Juhnke and A. Kwade, 2019. A Mathematical Approach to Consider Solid Compressibility in the Compression of Pharmaceutical Powders. Pharmaceutics 11, 121. https://doi.org/10.3390/pharmaceutics11030121.

Xie, X. and V. M. Puri, 2012. Powder Deposition in Three Parallel-Oriented Dies of Cylindrical and E Shapes. Advanced Powder Technology 23, 1-7. https://doi.org/10.1016/j.apt.2010.11.005.

Yohannes, B., M. Gonzalez, A. Abebe, O. Sprockel, F. Nikfar, S. Kang and A. M. Cuitino, 2015. The Role of Fine Particles on Compaction and Tensile Strength of Pharmaceutical Powders. Powder Technology 274, 372-378. https://doi.org/10.1016/j.powtec.2015.01.035.

York, P. and E. D. Baily, 1977. Dimensional Changes of Compacts after Compression. Journal of Pharmacy and Pharmacology 29, 70-74. https://doi.org/10.1111/j.2042-7158.1977.tb11248.x.

Yu, M., C. Omar, M. Weidemann, A. Schmidt, J. D. Litster and A. D. Salman, 2020. Roller Compaction: Infrared Thermography as a PAT for Monitoring Powder Flow from Feeding to Compaction Zone. International journal of pharmaceutics 578, 119114. https://doi.org/10.1016/j.ijpharm.2020.119114.

Yu, S., M. Adams, B. Gururajan, G. Reynolds, R. Roberts and C.-Y. Wu, 2013. The Effects of Lubrication on Roll Compaction, Ribbon Milling and Tabletting. Chemical Engineering Science 86, 9-18. https://doi.org/10.1016/j.ces.2012.02.026.

Yu, S., B. Gururajan, G. Reynolds, R. Roberts, M. J. Adams and C. Y. Wu, 2012. A Comparative Study of Roll Compaction of Free-Flowing and Cohesive Pharmaceutical Powders. International journal of pharmaceutics 428, 39-47. https://doi.org/10.1016/j.ijpharm.2012.02.033.

Zettler, A., J. Hilden, M. Koenig, C. Breslin, A. Aburub, M. Allgeier, P. Patel and B. Mitra, 2016. Evaluation of Small-Scale Powder Flow Characterization Tests in the Prediction of Large-Scale Process Failures. Journal of Pharmaceutical Innovation 11, 189-199. https://doi.org/10.1007/s12247-016-9258-5.

Zinchuk, A. V., M. P. Mullarney and B. C. Hancock, 2004. Simulation of Roller Compaction Using a Laboratory Scale Compaction Simulator. International journal of pharmaceutics 269, 403-415. https://doi.org/10.1016/j.ijpharm.2003.09.034.

Zuurman, K., K. Van der Voort Maarschalk and G. K. Bolhuis, 1999. Effect of Magnesium Stearate on Bonding and Porosity Expansion of Tablets Produced from Materials with Different Consolidation Properties. International journal of pharmaceutics 179, 107-115. https://doi.org/10.1016/S0378-5173(98)00389-5.

7 Appendix

7.1 Additional Figures

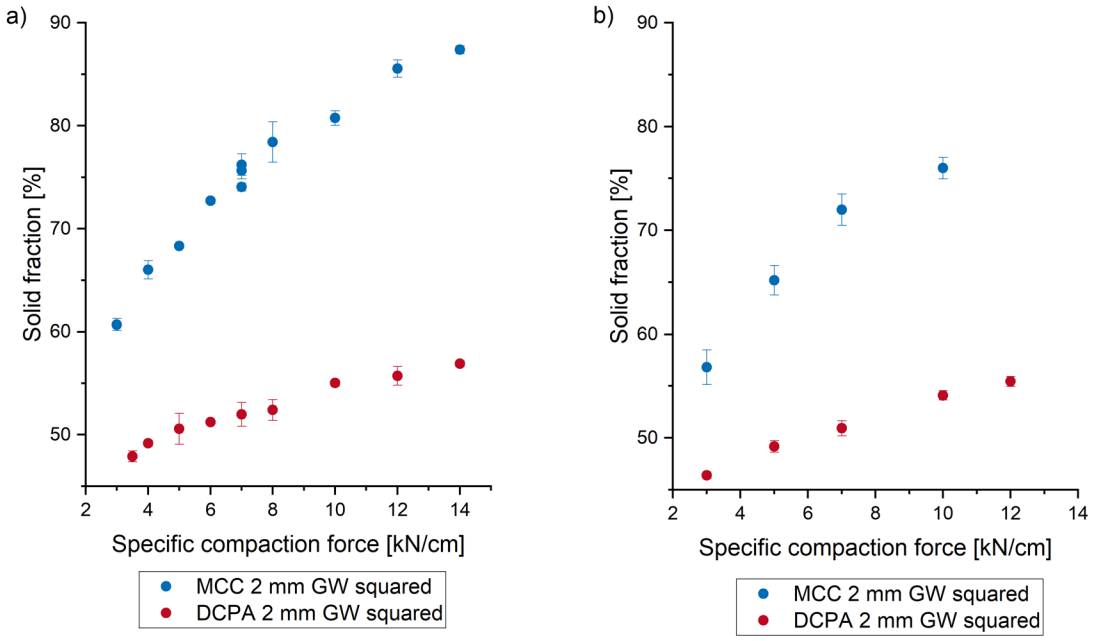

Figure 7.1-1: Comparison of ribbon solid fraction of MCC and DCPA in dependence on the specific compaction force for a) 25 mm and b) 40 mm roll width at a gap width of 2 mm with squared rolls; n=3; mean ± SD

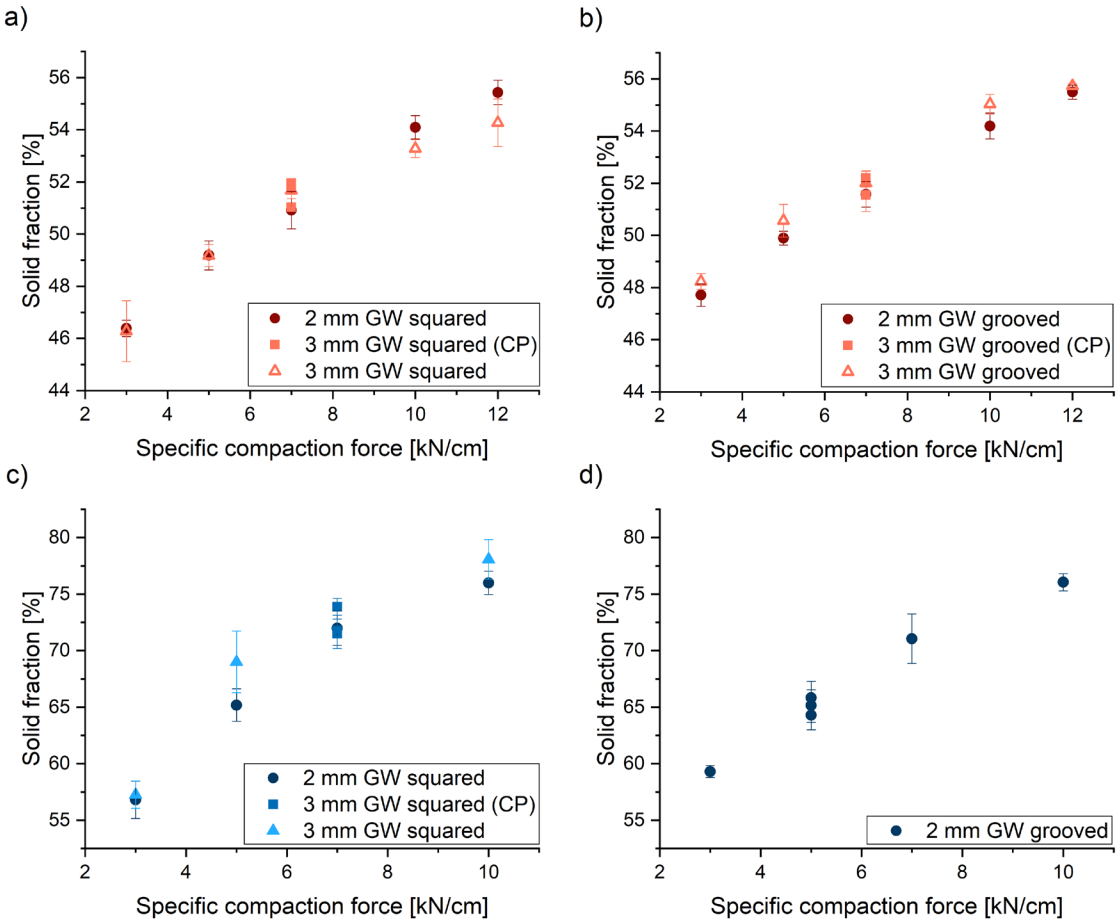

Figure 7.1-2: Influence of the gap width on the solid fraction of MCC and DCPA ribbons produced with 40 mm wide rolls; a) DCPA, squared rolls; b) DCPA, grooved rolls; c) MCC, squared rolls; d) MCC, grooved rolls; n=3, mean ± SD

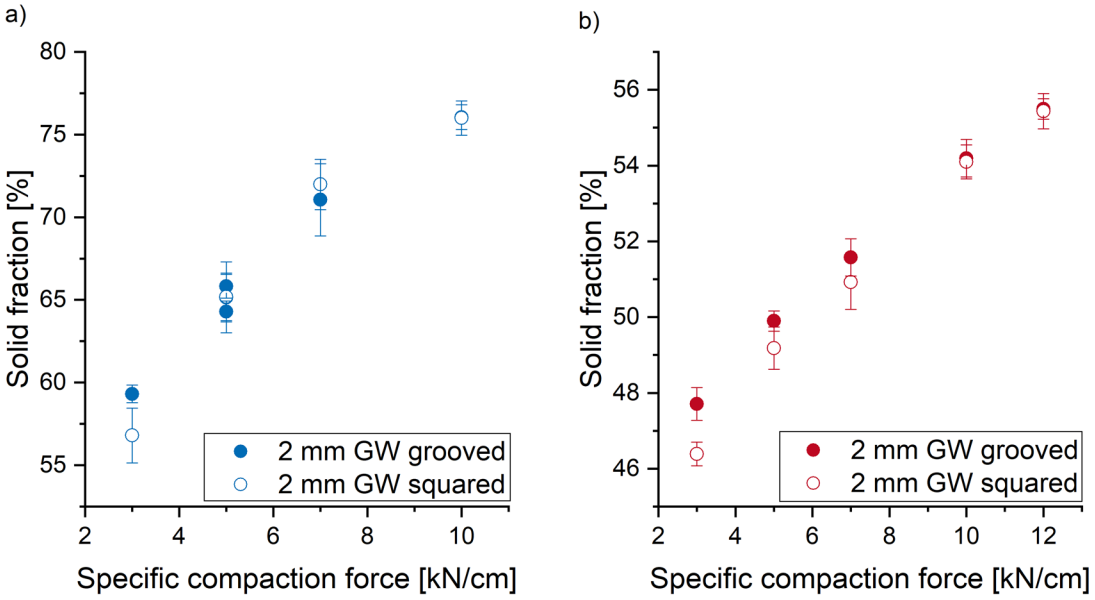

Figure 7.1-3: Comparison of ribbon solid fraction for grooved and squared rolls for (a) MCC and (b) DCPA at 2 mm gap width and 40 mm roll width; n=3; mean ± SD

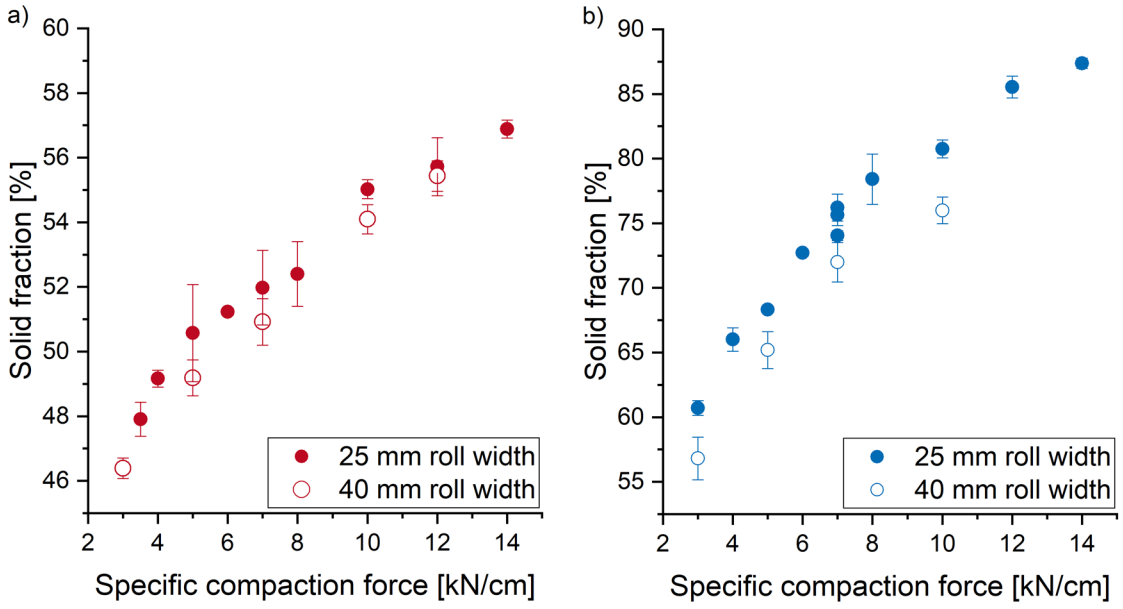

Figure 7.1-4: Influence of the roll width on the solid fraction of a) DCPA and b) MCC ribbons produced at 2 mm gap width and squared rolls; n=3; mean ± SD

8 Danksagung

Bei meinem Doktorvater Professor Peter Kleinebudde möchte ich mich ganz herzlich bedanken für die Aufnahme in seinen Arbeitskreis und für die Überlassung eines Dissertationsthemas, das mich von Beginn an fasziniert und begeistert hat. Vielen Dank, dass Sie sich immer die Zeit genommen haben sowohl für fachliche als auch für fachfremde Diskussionen und dass Sie zu jeder Zeit ein offenes Ohr und wertvolle Ratschläge für mich hatten.

Meinem Mentor Professor Jörg Breitkreutz danke ich für die Übernahme des Koreferats und für seine stets konstruktiven Ideen. Ich erinnere mich gerne an zahlreiche interessante Gespräche, in denen wir weit über den Tellerrand der pharmazeutischen Technologie hinausgeblickt haben.

Den beiden Professoren möchte ich außerdem für ihr unermüdliches Engagement für das Institut danken und für die Möglichkeit an insgesamt zwölf nationalen und internationalen Konferenzen teilgenommen zu haben.

I would like to express my sincere thanks to Medelpharm for the great cooperation, which was always characterised by mutual trust, close collaboration and a constant exchange of ideas. I would like to thank Ingrid Coyle and Bruno Villa for the warm welcome in Beynost at our project meetings, the acceptance into the Styl'One family and their constant support. I would like to thank Bruno Leclercq for the excellent supervision of my doctoral thesis on the part of Medelpharm, for his constructive feedback and for the numerous interesting discussions at our small and big project meetings. A big thanks goes to Guillaume Tardy, who has always supported me with his expertise in countless TeamViewer and WebEx sessions, incorporated our ideas into the Styl'One software and proofread my thesis. I would like to thank Régis Cazes for his helpful suggestions and ideas. And I would also like to say thank you to all the other employees at Medelpharm whom I have had the pleasure of meeting over the years. It was a real pleasure working with you!

Der Firma Alexanderwerk AG und Dr. Alexander Schmidt danke ich für die Möglichkeit, Versuchsreihen an der WP120 und WP200 zu realisieren. Bei Manfred Felder und Marcus Weidemann bedanke ich mich herzlich für die Unterstützung bei der Durchführung der Versuche, der spontanen Umplanung von Versuchsreihen und der Auswertung der Daten. Ein ganz herzliches Dankeschön auch für das Korrekturlesen von Teilen dieser Arbeit und die konstruktive fachliche Kritik.

Bei den Firmen JRS PHARMA & Co. KG und Chemische Fabrik Budenheim KG bedanke ich mich für das Bereitstellen von großen Mengen an Rohstoffen zur Walzenkompaktierung.

Bei Dr. Klaus Knop bedanke ich mich für das Korrekturlesen von Teilen dieser Arbeit, seine Hilfsbereitschaft in allen Belangen und die stets konstruktiven fachlichen Diskussionen.

Bei meinen Bürokolleginnen Kitti Szappanos-Csordás und Yasmin Thabet möchte ich mich herzlich bedanken für die vielen unvergesslichen lustigen und schönen Momente, die wir zusammen auf 00 erlebt haben. Ich habe selten so viel gelacht wie mit euch! Kitti danke ich außerdem von Herzen für ihre Einführung ins Walzenkompaktieren, ihre Ratschläge und Hilfsbereitschaft.

Meinem Bürokollegen Björn Fischer danke ich für eine großartige Zeit im Kellerbüro, für interessante Einblicke in die Welt der Spektroskopie und für unsere wundervollen sozioökonomischen Philosophiestunden.

Bei meinen Wahlpflichtfacht-Studentinnen Laura Osthege, Selina Wagner, Hanna Plappert und Nina Baumann bedanke ich mich für ihr großes Engagement und ihre Unterstützung bei der Untersuchung der elastischen Rückdehnung sowie bei der Kp-Faktor Bestimmung - und für die netten Gespräche bei dem ein oder anderen Chai Latte.

Bei Sabrina Berkenkemper möchte ich mich dafür bedanken, dass sie es mir so leicht gemacht hat ihre Diplomarbeit zu betreuen – und für unsere Fitness-Eskapaden nach einigen langen Boulder-Abenden.

Bei der Fokusgruppe Joggen bedanke ich mich für eine hervorragende Wettkampfvorbereitung und ein einmaliges Teamerlebnis beim Mud Master 2019 in Weeze.

Ein herzliches Dankeschön geht an Philipp und Olga Kiefer, die mich in den unterschiedlichsten Situationen immer großartig unterstützt haben und deren Wohnung zeitweise praktisch mein zweites Zuhause geworden ist. Vielen Dank für eure wundervolle Freundschaft!

Bei Bastian Hahn möchte ich mich bedanken für seine Freundschaft, seine gute Laune und zahlreiche Stunden Bouldern, die mich auf andere Gedanken gebracht haben. Außerdem war er für mich ein stetiger Ansporn beim Schreiben nicht aufzugeben und darüber aber nicht zu vergessen das Leben zu genießen.

Ard Lura danke ich für viele lustige Stunden an der Styl'One und dafür, dass die Tür zum Büro nebenan immer offen und immer Zeit zum Quatschen war.

Vincent Lenhart danke ich für seine Freundschaft von Anfang an und für seine Fähigkeit, mich zum Lachen zu bringen, auch wenn mir zum Heulen zumute ist.

Annika Wilms möchte ich danken für eine wunderschöne Zeit während meiner letzten Konferenz im schönen Lausanne. In Nürnberg war sie auch dabei, aber darüber darf nichts verraten werden…

Bastian Hahn und Philipp Kiefer möchte ich danken für die gemeinsame Organisation des PSSRC 2019 in Düsseldorf. Es hat die letzten Monate am Institut nicht unbedingt weniger stressig aber doch sehr viel lustiger gemacht.

Ein großes Dankeschön auch an alle nicht namentlich genannten Kollegen des Instituts, die eine tolle Arbeitsatmosphäre kreiert haben – ihr habt meine Zeit am Institut zu etwas ganz Besonderem gemacht!

Jana Reimer möchte ich ganz herzlich für das sprachliche Korrekturlesen dieser Arbeit danken und ihre Begeisterungsfähigkeit für ein für sie gänzlich fachfremdes Thema.

Bei Hans Lindner bedanke ich mich für den richtigen Hinweis zum richtigen Zeitpunkt – ohne ihn wäre diese Arbeit womöglich nicht entstanden.

Meinen Eltern Kerstin und Axel Reimer und meinem Bruder Bo Frederik Reimer danke ich dafür, dass sie mich immer in allem unterstützt haben, was ich mir vorgenommen habe. Meiner Oma Erika möchte ich Danke sagen für ihr Motto „Kartoffel für Kartoffel“, das mich vor allem in der Zeit des Schreibens immer wieder zum Weitermachen motiviert hat.

Meinem Mann Robert Keizer gilt mein ganz besonderer Dank. Durch deine grenzenlose Geduld, deine uneingeschränkte Unterstützung und dein Vertrauen habe ich es geschafft durchzuhalten und weiterzumachen, auch wenn es manchmal schwierig war.

9 Eigenständigkeitserklärung

Ich versichere an Eides Statt, dass die Dissertation “Hybrid modelling of roll compaction” von mir selbständig und ohne unzulässige fremde Hilfe unter Beachtung der “Grundsätze zur Sicherung guter wissenschaftlicher Praxis an der Heinrich-Heine-Universität Düsseldorf“ erstellt worden ist. Außerdem versichere ich, dass die vorgelegte elektronische mit der schriftlichen Version der Dissertation übereinstimmt und die Abhandlung in dieser oder ähnlicher Form noch nicht anderweitig als Promotionsleistung vorgelegt und bewertet wurde.

Hannah Lou Keizer